ACYL TRANSFER REACTIONS IN HYDROXYL ESTER DERIVATIVES, THEIR ANALOGS AND THE INVESTIGATION OF THE SYNTHETIC POTENTIAL OF RIGID INOSITOL DERIVATIVES

THESIS

SUBMITTED TO THE

SAVITRIBAI PHULE PUNE UNIVERSITY

FOR THE DEGREE OF

DOCTOR OF PHILOSOPHY

IN

CHEMISTRY

BY

TAMBOLI MAJID ISMAIL

RESEARCH SUPERVISOR

Dr. M. S. SHASHIDHAR

DIVISION OF ORGANIC CHEMISTRY

NATIONAL CHEMICAL LABORATORY

PUNE 411 008, INDIA

JANUARY 2016

Dedicated to my Beloved Family…

CERTIFICATE

This is to certify that the work incorporated in the thesis entitled "**Acyl transfer reactions in hydroxyl ester derivatives, their analogs and the investigation of the synthetic potential of rigid inositol derivatives**" submitted by **Tamboli Majid Ismail** was carried out by him under my supervision at the National Chemical Laboratory, Pune, India. Such materials, obtained from other sources have been duly acknowledged in the thesis.

Date:

(Dr. M. S. SHASHIDHAR)

Research Supervisor

Division of Organic Chemistry

National Chemical Laboratory

Pune-411 008, India

National Chemical Laboratory, Pune (India)

DECLARATION

I hereby declare that the thesis entitled **"Acyl transfer reactions in hydroxyl ester derivatives, their analogs and the investigation of the synthetic potential of rigid inositol derivatives"** submitted for Ph.D. degree to the Savitribai Phule Pune University has been carried out at National Chemical Laboratory, under the supervision of **Dr. M. S. Shashidhar**. This work is original and has not been submitted in part or full by me for any degree or diploma to any university.

Date:

Division of Organic Chemistry,
National Chemical Laboratory,
Pune-411 008

(TAMBOLI MAJID ISMAIL)

Acknowledgements

I wish to express my deep sense of gratitude and profound thanks to my research supervisor ***Dr. M. S. Shashidhar*** *for introducing me to the fascinating field of reaction in molecular crystals and inositol chemistry. His systematic working style, logical way of thinking, fruitful discussion, suggestion and humanitarianism is an attribute that I wish to take forward with me along with the chemistry that I learnt from him.*

No thanks can be enough to acknowledge the endless encouragement, care and support from Dr. ***R. G. Gonnade****. Once again I would like to my deep sense of gratitude and insightful thanks to Dr. R. G. Gonnade, for their great help in determining the x-ray structures and teaching x-ray crystallography and great support during my whole stay in NCL like great Teacher, Big brother.*

I would like to thank Dr. S. P. Chavan and Dr. (Mrs.) Radhika S. Kusurkar for their valuable suggestions and scientific discussion during assessment of my Ph.D. work. I wish to thank from bottom of my heart Dr. U. R. Kalkote for suggestion and help in and outside NCL.

My sincere thanks to scientists of the division; Dr. P. K. Tripathi, (HOD), Dr. N. N. Joshi, Dr. R. A. Joshi, Dr. (Mrs.) V. A. Kumar, Dr. N. P. Argade, Dr. G. J. Sanjayan, Dr. H. V. Thulasiram, Dr. C. V. Ramana, Dr. Reddy, Dr. Santosh Mhaske, Dr. S. Iyer, Dr. (Mrs.) A. P. Likhithe, Dr. (Mrs.) S. P. Maybhate, Dr. Muthukrishnan, Dr. A. T. Biju, Dr. Nitin. T. Patil and others. I wish to thank Mrs. Puranik and Mrs. Kolhe (SAC office) for their help.

Help from analytical units for characterization of compounds is gratefully acknowledged. I thank Dr. Rajmohanan for NMR, Shrikant, Mayur, Dinesh, Dr. H. B. Borate for analytical facilities, Mrs. S. P. Kunte, for HPLC, Dr. (Mrs.) Shanta Kumari for HR-MS, Dr. P. L. Joshi (and Mrs. Sawant, Mrs. Sanas and Mrs. Damse) for microanalysis and IR. I express my thanks to the office staff, Library members and administrative staff for their timely help.

I wish to thank Dr. Gurav, Dr. Vibhute, Dr. Kuberkar, Dr. P. A. Kulkarni, Dr. Dawane, Dr. M.A. Baseer, Dr. Shaikh Kabeer Ahmed of Yeshwant Mahavidyalaya, Nanded, Dr. Page, Dr. Murti., Dr. Joshi, Dr. (Mrs.) Vandana Kamble (Maharashtra Udaygiri Mahavidyalaya, Udgir), Khanapure Guruji, Kotwal guruji, Mane madam, sunil patil Sir, Bhatambre Sir, Mauzum Sir, Biradar sir, Bimshanker sir, Munjiwar sir, Patil Sir, Kalim Sir, Babu Sir, Ramesh belure sir, Imtiyaj Sir, Nagpure Sir, Sawant Sir and others for excellent teaching and time encouragement in my school and college level in Deoni.

It gives me immense pleasure to express my sincere thanks to my senior colleagues; Dr. Rajendra, Dr. Mrs. Shobhana, Alson Sir and especially Dr. Mrs. Madhuri Patil and Dr. Bharat, for their friendly nature, giving excellent training, valuable discussion and support. I am very much thankful to my labmates Richa, Nilesh, Rupesh, Debadi, Pranaya, Vir, Nivedita, Ekta, Samir, Nitai Sarkar, Jayendra, Niharika, Rohit, Santosh, Amartya, Priyadarshani, Permeshawary, Sanjay, awais for

maintaining cheerful atmosphere in the lab. Especially ***Shiridhar Thorat*** *and* ***Richa*** *for being best friend and I would like to thank Moreji for help and lab maintenance.*

I would like to thank Dr. (Mrs.) Vidya Shashidhar, Mrs. Vaishali Gonnade, for their advices and help.

I thank all my senior and Friends at NCL: Dr. Nagendra, Dr. Sharad, Dr. Pandurang, Ganesh Jogdand, Dr. Haval, Dr. Abasaheb, Dr. Manmath, Dr. Suleman, Dr. Ismail Todewale, Dr. Sudhir, Dr. Namdev, Dr. Bapu, Dr. Purude, Dr. Hamid, Dr.Satish Biradar, Abbas Biradar, Dr.Ravi, Dr.Kishor, Dr.Prakash, Dr.Pradeep, Dr.Lalit, Dr.Nilesh, Dr.Sumanta Dr.Seema, Dr.Venu, Dr.Manoj, Dr.Namrata, Tanaya, Dr.Debashish, Dr.Sujit, Dr.Prasanna, Rajesh, Animesh, Shiva B., Tukaram, Ganesh, Dr.Sangram, Dr.Ramesh, Dr.Arup, Sachin, Shiva, Dr.Vijayadas, Amol, Sanjeev, Suresh², Dr.Prashant, Dr.Mandeep, Ramesh, Pravat, Ravi, Sagar, Dr.Swati, Dr.Saikat, Dr.Pabhakar, Harshal, Dipesh, Shrikant, Kailash, Harshali, Sanket, Nitin, Dinesh, Appasaheb, Ambadas, Anupam, Vikas, Krishanu, Dr.Partha, Dr.Rahul, Brijesh, Raju, Rohan, sagar patil, Sumit Kamble, Dr.Pitambar, Dr.Rahul Patil, Dr.Sachin, Dr.Chandrababu, Dr.Yadagiri, Dr.Sunil, Ravindra, Narendra, Nagendra, Sachin Patil, Bala, Prabhu, Laxmi, Dr.Sanjay Negi, Ashok, Lenin, Ramsunder, Mujunath, Dr.Achinkya, Hemendra Chand, Ashish C, Remi reddy, Hanuman, Dr.Eldo, Dr. Rajesh T, Dr. Joby, Indravardhan, Dr. arijit, Dr. Tamas, Dr. Chandan, Chini, Rajan Pandey, Vasudev, Gajanan, Gorak, Rahul, Satish, Sitaram, Kishore, Pankaj, Ranjit, Milind, Sachin, Anupam, Trinath, Shanti, Santigopal, tony, Vishawanath, Jambu, Dr.Sangmesh, Dr. Prakash Sane, Dr. Ganesh Kokate, Dr.Abhijit, Dr. Asif, Dr. Raju Nanda, Dr. Kaushalji, Dr.Suleman Inamdar, Dr. Mohsin Pathan, Dr. Amol Hengane, Dr. Digamber Shinde, Dr. Pradeep Pachphule, Dr. Narayan, Dr. Nagesh Khupse, Dr. Sanjay Negi, Dr. Praksh Korke, Dr. Ganesh Kokate, Dr. Satish Yadav, Dr. Sandeep (Malak), Dr. Mujahid, Ijaj pathan, Narayan, Manoj Mane, Dr. Valmik, Dr. Rahul Aslam, Amol, Pradeep, Popat, Avinash, Manjur, Indradeep, Ravindra mule, Satej D, Praveen Shinde, Arun N, Shekhar, Yogesh Marathe, Praveen korra, Indrapal Karbhal, Roby Soni, Santosh Singh….. and others. I will cherish their company in NCL for long time.

I wish to thank my school and College friends: Ganesh, Raju, Dnyaneshwer, Ram, Praveen, Madhav, Milind, Anand, Balaji, Madhav, Sunil, Ramesh, Chetan, Musa, Satish, Rambau, Gajanan, Kore, Mahadev, dhage, Vikas kamble, Ravi, Vinod, Balu jagaye, Hemant, Ram ghatul, Sai Patil, Amjad, Jawed, Gutte, Jabbar, ram Ghatul, Parsuram, amol Shinde, Wagaj, Rupesh, Kishor Bodawar, Satish, Pathak and my senior Sachin Gurdharkar, Ziya, Pimpalpalle, Basir, Shanker², Manoj chopade, Balaji berve, Mohan Kalyankar, Gopi ……and others.

A lots of thanks goes to my dear friends Anil, Dr.Nagesh, Dr.Maroti, Dr.Shivaji, Dr.Dhiraj, Dr. Malba, Avinash pawade, Sharad parve, Dr. Mujahid, Dr. Sainath, Dr. Vilas, Dr. Samadhan, Manik, Vijay Kadam, Dr. Kaushalji, Govinda, who directly or indirectly helped me during my doctoral research.

My stay in NCL GJ hostel has been memorabale because of my core group of friends Dr.Deepak Bhau, Dr. Ankush, Dr. Pankaj Bharmwar, Dr. Kiran, Dr. Dhanraj, Dr. Mangesh, Dr. Asif, Dr. valmik Shinde, Dr. Chinmay, Dr. Bhausaheb Tawde, and at present Atul, Satish, Dnyaneshawar G, Arun N, Santosh L, Dnyaneshawar B, Sagar, Vinita, Nalini, and all my GJlites.

My special thanks to the ***Dr. Deepak Bhau***, ***Dr. Kiran Patil***, ***Dr. Sutar Sir***, ***Dr. Atul More***, ***Pranoy Banger*** *and Satish Biradar for their help and affection and love.*

I would like to express a deep sense of gratitude to each member of my Family and my friends for their blessing, love, care and constant encouragement throughout my life.

I would like to thanks many other people in and around NCL who helped me either directly or indirectly during my research career at NCL.

I would like to thank the Council of Scientific and Industrial Research (CSIR), New Delhi for the award of fellowship. I am thankful to Dr. P. K. Tripathi, Head of organic chemistry division and Director, NCL for opportunity to work in this prestigious research institute and providing all necessary infrastructure and facilities.

22th January 2016 *Tamboli Majid*

CONTENTS

Abbreviations

All	Allyl
Anhd.	Anhydrous
aq.	Aqueous
Bn	Benzyl
BnBr	Benzyl bromide
Bz	Benzoyl
BzCl	Benzoyl chloride
Calcd	Calculated
Cat.	Catalytic
Concd	Concentration
D_2O	Deuterium Oxide
DCM	Dichloromethane
dil.	Dilute
DIPEA	Di-isopropyl ethyl amine
DMAP	*N, N*-dimethylamino pyridine
DMF	*N, N*-Dimethylformamide
DMSO	Dimethyl sulfoxide
eq.	Equivalent
Et_3N	Triethylamine
El	Electrophile
g	Gram
h	Hour (s)
Hz	Hertz
i$BuNH_2$	*iso*-Butyl amine
IR	Infrared
LC-MS	Liquid chromatography-mass spectrometry
Mp	Melting point
Me	Methyl
MeOH	Methanol
mg	Milli gram
min.	Minute(s)

mL	Milliliter
mmol	Milli moles
NMR	Nuclear magnetic Resonance
Nu	Nucleophile
ORTEP	Oak Ridge Thermal Ellipsoid Plot Program
$Pd(OH)_2/C$	Palladium (II) Hydroxide on carbon
Ph	Phenyl
Py	Pyridine
rac-	Racemic
rt	Room temperature (23–30 ^oC)
Rf	Retention Factor
TMS	Trimethylsilyl
TLC	Thin layer chromatography
TsOH	4-Toluene sulfonic acid
s	singlet
d	doublet
t	triplet
q	quartet
m	multiplet
br.	broad

Abstract of the thesis

The thesis entitled **"Acyl transfer reactions in hydroxyl ester derivatives, their analogs and the investigation of the synthetic potential of rigid inositol derivatives"** consists of four chapters. A gist of the work described under each chapter is given below. Relevant references are cited. All the Chapters will include detailed experimental procedures, spectroscopic, crystallographic and analytical data relevant to the results described in the respective chapter and for the characterization of the compounds not previously reported in the literature.

Chapter 1: Identification of molecular crystals capable of undergoing acyl-transfer reaction based on intermolecular interactions in the crystal lattice: Acyl transfer reactions in 2,3-naphthalene diol derivatives.

Migration of acyl groups (inter and intramolecular) among the hydroxyl groups in polyhydroxy organic compounds, especially carbohydrates, their analogs and derivatives have attracted the attention of organic chemists for several decades. Although migration of acyl groups in the solution state is encountered frequently, such reactions in the solid state are rare. Investigation of the intermolecular acyl transfer reactivity in molecular crystals of *myo*-inositol orthoester derivatives (Scheme 1)[1-4] and its correlation with crystal structures enabled us to identify the essential parameters (a) and (b), to support efficient intermolecular acyl transfer reaction in crystals: (a) favourable relative geometry of the nucleophile (-OH, Nu) and the electrophile (-C=O, El) and (b) the molecular assembly, reinforced by C-H···π interactions, which supports a domino type of reaction in crystals (Figure 1).[1-4]

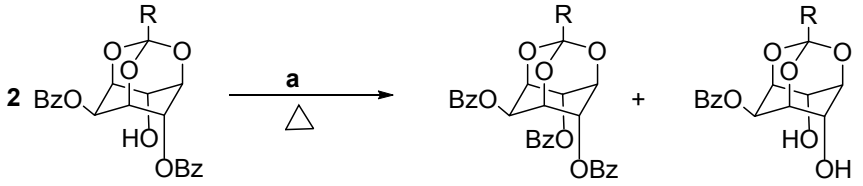

1 R = H ($P2_1/c$)
2 R = Me (Form I, $P2_1/n$)
2 R = Me (Form II, $C2/c$)
3 R = Ph ($P2_1/c$)
1·2 (Cc co-crystals)

4 R = H (47%)
5 R = Me (19%)
5 R = Me (42%)
6 R = Ph (49%)
4 + **5** (41%)

7 R = H (49%)
8 R = Me (21%)
8 R = Me (42%)
9 R = Ph (48%)
7 + **8** (35%)

Scheme 1: Transesterification reactions of *myo*-inositol orthoester derivatives in crystals (a) Anhydrous Na_2CO_3.

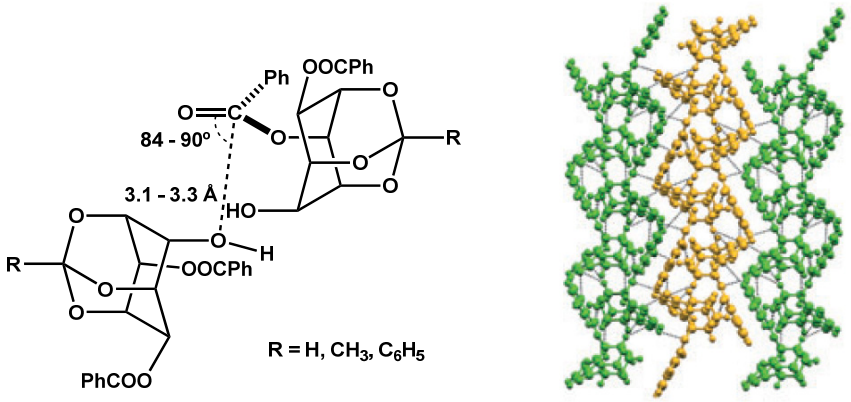

Figure 1: Schematic representation of the relative orientation of the reacting molecules between which acyl transfer occurs (left) in reactive crystals (of **1, 2, 3** and **1•2**) and the packing of molecules (right) required for efficient acyl group transfer in crystals. Each helix (green or orange) functions as a reaction channel for the propagation of acyl transfer between neighboring molecules.

In the current work, these parameters were used to identify other reactive crystals through a data-mining study of the Cambridge Structural Database. A 2:1 cocrystal of 2,3-naphthalene diol (**10**) and its di-*p*-methylbenzoate[5] (**11**) was selected (Figure 2) as a potentially reactive crystal and its reactivity was tested by heating the cocrystals in the presence of solid sodium carbonate. A facile intermolecular *p*-toluoyl group transfer was observed as predicted (Scheme 2).[6]

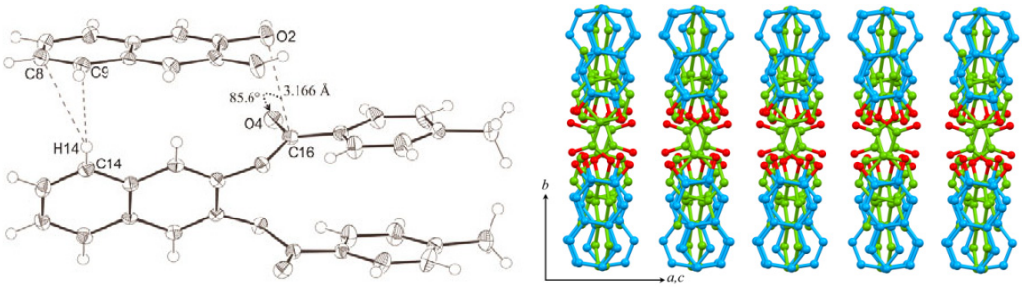

Figure 2: Relative orientation of the neighboring molecules of **10** and **11** in cocrystals **10•11** at 100 K (left); view of packing of the molecules to form discrete layers which function as reaction channels for acyl group transfer (right).

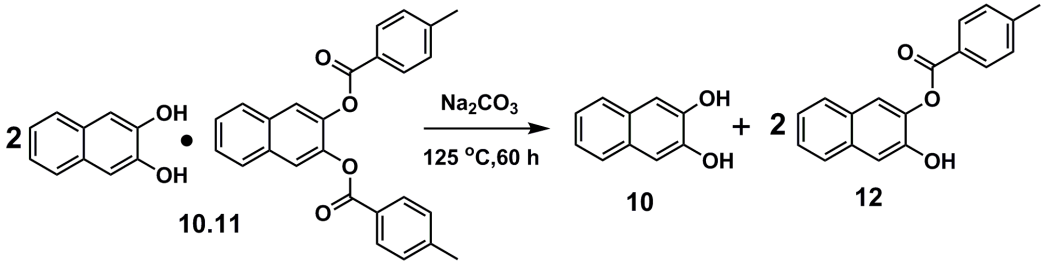

Scheme 2: Acyl transfer reaction in cocrystals **10•11** of naphthalene diol and its ditoluate.

The facility of the acyl transfer reaction in cocrystals **10•11** could be rationalized based on the packing of molecules in the cocrystal. Scheme 3 depicts the possible mechanism of acyl transfer in cocrystals **10•11**.

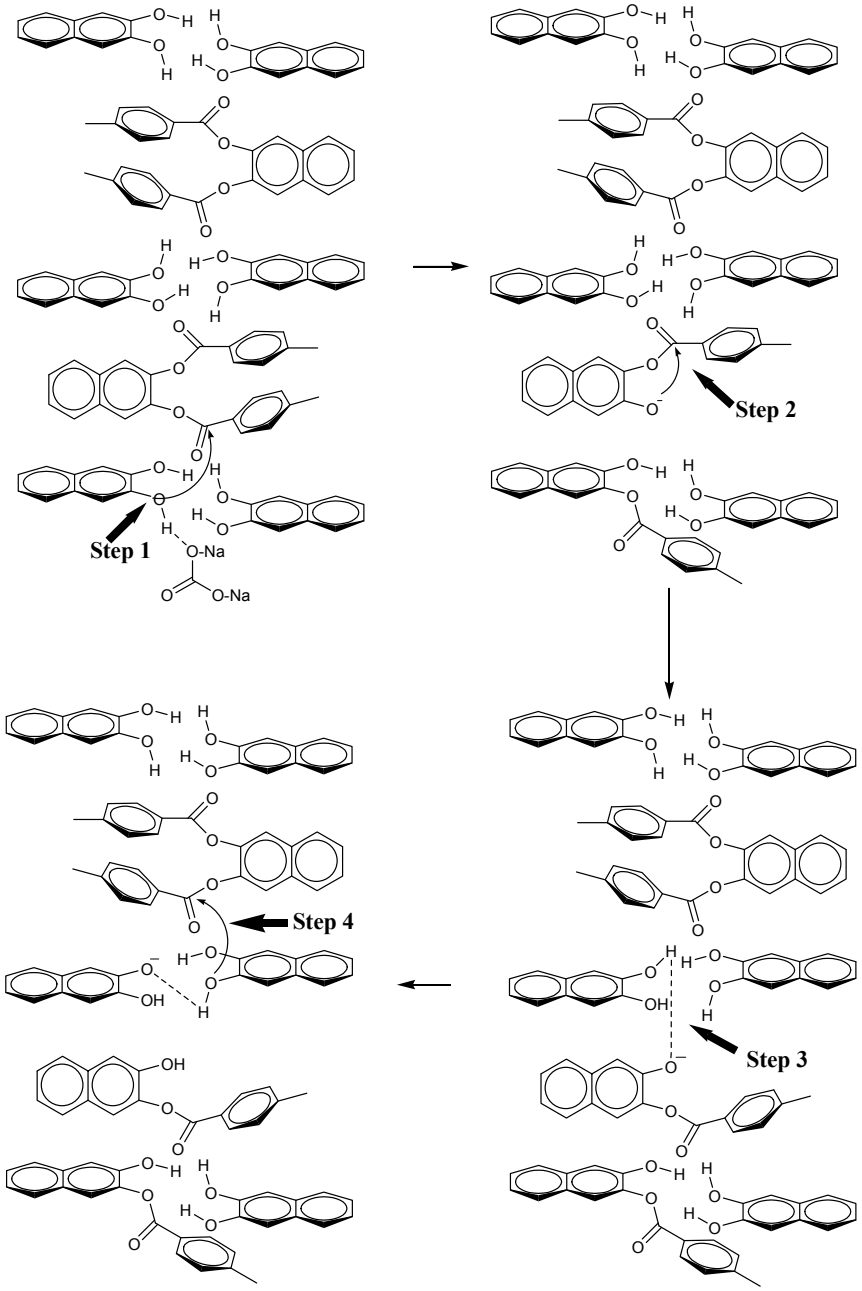

Scheme 3: Possible mechanism of acyl transfer in cocrystals **10•11**.

We also prepared cocrystals of the diol **10** with its mixed *p*-toluate and *p*-fluorobenzoate **13** (Scheme 4) hoping that such cocrystals could be of utility in understanding the mechanism of the acyl transfer reaction (shown in Scheme 3,

especially step 2). These cocrystals had structure and reactivity similar to that of cocrystals **10•11**. Studies towards unraveling the details of the mechanism of acyl transfer (Scheme 3) are in progress.

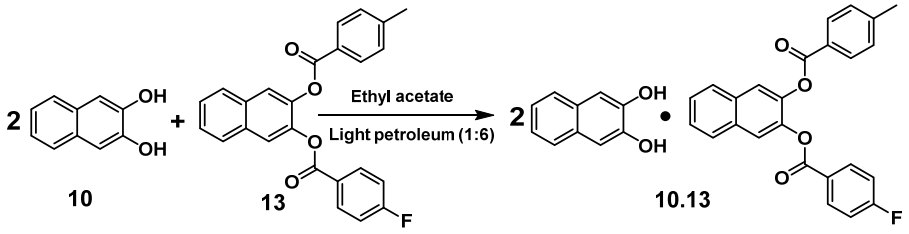

Scheme 4:

The successful identification of reactive crystals (from the CSD data base) opens up a novel method for the detection of molecular crystals capable of exhibiting acyl transfer reactivity and to predict the stability of hydroxyl esters in the crystalline state. Isomeric (*ortho*-, *meta*-, *para*-) ditoluates of the diol **10**, prepared during this work, exhibited interesting polymorphic and cocrystallization behavior; these results are published.

Chapter 2: Intramolecular cyclization of carbonate and thiocarbonate derivatives of *myo*-inositol 1,3,5-orthoformate in the solid state: Implications for acyl group transfer reactions in molecular crystals.

The results described in the previous chapter showed that certain crystal structure parameters based on non-covalent intermolecular interactions can be used to identify other molecular crystals that facilitate intermolecular acyl transfer reactions. Arriving at these parameters required the investigation of acyl transfer reaction in analogues and derivatives of *myo*-inositol orthoesters.[1-4,7-8] As a part of this study, we prepared carbonate and thiocarbonate derivatives of *myo*-inositol orthoformate and investigated their ability to undergo heat induced acyl transfer reaction in the solid state. It is pertinent to note that these derivatives have one oxygen atom extra [$R^1OC(O)OR^2$ or $R^1OC(S)OR^2$] in the vicinity of the carbonyl or thio carbonyl group as compared to esters [R^1COOR^2], which were the subject of previous studies.[1-4,7,8] The preparation of carbonate and thiocarbonate derivatives of *myo*-inositol orthoformate is shown in Scheme 5.

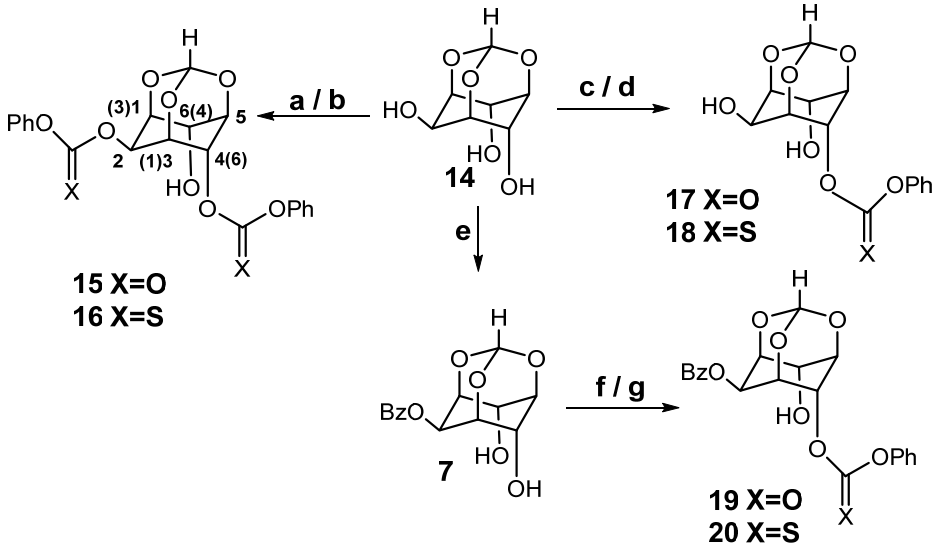

Scheme 5: (a) Pyridine, PhOCOCl (3 eq), -5 ^{o}C- rt, 1 h, 79%; (b) Pyridine, PhOCSCl (2.2 eq), -5 ^{o}C- rt, 2 h, 69 %; (c) PhOCOCl (1.2 eq), Et_3N, DMF, -5 ^{o}C- rt, 30 min., 64%; (d) PhOCSCl (1.2 eq), Et_3N, DMF, -5 ^{o}C- rt, 30 min., 66%; (e) PhCOCl, pyridine as in reference 24; (f) PhOCOCl (1.4 eq), Et_3N, DMF, -5 to 0 ^{o}C, 30 min, 55%; (g) PhOCSCl (1.3 eq), Et_3N, DMF, -5 to 0 ^{o}C, 30 min, 52%.

Racemic 4-*O*-phenoxycarbonyl and 4-*O*-phenoxythiocarbonyl derivatives of *myo*-inositol orthoformate underwent thermal intramolecular cyclization in the solid state to yield the corresponding 4,6-bridged carbonates and thiocarbonates respectively (Scheme 6). The thermal cyclization also occurred in the solution and molten states, but less efficiently, suggesting that these cyclization reactions are aided by molecular pre-organization, although not strictly topochemically controlled. Synthesis of C4,C6 bridged inositol derivatives by classical solution state synthesis have earlier been attempted due to their application potential in biology and in the development of functional materials.[9]

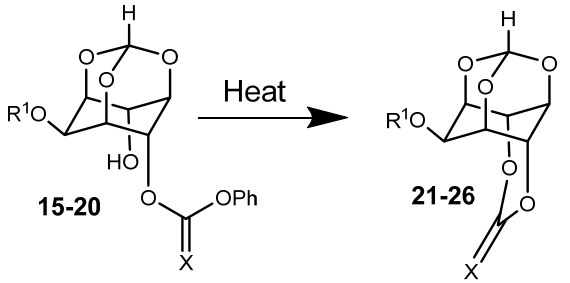

15, **21** X=O, $R^1 = C_6H_5OC{=}O$
16, **22** X=S, $R^1 = C_6H_5OC{=}S$
17, **23** X=O, R^1 = H

18, **24** X=S, R^1 = H
19, **25** X=O, $R^1 = C_6H_5C{=}O$
20, **26** X=S, $R^1 = C_6H_5C{=}O$

Scheme 6: Intramolecular cyclization reaction in carbonate and thiocarbonates.

Crystal structures of two carbonates (**17**, **19**) and a thiocarbonate (**20**) clearly revealed that the relative orientation of the electrophile and the nucleophile in the crystal lattice (Figure 3) facilitates the intramolecular cyclization reaction and forbids the intermolecular reaction (such as those encountered in Chapter 1, see Figure 1). The relatively wider range of intramolecular electrphile (El)···(Nu) nucleophile interaction parameters observed in reactive crystals is precedented by earlier observations of intramolecular acyl transfer in crystals of certain acetyl salicyclic acid derivatives.[10] The intermolecular El···Nu geometry observed in crystals that underwent cyclization reaction was consistently worse than the corresponding intramolecular geometry. The intermolecular El···Nu parameters in crystals of compounds **17** (5.362Å, 101.15°), **19** (5.373Å, 163.97°), and **20** (4.252Å, 134.85°) were very different as compared to those in molecular crystals of racemic 2,4-di-O-benzoyl-*myo*-inositol-1,3,5-orthoformate (3.216Å, 88.28°), which support intermolecular acyl transfer (Figure 3). The correlation observed between chemical reactivity and the non-covalent interactions in the crystal of reactants provides a way to estimate the chemical stability of analogous molecules in the solid state.

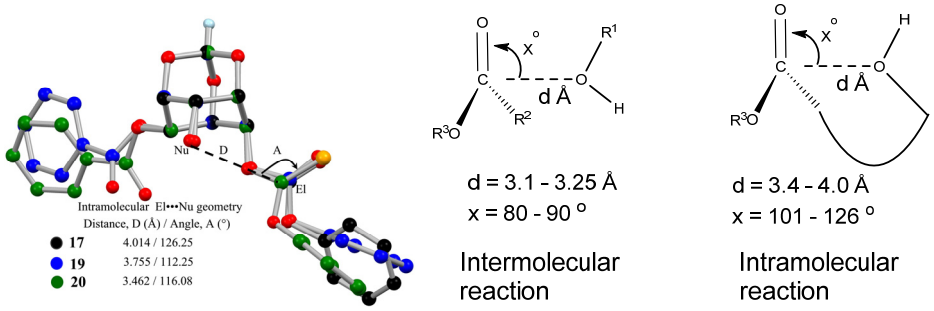

Figure 3: (a) Overlap of molecules present in crystals (at 23 °C) of carbonates **17**, **19** and the thiocarbonate **20** (left); (b) Range of electrphile···nucleophile interactions necessary for successful acyl group transfer in crystals leading to product formation (center and right).

We had also prepared *myo*-inositol orthoformate derivatives containing both the ester and the carbonate moieties (**30** and **31**, Scheme 7). The carbonate **30** as well as the thiocarbonate **31** did not exhibit acyl transfer reaction in their crystals (or solid state) when heated (140-145 °C, 72 h) in the presence of sodium carbonate. This result was consistent with their crystal structures. Geometrical parameters for the relative orientation of the electrophile and the nucleophile showed large deviation from that required for successful intermolecular acyl transfer reaction (Figure 3).

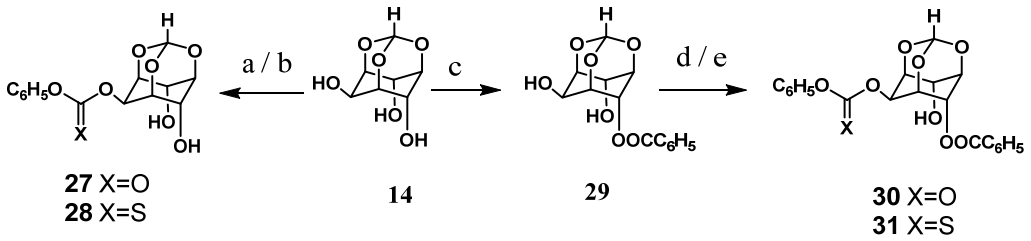

Scheme 7: (a) PhOCOCl, pyridine, DMF, -5 ^{o}C- rt, 2 h, 71%; (b) PhOCSCl, pyridine, DMF, -5 ^{o}C - rt, 2 h, 52%; (c) BzCl, Et_3N, DMF, 0^{o}C - rt, 8h, 48%; (d) PhOCOCl, pyridine, DMF, -5 - 0 ^{o}C, then rt, 6-7 h, 55%; (e) PhOCSCl, pyridine, DMF, -5 - 0 ^{o}C then rt, 10-12 h, 52%.

Chapter 3: Progress towards designing crystals capable of supporting intermolecular benzoyl group migration: polymorphism, reactivity, and crystal structure of racemates and enantiomers of *myo*-inositol orthoester dibenzoates.

There has been a revival in interest in polymorphism – a phenomenon which manifests in the differences in the solid state structure and properties of small molecules - in the recent past.[11] Although there are instances of chemical reactions taking place in molecular crystals and cocrystals, investigations on the polymorphism exhibited by these small molecules are scarce. We had reported the first instance of intermolecular benzoyl group transfer reactivity in crystals (Form **1I**) of racemic 2,4-di-*O*-benzoyl-*myo*-inositol-1,3,5-orthoformate, more than a decade ago.[1] This chapter presents results on the polymorphic and pseudo polymorphic structures of racemic 2,4-di-*O*-benzoyl-*myo*-inositol-orthoformate. Although we suspected the existence of polymorphs of this racemic dibenzoate, based on the occasional variation in the observed intermolecular benzoyl group transfer reactivity of racemic **1** in the solid state, isolating the polymorphic crystals suitable for X-ray diffraction analysis proved to be elusive. Screening racemic 2,4-di-*O*-benzoyl-*myo*-inositol-orthoformate for polymorphism by crystallization from different solvents yielded three polymorphs (Figure 4). Crystallization of the racemic dibenzoate **1** in the presence of (-)-D-2,6-di-*O*-benzoyl-*myo*-inositol-1,3,5-orthobenzoate in chloroform yielded a solvate, which was not stable under ambient conditions.

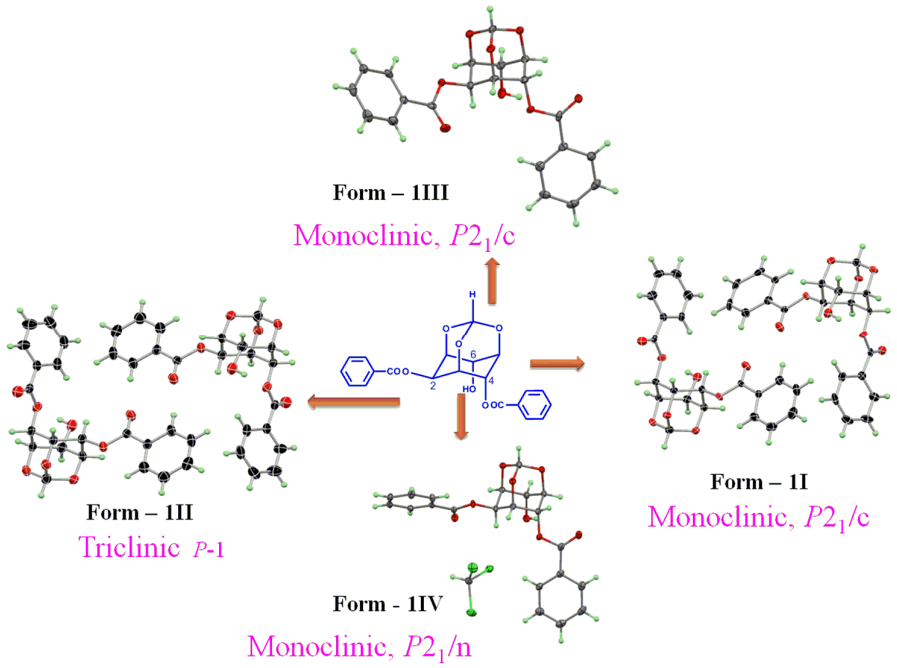

Figure 4: Polymorphism of racemic 2,4-di-*O*-benzoyl-*myo*-inositol-orthoformate (**1**). Two of the polymorphs (Form **1I** and Form **1II**) exhibited facile intermolecular benzoyl group transfer reaction. A comparison of the structure of the polymorphs could account for the observed differences in the benzoyl group-transfer reactivity of the polymorphs in the solid state. The observed differences in reactivity of the polymorphs accounts for the occasional variation of reactivity observed in bulk samples of crystalline racemic 2,4-di-*O*-benzoyl-*myo*-inositol-orthoformate. It is likely that under certain preparation and (un-specified) crystallization conditions, polymorphic crystals of racemic 2,4-di-*O*-benzoyl-*myo*-inositol-orthoformate (**1**) result, which have direct bearing on the observed reactivity of the bulk solid samples.

Distance (Å) / Angle (°)	**Form 1I**	**Form 1II**	**Form 1III**	**Form1IV**
O4(Nu)…C15(El)	3.240/3.160	3.198/3.190	5.635/3.602*	4.698
∠ O4(Nu)···C15-O7(El)	91.49/88.95	90.16/90.70	11.86/136.99*	33.90
∠H4*A*-O4(Nu)···C15(El)	108.36/116.62	113.37/113.23	55.95/76.76*	84.64
∠C4-O4(Nu)···C15 (El)	114.44/119.31	118.40/114.80	92.36/173.80*	73.37

Table 1: El···Nu interactions in polymorphs of racemic 2,4-di-*O*-benzoyl-*myo*-inositol-orthoformate (**1**) at 100K. * implies geometrical parameter of axial hydroxyl group with equatorial ester group.

Crystals of racemic dibenzoates of *myo*-inositol orthoesters had structures that supported facile benzoyl group transfer reaction in them (Chapter 1, Scheme 1). Each

helix (Chapter 1, Figure 1) which functioned as a reaction channel in these crystals consisted of one of the enantiomers of these dibenzoates, which clearly established that the benzoyl group transfer reaction in the crystalline racemate occurred between molecules having the same absolute configuration.[3] Hence it was of interest to see if these enantiomers formed chiral crystals on their own, having structure similar to the corresponding racemate, that supported benzoyl group transfer reaction, or whether presence of the opposite enantiomer in the crystal lattice was absolutely essential to stabilize the structure required to facilitate the benzoyl group transfer reaction. Accordingly, we prepared enantiomeric dibenzoates of *myo*-inositol orthoesters (Scheme 8) and compared their crystal structure and reactivity with those of the corresponding racemates. See chapter 4 for details on the preparation of diastereomers **32**, **33** and **dia34**.

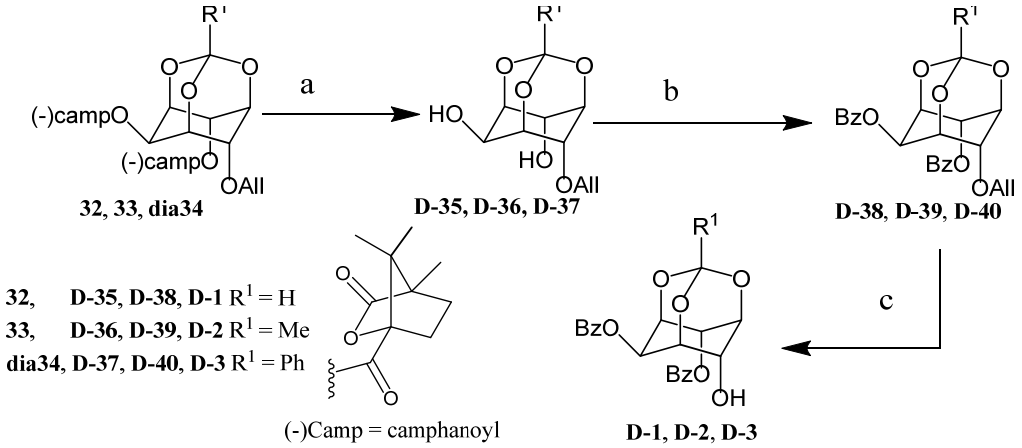

Scheme 8: (a) *iso*-Butyl amine, DCM, MeOH, reflux, 10-12 h, 96%; (b) benzoyl chloride, DMAP, pyridine, 0 ^{o}C - rt, 10-12 h, 90-93 %; (c) $Pd(OH)_2/C$, *iso*-propanol, reflux, 4-24 h, 66-80%. [Here only structure of **dia34** is used for representing the reaction sequence for synthesis of chiral dibenzoate orthoester, for **32** and **33** refer the structure in Scheme 11]

D-2,6-di-*O*-benzoyl-*myo*-inositol-1,3,5-orthobenzoate (**D-3**) forms polymorphic crystals, one of which (Form **D-3I**) has structure similar to its racemate (Figure 5) and (Form **D-3II**) has structure much different than its racemate (Figure 6)

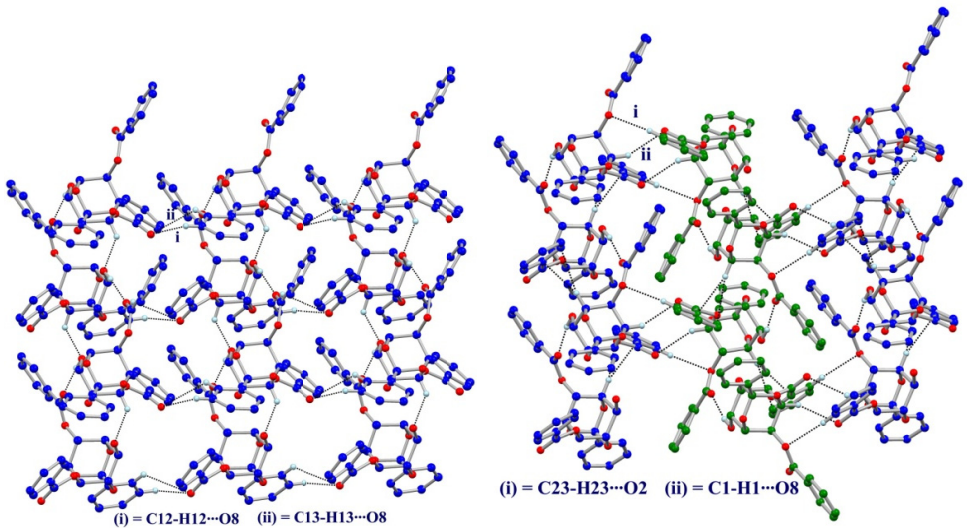

Figure 5: Packing of helices in crystals of Form **D-3I** (left), and its racemates **3** (right) (different colour of helices represent different enantiomer).

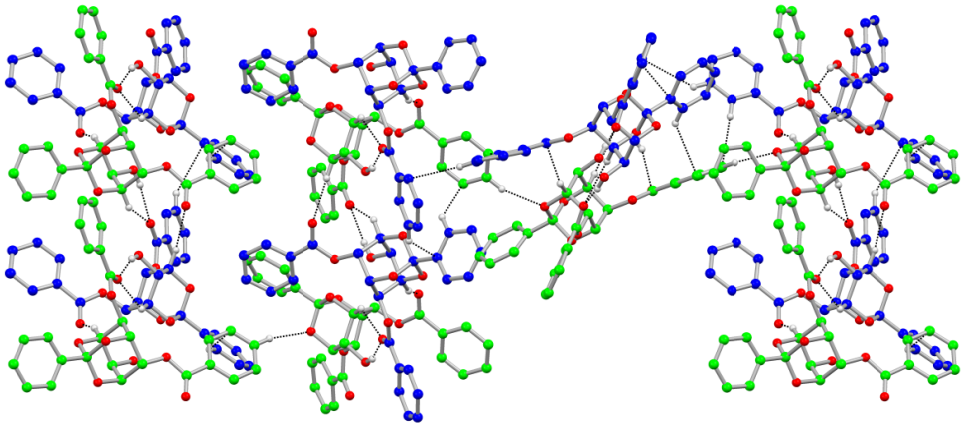

Figure 6: Packing of helices in crystals of Form **D-3II** revealing that the neighbouring helices are not discrete.

Distance(Å) / Angle(°)	**Form D-3I**	**Form D-3II**	**3**
OH(Nu)··· O=C(El)	3.196	4.612/4.394	3.1442(2)
∠O(Nu)···C=O(El)	83.00	36.28/32.04	85.6(1)
∠H-O(Nu)···C(El)	105.65	127.34/128.76	113(1)
∠C-O(Nu)···C (El)	99.66	92.75/95.99	111.1(1)

Table 2: El···Nu interactions in polymorphs of **D-3** and its recemate **3**.

Crystals of the racemate **3** as well as the enantiomer (**Form D-3I**) support intermolecular benzoyl transfer reaction (Scheme 9) due to helical assembly of molecules (Figure 5). This constitutes a rare case of a chiral compound exhibiting polymorphism and chiral as well as racemic crystals exhibiting same chemical reactivity in the crystalline state.

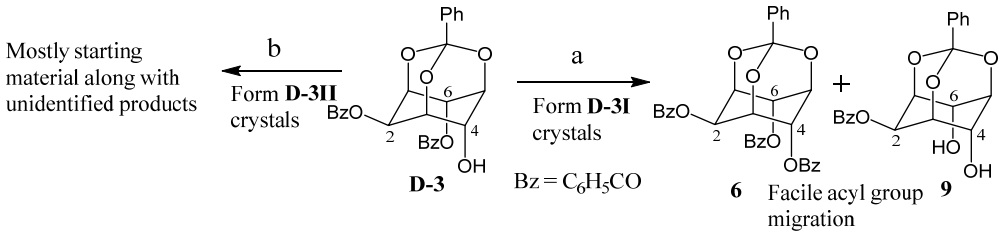

Scheme 9: (a) Na_2CO_3, 140 ^oC, 60 h; (b) Na_2CO_3, 130 ^oC, 60 h.

Although crystal structure of racemic 2,4-di-*O*-benzoyl-*myo*-inositol-1,3,5-orthoformate (**1**) and the corresponding racemic orthoacetate analog **2** were very similar to that of racemic orthobenzoate **3** and exhibited facile benzoyl group transfer reactivity, crystals of the enantiomers **D-1**, **D-2** (Scheme 3.2) have widely different structure (compared to crystals of racemates **1** and **2**, Scheme 1) and hence poor reactivity.

Chapter 4: Separation of diastereomeric dicamphanates of racemic 4-*O*-allyl-*myo*-inositol-1,3,5-orthoesters on gram scale by crystallization.

Since the discovery of the relationship between intracellular concentration of phosphoinositols and the release of calcium ions from intracellular sources, the chemistry and biology associated with naturally occurring inositol derivatives has expanded into a contemporary area of research with brisk activity.[12-13] Initial synthetic efforts were focused on the delineation of the relative reactivity of the inositol hydroxyl groups leading to the synthesis of suitably protected inositol derivatives as precursors for phosphoinositols.[14] With advances towards mapping of the various steps involved in the *myo*-inositol cycle and realization of the importance of glycoinositols, the focus shifted to the synthesis of chiral inositol derivatives. The known approaches for the preparation of chiral inositol derivatives include (a) use of chiral pool molecules (such as mannitol, glucose, galactose, quinic acid, cyclohexadiene diol) as starting materials; (b) classical resolution of racemic inositol derivatives *via* conversion to separable diastereomers; (c) desymmterization of symmetric *meso*-derivatives of inositol. As *myo*-inositol has the *meso*-configuration

generation of chiral *myo*-inositol derivatives necessarily involves the destruction of its symmetry (Scheme 10).

Orthoesters of *myo*-inositol have been extensively used as early intermediates for the synthesis of phosphoinositols, cyclitols and their derivatives, metal complexing agents and natural products containing the cyclitol moiety.[12-16] Considerable efforts have been invested in obtaining chiral *myo*-inositol derivatives from these rigid symmetric triols. However most of these methods involve tedious chromatographic separation of diastereomeric derivatives and/or provide chiral *myo*-inositol derivatives in small amounts.[17-22]

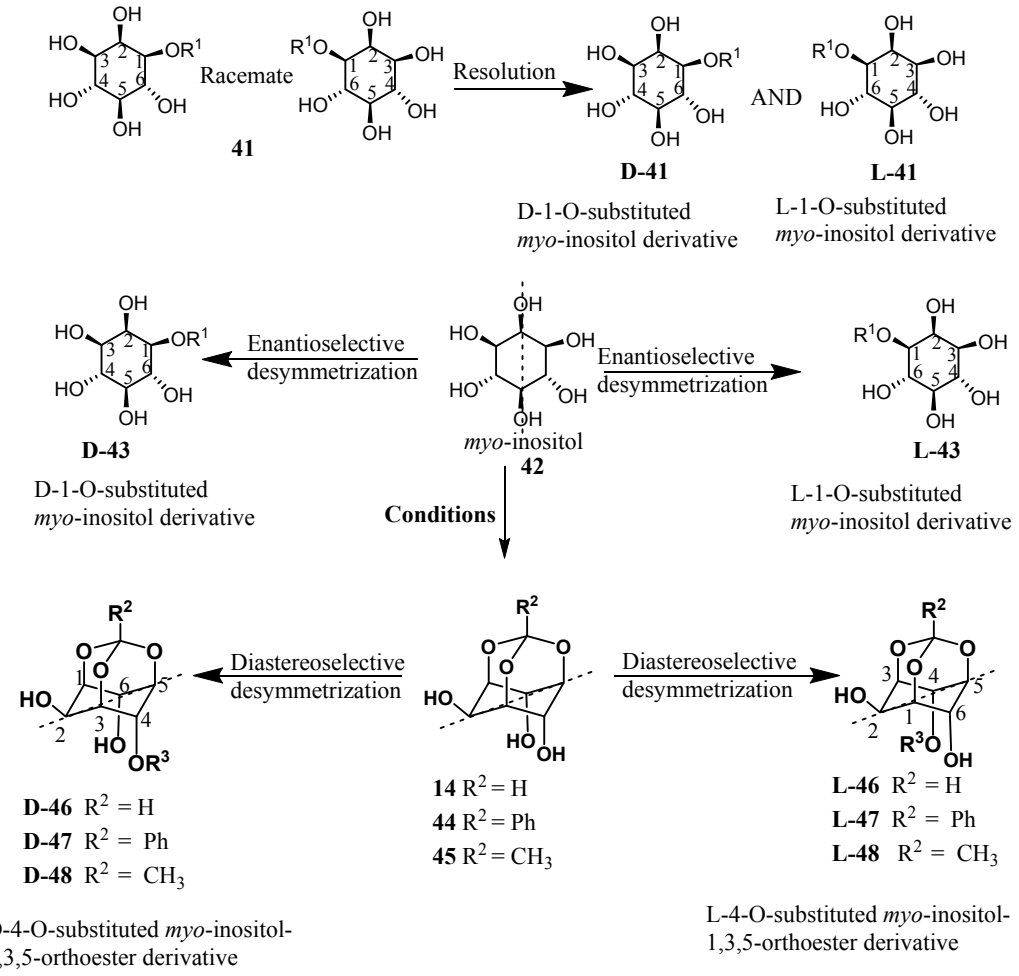

Scheme 10: Illustration of the generation of chiral derivatives of *myo*-inositol and its orthoesters as well as the conventional numbering of ring carbon atoms and the nomenclature of asymmetric inositol derivatives.

This chapter describes results on the separation of diastereomeric dicamphanates of racemic 4-*O*-allyl-*myo*-inositol-1,3,5-orthoesters (on gram scale) by crystallization. It is interesting to note that the procedures for the separation of diastereomeric *myo*-inositol orthoesters could be evolved due to the knowledge of crystal growth and crystal structures of inositol derivatives of comparable molecular structure (as seen in previous chapters). Scheme 11 summarizes the preparation and separation of diastereomeric dicamphanates of *myo*-inositol orthoesters. The diastereomeric purity of the solid dicamphanates obtained was at least 95%. The configuration of the diastereomeric orthoformates and the crystalline diastereomeric orthobenzoate were established by conversion to the known dicamphanates by cleavage of the allyl group.[23] This procedure showed **32** and **dia32** to be D-2,4-di-*O*-[(-)-ω-camphanoyl]-6-*O*-allyl-*myo*-inositol-1,3,5-orthoformate and D-2,6-di-*O*-[(-)-ω-camphanoyl]-4-*O*-allyl-*myo*-inositol-1,3,5-orthoformate respectively[17] and orthobenzoates **34** and **dia34** to be D-2,4-di-*O*-[(-)-ω-camphanoyl]-6-*O*-allyl-*myo*-inositol-1,3,5-orthobenzoate and D-2,6-di-*O*-[(-)-ω-camphanoyl]-4-*O*-allyl-*myo*-inositol-1,3,5-orthobenzoate respectively (Scheme 11).[19] The configuration of the diastereomeric orthoacetates was established by comparison of single crystal X-ray diffraction data of diastereomeric orthoformates (**32**) and orthoacetates (**33**) (Scheme 11). The configuration of the diastereomeric orthoacetates could be established by this process since dicamphanates of orthoacetates and orthoformates only differ at the orthoester position, which has no bearing on the configuration of the molecule. These diastereomeric dicamphanates were used for the preparation of enantiomeric dibenzoates (see Scheme 8).

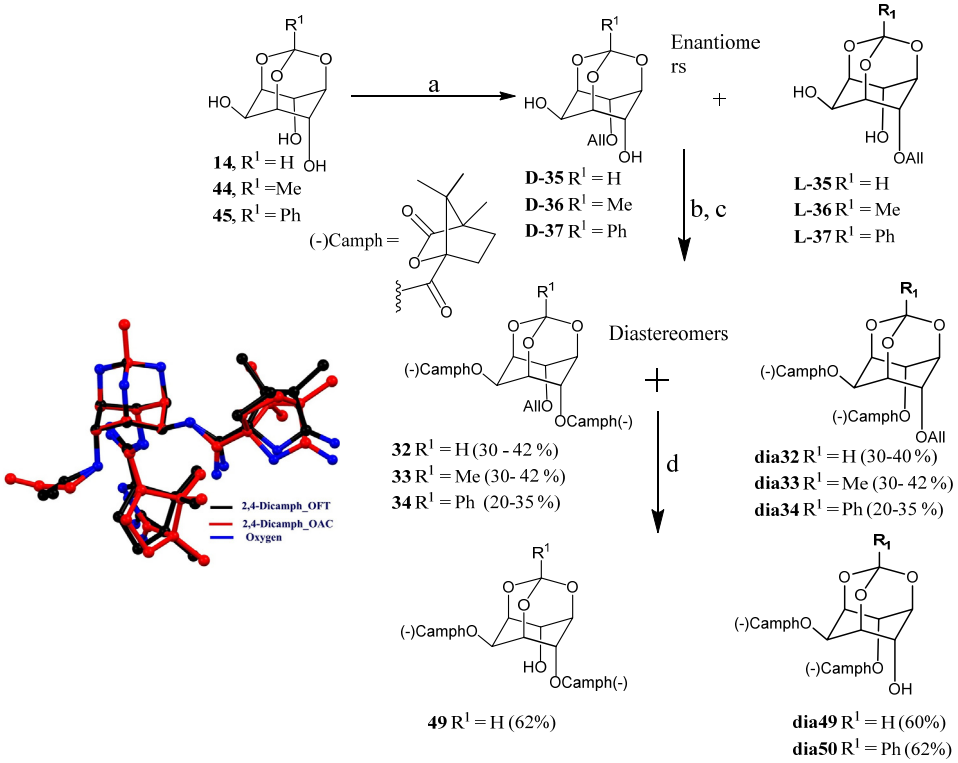

Scheme 11: (a) NaH, AllBr, DMF, 0 ^{o}C- rt, 8 h, 65 -70 %; (b) (1*S*)-(-) camphanoyl chloride, Et_3N, DMAP, pyridine, DCM reflux, for 2 days, 90-96 %; (c) crystallization from pentane/ methanol (for R^1 = H) or ethanol (for R^1 = Me) or *iso*-propanol (for R^1 = Ph); (d) $Pd(OH)_2/C$, *iso*-propanol, reflux, 24-30 h, 60-62%.

References:

[1] T. Praveen, U. Samanta, T. Das, M. S. Shashidhar, P. Chakrabharti, *J. Am. Chem. Soc.* **1998**, *120*, 3842-3845.

[2] C. Murali, M. S. Shashidhar, R. G. Gonnade, M. M. Bhadbhade, *Eur. J. Org. Chem.* **2007**, 1153-1159.

[3] M. P. Sarmah, R. G. Gonnade, M. S. Shashidhar, M. M. Bhadbhade, *Chem. Eur. J.* **2005**, *11*, 2103-2110.

[4] C. Murali, M. S. Shashidhar, R. G. Gonnade, M. M. Bhadbhade, *Chem. Eur. J.* **2009**, *15*, 261-269.

[5] S. Nakamatsu, K. Yoshizawa, S. Toyota, F. Toda, I. Matijasic, *Org. Biomol. Chem.* **2003**, *1,* 2231-2234.

[6] M. I. Tamboli, S. Krishnaswamy, R. G. Gonnade, M. S. Shashidhar, *Chem. Eur. J.* **2013**, *19*, 12867-12874.

[7] R. G. Gonnade, M. M. Bhadbhade, M. S. Shashidhar, *CrystEnggComm*, **2008**, *10*, 288- 296.

[8] S. Krishnaswamy, R. G. Gonnade, M. S. Shashidhar, M. M. Bhadbhade, *CrystEngComm*, **2010**, *12*, 4184–4197.

[9] D. Mansell, N. Veiga, J. Torres, L. L. Etchells, R. A. Bryce, C. Kremer, S. Freeman., *Tetrahedron*, **2010**, *66*, 8949-8957.

[10] K. Vyas, H. Manohar, *Mol. Cryst. Liq. Cryst.* **1986**, *137*, 37-43.

[11] A. J. Cruz-Cabeza, J. Bernstein, *Chem. Rev.* **2014**, *114*, 2170-219.

[12] (a) K. Hinchliffe, R. Irvine, *Nature*, **1997**, *390*, 123-124; (b) T. Schmittberger, H. Waldmann, *Synlett*. **1988**, 574-584; (c) *Phosphoinositides: chemistry, biochemistry and biochemical applications*, K. S. Bruzik, Ed.; ACS symposium series 718. American Chemical Society, Washington D. C. USA, **1999**.

[13] M. A. J. Ferguson, A. F. Williams, *Annu. Rev. Biochem.* **1988**, *57*, 285-320.

[14]. K. M. Sureshan, M. S. Shahsidhar, T. Praveen, T. Das, *Chem. Rev*. **2003**, 103, 4477 – 4503.

[15] B. Kilbas, M. Balci, *Tetrahedron,* **2011**, *67*, 2355 – 2389.

[16] B. P. Gurale, M. S. Shashidhar, R. G. Gonnade, *J. Org. Chem.* **2012**, *77*, 5801−5807 and references cited therein.

[17] M. A. Riley, M. F. Mohan, B. V. L. Potter, *Angew Chem. Int. Ed. Engl*. **1997**, *36*, 1472-1474.

[18] K. M. Sureshan, A. M. Riley, B. V. L. Potter, *Tetrahedron Lett.* **2007**, *48*, 1923-1926.

[19] A. M. Riley, H. Y. Godage, M. F. Mahon, B. V. L. Potter, *Tetrahedron Asymmetry*, **2006**, *17*, 171–174.

[20] S. W. Garrett, C. Liu, A. M. Riley, B. V. L. Potter, *J. Chem. Soc., Perkin Trans. 1*. **1998**, 1367-1368.

[21] K. S. Bruzik, M-D. Tsai, *J. Am. Chem. Soc.* **1992**, *114*, 6361– 6374.

[22] K. M. Sureshan, Y. Watanabe, *Tetrahedron Asymmetry*, **2004**, *15*, 1193–1198.

[23] A. Mart, M. S. Shashidhar, *Tetrahedron*, **2012**, *68*, 9769-9776.

[24] K. M.Sureshan, S. Devaraj, M. S. Shashidhar, *Tetrahedron*, **2009**, *65*, 2703-2710.

Note: Compound numbers in the Abstract of the thesis are different from those in the thesis and references are included separately for each chapter.

List of Publications

1. **M. I. Tamboli**, S**.** Krishnaswamy, R**.** G. Gonnade**,** M**.** S. Shashidhar, Identification of molecular crystals capable of undergoing acyl-transfer reaction based on intermolecular interactions in the crystal lattice, *Chem. Eur. J.* **2013**, *19*, 12867-12874.

2. **M. I. Tamboli**, S. Krishnaswamy, R. G. Gonnade, M. S. Shashidhar, Crystal-to-crystal thermal phase transformation of polymorphs of isomeric 2,3-naphthalene diol di-toluates: Mechanism and implications for molecular crystal formation and melting, *Cryst. Growth. Des.* **2014**, *14*, 4985−4996

3. **M. I. Tamboli**, V. Bahadur, R. G. Gonnade, M. S. Shashidhar, Correlation of the solid-state reactivities of racemic 2,4(6)-di-*O*-benzoyl-*myo*–inositol-1,3,5-orthoformate and its 4,4'–bipyridine cocrystal with their crystal structures, *Acta Cryst*. **2014**, *C70*, 1040-1045.

4. **M. I. Tamboli**, V. Bahadur, R. G. Gonnade, M. S. Shashidhar, Cocrystallization of 2,3-Dihydroxynaphthalene with its para-, meta-, and ortho-Ditoluates: Insight into Cocrystal Formation and Clues for the Construction of Supramolecular Assemblies Capable of Intermolecular Acyl Group Transfer Reactivity, *Cryst. Growth. Des.* **2015**, *15*, 1226–1232.

5. **M. I. Tamboli**, M**.** S. Shashidhar, R**.** G. Gonnade, S. Krishnaswamy, Intramolecular cyclization of carbonate and thiocarbonate derivatives of *myo*-inositol in the solid state: Implications for acyl group transfer reactions in molecular crystals, *Chem. Eur. J.* **2015**, *21*, 13676-13682.

6. **M. I. Tamboli**, M**.** S. Shashidhar, R. G. Gonnade, S. Krishnaswamy. Solid-state reactions by design: intermolecular transesterification in mixed cocrystals of 2,3-dihydroxynaphthalene and its di-*O*-acylated derivatives, *manuscript under preparation.*

7. **M. I. Tamboli**, V. Bahadur, R. G. Gonnade, M. S. Shashidhar. 'Intermolecular benzoyl group migration in crystals of enantiomers of unsymmetric dibenzoates of *myo*-inositol orthoesters: reactivity, structure and comparison with racemates, *manuscript under preparation.*

8. **M. I. Tamboli**, Nivedita T. Patil, R. G. Gonnade, M. S. Shashidhar. Separation of diastereomeric dicamphanates of racemic 4-*O*-allyl-*myo*-inositol-1,3,5-orthoesters on gram scale by crystallization: clues from crystal structures paves way to access chiral *myo*-inositol derived synthons, *to be Communicated.*

9. **M. I. Tamboli**, R. G. Gonnade, M. S. Shashidhar, 'The benzoyl group transfer reactivity of racemic 2, 4-di-*O*-benzoyl-*myo*-inositol-orthoformate in the solid state and its elusive polymorph' *to be Communicated.*

Poster presentations

1**. Majid I. Tamboli**, Shobhana Krishnaswamy, M. S. Shashidhar **" Prediction of acyl transfer reactivity in crystal"** Poster presented on National Science Day 2011 occasion at National Chemical Laboratory on 24^{th} -25^{th} Feb 2011.

2. **Majid I. Tamboli**, Shobhana Krishnaswamy, Rajesh G. Gonnade, Mysore S. Shashidhar **"Crystal-to-Crystal Thermal Phase Transition Amongst Conformational Polymorphs of Isomric Di-Toluate Derivatives of Naphthol".** Poster presented on National Science Day 2012 occasion at National Chemical Laboratory on 26^{th} -28^{th} Feb 2012.

3. **Majid. I. Tamboli**, S. Krishnaswamy, M. S. Shashidhar, **Acyl transfer reactions in co-crystals of 2, 3-naphthalene diol and its di-*p*-methylbenzoate**, Poster presented on XX International Conference on the Chemistry of the Organic Solid state at Indian institute of Science Bangalore. (June 26-30, 2011)

4. **Majid I. Tamboli**, Shobhana Krishnaswamy, Rajesh G. Gonnade and Mysore S. Shashidhar, **Identification of Molecular Crystals Capable of Undergoing Acyl-Transfer Reaction, based on intramolecular Interactions in the Crystal Lattice.** Poster presented on IX J-NOST Conference for Research Scholars at IISER Bhopal (December 04-06, 2013)

Chapter 1

Identification of molecular crystals capable of undergoing acyl-transfer reaction based on intermolecular interactions in the crystal lattice: Acyl transfer reactions in 2,3-naphthalene diol derivatives.

Most of the results presented in this chapter are published in three papers:

1. **M. I. Tamboli**, S. Krishnaswamy, R. G. Gonnade**,** M. S. Shashidhar, Identification of molecular crystals capable of undergoing acyl-transfer reaction based on intermolecular interactions in the crystal lattice, *Chem. Eur. J.* **2013**, *19*, 12867-12874.
2. **M. I. Tamboli**, V. Bahadur, R. G. Gonnade, M. S. Shashidhar, Cocrystallization of 2,3-Dihydroxynaphthalene with its para-, meta-, and ortho-Ditoluates: Insight into Cocrystal Formation and Clues for the Construction of Supramolecular Assemblies Capable of Intermolecular Acyl Group Transfer Reactivity, *Cryst. Growth Des.* **2015**, *15*, 1226–1232.
3. **M. I. Tamboli**, S. Krishnaswamy, R. G. Gonnade, M. S. Shashidhar, Crystal-to-crystal thermal phase transformation of polymorphs of isomeric 2,3-naphthalene diol di-toluates: Mechanism and implications for molecular crystal formation and melting, *Cryst. Growth Des.* **2014**, *14*, 4985−4996.

Introduction:

A large body of data on reactions in solutions, accumulated over more than a century, helped chemists to categorize organic reactions in terms of 'functional groups' and hence increased the probability of fairly accurate prediction of the facility of reactions of organic molecules and the structure of the possible products, based on the structure of the reactant molecules. The approach of 'functional groups' driven organic chemistry or synthesis appears to have inculcated organization and compartmentlization of organic reactions in teaching and research. Organic functional group transformations[1] are taught quite early on during chemical education and these reactions form the basis for numeous research publications in organic chemistry, more so in other areas of research that require preparation of organic compounds. A sound knowledge of functional group transformations (including C-C bond forming reactions) and stereochemistry allows us to develop 'retrosynthetic analyses' which form the starting point for complex multi-step syntheses. Most of these facts are however applicable to reactions in fluids, especially, reaction in the solution state. This is mainly because in fluids, non-covalent intermolecular reactions, which have the potential to alter the reactivity of molecules are negeligible and individual molecules have greater degree of freedom. In the solution state, solvents reduce or even completley remove the effect of non-covalent intermolecular interactions between the reactant molecules, allowing them to orient with respect to each other for successful covalent bond formation. Solvents however, bring in solvent – solute non-covalent interctions (solvent effects), which are often exploited in organic syntheses. Hence the concept of 'functional groups' allows chemists to predict the products of a reaction in the fluid state, with fairly good confidence and probability.

In contrast, the complex nature of non-covalent intermolecular interactions precludes the design and synthesis of crystals (or molecular solids in general) that contain the reactive centres (of constituent molecules) in the right relative orientation for successful covalent bond formation. The prevalence of polymorphic modifications and their thermal phase transitions in the solid state also contribute to the uncertainty in prediction of the reactivity of molecules in their crystals. The results presented in this chapter show that the knowledge generated by systematic analysis of crystal structures which facilitate a chemical reaction, can be utilized in identifying other reactive crystalline solids. We hope that eventually, such an approach could aid the evolution of 'reactive group' aided solid state organic reactions. This implies that, just

as greater understanding of molecular strucutre allows one to predict their reactivity in the fluid state, greater understanding of solid state strucutre would allow one to predict their reactivity in the solid state.

Carbon–carbon and carbon–hetero atom (O, N, S) bond formation reactions in molecular crystals have been investigated in the last few decades because of their facility and often, unique product selectivity.[2-6] The crystal lattice provides structured environment for specific reactions which results in high product selectivity compared to the corresponding solution state reactions. Reactions in solids, apart from being potential environmentally green or benign reaction systems, also contribute to the understanding of differences in the stability of small molecules in different phases, including drug formulations.[7-10] The pioneering work of Schmidt[11-13] and later others[14-19] helped formulate requirements in terms of inter-atomic distances, design and create templates and novel substrates for the addition reactions of olefins in crystals, resulting in C-C bond formation (scheme 1.1).

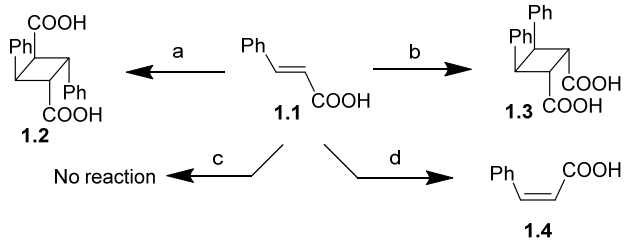

Scheme 1.1: C-C bond forming reaction in crystals; these reactions also illustrate the difference in reactivity of same molecules in different phases. (a) hν, α – crystal form; (b) hν, β – crystal form; (c) hν, γ – crystal form; (d) hν, solution.

It is significant to mention that since the facility of covalent bond formation in the solid state is dependent on the relative orientation of the molecules involved in a chemical reaction, the observed facility of the reaction could vary from one solid form (phase) to another solid form (phase) consisting of the same molecules. Also polymorphic modifications of crystal forms can have profoundly different reactivity (as illustrated by the solid state reactivity of cinnamic acid **1.1**). Hence tracking thermal changes in molecular solids becomes more or less mandatory during the study of chemical reactions in the solid state.

In contrast, most of the reports on reactions in molecular crystals involving migration of relatively larger group of atoms between the reacting centers have been sporadic

stand-alone examples.[20-24] This is perhaps because most of these reactive crystals were comprised of one chemical entity and hence the reactions investigated were either intramolecular reactions or homomolecular reactions (implying reactions between one kind of molecules). Heteromolecular reactions i.e. reaction between different kinds of molecules, in crystals are far and few.[14b,24] This is because heteromolecular reactions in crystals require cocrystals (scheme 1.2) of the potential reactants, and there appear to be no straight forward way to cocrystallize desired different organic molecules.

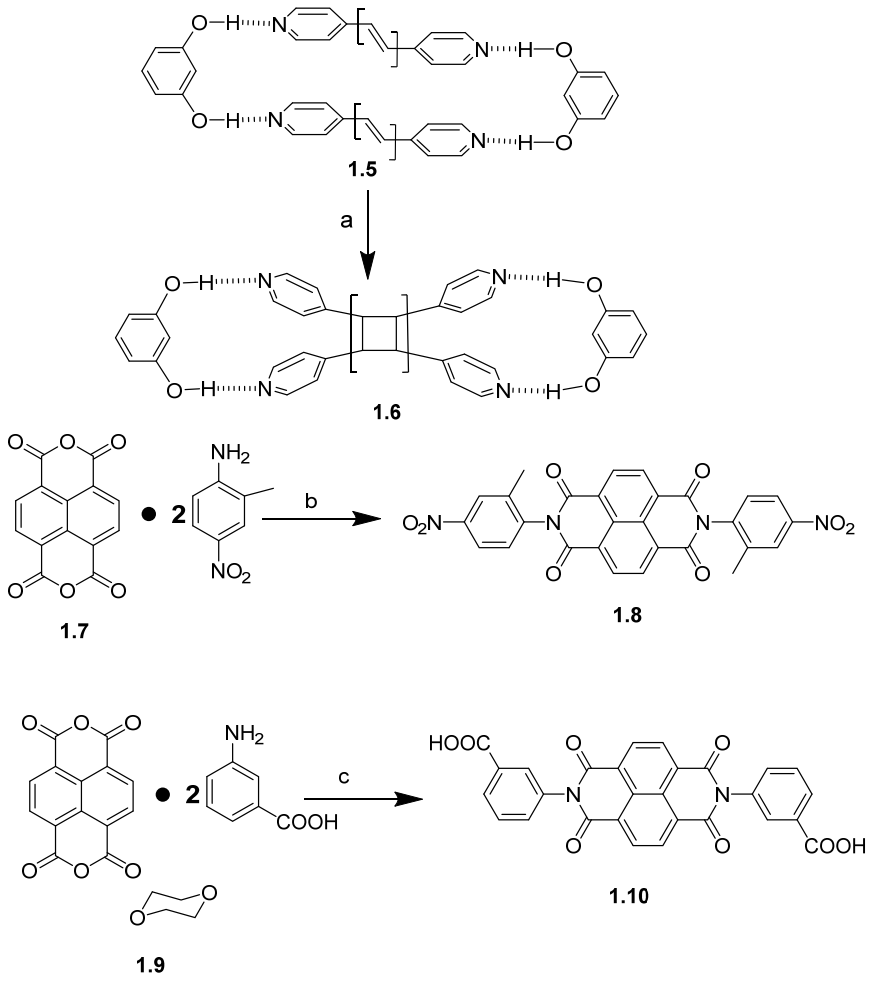

Scheme 1.2: Homo and hetero molecular reactions in cocrystals (a) hν; (b) 180 ^{o}C, 3h; (c) 200 ^{o}C, 24 h.

Transesterification reactions which involve nucleophilic addition to carbonyl groups (followed by elimination) are frequently encountered organic reactions in the solution state and in living systems. Acyl group transfer reactions, albeit few, have

also been reported to occur in the organic solid-state.[7-9,25,26] The earliest report was the thermally induced intramolecular O → N acyl migration in *O*-acylsalicylamide.[25] Vyas and co-workers correlated the facile intramolecular acyl group migration with the geometry of the reactive centres in the crystalline state.[26] Transacylation was also observed in tablet mixtures of aspirin and drugs with easily acylated functionalities such as phenylephrine hydrochloride, codeine and acetaminophen (Scheme 1.3).[7-9]

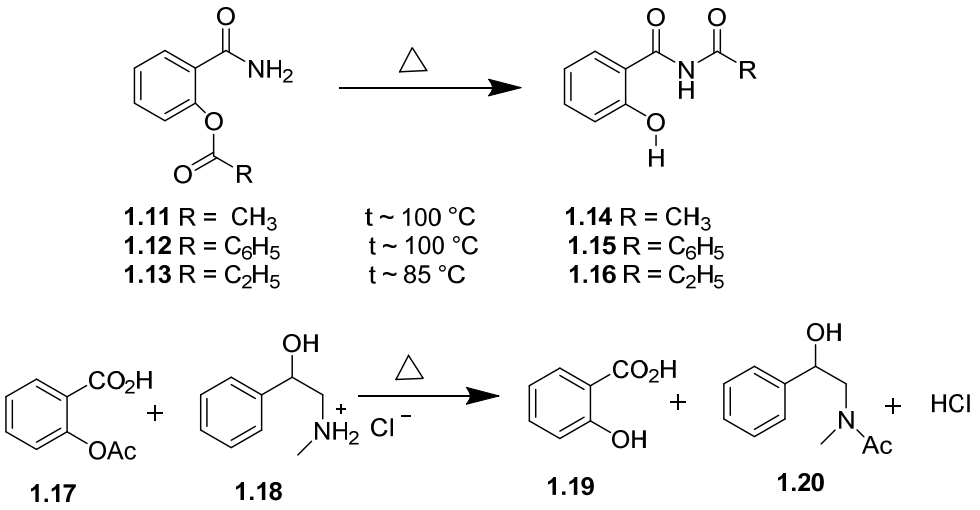

Scheme 1.3: O → N acyl group migration reactions in the solid state.

We had reported (the first instance[27] of) a facile intermolecular benzoyl group transfer reaction in crystals of racemic 2,4-di-*O*-benzoyl-*myo*-inositol 1,3,5-orthoformate (**1.21**), its orthoacetate **1.22**, orthobenzoate **1.23**, analogs,[28] as well as in cocrystals **1.21•1.22**[29] (Scheme 1.4), which yielded the corresponding tribenzoates **1.24 - 1.26** and the diols **1.27- 1.29**.

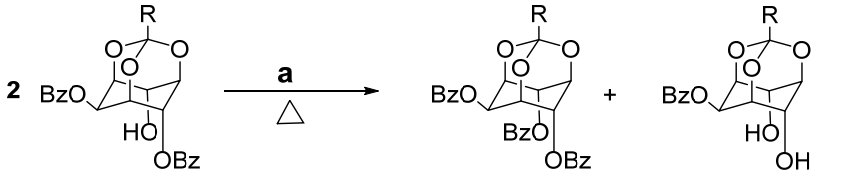

Scheme 1.4: Transesterification reactions of *myo*-inositol orthoester derivatives in crystals (a) Anhydrous Na_2CO_3.

A comparison of the crystal structures of all the compounds in which the intermolecular acyl transfer reaction occurred and their polymorphs in which the corresponding reaction was not facile, helped us determine the minimum conditions necessary for the occurrence of intermolecular acyl transfer reaction in molecular crystals.[28, 30,31] The present chapter describes identification of a molecular cocrystal (in the light of prior knowledge generated in our laboratory), by search of the Cambridge Structural Database (CSD, Version 5.34, November 2012) which had the potential to support intermolecular acyl transfer between its constituent molecules and the experimental verification of the facility of acyl transfer reaction as anticipated. Results pertaining to the preparation and reactivity of cocrystals of 2,3-napththalene diol with its di-*m*-toluate and a mixed diester (*p*-toluate and *p*-fluorobenzoate) are also presented in this chapter.

Results and Discussion:

Efficient intermolecular oxygen to oxygen benzoyl group transfer reactions were observed in *myo*-inositol orthoester derivatives **1.21**, **1.22**, **1.23** and cocrystals **1.21•1.22**. Single crystal X-ray diffraction analysis of these reactive crystals[28,29] revealed that the distance between the reaction centers (HO···C=O), and the angle of approach of the –OH (Nucleophile, -Nu) towards the ester carbonyl group, C=O (Electrophile, -El) lay in the range of 3.1-3.3 Å and 84-90° respectively.[28] These interatomic distances and angles are close to those arrived for El···Nu interactions via the study of crystal structures and theoretical calculations on a model system, by Bürgi and Dunitz.[32] Their results (from crystal structure data) indicated that the N···C=O and O···C=O angles were in the range 105 ± 5° for all the distances smaller than 2.5 Å between the electrophile and the nucleophile (Figure 1.1). Hydroxy acids with intramolecular O···C=O angles of ~98° show the highest rate of intramolecular lactonization[33] and Bender[34] also postulated that a perpendicular approach of the nucleophile to the π - electron system should be preferred over a coplanar approach in order to maximize the overlap between the nucleophile and π-electrons of the carboxyl group during intramolecular lactonisation.

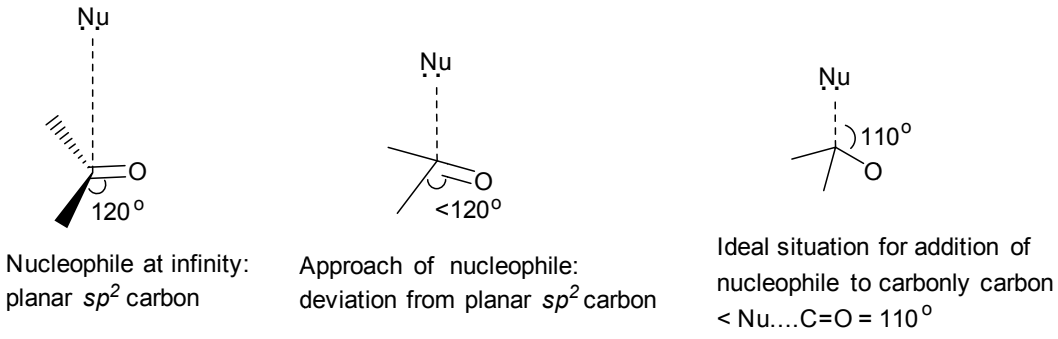

Figure 1.1: Consequence of the approach of a nucleophile (Nu) to a carbony group as delineated in references 32-34.

Hence it is reasonable to expect larger deviation of O···C=O angle (from the tetrahedral angle) as the El···Nu distance increases (beyond 2.5 Å), as observed in reactive crystals of *myo*-inositol orthoester derivatives. Subsequent investigations of structure and benzoyl group transfer reactions in crystals of other *myo*-inositol 1,3,5-orthoester derivatives[29-31] helped us realize the importance of helical molecular pre-organization in reactive crystals,[35] which functions as a reaction channel and contributes to the facility and almost quantitative conversion of the reactants to products. Hence we wondered whether (a) El···Nu geometry between potentially reactive centers in molecules; (b) the assembly of these reacting pairs in the crystal, in the form of a channel for the reaction to propagate; and (c) weak intermolecular interactions[36,37] such as C-H···π[38,39] which help to maintain the topochemical control, could be used as parameters to predict the facility of acyl group transfer reactivity in molecular crystals (Figure 1.2).

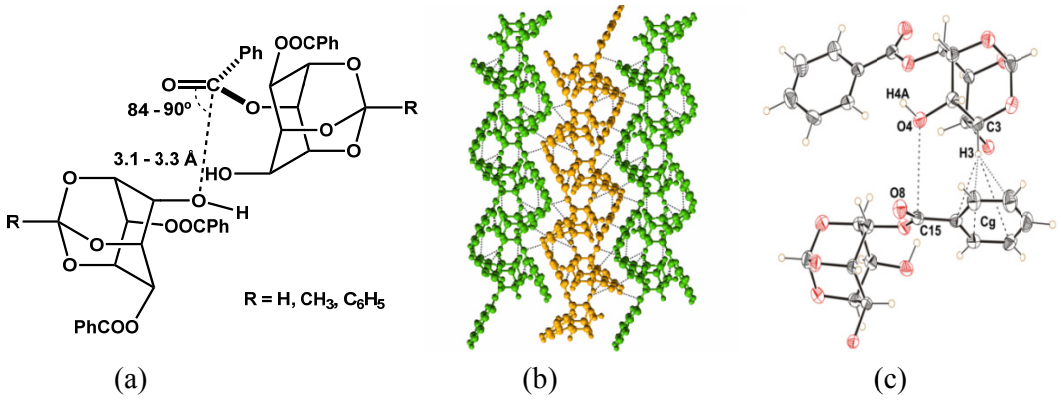

Figure 1.2: Necessary conditions for acyl migration reaction in the solid state. (a) Relative orientation of the reacting molecules between which acyl transfer occurs in

reactive crystals; (b) the packing of molecules required for efficient acyl group transfer in crystals; (c) C-H···π interaction for the maintenance of topochemical control.

A survey of the CSD for compounds containing a carbonyl group and an oxygen nucleophile revealed that when the distance between the electrophile and the nucleophile was lesser than the sum of their van der Waals radii (3.22 Å), the angle of approach of the nucleophile towards the electrophile lay mostly in the range of 80 - 100°.[31] The CSD searches, depending on the distance between the ester carbonyl carbon (El) and the hydroxyl oxygen (Nu) (HO···C=O, 3.1–3.5Å, defined as a non-bonded contact) and the corresponding angle (85-95^0, see Figure 1), yielded ~200 hits. About 100 of these structures were scrutinized and some were selected as 'potentially reactive' crystals (Scheme 1.5).[40-49]

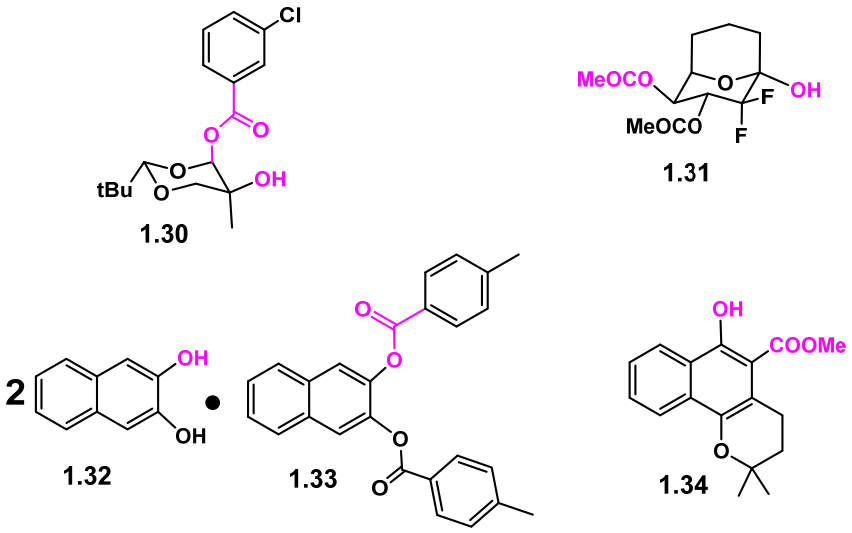

Scheme 1.5: Some of the 'potentially reactive' (with regard to intermolecular acyl group transfer) molecules in their crystals found from a CSD search.

The cocrystal **1.32•1.33** (CSD reference code: IJAGIJ) was chosen for the actual experiment due to its ease of preparation in larger amounts and also due to contemporary interest in the preparation and the study of properties of cocrystals.[14b,24] The grounds for rejection of other 'hits' in the CSD were (i) crystal comprising of one kind of molecule (i.e., El and Nu present in the same molecule) since we had earlier reported[27.28] reactions in such crystals; (ii) solvated crystal - potential loss of solvent and hence possibility of phase change on heating which could

make the structure-reactivity correlation difficult; (iii) multi-step synthesis for obtaining the desired molecule and hence its crystal; (iv) compound obtained by isolation in small quantities from natural sources; (v) hydrated crystal - potential loss of water and/or possibility of hydrolysis during the acyl transfer reaction in crystals. In the 2:1 cocrystal **1.32●1.33** of 2,3-naphthalene-diol (**1.32**) and its di-*p*-methylbenzoate (**1.33**) the distance between the nearest Nu (-OH of **1.32**) and the El (C=O of **1.33**) was 3.166 Å and the angle of approach of Nu towards El was 85.6° (Figure 1.3).

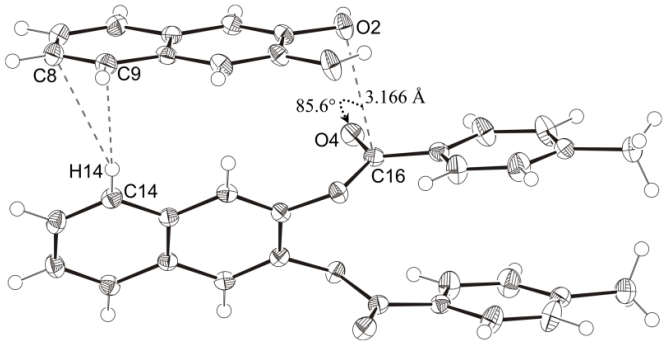

Figure 1.3: Relative orientation of the neighboring molecules of **1.32** and **1.33** in cocrystals **1.32●1.33** at -173 °C. Thermal ellipsoids are drawn at 50% probability level and H-atoms are depicted as spheres of arbitrary radii. (for similar association at higher temperatures, see Figures A1-A4, Appendix I)

A view of the crystal packing along the *ab*-diagonal (Figure 1.4a) revealed a layered structure wherein the naphthalene rings of **1.32** and **1.33** are perpendicular to each other. Such a molecular assembly brings the hydroxyl oxygen (Nu) of the diol **1.32** in close proximity to the carbonyl carbon (El) of the adjacent diester **1.33**, and generates a short El···Nu contact (O2···C16=O4), satisfying one of the pre-requisites for the acyl group migration from **1.33** to **1.32** (Figure 1.3, Table 1.1).

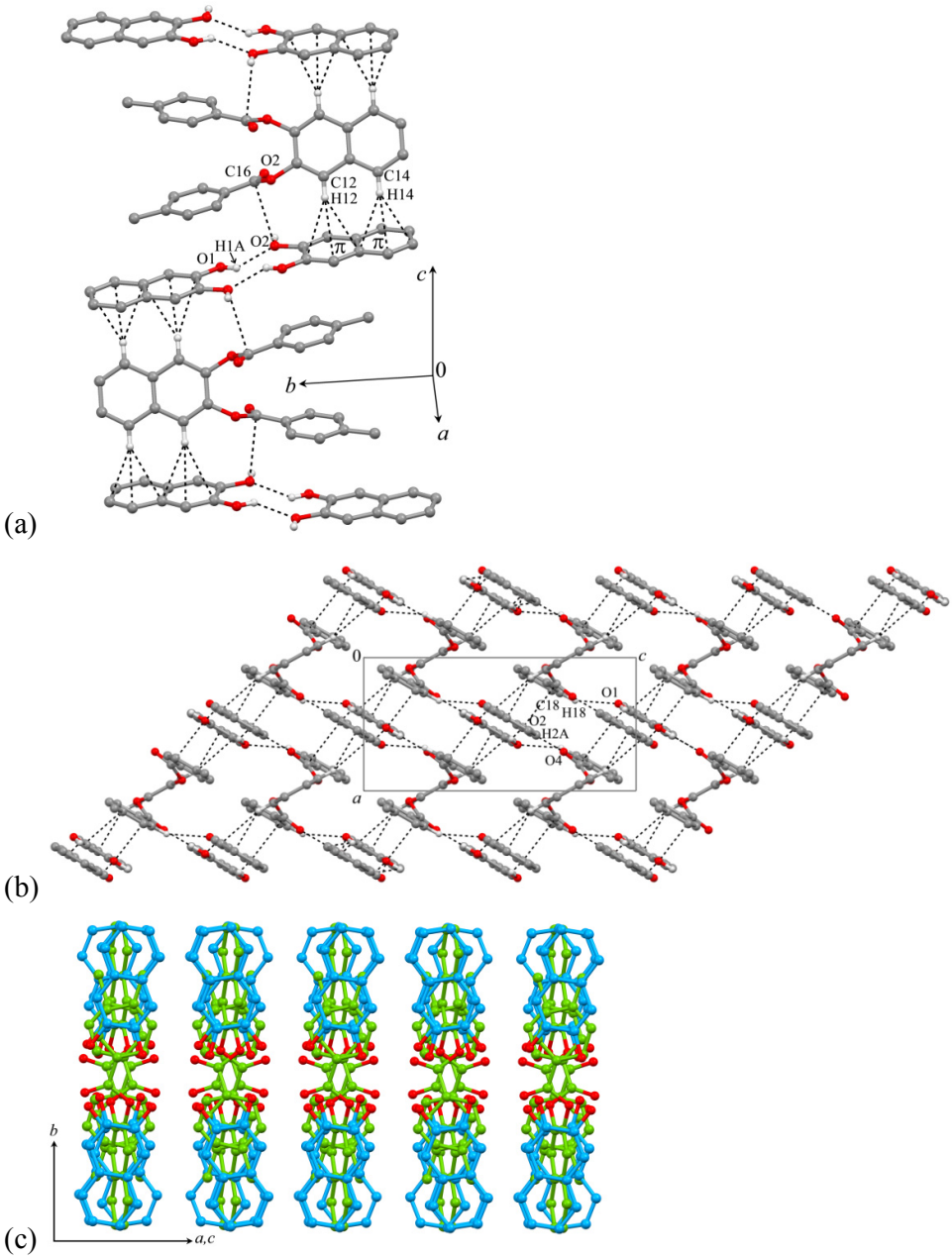

Figure 1.4: Packing of molecules in cocrystal **1.32●1.33**. (a) Layered structure of molecules in crystals of **1.32●1.33** displaying sandwiched arrangement of diol molecules between the diesters; (b) Molecular packing viewed down *b*-axis revealing bridging of neighbouring reactive layers via strong O-H···O and C-H···O interactions. Dotted lines indicate hydrogen bonding interactions; (c) View of the packing of molecules down the reaction channel showing discrete alignments of the layers. Blue molecules depict the diol **1.32**; green: diester **1.33**, and oxygen atoms are shown in red.

El···Nu Parameter	**-173**	**25**	**100**	**125**	**25[a]**
C16···O2	3.162	3.272	3.341	3.269	3.277
∠O4=C16···O2	85.8	84.6	84.4	84.7	84.5
∠H2A-O2···C16	82	84	85	82	84
∠C3-O2···C16	102.4	101.3	100.7	101.3	101.1

[a] Crystal heated to 136 °C on hot stage microscope and then allowed to cool to 25 °C.

Table 1.1: El···Nu parameters for the reacting molecules in the cocrystal **1.32●1.33** at various temperatures (°C).

This molecular architecture is further supported by the formation of off-centered C-H···π interactions involving naphthalene ring protons of the diester **1.33** and π-cloud of the adjacent diol **1.32** molecules (Figure 1.4a). The neighboring layers are connected to each other *via* strong intermolecular O-H···O hydrogen bonds (O2-H2A···O4), and linear C-H···O (C18-H18···O1) interactions (Table A2, Appendix I), thus providing well directed discrete reaction channels throughout the crystal lattice (Figures 1.4b and 1.4c). Hence the cocrystal **1.32●1.33** had all the structural features [(a) to (c) mentioned above], for an intermolecular *p*-toluoyl group transfer reaction between **1.32** and **1.33** (Scheme 1.6).

The experiment for verifying the expected reactivity in cocrystals **1.32●1.33** was interesting because the structure of the constituent molecules (inositol orthoester derivatives) of crystals which were used to arrive at the necessary conditions for intermolecular acyl transfer are hugely different from the constituent molecules (naphthalene derivatives) of cocrystals **1.32●1.33** in which the reaction was expected to occur. The acyl transfer reactivity in **1.32●1.33** was tested by heating a ground mixture of **1.32●1.33** and sodium carbonate (as described in the experimental section) to obtain the *p*-toluate **1.35** in very good isolated yield (91%). Since the diol **1.32** and the diester **1.33** are present in the molar ratio of 2:1 in the cocrystal, ~ 1 equivalent of the diol **1.32** was also obtained at the end of the reaction.

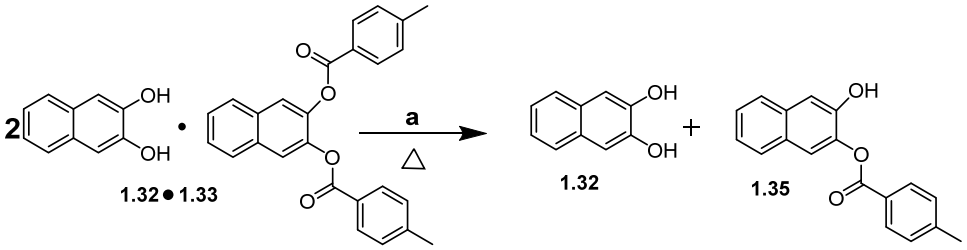

Scheme 1.6: Intermolecular toluoyl group transfer in cocrystals **1.32●1.33**; (a) Anhydrous Na_2CO_3.

No acyl transfer reactivity was observed at temperatures below 110 °C or in the absence of sodium carbonate. The acyl transfer reaction was less efficient above the melting point of cocrystals **1.32●1.33** (140-145 °C, 5 h, 46% yield of **1.35**) as compared to the reaction below the melting point (122-125 °C, 6 h, 80% yield of **1.35**). Isolation of *p*-toluic acid as one of the products in the reaction above the melting point of the cocrystals **1.32●1.33** indicated that the acyl transfer reaction was less specific in the molten state (due to loss of topochemical control) and was accompanied by hydrolysis of the ester group. The diester **1.33** predominantly underwent hydrolysis in DMF solution, when allowed to react with **1.32** in the presence of sodium carbonate. Use of *p*-xylene as the solvent for the acyl transfer reaction resulted in the formation of the monotoluate **1.35** (9%) and about 40% of the unreacted **1.33** was recovered. A comparison of all these results clearly indicates the role played by the crystal lattice during the reaction between **1.32** and **1.33** in their cocrystals **1.32●1.33**.

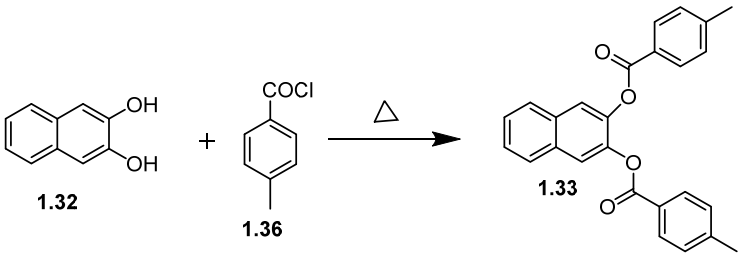

Scheme 1.7: Preparation of the diester **1.33**.

The cocrystal **1.32●1.33** was reported[42] as an intermediate in the solvent-free acylation of the diol **1.32** with *p*-toluoyl chloride at or below 125 °C (Scheme 1.7).

The existence of this intermediate in the reaction mixture was revealed by IR spectroscopy, and the same intermediate was later crystallized using **1.32** and **1.33**. Although the cocrystal **1.32●1.33** was described as an intermediate during the *O*-acylation of **1.32**, it was not clear whether cocrystals **1.32●1.33** functioned as reactive intermediates during the solvent free acylation of **1.32** with *p*-toluoyl chloride. This is especially because the solvent free benzoylation of **1.32** with *p*-toluoyl chloride at 120 °C, was complete in 15 min to yield the diester **1.33**. The acyl transfer reaction in cocrystals **1.32●1.33** on the other hand, needed several hours above 120 °C for completion. Hence it is unlikely that the acylation of **1.32** under solvent free conditions[42] proceeded exclusively through a topochemically controlled benzoyl group transfer reaction in the intermediate cocrystals **1.32●1.33**.

The facile formation of cocrystals **1.32●1.33** just by co-grinding the diol **1.32** and its diester **1.33** revealed strong affinity between these two molecules (Figure A9, Appendix I). The significant interactions observed between the diol **1.32** and the ditoluate **1.33** in their cocrystals were, (i) O-H···O hydrogen bonding interactions between OH of **1.32** and the C=O group of **1.33**; (ii) short El (C=O) and Nu (OH) contact (Figure 1.3); (iii) C-H···O contacts and (iv) C-H···π interactions between the naphthalene ring proton of **1.33** and aromatic ring of the diol **1.32** (Figure 1.4). An estimation of the lattice energy[50] of the cocrystal **1.32●1.33** gave a value of -233 kJ/mole. The computation of interaction energies for significant interactions between **1.32** and **1.33** revealed comparable values for H-O···C=O i.e. El···Nu contact (-67.8 kJ/mole) and O-H···O hydrogen bonding interaction (-70.7 kJ/mole) whereas, interaction energies for C-H···O (-19.6 kJ/mole) and C-H···π contacts (-5.3 kJ/mole) were noticeably lower. These values reveal the relative importance of the El···Nu contacts (O2···C16=O4) in the layered arrangement of one diester **1.33** and two diol **1.32** molecules (Figure 1.4) in cocrystal **1.32●1.33**.

The El···Nu parameters as well as the molecular assemblies shown in Figures 1.3 and 1.4 are derived from the X-ray diffraction data of cocrystals **1.32●1.33** collected at low temperature. However, the acyl-transfer reaction in **1.32●1.33** occurred at much higher temperature. Hence, we wanted to observe the effect of temperature on the crucial intermolecular interactions shown in Figures 1.3 and 1.4. The X-ray diffraction intensity data measurement at 100 °C was carried out successfully,

however data collection at temperatures higher than 100 °C was not initially successful due to changes at the crystal surface (Figure A6, Appendix I) leading to fragmentation of the exterior into small crystallites (the interior of the crystal was intact). The diffraction spots confirmed the single crystalline nature but high mosaicity and bad least squares of the orientation matrix suggested a phase change (this could be responsible for a small endothermic hump in DSC of **1.32●1.33** prior to melting, (Figure A8, Appendix I). Removal of the small crystallites from the surface and rapid collection of the data sets (at 125 °C) gave the structure of the cocrystal **1.32●1.33** with good R-value. We also determined the structure of the cocrystal **1.32●1.33** (at 25 (2) °C), which was heated up to 136 °C (close to melting temperature 139 °C) on hot stage polarising microscope and then cooled to room temperature. The structure overlay of the reacting molecules at different temperatures matched very well (Figure A5, Appendix I).

These experiments revealed that there were no major changes in the intermolecular El···Nu contacts, with variation in temperature (Table 1, Figure A5, Appendix I). The variable temperature powder X-ray diffraction patterns recorded at 25 °C, 80 °C and 125 °C matched reasonably well (Figures A11, Appendix I), thus suggesting modest effect of heating on the packing arrangements of molecules in the crystal lattice of cocrystals **1.32●1.33**. Interestingly, the thermal anisotropies of molecules of the diol **1.32** and the ditoluate **1.33** in cocrystals **1.32●1.33** at 100 °C showed significant change; the lone pair on the oxygen of the hydroxyl group was found to be better oriented towards the carbonyl carbon, as compared to that observed at other temperatures (Figure 1, Figure A1–A4, Appendix I). The thermal motion analysis of the reactants revealed larger internal motion of O2 towards C16 (Figure 1.3) at 100 °C. This motion diminished at 125 °C suggesting stabilization of the movement of these groups towards each other at higher temperatures. This perhaps implies the onset of the acyl transfer reaction between the diol **1.32** and the ditoluate **1.33** in cocrystals **1.32●1.33**.

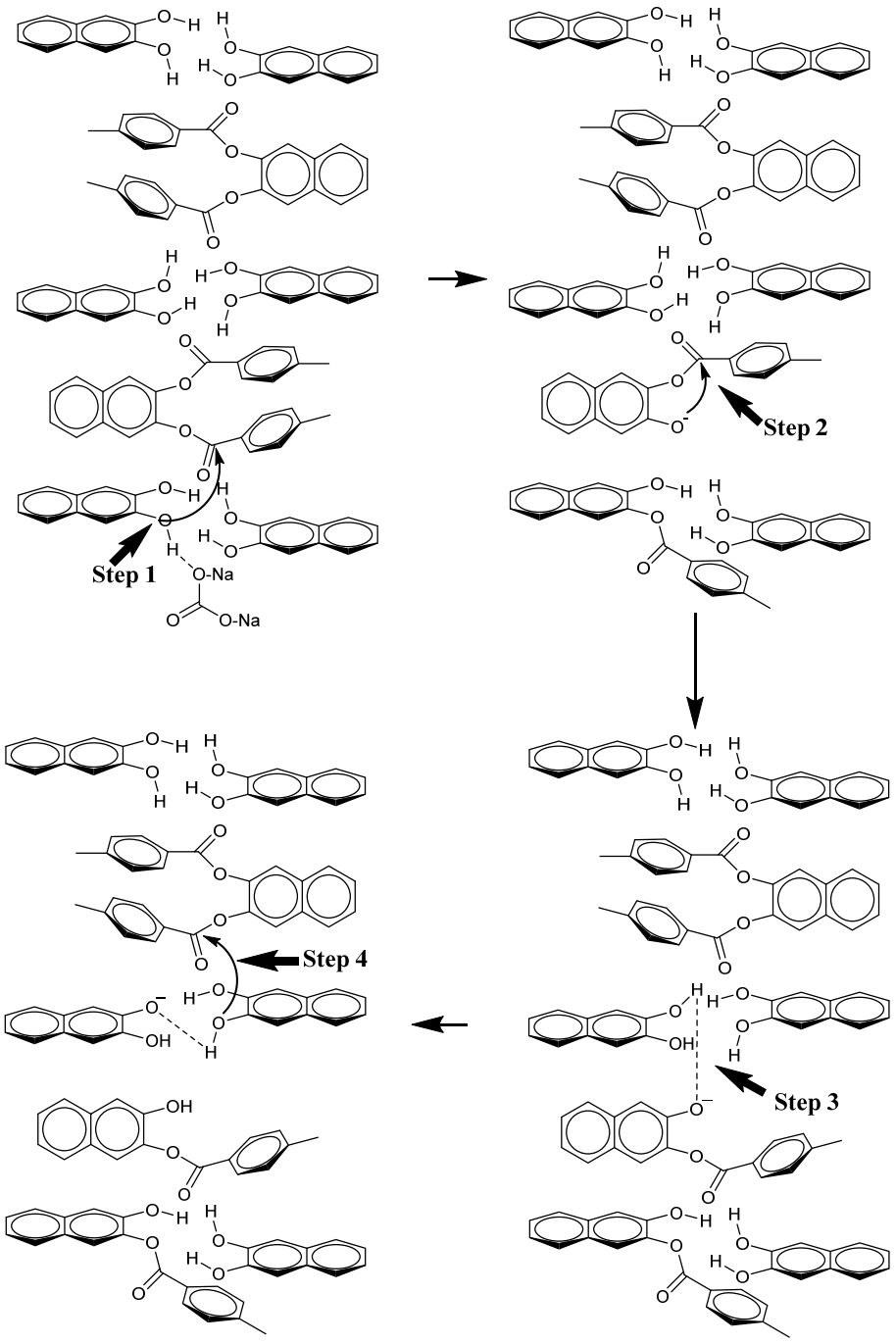

Scheme 1.8: A mechanism for the acyl group transfer from the ditoluate **1.33** to the diol **1.32** in cocrystals **1.32●1.33**.

The mechanism of the acyl transfer reaction depicted in Scheme 1.8, rationalizes the experimentally observed high extent of conversion of reactants to product. Sodium carbonate possibly initiates the reaction at the base of a molecular layer (step 1) after which the reaction progresses by successive proton and *p*-toluoyl group transfers, resulting in a clean reaction and high yield of the mono ester **1.35**. High percentage of conversion of reactants to products observed is consistent with this mechanism since the acyl transfer reaction initiated at the surface of the crystals by the base (sodium carbonate, Step 1, Scheme 1.8) can progress well into the crystal, by generation of phenoxide ions due to a series of intramolecular toluoyl group transfer (Step 2, Scheme 1.8) and proton transfer (Step 3-4, Scheme 1.8).

The intramolecular toluoyl group transfer proposed in step 2 of Scheme 1.8 is supported by the perpendicular approach of the phenolic oxygen (Nu) of **1.33** towards the ester carbonyl group (C=O, El) of the same molecule in cocrystal **1.32●1.33** (Figure 1.5). The El···Nu distance observed in the cocrystal of **1.32●1.33** for intramolecular toluoyl group transfer is 2.935(2) Å and the angle of approach is 80.9°. The intramolecular transfer of the toluoyl group is necessary to sustain a domino type of reaction in cocrystals **1.32●1.33**.

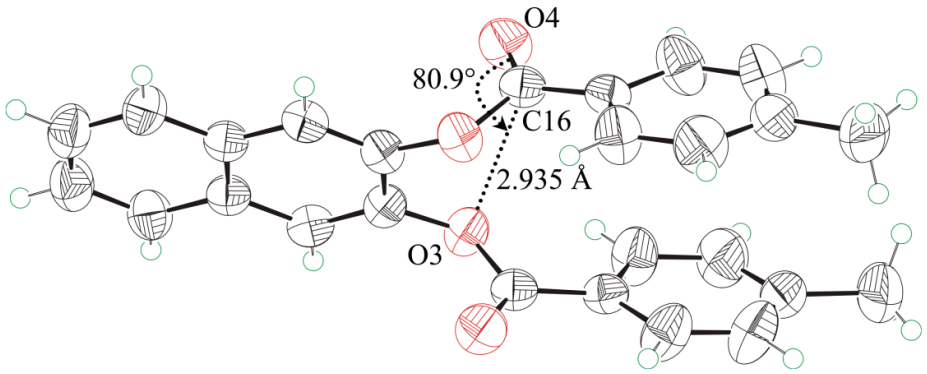

Figure 1.5: ORTEP of the diester **1.33** in a cocrystal **1.32●1.33** showing relative orientation between phenolic oxygen and ester carbonyl group at 125 °C. Thermal ellipsoids are drawn at 50% probability level and H-atoms are depicted as spheres of arbitrary radii.

We also solved the crystal structure of the product **1.35** (Figure A7, Table A1, Appendix I) for comparison with the structure of the cocrystal **1.32●1.33** and to

inspect the El···Nu geometry for inter as well as intramolecular acyl transfer. The intramolecular geometry (El···Nu distance O2···C11 = 2.937Å and angle O2···C11-O3 = 80.9°) for acyl transfer in crystals of the monoester **1.35** matches (Figure 1.6 with the parameters observed for the diester **1.33** in its cocrystal **1.32●1.33**, supporting the possibility of intramolecular acyl transfer during the process shown in Scheme 1.8.

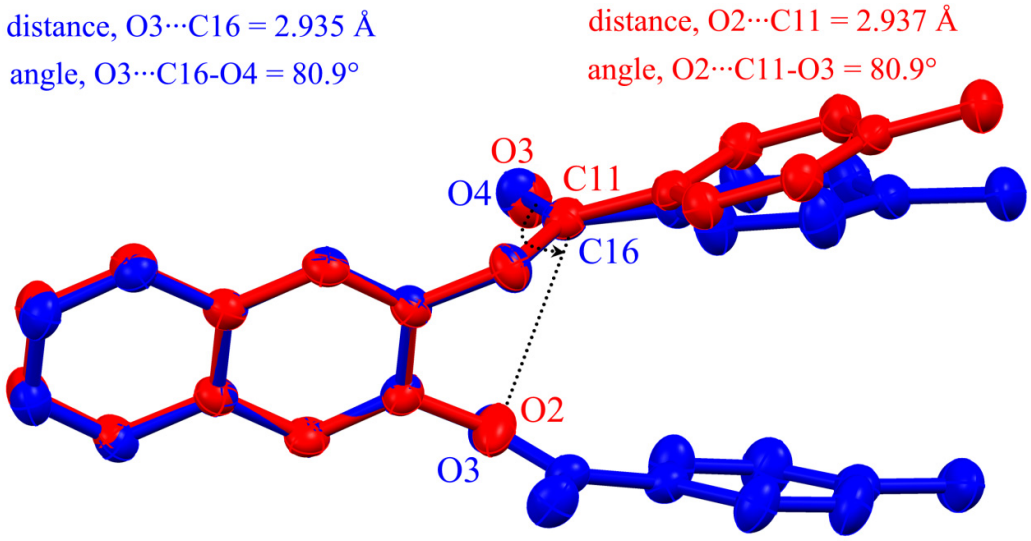

Figure 1.6: Molecular overlap of the ditoluate **1.33** (blue) in a cocrystal **1.32●1.33** and the monotoluate **1.35** (red) in its crystal.

However, a catemeric association of the *c*-glide related molecules through strong O-H···O (O2-H2A···O3) hydrogen bonding interactions between the carbonyl oxygen atom and the hydroxyl group (potential reaction centers) of adjacent molecules precludes the possibility of intermolecular acyl transfer reaction in crystals of **1.35** (Figure 1.7, Table A3, Appendix I).

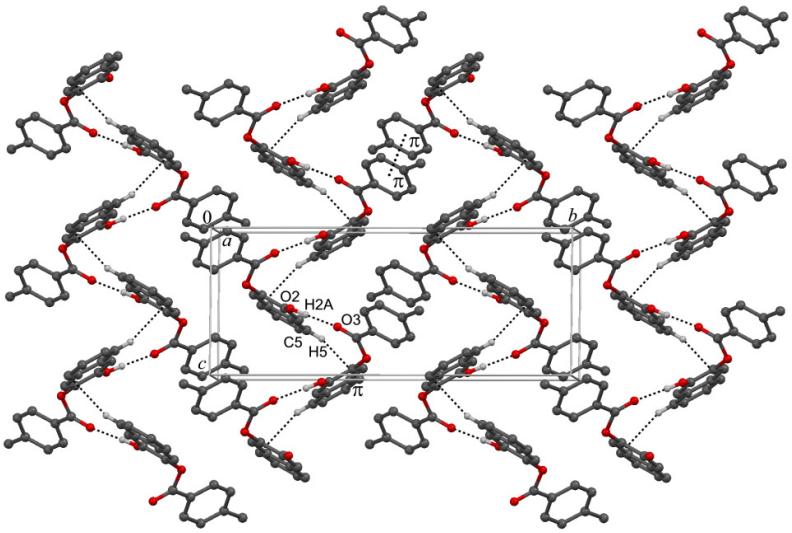

(a)

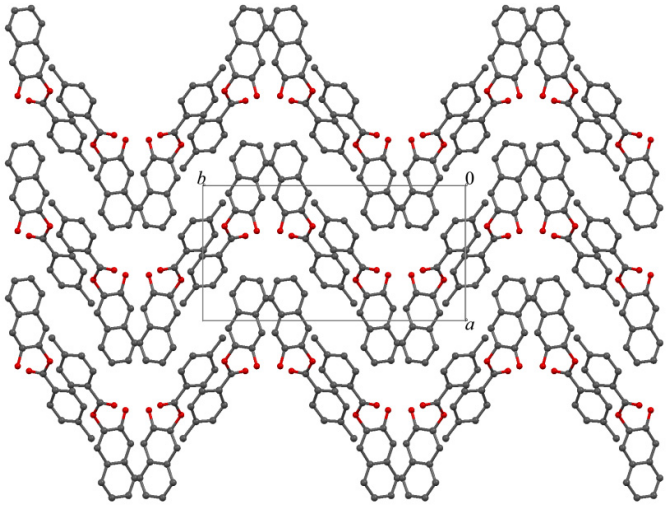

(b)

Figure 1.7: Packing of molecules in crystals of the monotoluate **1.35**. (a) Packing viewed down *a*-axis shows the formation of anti-parallel chains through O-H···O hydrogen bonding; (b) Arrangement along the *c*-axis reveals corrugated sheet like structure. Dotted lines indicate hydrogen bonding interactions. Some hydrogen atoms are omitted for clarity.

Cocrystallization of 2,3-dihydroxynaphthalene (1.32) with its *meta*-ditoluate (1.37):

We also attempted the cocrystallization of the *m*-ditoluate **1.37** and the *o*-ditoluate **1.38** with the diol **1.32** in order to see the effect of the position of the methyl group on cocrystallization behaviour of these diesters with the diol **1.32**. It was also of interest to see if the resultant cocrystals exhibited acyl transfer reactivity. Cocrystals of the diol **1.32** and the *m*-ditoluate **1.37** could be obtained either by cocrystallization from their solution or by solvent-drop grinding. The ratio of the diol **1.32** and the *m*-ditoluate **1.37** in cocrystals **1.32●1.37** was 1**:**1. Similar attempts at cocrystallization of the diol **1.32** and the *o*-ditoluate **1.38** only resulted in crystallization of the two components separately.

The cocrystals **1.32●1.37** turned out to be less reactive (Scheme 1.9) than the cocrystals **1.32●1.33** of the *p*-ditoluate. The extent of conversion of the reactants to products in cocrystal **1.32●1.37** was 30% (95 ^{o}C, 72 h) as compared to 91% in cocrystal **1.32●1.33**. (125 °C, 60 h). The same reaction in the solution and molten states were much less facile and less selective. The difference in observed reactivity could be explained by a comparison of the structure of the two cocrystals.

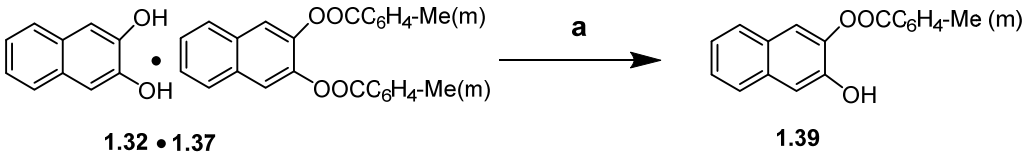

1.32 • 1.37 **1.39**

Scheme 1.9: Toluoyl group transfer reaction in cocrystals **1.32●1.37** (a) Anhydrous Na_2CO_3.

In cocrystal **1.32●1.37**, both the diester molecules occupy a special position (two-fold, as observed in cocrystal **1.32●1.33**), therefore only half the molecule of each diester (primed and unprimed) is present in the asymmetric unit while the other half is generated by two-fold symmetry operation. In contrast, the diol molecule in **1.32●1.37** occupies a general position. Therefore the ratio of the components in cocrystal **1.32●1.37** is 1:1. Overlay of the molecular structure of both the symmetry independent ditoluates in **1.32●1.37** revealed slight difference in the conformation of the ester group (Figure 1.8a). However, significant change was observed between the

conformation of the *p*- and the *m*-ditoluates in cocrystals **1.32●1.33** and **1.32●1.37** (Figure 1.8b). In cocrystals **1.32●1.33**, proximity of the *p*-toluoyl groups facilitate intramolecular face-to face π···π alignment between the phenyl rings (albeit longer and offset stacking). But, *m*-toluoyl groups in cocrystal **1.32●1.37** are farther apart from each other precluding face-to face π···π association between the phenyl rings.

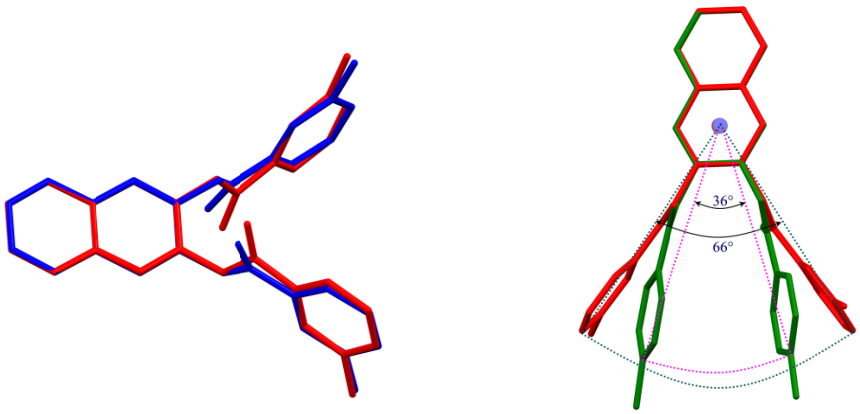

(a) (b)

Figure 1.8: (a) Overlay of the molecular structure of the symmetry-independent *m*-ditoluate molecules (red and blue) in **1.32●1.37**. (b) Overlay of the *p*-ditoluate molecule (green) in cocrystal **1.32●1.33** and one of *m*-ditoluate molecule (red) in cocrystal **1.32●1.37**.

A view (Figure 1.9a) of molecular packing in cocrystal **1.32●1.37** showed a layered arrangement of the *m*-ditoluate **1.37** and the diol **1.32** molecules. Both symmetry independent *m*-ditoluate **1.37** molecules form separate layers extended along the *a*-axis. The adjacent layers (red, blue) are connected to each other through the diol molecules *via* conventional O-H···O hydrogen bonding interactions, namely O2-H2A···O3' (entry 2, Table A6, Appendix I) and O1-H1A···O3 (entry 1, Table A6, Appendix I) engaging both –OH groups of the diol **1.32** and carbonyl oxygens of both the *m*-ditoluate **1.37** molecules (Figure 1.9b).

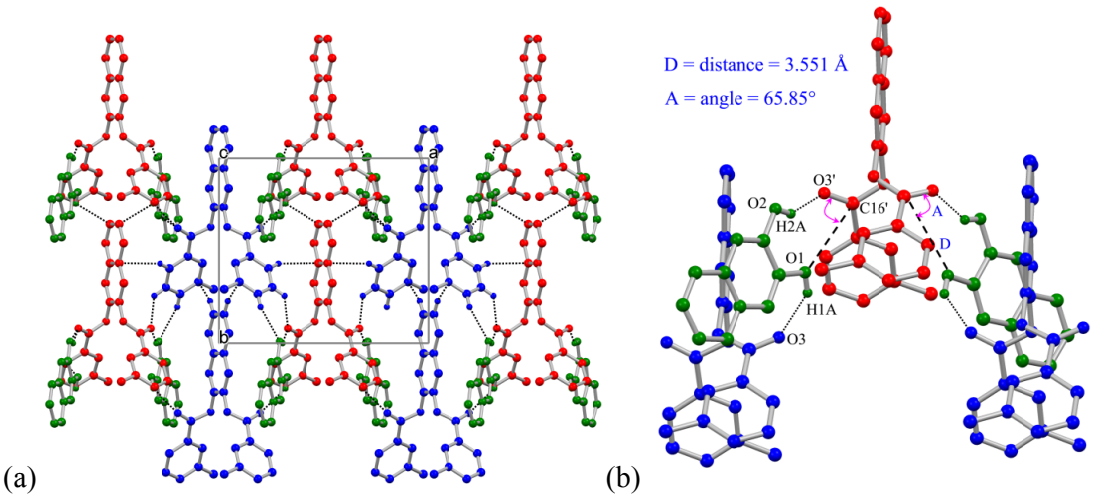

Figure 1.9: Views of the molecular packing in cocrystals **1.32●1.37**. (a) down the *c*-axis; (b) El···Nu geometry between the nearest diol and the *m*-ditoluate molecules.

The diol **1.32** molecules are also associated with the *m*-toluoyl groups of the ditoluate **1.37** molecules through C-H···O (C20-H20···O2) (entry 3, Table A6, Appendix I), C-H···π (C23-H23*A*···π (Cg10) (entry 6, Table A6, Appendix I) and C23'-H23*F*···π (Cg9) (entry 7, Table A6, Appendix I) interactions (Figure 1.10), to generate extended chain along the *a*-axis. In contrast, in cocrystal **1.32●1.33** (as mentioned above) the diol molecules are engaged *via* O···C=O short contact and C-H···π interactions with the naphthalene ring protons of the *p*-ditoluate **1.33** molecules.

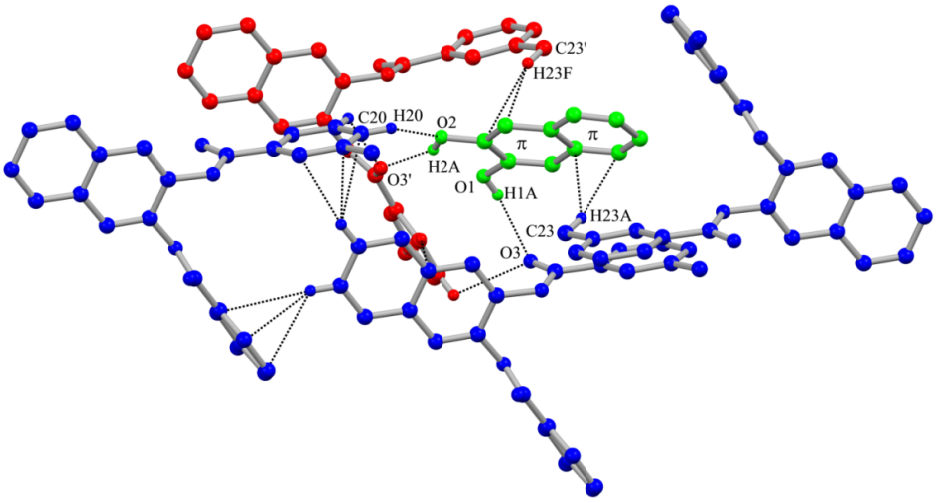

Figure 1.10: Interaction between the diol **1.32** molecules with the *m*-ditoluate **1.37** in cocrystal **1.32●1.37**.

Analysis of the geometrical parameters for the El···Nu (primed *m*-toluate O=C···OH of the diol) interactions in cocrystal **1.32●1.37** revealed that the hydroxyl group and the *m*-toluate carbonyl group were not well placed for the acyl transfer reaction. The closest distance and angle of the El···Nu geometry was found to be 3.551 Å and 65.85° which significantly deviates from the El···Nu geometry observed in cocrystal **1.32●1.33** (3.269 Å, 84.7°). Secondly, the arrangement of molecules of the diol **1.32** and diester (primed) **1.37** in crystals of **1.32●1.37** does not create chains (as in crystals of **1.32●1.33**) which facilitate intermolecular acyl transfer reaction in a domino fashion (Figure 1.4a). The growth of the assembly of (diol **1.32** and primed *m*-ditoluate (red) **1.37**) molecules to form a chain is prevented by the intervention of the second symmetry independent umprimed *m*-ditoluate **1.37** molecule (blue). Hence the extent of *m*-toluoyl group transfer reaction in cocrystals **1.32●1.37** (Scheme 1.9) turned out to be low.

Polymorphism of isomeric ditoluates of 2,3-naphthalene diol:

Isomeric *para* - (**1.33**) and *meta*- (**1.37**) ditoluate derivatives of naphthalene 2,3-diol **1.32** exhibited polymorphism producing three (Forms **1.33I**, **1.33II**, **1.33III**) and two (Forms **1.37I**, **1.37II**) polymorphs each respectively, depending on the solvent and conditions of crystallization. Crystal forms **1.33I**, **1.33II** and **1.37I** could be obtained repeatedly while crystal forms **1.33III** and **1.37II** were obtained (separately) in one of the crystallization experiments, each. All the crystal forms were stable at ambient conditions, except Form **1.37II**, which disintegrated to a powder over 4-5 days under ambient conditions. In contrast, the *o*-ditoluate **1.38** of naphthalene 2,3-diol **1.32** did not exhibit polymorphism; it yielded fibrous chiral crystals from different solvents / conditions. Crystal structure analysis of all these polymorphs revealed dominance of energetically similar weak intermolecular interactions such as C-H···O, C-H···π, π···π and their interplay in molecular aggregation resulting in polymorphic modifications. DSC, hot stage microscopy, single crystal and powder X-ray diffraction measurements revealed crystal-to-crystal thermal transformation of Forms **1.33I** and **1.33II** crystals to Form **1.33III** crystals and Form **1.37II** crystals to Form **1.37I** crystals. Crystal structures of these polymorphs are not discussed here since it is not directly related to the topic of this thesis. Details of polymorphism of the isomeric

ditoluates encountered are published; [51]however, some details are given in [Appendix I].

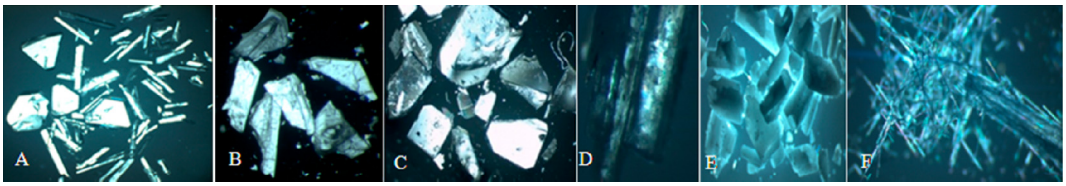

Figure 1.11: Photomicrographs of crystals of ditoluates **1.33**, **1.37**, and **1.38**. (A) Form **1.33I** (needles) and Form **1.33II** (plates) crystals; (B) From **1.33III** crystals; (C) Form **1.37I** crystals; (D) Form **1.37II** crystals; (E) opaque crystals obtained by exposure of Form **1.37II** crystals to air; (F) fibrous crystals of **1.38**.

We also screened the ability of naphthalene-2,3-diol to form cocrystals with its diesters of other substituted benzoic acids hoping to obtain cocrystals having the ability to support intermolecular acyl transfer reactions. We are however aware that small changes in molecular structures could profoundly influence the organization of molecules in the cocrystal lattice. Scheme 1.10 below shows the diesters prepared from 2,3-naphthalene diol.

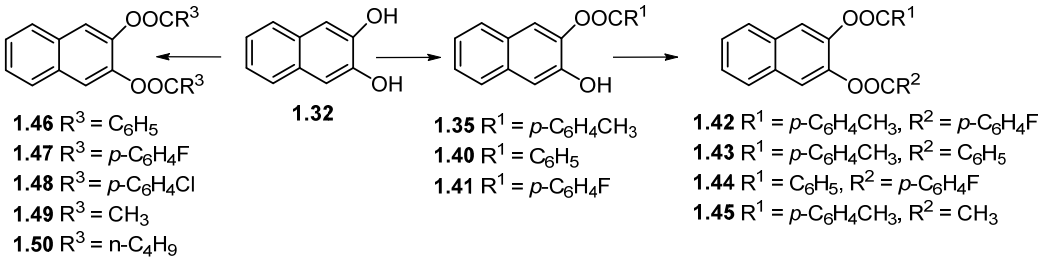

Scheme 1.10: Acylation of 2,3-dihydroxy naphthalene (**1.32**) and its monoesters.

The diesters **1.42-1.50** were screened for cocrystallization with 2,3-naphthalene diol (**1.32**) in common organic solvents. We obtained 1:2 cocrystals **1.32●1.42** of the diester **1.42** with the diol **1.32** by crystallization from ethyl acetate – light petroleum mixture (1:6). The cocrystals **1.32●1.42** could not be obtained by solvent drop grinding method (as revealed by IR spectroscopy and DSC). Crystallization of **1.32** and **1.42** in the molar ratio 1:1 or 1:2 or 1:3 or 2:1 or 3:1 also yielded 2:1 cocrystals **1.32●1.42**. Use of other solvents (diethyl ether, dichloromethane, chloroform,

methanol, acetone, toluene and nitro methane) instead of ethyl acetate failed to yield cocrystals. All our attempts to cocrystallize other diesters in scheme 1.10 with diol **1.32** failed.

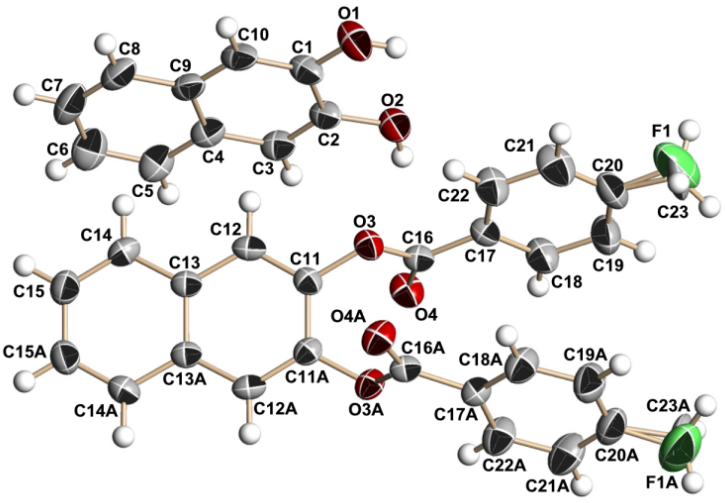

Figure 1.12: Representative ORTEP of the molecules in cocrystals **1.32●1.42**. The displacement ellipsoids are drawn at 40% probability level and H atoms are shown as small spheres of arbitrary radii.

The cocrystal **1.32●1.42** is isomorphous and isostructural with the cocrystal **1.32●1.33** formed from 2,3-naphthalene diol and its di-*p*-toluate (Figures 1.12 and 1.13). The structure of **1.32●1.42** showed substitutional disorder where the fluorine atom and the methyl group at the *para*-position of the diester occupy the same position (Figure 1.12).

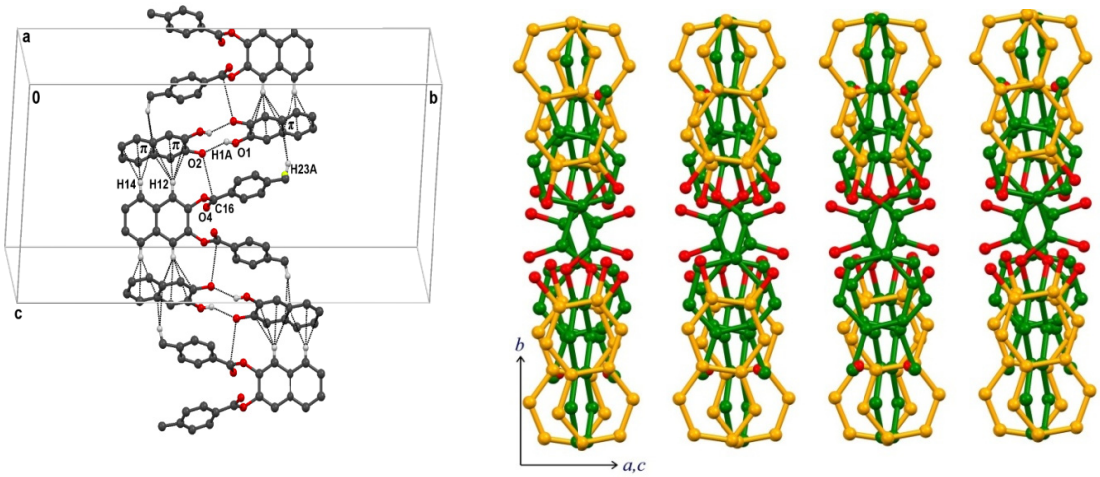

(a) (b)

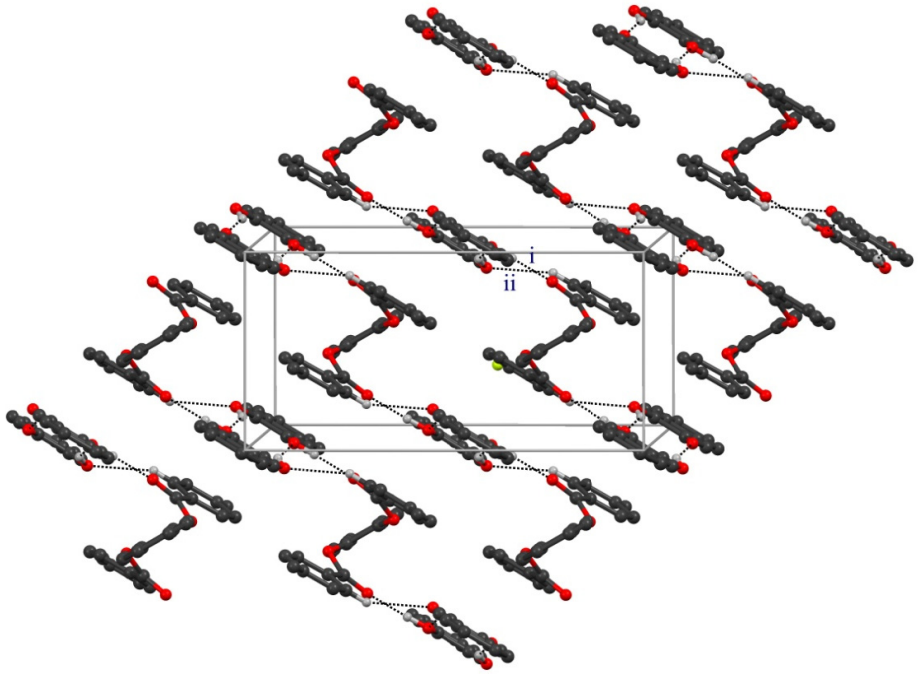

(c)

Figure 1.13: (a) Molecular layer formed from the diol **1.32** molecules sandwiched between the diesters **1.42**; (b) view of the packing of molecules down the reaction channel showing discrete alignment of the layer; (c) adjacent layers are bridged along the *c*-axis through O-H···O (i) O2-H2A···O4 and C-H···O (ii) C18-H18···O1 interactions. Hydrogen atoms not involved in hydrogen bonding are omitted for the sake of clarity.

The diol molecules **1.32** associate in pairs through O-H···O hydrogen bonding interactions (O1-H1A···O2), and are sandwiched between the diesters **1.42** along the *ab* diagonal plane. The naphthalene ring of the diol **1.32** is perpendicular to the naphthalene ring of the adjacent diester **1.42** with the formation of weak C-H···π interactions between the π cloud of the former and aromatic protons of the latter. The layer-like assembly results in the nucleophile (Nu: -OH of diol **1.32**) stationed in close proximity to the electrophile (El: C=O of the diester **1.42**), generating a short El-Nu contact (O2···C16=O4), fulfilling one of the conditions for transesterification (Figure 1.14a). Neighbouring layers are connected to each other through strong intermolecular O-H···O hydrogen bonds (O2-H2A···O4), and linear C-H···O (C18-H18···O1) interactions, providing well-directed discrete reaction channels throughout the crystal lattice (Figure 1.13b and 1.13c). The electrophile - nucleophile geometry in **1.32●1.42** is comparable with that observed in the related cocrystal **1.32●1.33** composed of 2,3-naphthalene diol and its di-*p*-toluate (Table 1.1). Hence their intermolecular acyl transfer reactivity in cocrystals **1.32●1.42** is expected to be similar to that observed in cocrystals **1.32●1.33.**

The cocrystals **1.32●1.42** were subjected to acyl-transfer reaction (below its melting point) in the presence of sodium carbonate; the result is shown in Scheme 1.11. The yield obtained at the same temperature in 24 h was 72%. There was no reaction below 90 ºC. The acyl transfer reaction did not occur in the absence of sodium carbonate. The two mono esters **1.35** and **1.41** were not easily separable and hence their ratio almost (1:1) was estimated by ^{1}H NMR spectroscopy.

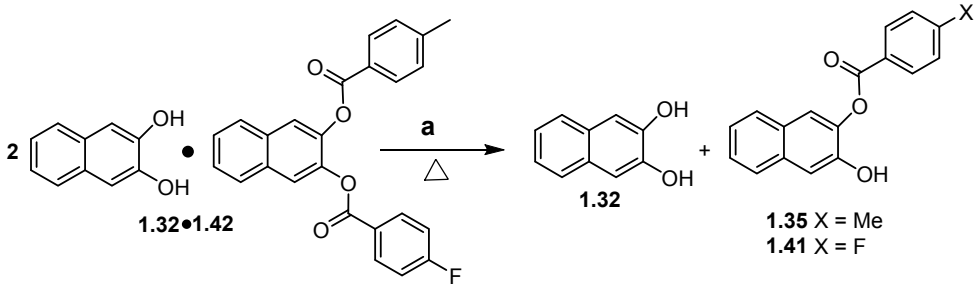

Scheme 1.11: Intermolecular acyl group migration in cocrystals **1.32●1.42** at (a) Anhydrous Na_2CO_3, 100-105 ^{o}C (72 h); yield of the mono esters **1.35** and **1.41** was 94%.

The structure overlay of the cocrystal **1.32●1.42** at different temperatures suggested that the molecular skeleton remains intact with slight change in the orientation in methyl proton (Figure 1.14b). There is also not much variation in geometrical parameter of El···Nu interactions in the crystal lattice (Table 1.2).

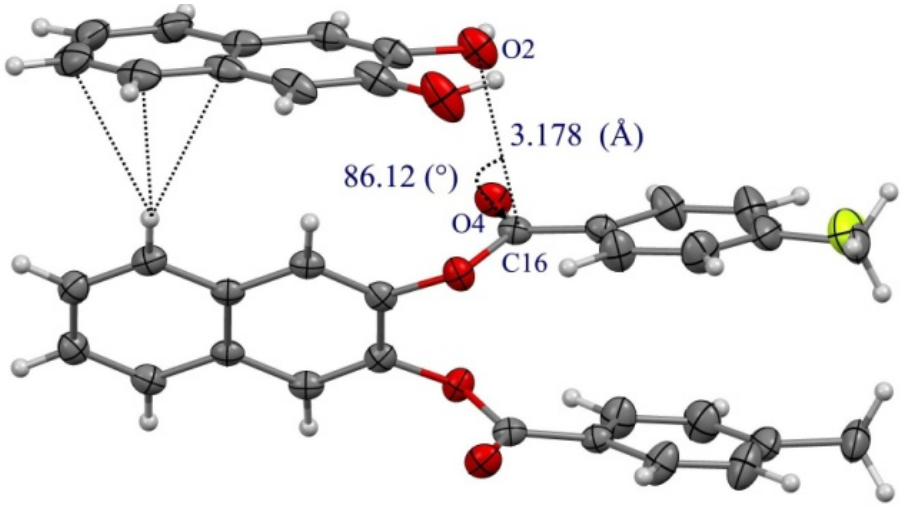

(a)

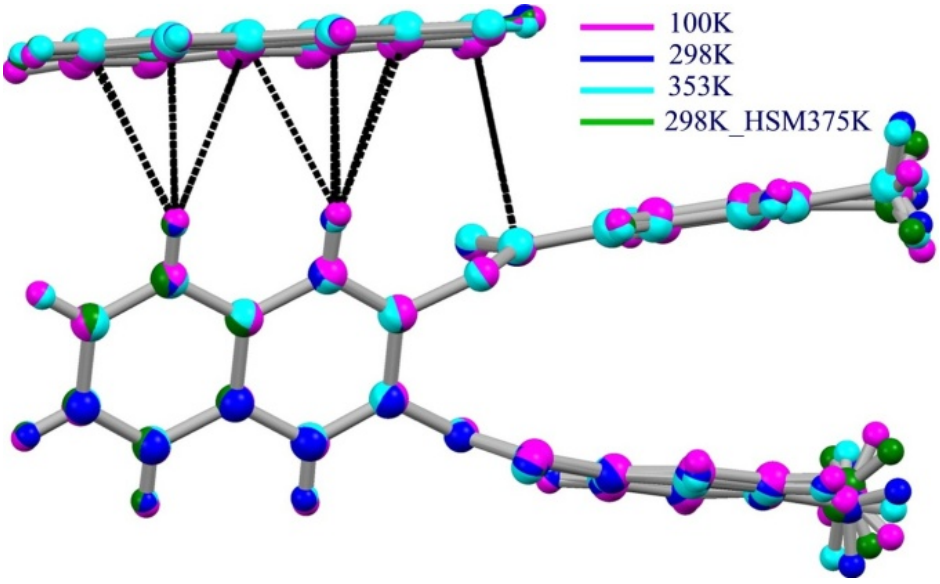

(b)

Figure 1.14: (a) Relative orientation of the neighboring molecules of **1.32** and **1.42** in cocrystals **1.32●1.42** at 100 K; (b) structure overlay of reacting molecules in cocrystal at different temperatures.

El···Nu parameter	**-173**	**25**	**80**	**25$^{\$}$**
C16···O2	3.178	3.285	3.325	3.282
∠O4=C16···O2	86.12	85.07	84.50	85.16
∠H2A-O2···C16	81.45	81.24	83.74	84.50
∠C2-O2···C16	102.9	101.54	101.12	101.67

$^{\$}$Crystal heated to 102 ^{o}C on hot stage microscope and then allowed to cool to 25 ^{o}C.

Table 1.2: El···Nu parameters for the reacting molecules in the cocrystal **1.32●1.42** at various temperatures in ^{o}C.

The powder X-ray diffraction pattern recorded after grinding the mixture of cocrystals **1.32●1.42** and solid sodium carbonate revealed presence of diffraction peaks of individual components i.e. cocrystal **1.32●1.42** and sodium carbonate, thus eliminating the possibility of generation of any new crystalline phase during grinding (Figure 3.15 and 3.16). Variable temperature PXRD of cocrystals **1.32●1.42** (Figure 3.17) were recorded in the range (35 to 105 ^{o}C) to see the effect of heat on the cocrystal **1.32●1.42**. The results revealed that the crystal lattice remained undisturbed till the reaction temperature (100-105 ^{o}C). This allowed us to correlate the reactivity in the solid state with the crystal structure of cocrystals **1.32●1.42** at room temperature.

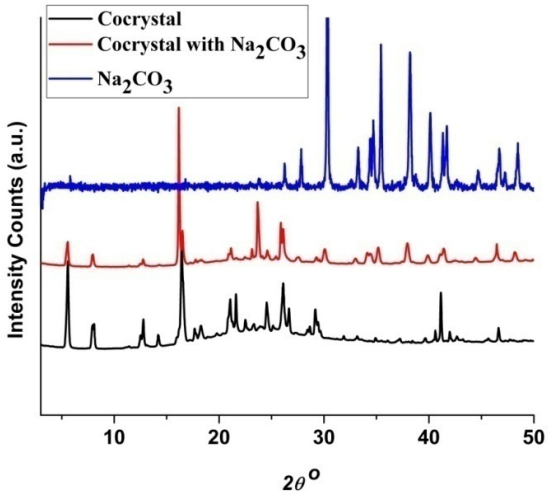

Figure 1.15: PXRD of profiles of cocrystals **1.32●1.42**, cocrystals **1.32●1.42** ground with anhydrous sodium carbonate at room temperature and anhydrous sodium carbonate.

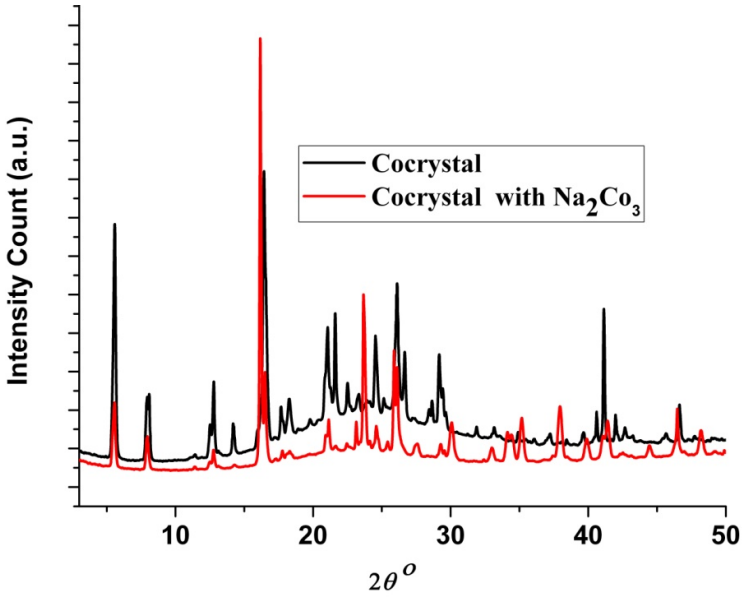

Figure 1.16: PXRD of cocrystals **1.32●1.42** and **1.32●1.42** ground with anhydrous sodium carbonate at room temperature.

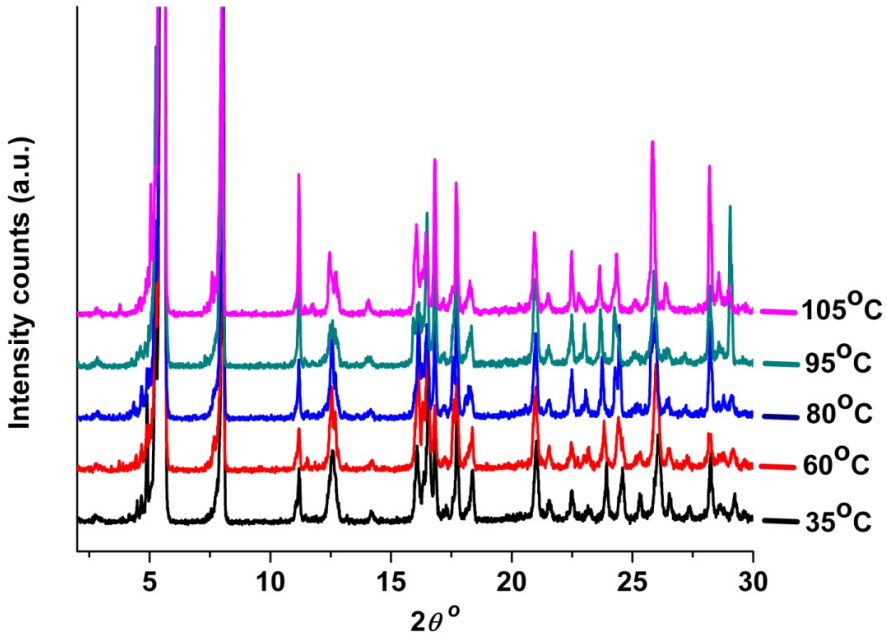

Figure 1.17: Variable temperature PXRD of cocrystals **1.32●1.42**.

Conclusions:

Investigation of the intermolecular acyl transfer reactivity in molecular crystals of *myo*-inositol orthoester derivatives and its correlation with crystal structures enabled us to identify the essential parameters to support efficient acyl transfer reaction in crystals: (a) the favourable geometry of the nucleophile (-OH) and the electrophile (C=O) and (b) the molecular assembly, reinforced by C-H···π interactions, which supports a domino type of reaction in crystals. These parameters were used to identify another reactive crystal through a data-mining study of the Cambridge Structural Database. A 2:1 cocrystal of 2,3-naphthalene diol and its di-*p*-methylbenzoate was selected as a potentially reactive crystal and its reactivity was tested by heating the cocrystals in the presence of solid sodium carbonate. A facile intermolecular *p*-toluoyl group transfer was observed as predicted. The successful identification of reactive cocrystals opens up a novel method for the detection of molecular crystals capable of exhibiting acyl transfer reactivity.

Cocrystals and molecular complexes have gained prominence in the last two decades with numerous studies devoted to developing methods of synthesis and potential applications.[52-61] Solid-state reactions in such multi-component crystals are rare and constitute a largely unexplored field due to inherent difficulties in obtaining molecular crystals wherein the reacting centers are aligned in the proper orientation for the desired reaction. Our investigations illustrate the importance of systematic studies of group transfer reactions in crystals paving the way for identification of reactive crystals and cocrystals from the crystal structure database. This provides a novel route to obtain crystals that are capable of undergoing chemical reactions. Structure-reactivity correlation studies in crystals could also provide methods for evaluating the chemical stability of functional multi-component solids.

Experimental Section:

General Experimental Methods:

All the solvents were purified according to the literature procedure[62] before use. All air or moisture sensitive reactions were carried out in an atmosphere of argon or nitrogen. Sodium hydride used in experiments was 60% suspension in mineral oil. Thin layer chromatography was performed on E. Merck pre-coated 60 F_{254} plates and the spots were rendered visible either by shining UV light or by charring the plates with chromic acid solution. Column chromatographic separations (60-120, 100–200 mesh) and flash column chromatographic separations (silica gel, 230–400 mesh) were carried out with light petroleum–ethyl acetate mixtures as eluent. 'Usual work-up' implies washing of the organic layer with water followed by brine, drying over anhydrous sodium sulfate, and removal of the solvent under reduced pressure using a rotary evaporator. IR spectra were recorded (in $CHCl_3$ solution, or as a Nujol mull or as a neat film, solid unless otherwise mentioned) with a Shimadzu FTIR-8400 or Perkin–Elmer spectrophotometer or Bruker Alpha spectrophotometer. ^1H and ^{13}C NMR spectra were recorded on Bruker AV 200 MHz or Bruker AV 400 MHz, or Bruker AV 500 MHz or JEOL ECX 400 MHz spectrometer. Chemical shifts (δ, ppm) reported are referred to internal tetramethylsilane (0 ppm) for ^1H NMR and $CDCl_3$ (77 ppm) for ^{13}C NMR. ^{19}F NMR spectra were recorded on bruker 400 MHz spectrometer with C_6F_6 (hexa-flurobenzene) as internal standard. Microanalytical data were obtained using a Carlo-Erba CHNS-0 EA 1108 or Flash EA 1112 series CHNS elemental analyzer. All the melting points reported are uncorrected and were recorded using a Büchi B-540 electro-thermal melting point apparatus. Yields refer to chromatographically and spectroscopically pure compounds. All the asymmetrically substituted *myo*-inositol derivatives reported are racemic; however only one of the enantiomers is shown in all the schemes for convenience and clarity. Compounds previously reported in the literature were characterized by comparison of their melting points and/or ^1H NMR spectra with the reported data.

Crystallization: Naphthalene-2,3-diol (**1.32**, 0.32 g, 2 mol) and its di-*p*-methyl benzoate[42] **1.33** (0.396 g, 1 mmol) were dissolved in ethyl acetate (10 mL) by warming; light petroleum (90 mL) was added and the resulting solution was stored in an open container, at ambient temperature. Crystallization was complete in a few

hours to yield the 2:1 cocrystals **1.32●1.33** (0.716 g), MP = 139-140 °C. The structure of the cocrystals **1.32●1.33** revealed by single crystal X-ray diffraction analysis was identical to that retrieved from the CSD.[42] Crystallization of a mixture of **1.32** and **1.33** in the molar ratio 1:1 or 1:2 or 1:3 also yielded 2:1 cocrystals **1.32●1.33** consistently. The cocrystals **1.32●1.33** could also be obtained by grinding a mixture of the diol **1.32** (0.160 g, 1.0 mmol), the diester **1.33** (0.198 g, 0.50 mmol) and two-three drops of ethyl acetate, using a pestle and mortar.

Solid-state reactivity of cocrystals 1.32●1.33: A mixture of freshly grown crystals of **1.32●1.33** (0.093 g, 0.13 mmol) and activated sodium carbonate (0.110 g, 1.03 mmol) was ground into a fine powder using a mortar and pestle. The mixture was transferred to a test tube filled with argon, and heated in an oil bath (122-125 °C) for 60 h. The reaction mixture was cooled to ambient temperature, suspended in water (20-30 mL) and then extracted with ethyl acetate (20-30 mL). The organic extract was washed with water, followed by brine. The organic layer was dried over anhydrous sodium sulphate and evaporated under reduced pressure. The residue obtained was purified by column chromatography (silica gel 100-200 mesh; eluent, ethyl acetate/light petroleum 10/90, v/v) to obtain **1.35** (0.066 g, 91%) as a solid, Mp. 197-198 °C (crystals from chloroform); **TLC** (35/65 ethyl acetate/light petroleum, v/v): R_f : 0.6; **IR** (Nujol): $\bar{\nu}$ 1723, 3391 cm^{-1}; **^{1}H NMR** ($CDCl_3$, 200MHz): δ 2.48 (s, 3H), 5.70 (s, 1H, D_2O exchangable), 7.30-7.50 (m, 5H, Ar H), 7.69-7.80 (m, 3H, Ar H), 8.12-8.20 (m, 2H, Ar H); **^{13}C NMR** (Acetone-d_6, 50MHz): δ 22.0, 112.3, 121.9, 124.9, 127.1, 127.2, 128.2, 128.4, 129.6, 130.5, 131.3, 134.2, 141.8, 145.6, 149.7, 165.7 **Elemental analysis**: calcd (%) for $C_{17}H_{24}O_3$ (278.31): C 77.68, H 5.07; found, C 77.30, H 4.81. The diol **1.32** (0.022 g, 53%) was recovered on elution with ethyl acetate/light petroleum (25/75 v/v) (Figures A12-A14, Appendix I).

Reaction of 1.32●1.33 in melt: The cocrystals **1.32●1.33** (0.179 g, 0.25 mmol) and sodium carbonate (0.212 g, 2 mmol) were ground together. The mixture obtained was placed in a test tube and immersed in an oil bath pre-heated to 145 °C (reaction time 5 h). The reaction mixture was worked up as above. The residue obtained from the ethyl acetate layer was chromatographed over silica gel (100-200 mesh) to obtain the mono-*p*-toluate **1.35** (eluent, ethyl acetate/light petroleum, 10/90 v/v, 0.064 g, 46%), the diol **1.32** (eluent, ethyl acetate/light petroleum, 20/80 v/v, 0.080 g, 67%) and the

diester **1.33** (0.014 g, 14%). The aqueous layer was acidified with hydrochloric acid and extracted with ethyl acetate. The organic extract was dried over anhydrous sodium sulfate and evaporated to obtain *p*-toluic acid (0.013 g, 19%).

Reaction between 1.32 and 1.33 in solution: The diol **1.32** (0.032 g, 0.2 mmol), the diester **1.33** (0.040 g, 0.1 mmol), sodium carbonate (0.085 g, 0.8 mmol) and dry *p*-xylene (2.5 mL) were heated (125 °C) for 24 h. Excess of dry *p*-xylene (2.5 mL) was added and the heating continued for further 36 h. The reaction mixture was concentrated under reduced pressure and the residue worked up as above. Column chromatographic separation yielded **1.33** (0.016 g, 40%) and the monotoluate **1.35** (0.005 g, 9%). Use of dry DMF (instead of *p*-xylene) as the solvent for the same reaction resulted predominantly in the hydrolysis of **1.33** and formation of **1.35** was not observed.

DSC Analysis: The thermal behaviour of crystals were recorded on a Mettler Differential Scanning Calorimeter or Waters DSC instrument. Crystals (~ 3 mg) were placed in a sealed aluminium pan (40 µl) and were analyzed from ambient temperature to ~ 20 °C above the melting point of the compound using an empty pan as the reference. The heating rate was 5 °C min^{-1} (10 °C min^{-1} in some experiments) and nitrogen gas was used for purging.

X-ray Crystallography:

Single-crystal X-ray intensity data measurements were recorded on a Bruker SMART APEX II and SMART APEX I single crystal X-ray CCD diffractometer respectively, with graphite-monochromatised (Mo-Kα = 0.71073 Å) radiation. The X-ray generator was operated at 50 kV and 30 mA. Diffraction data were collected with a ω scan width of 0.3° for those collected on (SMART APEX I) (φ settings 0, 90, 180 and 270°; the detector position (2θ) was fixed at -28°) and 0.5° for those (SMART APEX II) (at different settings of φ and 2θ). The sample-to-detector distance was fixed at 6.145 cm for those collected on (SMART APEX I) and 5.00 cm for for those (SMART APEX II). The X-ray data acquisition was monitored by SMART (for for those collected on (SMART APEX I))[65] or APEX II (for SMART APEX II) programs.[66] All the data were corrected for Lorentz-polarization and absorption effects using SAINT and SADABS programs integrated in APEX II program

package.[66] The structures were solved by direct method and refined by full matrix least squares, based on F^2, using SHELX-97[67]. Molecular diagrams were generated using ORTEP-32[68] and packing diagrams were prepared using Mercury-3.3.[69] Geometrical calculations were performed using SHELXTL and PLATON.[70] (see Table A1-A2, Appendix I)

PXRD Analysis: Powder X-ray diffraction patterns were recorded on PANalytical X'PERT PRO instrument at a continuous scanning rate of 2° 2θ/min using Cu Kα radiation (40 kV, 30 mA) with the intensity of the diffracted X-ray being collected at intervals of 0.017° 2θ. Or recorded on Rigaku Micromax-007HF instrument (High intensity microfocous rotating anode X-ray Generator) with R-axis detector IV++ at a continuous scanning rate of 2° 2θ/min using Cu Kα radiation (40 kV, 30 mA) with the intensity of the diffracted X-ray being collected at intervals of 0.1° 2θ. A nickel filter was used to remove Cu K$_\beta$ radiation. The powder X-ray diffraction pattern of the mixture of cocrystals **1.32●1.33** and solid sodium carbonate obtained by grinding them together revealed presence of diffraction peaks of individual components i.e. of **1.32●1.33** and sodium carbonate, thus eliminating the possibility of generation of any new crystalline phase during grinding (Figures A10, Appendix I).

Preparation of Naphathalene-2,3-diol ditoluates 1.33, **1.37** and **1.38:** The *p*-ditoluate **1.33** was prepared as reported earlier.[42] The ditoluates **1.37** and **1.38** were synthesized by the acylation of naphthalene-2,3-diol (**1.32**) with *m*-toluoyl chloride (for **1.37**) and *o*-toluoyl chloride (for **1.38**) at 115−120 °C. [See Appendix I for details and compound characterization data]

Preparation of naphathalene-2,3-diol-*m*-ditoluate (1.37): To 3-methyl benzoic acid (4.080 g, 30 mmol), thionyl chloride (8.210 g, 69 mmol) was added and the reaction mixture was stirred at 85-90 ^oC for 4 h. The reaction mixture was cooled and thionyl chloride was removed under reduced pressure. The residue was mixed with naphthalene-2,3-diol, (2.000 g, 12.5 mmol) and heated with stirring in a dry round bottom flask at 110-115 ^oC for 3 h. The reaction mixture was cooled to room temperature and stirred with aqueous solution of sodium carbonate. The undissolved solid was extracted into ethyl acetate. The ethyl acetate extract was washed with water followed by brine and dried over anhydrous Na_2SO_4. The organic extract was evaporated under reduced pressure to obtain the crude product, which was purified by

column chromatography (silica gel 100-200 mesh; eluent 5:95 ethyl acetate: light petroleum) to get **1.37** (4.300 g, 87%) as a colorless solid.

Data For **1.37:** TLC R_f : 0.6 (1:4 ethyl acetate - light petroleum); **MP** = 91-92 ^oC (crystals from ethanol); **IR** (Nujol): $\bar{\nu}$ 1733, 1746 cm^{-1}; **^{1}H NMR** ($CDCl_3$, 200 MHz): δ 2.27 (s, 6H, CH_3), 7.37-7.21 (m, 4H, Ar H), 7.57-7.47 (m, 2H, Ar H), 7.95-7.80 ppm (m, 8H, Ar H); **^{13}C NMR** ($CDCl_3$, 50 MHz): δ 21.0, 120.9, 126.3, 127.3, 127.5, 128.3, 128.7, 130.6, 131.5, 134.3, 138.23, 141.3, 164.6 ppm; **Elemental analysis** calcd for $C_{26}H_{20}O_4$ (396.44): C, 78.77; H, 5.09; found, C, 78.27; H, 5.03%.

Preparation of naphathalene-2,3-diol-*o*-ditoluate (1.38): The ditoluate **1.38** was prepared as above using 2-methyl benzoic acid (instead of 3-methyl benzoic acid); yield 4.450 g (90%).

Data for **1.38:** TLC R_f: 0.6 (1:4 ethyl acetate - light petroleum); **MP** = 110 ^oC (crystals from dichloromethane); **IR** (Nujol): 1738 cm^{-1}; **^{1}H NMR** ($CDCl_3$, 200 MHz): δ 2.59 (s, 6H, CH_3), 7.10-7. 20 (m, 4H, Ar H), 7.46-7.36 (m, 2H, Ar H), 7.56-7.48 (m, 2H, Ar H), 7. 92-7.81 (m, 4H, Ar H), 8.06-8.03 (dd, 2H, Ar H) ppm; **^{13}C NMR** ($CDCl_3$, 50 MHz): δ 21.7, 121.1, 125.8, 126.3, 127.5, 127.7, 131.2, 131.7, 131.8, 132.8, 141.5, 165 ppm; **HRMS** $[C_{26}H_{20}O_4 + Na]^+$ = 419.1248, found = 419.1254.

Crystallization: Solubility of the ditoluates **1.33**, **1.37**, and **1.38** was similar in common organic solvents. A clear solution was obtained by vigorous shaking and/or warming of the ditoluate in the desired solvent, and the solution was allowed to evaporate at room temperature over 2-3 days. Crystallization of **1.33** from diethyl ether produced needle-shaped crystals in 10−12 h (Form **1.33I**, Figure 1.11A), whereas thick plates (Form **1.33II**, Figure 1.11A) appeared after 1−2 days in the same crystallization flask; the quantity of the needles obtained was always more than the plates, consistently. Crystallization of **1.33** from ethyl acetate, acetone, toluene, nitromethane, dichloromethane, chloroform, carbon tetrachloride (CCl_4), and tetrahydrofuran (THF) yielded Form **1.33I** crystals exclusively, whereas Form **1.33II** crystals were obtained from acetonitrile, 2-propanol, methanol, and benzene. In one of the experiments, Form **1.33III** crystals (blocks, Figure 1.11B) were obtained from a hot solution of methanol, but several attempts to obtain these crystals again yielded only Form **1.33II** crystals. Crystallization of **1.37** from ethyl acetate, acetone, toluene,

nitromethane, dichloromethane, chloroform, acetonitrile, 2-propanol, methanol, benzene, CCl_4, and THF yielded thick plates (Form **1.37I**, Figure 1.11C) exclusively. Crystallization of **1.37** from ethanol once produced only needle type crystals (Form **1.37II**, Figure 1.11D). However, further attempts to obtain Form **1.38II** crystals yielded only Form **1.37I** crystals. Form **1.37II** crystals turned opaque at ambient conditions within 2-3 days (Figure 1.11E) and completely disintegrated into a powder in 4-5 days. Crystallization of the *o*-toluate **1.38** from all the solvents mentioned above produced fibrous crystals (Figure 1.11F).

Details of X-ray diffraction data collection, structure solution and refinement, differential scanning calorimetry (DSC) analysis, hot stage microscopy (HSM), and powder X-ray diffraction (PXRD) studies are given in the Appendix I.

Cocrystallization: The diol **1.32** (0.32 g, 2 mmol) and the *m*-ditoluate **1.37** (0.792 g. 2 mmol) were dissolved in ethyl acetate (10-15 mL) by warming. Light petroleum (80-90 mL) was added and the resulting solution was stored in an open container, at ambient temperature. Evaporation of the solvent was complete in 2-4 days to yield large, square, reddish cocrystals **1.32●1.37** (1.00 - 1.10 g).

Data for **1.32●1.37:** MP = 110 ^{o}C; **IR** (Nujol): $\bar{\nu}$ 1722, 1734, 3433, 3497 cm^{-1}; **^{1}H NMR** (*Acetone-d_6*, 200 MHz): δ 2.31 (s, 6H), 7.30-7.16 (m, 4H, Ar H), 7.5-7.32 (m, 4H, Ar H), 7.70-7.55 (m, 4H, Ar H), 7.97-7.83- (m, 4H, Ar H), 8.00-8.14 (m, 4H, Ar H), 8.46 ppm (br. s, 2H, Ar OH exchangeable with D_2O); **^{13}C NMR** (*Acetone-d_6*, 50 MHz): δ 21.0, 110.4, 121.8, 124.1, 126.7, 127.3, 127.9, 128.3, 129.4, 129.6, 130.3, 131.1, 132.5, 135.4, 139.4, 142.5, 147.1, 164.9 ppm; **Elemental analysis** calcd for $C_{36}H_{28}O_6$ (556.19): C, 77.68; H, 5.07; found, C, 77.87; H, 4.89 %.

Use of acetone as the solvent also yielded the cocrystals **1.32●1.37**. The cocrystals **1.32●1.37** could also be obtained (See Figure A36, Appendix I) by the solvent (ethyl acetate) drop-grinding method, from a 1:1 mixture of the two components. The cocrystals were fully characterized by IR and NMR spectroscopy (solution and solid state), elemental analysis, thermal analysis, powder X-ray diffraction and single crystal X-ray diffraction analysis (See Appendix I for data). The molar ratio of the two components in cocrystals **1.32●1.37** was 1:1 as revealed by single crystal X-ray

diffraction analysis and ^{1}H NMR spectroscopy. Crystallization using **1.32** and **1.37** in the molar ratio 1:1 or 1:2 or 1:3 also yielded 1:1 cocrystals **1.32●1.37**.

Acyl transfer reactivity of cocrystals 1.32●1.37: Procedure A: A mixture of freshly grown cocrystals **1.32●1.37** (0.417 g, 0.75 mmol) and activated sodium carbonate (0.636 g, 6 mmol) was ground into a fine powder using a mortar and pestle. The mixture was transferred to a test tube filled with argon, and heated in an oil bath (90-95 ^{o}C) for 72 h. The reaction mixture was cooled to ambient temperature, suspended in water (80-100 mL) and then extracted with ethyl acetate (120-160 mL). The organic extract was washed with water, followed by brine. The organic layer was dried over anhydrous sodium sulphate and evaporated under reduced pressure. The residue obtained was subjected to column chromatography (silica gel 100-200 mesh) to obtain the unreacted ditoluate **1.37** (0.094 g, 31%, eluent, ethyl acetate/light petroleum, 1/19 v/v); the monotoluate **1.39** (0.0126 g, 30%, eluent, ethyl acetate/light petroleum 1/9, v/v); and the diol **1.32** (0.097 g, 80%, mp. 162-165 ^{o}C, eluent, ethyl acetate/light petroleum, 1/4 v/v). Conc. hydrochloric acid was added drop wise to the aqueous layer (till acidic) and extracted with ethyl acetate. The organic extract was washed with water, dried over anhydrous sodium sulfate and evaporated under reduced pressure. The residue obtained was subjected to column chromatography (silica gel 100-200 mesh) to obtain *m*-toluic acid (0.024 g, 12%, eluent, ethyl acetate/light petroleum, 1/3 v/v).

Data for **1.39:** TLC R_f: 0.6 (ethyl acetate/light petroleum, 7/13 v/v); MP = 190 ^{o}C (crystals from chloroform); **IR** (Nujol): $\bar{\nu}$ 1720, 3383 cm^{-1}; **^{1}H NMR** (*Acetone-d_6*, 200 MHz): δ 2.46 (s, 3H, CH_3), 7.60-7.25 (m, 5H, Ar H), 7.90-7.65 (m, 3H, Ar H), 8.05-8.0 (m, 2H, Ar H), 9.03 ppm (s, 1H, OH - D_2O exchangeable); **^{13}C NMR** (*Acetone-d_6*, 50 MHz): δ 21.2, 111.9, 121.5, 124.5, 126.1, 126.7, 128.08, 129.5, 130.5, 131.3, 133.9, 135.1, 139.4, 141.4, 149.3, 165.4 ppm; **HRMS** $(C_{18}H_{15}O_3+H)^+$ (279.1016); Found = 279.1015.

Procedure B (in melt): The cocrystals **1.32●1.37** (0.030 g, 0.054 mmol) and sodium carbonate (0.046 g, 0.43 mmol) were ground together. The mixture obtained was placed in a test tube and immersed in an oil bath pre-heated to 140 ^{o}C (reaction time 5 h). The reaction mixture was suspended in ethyl acetate (20 mL) and washed with

water. Ethyl acetate solution was dried over anhyd. sodium sulfate and evaporated under reduced pressure. TLC analysis (ethyl acetate/ light petroleum, 3/17 v/v) of the residue showed the presence of the diol **1.32**, the diester **1.37** and the monoester **1.39**. No attempt was made to seprate them. The *m*-toluic acid (0.0045 g, 32%) was obtained from the aqueous layer (as in Procedure A).

Procedure C (in solution): The cocrystals **1.32●1.37** (0.056 g, 0.1 mmol), sodium carbonate (0.085 g, 0.8 mmol) and dry *p*-xylene (3 mL) were heated at 90-95 ^{o}C for 72 h. The reaction mixture was concentrated under reduced pressure and the residue worked up as above. The products were separated by column chromatography (as in Procedure A) to obtain the ditoluate **1.37** (0.012 g, 30%), the monotoluate **1.39** (0.015 g, 27%) and the diol **1.32** (0.012 g, 75%). A minor amont of *m*-toluic acid (0.004 g, 15%) was obtained from the aqueous layer (as in Procedure A).

General procedure for synthesis of diester:

All the acid chlorides were synthesised by heating the corresponding acid at 80-90 ^{o}C with freshly distilled thionyl chloride for 3 h; excess of thionyl chloride was removed under reduced pressure.[63] Acyl chloride obtained was used in next reaction without further purification.

General procedure for the acylation of the diol 1.32: A mixture of the diol **1.32** and the required acid chloride was heated (100-120 ^{o}C) with stirring for 3-4 h in a flask fitted with a calcium chloride guard tube. HCl gas generated was trapped by using calcium chloride guard tube above reaction set up. The reaction mixture was cooled to room temperature, suspended in aq. Na_2CO_3 solution and extracted with ethyl acetate or DCM. The organic layer was washed with water followed by brine and dried over anhydrous Na_2SO_4. The solvent was evaporated under reduced pressure to obtain the crude product, which was purified by column chromatography (silica gel 100-200 mesh). The detail for each reaction is shown in Table 1.3.

Entry	Substrate (mmol)	Acylating agent (mmol)	Reaction, Temp °C, (time, h)	Products (yield %)	Melting point (°C)
1	Diol **1.32** (25)	*p*-toluoyl Chloride (35)	110 (3)	mono-*p*-toluate **1.35** (27) Ditoluate **1.33** (42)	197-198[64] 145[42]
2	Diol **1.32** (10)	Benzoyl Chloride (14)	110 (3)	mono-benzoate **1.40** (31) dibenzoate **1.46** (32)	222-224
3	Diol **1.32** (8)	*p*-fluro Benzoyl Chloride (13)	110 (3)	mono-*p*-flurobenzoate **1.41** (21)	228-230
4	Diol **1.32** (10)	Benzoyl Chloride (30)	120 (4)	Dibenzoate **1.46** (87)	149-151
5	Diol **1.32** (2)	*p*-fluro Benzoyl Chloride (5)	120 (4)	Di-*p*-flurobenzoate **1.47** (69)	171-173
6	Diol **1.32** (2)	*p*-Chloro Benzoyl Chloride (15)	120 (4)	Di-*p*-chlorobenzoate **1.48** (36)	169
7	Diol **1.32** (2)	Acetic anhydride (6)	110 (3)	Di-acetate **1.49** (63)	88
8	Diol **1.32** (2)	Pentanoyl Chloride (6)	80 -90 (4)	Di-pentanoate **1.50** (51)	Liquid
9	Mono **1.35** (1)	Acetic anhydride (3)	110 (3)	*2*-acetate-3- toluate **1.45** (66)	156-158
10	Mono **1.35** (1)	Benzoyl Chloride (2)	120 (4)	*2-p*-toluate-3- benzoate **1.43** (91)	116
11	Mono **1.35** (7.2)	*p*-fluro Benzoyl Chloride (13)	120 (4)	*2-p*-flurobenzoate-3- toluate **1.42** (89)	122-125
12	Mono **1.40** (1.5)	*p*-fluro Benzoyl Chloride (3.8)	120 (4)	*2-p*-flurobenzoate-3-benzoate **1.44** (77)	151

Table 1.3: Acylation of 2,3-dihydroxy naphthalene (**1.32**) and its monoesters.

Eluent for column chromatography, ethyl acetate: light petroleum, v/v: entry 1 – 5:95 for **1.33**, 15:85 for **1.35**; entry 2 – 5:95 for **1.46**, 15:85 for **1.40**; entry 3 –15:85 for **1.41**; entry 4 – 5:95; entry 5 – 5-7:95-93; entry 6 – 7:93; entry 7 – 10-12:90-88; entry 8 – 7:93; entry 9 – 10:90; entry 10 – 5:95; entry 11 – 5-7:95-93; entry 12 – 5-7:95-93.

3-hydroxynaphthalen-2-yl benzoate (1.40):

Data for **1.40:**TLC R_f: 0.7 (35% ethyl acetate in light petroleum); **MP** = 222-224 °C (crystals from acetonitrile); **IR** (Nujol): $\bar{\nu}$ 1724, 3300-3450 cm^{-1}; **^{1}H NMR** ($CDCl_3$, 200 MHz): δ 7.29-7.51 (m, 3H, Ar H), 7.58-7.70 (m, 2H, Ar H), 7.71-7.89 (m, 4H, Ar H), 8.19-8.31 (m, 2H, Ar H), 9.09 ppm (s, 1H, D_2O exchangeable, Ar OH); **^{13}C NMR** (DMF-d_7, 50 MHz,): δ 111.2, 121.0, 123.8, 126.2, 127.6, 128.4, 129.2, 129.9, 130.3, 133.4, 134.1, 141.1, 149.3, 165.0 ppm; **Elemental analysis** calcd for $C_{17}H_{12}O_3$ (264.28): C, 77.26; H, 4.58; found, C, 77.27; H, 4.37 %.

3-hydroxynaphthalen-2-yl (4-flurobenzoate) (1.41):

Data for **1.41:** TLC R_f : 0.6 (35% ethyl acetate in light petroleum); **MP** = 228-230 ^oC (crystals from Ethyl acetate); **IR** (solid): $\bar{\nu}$ 1738, 3350-3450 cm^{-1}; **^{1}H NMR** (*Acetone-d_6*, 500 MHz): δ 7.31 - 7.45 (m, 5 H, Ar H), 7.70 - 7.76 (m, 2 H, Ar H), 7.81 (d, *J* = 8.5 Hz, 1 H, Ar H), 8.25 – 8.35 (m, 2 H, Ar H), 9.12 ppm (s, 1 H, D_2O exchangeable, Ar OH); **^{13}C NMR** (*Acetone-d_6*, 126 MHz): δ 112.0, 116.5, 116.7, 121.5, 124.5, 126.80, 126.84, 127.0, 128.1, 129.2, 133.7, 133.8, 133.9, 141.3, 149.2, 164.4, 166.9 ppm (d, J_{C-F} = 253 Hz); ^{1}H-decoupled **^{19}F NMR** (*Acetone-d_6*, C_6F_6 as reference, 376.5 MHz): -104.95 ppm; **Elemental analysis** calcd for $C_{17}H_{11}FO_3$ (282.27): C, 72.34; H, 3.93; found, C, 72.08; H, 3.67 %.

2-*O*-(4-fluorobenzoyl)-3-*O*-(4-methylbenzoyl)-naphthalene (1.42):

Data for **1.42:** TLC R_f : 0.5 (1:9 ethyl acetate: light petroleum); **MP** = 122-125 ^oC (Plate shaped crystals obtained by cooling ethyl acetate : light petroleum (1:9) solution in a freezer; **IR** (Nujol): $\bar{\nu}$ 1738, 1746 cm^{-1}; **^{1}H NMR** ($CDCl_3$, 400 MHz): δ 2.39 (s, 3H), 7.00-7.10 (m, 2H, Ar H), 7.14 – 7.22 (m, 2H, Ar H), 7.45-7.57 (m, 2H, Ar H), 7.78-7.90 (m, 4H, Ar H),7.93 – 8.00 (m, 2H, Ar H), 8.05-8.15 ppm (m, 2H, Ar H); **^{13}C NMR** ($CDCl_3$, 50 MHz): δ 21.6, 115.4, 115.9, 120.9, 121.1, 125.0, 125.1, 125.9, 126.4, 127.5, 129.2, 130.2, 131.6, 131.7, 132.7, 132.9, 141.27, 141.33, 144.6, 164.5, 166.1 ppm (d, J_{C-F} = 256 Hz); ^{1}H-decoupled **^{19}F NMR** ($CDCl_3$, C_6F_6 as reference, 376.5 MHz): -105.03 ppm; **Elemental analysis** calcd for $C_{25}H_{17}FO_4$ (400.40): C, 74.99; H, 4.28; found, C, 75.14; H, 4.23 %.

2-*O*-(benzoyl)-3-*O*-(4-methylbenzoyl)-naphthalene (1.43):

Data for **1.43:** TLC R_f : 0.5 (1:9 ethyl acetate: light petroleum); **MP** = 116 ^oC; **IR** (Nujol): $\bar{\nu}$ 1739 cm^{-1}, **^{1}H NMR** ($CDCl_3$, 200 MHz): δ 2.38 (s, 3 H), 7.17 (d, *J* = 8 Hz, 2 H, Ar H), 7.32 - 7.44 (m, 2 H, Ar H), 7.46 - 7.61 (m, 3 H, Ar H), 7.81 - 7.91 (m, 4 H, Ar H), 7.94-8.02 (m, 2 H, Ar H), 8.04-8.14 ppm (m, 2 H, Ar H); **^{13}C NMR** ($CDCl_3$, 50 MHz): δ 21.7, 121.0, 121.1, 126.0, 126.3, 127.5, 128.4, 128.8, 129.2, 130.15, 130.18, 131.59, 131.65, 133.6, 141.4, 144.5, 164.6 ppm; **Elemental analysis** calcd for $C_{25}H_{18}O_4$ (382.41): C, 78.52; H, 4.74; found, C, 78.32; H, 4.53 %.

3-(benzoyl) naphthalene-2-yl 4-flurobenzoate (1.44):

Data for **1.44:** TLC R_f **:** 0.32 (5% ethyl acetate in light petroleum); **MP** = 150-151 ^oC (crystals from ethyl acetate - light petroleum mixture); **IR** (Nujol): $\bar{\nu}$ 1739, 1749cm^{-1}; **^{1}H NMR** ($CDCl_3$, 200 MHz): δ 6.95-7.10 (m, 2H, Ar H), 7.32-7.62 (m, 5H, Ar H), 7.80-7.92 (m, 4H, Ar H), 8.06-8.16) ppm (m, 4H, Ar H); **^{13}C NMR** ($CDCl_3$, 50 MHz): δ 115.5, 115.9, 121.0, 121.1, 124.9, 125.0, 126.4, 127.5, 128.5, 128.6, 130.1, 131.6, 131. 64, 132.7, 132.9, 133.7, 141.17, 141.22, 164.5, 166.1 ppm (d, J_{C-F} = 256 Hz); ^{1}H-decoupled **^{19}F NMR** ($CDCl_3$, C_6F_6 as reference, 376.5 MHz): -105.24 ppm; **Elemental analysis** calcd for $C_{24}H_{15}FO_4$ (386.37): C, 74.61; H, 3.91; found, C, 74.44; H, 3.66 %.

3-(4-methylbenzoyl) naphthalene-2-yl acetate (1.45):

Data for **1.45:** TLC R_f : 0.5 (15:85 ethyl acetate: light petroleum); **MP** = 156-158 ^oC [needle shaped crystals obtained from ethyl acetate in hexane (15:85)]; **IR** (Nujol): $\bar{\nu}$ 1735, 1766 cm^{-1}; **^{1}H NMR** ($CDCl_3$, 200 MHz): δ 2.18 (s, 3 H), 2.47 (s, 3 H), 7.30 – 7.38 (m, 2 H, Ar H), 7.45 – 7.55 (m, 2 H, Ar H), 7.69 (s, 1 H, Ar H), 7.74 - 7.88 (m, 3 H, Ar H), 8.06 - 8.15 ppm (m, 2 H, Ar H); **^{13}C NMR** ($CDCl_3$, 50 MHz): δ 20.6, 21.8, 120.9, 121.1, 126.1, 126.3, 127.5, 129.5, 130.3, 131.6, 131.7, 141.2, 141.3, 144.8, 168.8 ppm; **HRMS** $[C_{20}H_{16}O_4 + Na]^+$ = 343.0941, found = 342.0934.

Naphthalene-2, 3-diyl bis(benzoate) (1.46):

Data for **1.46:**TLC R_f : 0.5 (1:9 ethyl acetate: light petroleum); **MP** = 149-151 ^oC (Long needle shaped crystals obtained from chloroform); **IR** (Nujol): $\bar{\nu}$ 1741 cm^{-1}; **^{1}H NMR** ($CDCl_3$, 200 MHz): δ 7.31 - 7.44 (m, 4 H, Ar H), 7.48 - 7.61 (m, 4 H, Ar H), 7.81 - 7.93 (m, 4 H, Ar H), 8.07 – 8.12 ppm (m, 4 H, Ar H); **^{13}C NMR** ($CDCl_3$, 50 MHz): δ 121.1, 126.4, 127.6, 128.5, 128.7, 130.2, 131.6, 133.7, 141.3, 164.6 ppm; **Elemental analysis** calcd for $C_{24}H_{16}O_4$ (368.39): C, 78.25; H, 4.38; found, C, 77.85; H, 4.59 %.

Naphthalene-2, 3-diyl bis(4-fluorobenzoate) (1.47):

Data for **1.47:** TLC R_f : 0.4 (5% ethyl acetate in light petroleum); **MP** = 171-173 ^oC (crystals from ethyl acetate - light petroleum mixture); **IR** (Nujol) $\bar{\nu}$ 1737, 1745 cm^{-1}; **^{1}H NMR** ($CDCl_3$, 200 MHz): δ 6.97-7.12 (m, 4H, Ar H), 7.46-7.58 (m, 2H, Ar H), 7.80-7.90 (m, 4H, Ar H), 8.05-8.15 ppm (m, 4H, Ar H); **^{13}C NMR** ($CDCl_3$, 50 MHz):

δ 115.6, 116, 121.1, 124.9, 125, 126.5, 127.6, 131.7, 132.7, 132.8, 141.1, 163.5, 166.2 ppm (d, J_{C-F} = 255.79 Hz); ^{1}H-decoupled ^{19}**F NMR** ($CDCl_3$, C_6F_6 as reference, 376.5 MHz): -104.93 ppm; **Elemental analysis** calcd for $C_{24}H_{14}F_2O_4$ (404.36): C, 71.29; H, 3.49; found, C, 71.06; H, 3.36 %.

Naphthalene-2, 3-diyl bis(4-chlorobenzoate) (1.48):

Data for **1.48:** TLC R_f: 0.5 (1:9 ethyl acetate: light petroleum); **MP** = 169 ^{o}C (needle shaped crystals obtained by chloroform); **IR** (Nujol): $\bar{\nu}$ 1750,1741 cm^{-1}; ^{1}**H NMR** ($CDCl_3$, 200 MHz): δ 7.32 - 7.42 (m, 4 H, Ar H), 7.50-7.59 (m, 2 H, Ar H), 7.81 - 7.90 (m, 4 H, Ar H), 7.96 - 8.06 ppm (m, 4 H, Ar H); ^{13}**C NMR** ($CDCl_3$, 50 MHz): δ 121.1, 126.6, 127.1, 127.6, 129.0, 131.5, 131.7, 140.4, 141.0, 163.7 ppm; **HRMS** $[C_{24}H_{14}O_4Cl_2 + Na]^+$ = 459.0161, found = 459.0161.

Naphthalene-2, 3-diyl bis-acetate (1.49):

Data for **1.49:** TLC R_f: 0.3 (15:85 ethyl acetate: light petroleum); **MP** = 88 ^{o}C [Thin plate shaped crystals obtained from ethyl acetate - hexane (20:80)]; **IR** (Nujol): $\bar{\nu}$ 1763 cm^{-1}; ^{1}**H NMR** ($CDCl_3$, 200 MHz): δ 2.35 (s, 6 H), 7.42 - 7.52 (m, 2 H, Ar H), 7.66 (br. s, 2 H, Ar H), 7.73 - 7.84 ppm (m, 2 H, Ar H); ^{13}**C NMR** ($CDCl_3$, 50 MHz): δ 20.7, 120.9, 126.3, 127.4, 131.5, 140.9, 168.5 ppm; **HRMS** $[C_{14}H_{12}O_4 + Na]^+$ = 267.0628, found = 267.0625.

Naphthalene-2, 3-diyl bis-pentanoate (1.50):

Data for **1.50:** TLC R_f**:** 0.4 (1:9 ethyl acetate: light petroleum); **IR** (Neat): $\bar{\nu}$ 1712, 1767 cm^{-1}; ^{1}**H NMR** ($CDCl_3$, 200 MHz): δ 0.97 (t, J = 7.2 Hz, 6 H), 1.34 – 1.57 (m, 4 H), 1.67 - 1.88 (m, 4 H), 2.58 (t, J = 7.5 Hz, 4 H), 7.38 – 7.49 (m, 2 H, Ar H), 7.63 (s, 2 H, Ar H), 7.73 – 7.8 ppm (m, 2 H, Ar H); ^{13}**C NMR** ($CDCl_3$, 50 MHz): δ 13.6, 22.2 (CH_2), 26.9 (CH_2), 33.7 (CH_2), 120.8, 126.1, 127.3, 131.4, 141.0, 171.3 ppm; **HRMS** $[C_{20}H_{24}O_4\,Na]^+$ = 351.1567, found = 351.1560.

Procedure of cocrystallization of 1.42:

The diol **1.32** (0.64 g, 4 mmol) and its diester **1.42** (0.800 g. 2 mmol) were dissolved in ethyl acetate (15 mL) by warming. Light petroleum (90 mL) was added and the resulting solution was stored in an open container, at ambient temperature and the

solvent was allowed to evaporate. Crystallization was complete in 6-8 days to yield reddish needle shaped 2:1 cocrystals **1.32●1.42** (~ 1.300 g, **MP** = 120-122 ^{o}C).

The cocrystals **1.32●1.42** were characterized by IR, NMR spectroscopy (^{1}H, ^{13}C, ^{19}F), elemental analysis, thermal analysis and single crystal X-ray diffraction, and powder X-ray diffraction.

DSC analyses of the diester **1.42**, cocrystal **1.32●1.42** as well as physical mixture of **1.32** and **1.42** in the ratio 2:1 were carried. DSC of the diester **1.42** and cocrystal **1.32●1.42** showed single endothermic peak corresponding to their melting at 131 °C, and 120 °C respectively (Figure A82-A84, Appendix I) revealed that there is no phase change before melting.

Data for **1.32●1.42:**

MP = 120-122 ^{o}C (Reddish needle shape crystals obtained by ethyl acetate - light petroleum solution); **IR** (Nujol): $\bar{\nu}$ 3450 - 3500, 3250 - 3350, 1729 cm^{-1}; **^{1}H NMR** ($CDCl_3$, 400 MHz): δ 2.36 (s, 3H), 5.79 (s, 4H, Ar- OH), 6.90-7.32 (m, 12H, Ar H), 7.45-7.65 (m, 6H, Ar H), 7.7 – 7.9 (m, 4H, Ar H), 7.92 – 8.1, ppm (m, 4H, Ar H); **^{13}C NMR** ($CDCl_3$, 100 MHz): δ 21.7, 110.1, 115.7, 115.9, 121.0, 121.2, 124.1, 124.94, 124.97, 125.8, 126.2, 126.48, 126.51, 127.6, 129.3, 129.5, 130.2, 131.6, 131.7, 132.8, 132.9, 141.2, 141.25, 144.2, 144.9, 163.9, 166.3 ppm (d, $J_{C\text{-}F}$ = 245.84 Hz) ; **^{19}F NMR** ($CDCl_3$, drop of C_6F_6, 376.5MHz): -105.03 ppm; **Elemental analysis** calcd for $C_{45}H_{33}FO_8$ (720.75): C, 74.99; H, 4.62; found, C, 74.63; H, 4.30%.

Solid-state reactivity of cocrystals (1.32●1.42): A mixture of freshly grown crystals **1.32●1.42** (0.050 g, 0.069 mmol) and activated sodium carbonate (0.059 g, 0.6 mmol) was ground into a fine powder using a mortar and pestle. The mixture was transferred to a test tube filled with argon, and heated in an oil bath (100-105 ºC) for 72 h. [The workup and isolation of product could also done by earlier procedure i.e, as in solid state reaction of cocrystal **1.32●1.33**] The reaction mixture was cooled to ambient temperature; the solid was extracted with dichloromethane and the residue was separated by filtration. The DCM solution was washed with water, dried over anhydrous Na_2SO_4 and evaporated to dryness. TLC analysis of the residue showed it to be a mixture of monoesters **1.35** and **1.41** and a minor amount of the unreacted diester **1.42**. The mixture of monoesters **1.35** and **1.41** (0.036 g, 94%) was separated

by column chromatography (silica gel 100-200 mesh; eluent, ethyl acetate/light petroleum 1/9, v/v).

The residue (left behind after extraction with DCM) was extracted with ethyl acetate (2 X 20 mL). The combined ethyl acetate extract was washed with water, dried over Na_2SO_4 and evaporated under reduced pressure to obtain a solid. The solid was purified over a short column of silica gel (100-200 mesh, elute: 1:4 ethyl acetate:light petroleum) to obtain the diol **1.32** (0.011 g, 50%); MP = 160 -162 ºC. Lit. (Aldrich catalogue) MP = 162 ºC.

Data for mixture of **1.35** and **1.41:** TLC R_f : 0.6 (35:65 ethyl acetate : light petroleum); **IR** (Nujol): $\bar{\nu}$ 3300 - 3400, 1724cm^{-1}; **^{1}H NMR** (*Acetone-d_6*, 400MHz): δ 2.46 (s, 3H, CH_3), 7.30-7.50 (m, 10H, Ar H), 7.7-7.85 (m, 6H, Ar H), 8.12 (d, *J* = 8.3 Hz, 2H, Ar H), 8.29-8.34 (m, 2H, Ar H), 9.02 (s, 1H, Ar OH, D_2O Exchangable), 9.06 ppm (s, 1H, Ar OH, D_2O Exchangable); **^{13}C NMR** (*Acetone-d_6*, 100MHz): δ 21.6, 111.9, 112.0, 116.5, 116.7, 124.6, 124.5, 125.5, 126.7, 126.82, 126.83, 126.86, 127.8, 128.07, 128.1, 129.22, 129.25, 130.2, 131.0, 133.7, 133.8, 133.9, 141.2, 141.4, 145.3, 164.3, 164.4, 166.7 ppm (d, $J_{C\text{-}F}$ = 252.78 Hz); ^{1}H-decoupled **^{19}F NMR** (*Acetone-d_6* + drop of C_6F_6, 376.5 MHz): -104.96.

Reaction of 1.32●1.42 in melt: The cocrystals **1.32●1.42** (0.030 g, 0.042 mmol) and sodium carbonate (0.35 g, 0.33 mmol) were ground together. The mixture obtained was placed in a test tube and immersed in an oil bath pre-heated to 130 ºC (reaction time 5 h). The reaction mixture was cooled to ambient temperature to obtain a solid. TLC analysis of the solid reveled the presence of major amount of the diol **1.32** and minor amounts of **1.35**, **1.41**, **1.42**. The solid was extracted with ethyl acetate (3X20 mL) and the residue was discarded. Then combined ethyl acetate extract was evaporated under reduced pressure. The residue was column chromatographed (silica gel 100-200 mesh, eluent: ethyl acetate) to isolate the diol **1.32** (0.016 g, 80%). The initial fractions obtained on elution with ethyl acetate – light petroleum (gradient elution) consisted of a mixture of **1.35**, **1.41**, **1.42** which were discarded. This expt revealed that the considerable amount of the diester underwent hydrolysis to yield the diol **1.32** as the major product.

Reaction of 1.32●1.42 in solution: The cocrystals **1.32●1.42** (0.030 g, 0.042 mmol), sodium carbonate (0.035 g, 0.33 mmol) and dry *p*-xylene (2.5 mL) were heated at 100-105 ºC for 72 h. The reaction mixture was concentrated under reduced pressure and the residue worked up as above (as in the solid state reaction). Column chromatographic sepration yielded a mixture of **1.35** and **1.41** (0.012 g, 51%) , the diol **1.32** (0.008 g, 59%) along with minor amount of the diester **1.42** (0.002 g 12%).

Crystal data	**1.32●1.42 at 100K**	**1.32●1.42 at 298K**	**1.32●1.42 at 353K**	**1.32●1.42 at 298K$**	**1.41 at 100K**
Formula	$C_{25}H_{17}O_4F$, $2(C_{10}H_8O_2)$	$C_{25}H_{17}O_4F$, $2(C_{10}H_8O_2)$	$C_{25}H_{17}O_4F$, $2(C_{10}H_8O_2)$	$C_{25}H_{17}O_4F$, $2(C_{10}H_8O_2)$	$C_{17}H_{11}O_3F_1$
M_r	720.71	720.71	720.71	720.71	282.26
Crystal size, mm	0.58 × 0.15 × 0.10	0.45 × 0.34 × 0.23	0.68 × 0.15 × 0.10	0.72 × 0.23 × 0.22	0.31 × 0.24 × 0.17
Temp. (*K*)	100(2)	296(2)	353(2)	296(2)	100(2)
Crystal system	orthorhombic	orthorhombic	orthorhombic	orthorhombic	Monoclinic
space group	*Pbcn*	*Pbcn*	*Pbcn*	*Pbcn*	$P2_1/c$
a [Å]	7.4293(2)	7.6234(8)	7.6930(18)	7.615(2)	9.5284(2)
b [Å]	31.4440(10)	31.556(4)	31.559(8)	31.572(10)	18.8191(4)
c [Å]	15.2990(5)	15.2927(16)	15.328(4)	15.309(5)	7.40220(10)
β[°]	90	90	90	90	102.1590(10)
V [Å^3]	3573.95(19)	3678.9(7)	3721.4(16)	3680.9(19)	1297.56(4)
Z	4	4	4	4	4
F(000)	1504	1504	1504	1504	584
D_{calc} [g cm^{-3}]	1.339	1.301	1.231	1.301	1.445
μ [mm^{-1}]	0.095	0.092	0.091	0.092	0.108
Ab.correction T_{min} T_{max}	multi-scan 0.9473 0.9905	multi-scan 0.963 0.979	multi-scan 0.9405 0.9909	multi-scan 0.9365 0.9800	multi-scan 0.9672 0.9818
$2\theta_{max}$	50.50	57.00	50.00	50.00	51.00
reflns. collected	23080	19681	102578	15112	13544
Unique reflns.	3246	4611	3285	3248	2412
Observed reflns.	2976	2236	1678	2413	2120
h, k, l (min, max)	(-8, 8), (-34, 37), (-18, 13)	(-9, 10), (-17, 42), (-20, 20)	(-9, 9), (-37, 37), (-18, 18)	(-7, 9), (-37, 18), (-18, 11)	(-11, 11), (-22, 22), (-8, 8)
R_{int}	0.0256	0.0440	0.1912	0.0287	0.0278
No. of para	315	257	255	257	195
R_1 [I>2σ(I)]	0.0484	0.0538	0.0651	0.0440	0.0307
wR_2 [I>2σ(I)]	0.1114	0.1190	0.1147	0.1039	0.0709
R_1 (all data)	0.0528	0.1308	0.1398	0.0629	0.0360
WR_2 (all data)	0.1134	0.1463	0.1482	0.1143	0.0739
goodness-of-fit	1.279	1.013	1.098	1.066	1.021
$\Delta\rho_{max}$,$\Delta\rho_{min}$(eÅ^{-3})	0.207 , -0.176	0.153 , -0.118	0.141 , -0.141	0.153 , -0.111	0.218, -0.179

Table 1.4: Crystallographic data for cocrystal **1.32●1.42** at various temps and **1.41**

	D-H···A	D-H (Å)	H···A (Å)	D···A (Å)	D-H···A (°)	Symmetry codes
1.32●1.42 at 100K	O2-H2A···O4	0.88(3)	1.79(3)	2.673(2)	178(4)	*1-x,y,1/2-z*
	O1-H1A···O2	0.94(3)	1.95(3)	2.761(2)	144(3)	*1-x,-y,1-z*
	C18-H18···O1	1.00(3)	2.43(3)	3.369(3)	156(2)	*x,-y,-1/2+z*
	C12-H12···π (Cg5)	1.029	2.60(2)	3.471(2)	141.9(16)	*x,y,z*
	C14-H14···π (Cg6)	0.975	2.64(2)	3.428(2)	138.0(17)	*x,y,z*
	C5-H5···π(Cg3)	0.955	2.85(2)	3.588(2)	135.2(17)	*1+x,y,z*
	C5-H5···π(Cg3)	0.955	2.85(2)	3.588(2)	135.2(17)	*1-x,y,1/2-z*
1.32●1.42 at 298K	O2-H2A···O4	0.82	1.87	2.691(2)	177	*1-x,y,3/2-z*
	O1-H1A···O2	0.82	2.10	2.790(2)	142	*1-x,1-y,2-z*
	C18-H18···O1	0.93	2.56	3.417(3)	153	*x,1-y,-1/2+z*
	C12-H12···π (Cg5)	0.93	2.74	3.5587(19)	148	*x,y,z*
	C14-H14···π (Cg6)	0.93	2.75	3.505(2)	139	*x,y,z*
	C5-H5···π(Cg3)	0.929	2.92	3.671(3)	138	*1+x,y,z*
	C5-H5···π(Cg3)	0.929	2.92	3.671(3)	138	*1-x,y,3/2-z*
1.32●1.42 at 353K	O2-H2A···O4	0.82	1.88	2.701(3)	177	x,-y,-1/2+z
	O1-H1A···O2	0.82	2.14	2.799(4)	137	*1-x,-y,1-z*
	C18-H18···O1	0.929	2.605	3.446	150.69	1- *x, y,* 3/2- *z*
	C12-H12···π (Cg5)	0.931	2.77	3.597(4)	148	*1-x,-y,1-z*
	C14-H14···π (Cg6)	0.929	2.77	3.535(4)	140	*1-x,-y,1-z*
	C5-H5···π(Cg3)	0.929	2.94	3.698(4)	140	*2-x,-y,1-z*
	C5-H5···π(Cg3)	0.929	2.94	3.698(4)	140	*x,-y,-1/2+z*
1.32●1.42 at 298K$	O2-H2A···O4	0.82	1.87	2.691(2)	177	*-1+x,1-y,-1/2+z*
	O1-H1A···O2	0.82	2.10	2.791(2)	142	*-x,2-y,-z*
	C18-H18···O1	0.93	2.57	3.417(3)	153	*1-x,-1+y,1/2-z*
	C12-H12···π (Cg5)	0.93	2.74	3.562(2)	148	*1-x,1-y,1-z*
	C14-H14···π (Cg6)	0.929	2.75	3.505(3)	139	*1-x,1-y,1-z*
	C5-H5···π(Cg3)	0.93	2.92	3.669(3)	138	*-x,1-y,1-z*
	C5-H5···π(Cg3)	0.93	2.92	3.669(3)	138	*-1+x,1-y,-1/2+z*
1.41	O2-H2A···O3	0.880(15)	1.845(15)	2.7135(12)	168.6(14)	*x,3/2-y,-1/2+z*
	C3-H3···π (Cg1)	0.950	2.90	3.7178(12)	145	*x,3/2-y,-1/2+z*
	C5-H5···π (Cg2)	0.950	2.69	3.4218(12)	134	*x,3/2-y,-1/2+z*
	C8-H8···π (Cg3)	0.950	2.92	3.6470(12)	135	*-1+x,y,z*
	π (Cg3)···π (Cg3)			3.8249(7)	0	*2-x,2-y,1-z*

α = Dihedral angle between phenyl rings, Cg is the centroid of the ring, In **1.32●1.42** ocrystal Cg3 = C(13) - C(13)a, Cg5 = C1 – C10, Cg6 = C4 – C9;In **1.41** Cg1=C1- C10, Cg2=C4- C9, Cg1=C12- C17. $=**1.32●1.42** heated to 373K and cooled to 298K

Table1.5: Geometrical parameters for intermolecular interactions in cocrystals of **1.32●1.42** at different temperatures and **1.41**.

	1.40	**1.42**	**1.45**	**1.46**	**1.48**	**1.49**
Chemical formula	$C_{17}H_{12}O_3$	$C_{25}H_{17}FO_4$	$C_{20}H_{16}O_4$	$C_{24}H_{16}O_4$	$C_{24}H_{14}Cl_2O_4$	$C_{14}H_{12}O_4$
M_r	264.27	400.39	320.33	368.37	437.25	244.24
Temperature (K)	297(2)	297(2)	296(2)	297(2)	100(2)	100(2)
Morphology	plate	Plate	Needle	Plate	Needle	Plate
Crystal size (mm)	0.29 × 0.260 × 0.05	0.39 × 0.11 × 0.07	0.43 × 0.32 × 0.17	0.72 × 0.12 × 0.09	0.30×0.23×0.21	0.45 × 0.34 × 0.21
Crystal system	Orthorhombic	Monoclinic	Monoclinic	Orthorhombic	Orthorhombic	Monoclinic
Space group	*Pca*2_1	*P*2_1/*c*	*P*2_1/*c*	*Pbcn*	*Pcca*	*C*2/*c*
a (Å)	12.035(4)	12.434(3)	9.2744(9)	17.587(2)	19.3833(14)	18.3645(10)
b (Å)	14.519(5)	9.793(3)	10.5202(9)	13.9460(17)	14.6136(10)	9.1236(5)
c (Å)	7.522(3)	20.175(4)	19.4402(14)	7.4996(10)	7.0200(4)	14.6229(8)
α (°)	90	90	90	90	90	90
β (°)	90	125.510(10)	118.494(3)	90	90	104.720(3)
γ (°)	90	90	90	90	90	90
V (Å^3)	1314.4(8)	1999.7(9)	1667.0(2)	1839.4(4)	1988.5(2)	2369.7(2)
Z D_{calc} (g cm^{-3})	4 1.335	4 1.330	4 1.276	4 1.330	4 1.461	8 1.369
μ(mm^{-1}) *F(000)*	0.091 552	0.096 832	0.089 672	0.090 768	0.356 896	0.101 1024
T_{min} T_{max}	0.9735 0.9954	0.9640 0.9938	0.9628 0.9851	0.9379 0.9924	0.9007 0.9290	0.9561 0.9791
h, k, l (min, max)	(-6,14), (-17,17), (-8,8)	(-14,14), (-11,11), (-23, 19)	(-11,11), (-12,12), (-23,23)	(-19,20), (-16,14), (-8,8)	(-23,21) (-16,17) (-8,7)	(-21,22), (-11,11), (-17,17)
Reflns collected	6276	9753	17327	8568	15506	8554
Unique reflns	2229	3513	2363	1621	1811	2202
Observed reflns R_{int}	1911 0.0320	2112 0.0334	1624 0.0352	1376 0.0364	1501 0.0354	1857 0.0195
No. of parameters	185	272	220	127	136	166
GoF	1.182	1.109	0.979	1.058	1.187	1.032
$R_1[I > 2\sigma(I)]$	0.0544	0.0757	0.0371	0.0420	0.0481	0.0304
$WR_2[I > 2\sigma(I)]$	0.1229	0.1498	0.1002	0.0996	0.1028	0.0753
R_1_all data	0.0662	0.1302	0.0594	0.0501	0.0621	0.0385
Wr_2_all data	0.1383	0.1681	0.1094	0.1040	0.1112	0.0812
$\Delta\rho_{max}$, $\Delta\rho_{min}$ (e Å^{-3})	0.22, -0.18	0.16, -0.15	0.107, -0.097	0.13, -0.24	0.310, -0.406	0.225,-0.160

Table 1.6: Crystallographic data table of mono and diesters of naphthalene 2,3 diol.

Crystal	D-H···A	D-H (Å)	H···A (Å)	D···A (Å)	D-H···A /α (°)	Symmetry codes
1.40	O2-H2*A*···O3	0.89(7)	1.86(7)	2.728(5)	165(5)	*3/2-x,y,1/2+z*
	C5-H5···Cg2	0.93	2.82	3.539(5)	135	*3/2-x,y,1/2+z*
	C10-H10···Cg2	0.93	2.81	3.530(5)	136	*1-x,1-y,-1/2+z*
	C15-H15...O3	0.93	2.79	3.615(6)	148	*-1/2+x,2-y,z*
	C16-H16...O2	0.93	2.80	3.399(6)	123	*1-x,2-y,-1/2+z*
1.42	C18-H18*C*···Cg1	0.96	2.90	3.702(5)	141	*x,3/2-y,1/2+z*
	C6-H6...F1	0.93	2.69	3.454	140	*x,3/2-y,-1/2+z*
	Cg4...Cg4			3.980(3)	0	*1-x,1-y,2-z*
1.45	C13-H13···πCg2	0.929	2.72	3.595(2)	158	*1+x,y,z*
	C14-H14···πCg1	0.929	2.96	3.700(2)	138	*1+x,y,z*
1.46	C9-H9···O2	0.93	2.71	3.338(2)	125	*1/2-x,1/2+y,z*
	C12-H12···Cg1	0.93	2.79	3.4710(17)	131	*1-x,-y,1-z*
1.48	C12-H12...O2	0.95	2.34	3.212(3)	153	*3/2-x,1-y,z*
	C2-H2···πCg3	0.95	2.98	3.668(3)	130	*x,1-y,1/2+z*
	C8-H8···πCg1	0.95	2.71	3.347(3)	125	*1-x,1-y,1-z*
	C8-H8···πCg1	0.95	2.71	3.347(3)	125	*x,1-y,1/2+z*
	C9-H9···πCg2	0.95	2.85	3.565(3	133	*1-x,1-y,1-z*
	C9-H9···πCg2	0.95	2.85	3.565(3	133	*x,1-y,1/2+z*
1.49	C14-H14*C*···O3	0.98	2.45	3.4099(16)	168	*x,-y,1/2+z*
	C12-H12*B*···πCg1	0.98	2.98	3.6253(14)	125	*1/2-x,-1/2+y,1/2-z*
	πCg1···πCg2			3.9921(7)	2.23(6)	*-x,1-y,-z*
	πCg2···πCg1			3.9922(7)	2.23(6)	*-x,1-y,-z*
	α = Dihedral angle between phenyl rings, Cg is the centroid of the phenyl ring In **1.40** Cg2 = C4 – C9; In **1.42** Cg1 = C1 – C10; Cg4 = C20 – C25; In **1.46** Cg1 = C1 – C1A, Cg2 = C3 – C3A; In **1.48**, Cg1 = C1 – C(1)a, Cg2 = C3 – C(3)a, Cg3 = C7 – C12; In **1.49** and **1.45** Cg1 = C1 – C10, Cg2 = C4 – C9.					

Table1.7: Geometrical parameters for intermolecular interactions table for mono and diesters of naphthalene 2,3 diol.

References:

[1] (a) S. Patai series of books; (b) R. C. Larock, *Comprehensive Organic Transformation,* Wiley -VCH **1999**.

[2] (a) V. Ramamurthy, K. Venkatesan, *Chem. Rev.***1987**, *87,*433-481; (b)Y. Ohashi, *Reactivity in Molecular Crystals*, WILEY -VCH, Weinheim, **1993**.

[3] H. Kanazawa, Y. Ohashi, *Mol. Cryst. Liq. Cryst.* **1996**, *277*, 45-54.

[4] I. Rubinstein, G. Clodic, G. Bolbach, I. Weissbuch, M. Lahav, *Chem. Eur. J.* **2008**, *14*, 10999-11009.

[5] A. E. Keating, M. A. Garcia-Garibay, *Mol. Supramol. Photochem*. **1998**, *2,* 195-248.

[6] D. Braga, F. Grepioni, *Angew. Chem. Int. Ed.* **2004**, *43,* 4002-4011.

[7] A. E. Troup, H. Mitchner, *J. Pharm. Sci.* **1964**, *53,* 375-379.

[8] A. L. Jacobs, A. E. Dilatush, S. Weinstein, J. J. Windheuser, *J. Pharm. Sci.* **1966***, 55,* 893-895.

[9] K. T. Koshy, A. E. Troup, R. N. Duvall, R. N. Conwell, L. L. Shankle, *J. Pharm. Sci.* **1967**, *56,* 1117-1121.

[10] R. S. Sardessai, S. Krishnaswamy, M. S. Shashidhar, *CrystEngComm*. **2012**, *14,* 8010 - 8016.

[11] M. D. Cohen, G. M. J. Schmidt, *J. Chem. Soc*. **1964**, 1996-2000.

[12] M. D. Cohen, G. M. J. Schmidt, F. I. Sonntag, *J. Chem. Soc.* **1964**, 2000-2013.

[13] G. M. J. Schmidt, *J. Chem. Soc.* **1964**, 2014-2021.

[14] (a) L. R. MacGillivray, G. S. Papaefstathiou, T. Friščić, D. B. Varshney, T. D. Hamilton, *Top. Curr. Chem.* **2004**, *248,* 201-221; (b) T. Friščić, L. R. MacGillivray, *Croatica Chemica Acta*, **2006**, *79*, 327-333 and reference cited in.

[15] J. Yang, M. B. Dewal, S. Profeta, Jr. M. D. Smith, Y. Li, L. S. Shimizu, *J. Am. Chem. Soc.* **2008**, *130,* 612-621.

[16] L. R. Macgillivray, G. S. Papaefstathiou, T. Friščić, T. D. Hamilton, D.-K. Bucar, Q. Chu, D. B. Varshney, I. G. Georgiev, *Acc. Chem. Res.* **2008**, *41,* 280-291.

[17] M. W. Ghosn, C. Wolf, *J. Org. Chem.* **2010**, *75,* 6653-6659.

[18] M. H. Mir, L. L. Koh, G. K. Tan, J. J. Vittal, *Angew. Chem. Int. Ed.* **2010**, *49,* 390-393.

[19] A. Gavezzotti, M. Simonetta, *Nouv. J. Chim.* **1978**, *2,* 69-72.

[20] P. Venugopalan, K. Venkatesan, J. Klausen, E. Novotny-Bregger, C. Leumann, A. Eschenmoser, J. D. Dunitz, *Hel*v. *Chim. Acta.* **1991**, 74, 662-669.

[21] R. Sekiya, K. Kiyo-oka, T. Imakubo, K. Kobayashi, *J. Am. Chem. Soc.* **2000**, *122,* 10282-10288.

[22] K. Tanaka, A. Tomomori, J. L. Scott, *Eur. J. Org. Chem.* **2003**, 2035-2038.

[23] K. M. Sureshan, T. Murakami, T. Miyasou, Y. Watanabe, *J. Am. Chem. Soc.* **2004**, *126,* 9174-9175.

[24] M. L. Cheney, G. J. McManus, J. A. Perman, Z. Wang, M. J. Zaworotko, *Cryst. Growth Des.* **2007**, *7,* 616-617.

[25] A. J. Gordon, *Tetrahedron*, **1967**, *23,* 863-870.

[26] K. Vyas, H. Manohar, K. Venkatesan, *J. Phys. Chem.* **1990**, *94,* 6069-6073.

[27] T. Praveen, U. Samanta, T. Das, M. S. Shashidhar, P. Chakrabarti, *J. Am. Chem. Soc*. **1998**, *120,* 3842-3845.

[28] C. Murali, M. S. Shashidhar, R. G. Gonnade, M. M. Bhadbhade, *Chem. Eur. J.* **2009**, *15,* 261-269.

[29] M. P. Sarmah, R. G. Gonnade, M. S. Shashidhar, M. M. Bhadbhade, *Chem. Eur. J.* **2005**, *11,* 2103-2110.

[30] S. Krishnaswamy, R. G. Gonnade, M. S. Shashidhar, M. M. Bhadbhade, *CrystEngComm*. **2010**, *12,* 4184-4197.

[31] S. Krishnaswamy, M. S. Shashidhar, M. M. Bhadbhade, *CrystEngComm*. **2011**, *13,* 3258-3264.

[32] H. B. Bürgi, J. D. Dunitz, *Acc. Chem. Res.* **1983**, *16,* 153-161.

[33] D. R. Storm, D. E. Koshland, *J. Am. Chem. Soc.* **1972**, *94,* 5815-5825.

[34] M. L. Bender, *Chem. Rev.* **1960**, *60,* 53-113.

[35] I. Weissbuch, L. Leiserowitz, M. Lahav, *Top. Curr. Chem.* **2005**, *259*, 123–165.

[36] G. R. Desiraju, T. Steiner, *The Weak Hydrogen Bond in Structural Chemistry and Biology*, Oxford University Press: Oxford, **1999**.

[37] J. Bernstein, M. C. Etter, L. Leiserowitz in *Structure Correlation: The role of hydrogen bonding in Molecular Assemblies,* Vol. 1 (Eds: H. B. Bürgi, J. D. Dunitz), WILEY-VCH, Weinheim, **2008**, pp. 431-507

[38] M. Nishio, Y. Umezawa, K. Honda, S. Tsuboyama, H. Suezawa, *CrystEngComm,* **2009**, *11*, 1757-1788.

[39] R. Boese, T. Clark, A. Gavezzotti, *Helv. Chim. Acta,* **2003**, *86*, 1085-1100.

[40] M. Chino, K. Nishikawa, T. Tsuchida, R. Sawa, H. Nakamura, K. T. Nakamura, Y. Muraoka, D. Ikeda, H. Naganawa, T. Sawa, T. Takeuchi, *J. Antibiot*. **1997**, *50*, 143-146.

[41] K. Tanaka, D. Fujimoto, A. Altreuther, T. Oeser, H. Irngartinger, F. Toda, *J. Chem. Soc., Perkin Trans. 2*, **2000**, 2115-2120.

[42] S. Nakamatsu, K. Yoshizawa, S. Toyota, F. Toda, I. Matijasic, *Org. Biomol. Chem*. **2003**, *1*, 2231-2234.

[43] S. A. Talipov, B. T. Ibragimov, K. M. Beketov, K. D. Praliev, T. F. Aripov, *Kristallografiya (Crystallogr. Rep.*), **2004**, *49*, 841-843.

[44] K. Ghosh, M. Datta, R. Frohlich, N. C. Ganguly, *J. Mol. Struct*. **2005**, *737*, 201-206.

[45] H-Y. Peng, C. K. Lam, T. C. W. Mak, Z. Cai, W-T. Ma, Y-X. Li, H. N. C. Wong, *J. Am. Chem. Soc*. **2005**, *127*, 9603-9611.

[46] J-B.Yu, S-W. Chen,G-R. Zheng, L-Y. Dai, *Acta Crystallogr. Sect. E*: *Struct. Rep.* **2008**, *64*, o1653.

[47] G. A. Wallace, T. D. Gordon, M. E. Hayes, D. B. Konopacki, S. R. Fix-Stenzel, X. Zhang, P. Grongsaard, K. P. Cusack, L. M. Schaffter, R. F. Henry, R. H. Stoffel, *J. Org. Chem.* **2009**, *74*, 4886-4889.

[48] E-Y. Xia, J. Sun, R. Yao, C-G. Yan, *Tetrahedron*, **2010**, *66*, 3569-3574.

[49] S. Varughese, G. R. Desiraju, *Cryst. Growth Des*. **2010**, *10*, 4184-4196.

[50] A. Gavezzotti, *Acc. Chem. Res.* **1994**, *27,* 309–314.

[51] M. I. Tamboli, S. Krishnaswamy, R. G. Gonnade, M. S. Shashidhar, *Cryst. Growth Des*. **2014**, *14*, 4985- 4996.

[52] T. Friščić, S. L. Childs, S. A. A. Rizvi, W. Jones, *CrystEngComm*. **2009**, *11,* 418-426.

[53] R. Kuroda, J. Yoshida, A. Nakamura, S. Nishikiori, *CrystEngComm*. **2009**, *11,* 427-432.

[54] T. Friščić, W. Jones, *Cryst. Growth Des.* **2009**, *9,* 1621-1637.

[55] D. P. McNamara, S. L. Childs, J. Giordano, A. Iarriccio, J. Cassidy, M. S. Shet, R. Mannion, E. O'Donnell, A. Park, *Pharm. Res.* **2006**, *23,* 1888-1897.

[56] S. Basavoju, D. Bostrom, S. P. Velaga, *Pharm. Res.* **2008**, *25,*530-541.

[57] D. Daurio, C. Medina, R. Saw, K. Nagapudi, F. Alvarez-Nùñez, *Pharmaceutics*. **2011**, *3,* 582-600.

[58] T. Friščić, W. Jones, *J. Pharm. Pharmacol.* **2010**, *62,* 1547-1559.

[59] T. Itoh, T. Suzuki, T. Uno, M. Kubo, N. Tohnai, M. Miyata, *Angew. Chem. Int. Ed.* **2011**, *50,* 2253-2256.

[60] D. H. Oswald, C. R. Pulham, *CrystEngComm.* **2008**, *10*, 1114-1116.

[61] J. Bernstein, J. J. Novoa, R. Boese, S. Cirkel, *Chem. Eur. J.* **2010**, *16*, 9047-9055.

[62] D. D. Perrin, W. L. F. Armarego, *Purification of Laboratory Chemicals*, 2nd edition, Pergamon Press, Oxford, U.K., **1988**.

[63] *Vogel's Textbook of Practical Organic Chemistry*, 5th edition, Longman, UK, **1989**.

[64] M. I. Tamboli, S. Krishnaswamy, M. S. Shashidhar, R. G. Gonnade, *Chem. Eur. J.* **2013**, 19, 12867-12874.

[65] Bruker (**2003**). SADABS Version 2.05, SMART Version 5.631 and SAINT Version 6.45. Bruker AXS Inc., Madison, Wisconsin, USA.

[66] Bruker (**2006**). *APEX2*, *SAINT* and *SADABS*. Bruker AXS Inc., Madison, Wisconsin, USA.

[67] G. M. Sheldrick, *Acta Crystallogr.* **2008**, A*64*, 112-122.

[68] L. J. Farrugia, *J. Appl. Crystallogr.* **1997**, *30*, 565.

[69] C. F. Macrae, P. R. Edgington, P. McCabe, E. Pidcock, G. P. Shields, R. Taylor, M. Towler and J. van de Streek, *J. Appl. Crystallogr.* **2006**, *39*, 453-457

[70] A. L. Spek, *J. Appl. Crystallogr.* **2003**, *36*, 7-13.

Appendix I given in Pen Drive, along with Thesis

List of the content in Appendix I

Chapter 2

Intramolecular cyclization of carbonate and thiocarbonate derivatives of *myo*-inositol 1,3,5-orthoformate in the solid state: Implications for acyl group transfer reactions in molecular crystals.

Most of the work reported in this thesis is published in

M. I. Tamboli, M. S. Shashidhar, R. G. Gonnade, S. Krishnaswamy, Intramolecular cyclization of carbonate and thiocarbonate derivatives of *myo*-inositol in the solid state: Implications for acyl group transfer reactions in molecular crystals, *Chem. Eur. J.* **2015**, *21*, 13676-13682.

Introduction:

Addition of a nucleophile to a carbonyl group is the primary step for the transformation of several organic chemical functional groups in living and nonliving ensemble of molecules. Nucleophilic addition to a carbonyl group followed by elimination retains the sp^2 hybridized carbonyl carbon, leading to transacylation reactions (such as esterification, transesterification, amidation, hydrolysis of esters and amides). Perhaps thousands of publications in journals have resulted from the investigation of these reactions in the solution state and in living systems. However this fundamental process of nucleophilic addition to carbonyl groups has seldom been observed in the solid state. This could be mainly due to the difficulty in identifying molecular solids that undergo specific chemical reactions and the uncertainty in obtaining solids (amorphous or crystalline) with desired specific (chemical) properties. Consequently, most known chemical reactions in molecular solids in general and crystals in particular[1] are serendipitous observations or results of random (or at best educated guess) experimentation.

However, results described in previous chapters do show that certain crystal structure parameters based on non-covalent intermolecular interactions can be used to identify other molecular crystals that facilitate intermolecular acyl transfer reactions.[2] This required the investigation of acyl transfer reaction in analogues and derivatives of *myo*-inositol orthoesters (see references cited in reference 2). As a part of this study, we prepared carbonate and thiocarbonate derivatives of *myo*-inositol orthoformate and investigated their ability to undergo heat induced acyl transfer reaction in the solid state (as well as in solution and molten states, for comparison). It is pertinent to note that these derivatives have one oxygen atom extra [$R^1OC(O)OR^2$ or $R^1OC(S)OR^2$] in the vicinity of the carbonyl or the thio carbonyl group, as compared to esters [R^1COOR^2], which were the subject of study in the previous chapter. These carbonates and thiocarbonates underwent intramolecular cyclization in the solid state to provide the corresponding C4,C6-bridged carbonate and thiocarbonate derivatives of *myo*-inositol orthoformate. The single crystal X-ray diffraction structures of two of the carbonates and a thiocarbonate revealed the reason for the facility of intramolecular cyclization reaction and the non-occurrence of intermolecular acyl-transfer in these molecular solids. The present chapter attempts to arrive at a

correlation between crystal structure and specific chemical reactivity in these molecular solids. This could have wider implications for the development of solid state organic reactions as a tool for organic synthesis. Synthesis of C4,C6 bridged inositol derivatives by classical solution state synthesis have earlier been attempted due to their application potential in biology and in the development of functional materials.[3]

Results and Discussion:

The racemic carbonate and thiocarbonate derivatives **2.2**-**2.7**, of *myo*-inositol orthoformate **2.1** were prepared as shown in Scheme 2.1, with prior knowledge of the regioselectivity of *O*-substitution of the hydroxyl groups of the triol **2.1** under different reaction conditions.[4]

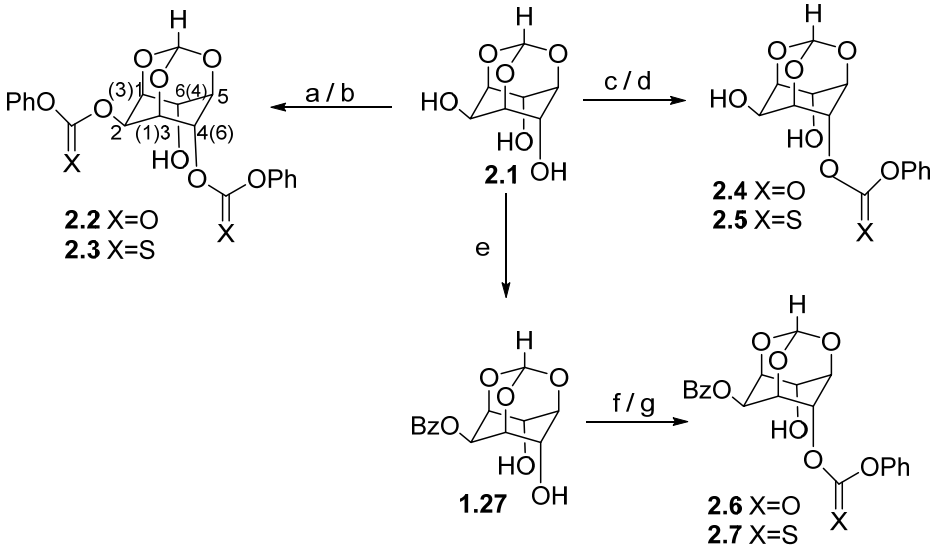

Scheme 2.1: (a) Pyridine, PhOCOCl (3 eq), -5 ^{o}C- rt, 1 h, 79%; (b) Pyridine, PhOCSCl (2.2 eq), -5 ^{o}C- rt, 2 h, 69 %; (c) PhOCOCl (1.2 eq), Et_3N, DMF, -5 ^{o}C- rt, 30 min., 64%; (d) PhOCSCl (1.2 eq), Et_3N, DMF, -5 ^{o}C- rt, 30 min., 66%; (e) PhCOCl, pyridine as in reference 4; (f) PhOCOCl (1.4 eq), Et_3N, DMF, -5 to 0 ^{o}C, 30 min, 55%; (g) PhOCSCl (1.3 eq), Et_3N, DMF, -5 to 0 ^{o}C, 30 min, 52%.

The regioselectivity of the reaction of the triol **2.1** can be controlled exploiting (a) the presence of intramolecular hydrogen bonding between the C4- and C6-hydroxyl groups; and (b) the ability of *O*-substituted derivatives of the orthoformate **2.1** to chelate with metal ions (Scheme 2.2). [4]

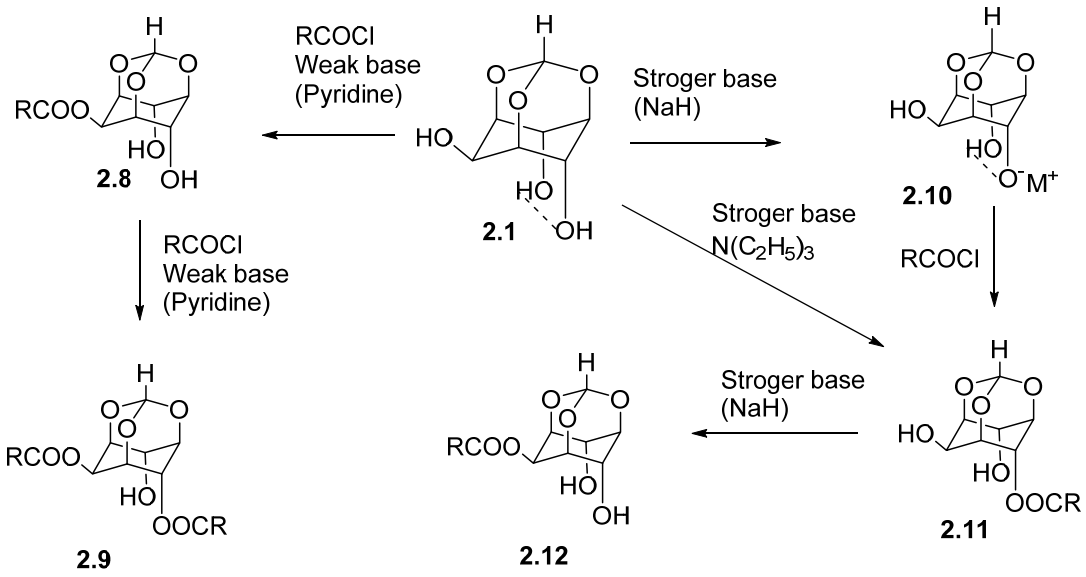

Scheme 2.2: The regioselectivity of the reaction of the triol **2.1** under different reaction conditions.

The carbonates **2.4**, **2.6** and the thiocarbonate **2.7** crystallized in the monoclinic crystal system (space group $P2_1/c$, Z' = 1) but **2.2** and **2.5** could not be obtained in the crystalline form. The thiocarbonate **2.3** crystallized as benzene solvate in one of the attempts at its crystallization, but this crystalline solvate could not be obtained again. Crystal structure data is given in (Table A2, Appendix II).

The melting point of the carbonates and thiocarbonates varied to considerable extent when determined more than once for the same sample, indicating irreversible change in these solids due to heating. The thiocarbonate **2.5** melted between 146 and 150 ^{o}C and subsequently turned to a solid which melted (with decomposition) finally between 260 and 280 ^{o}C suggesting a drastic change in the composition of **2.5**. These observations were substantiated by the DSC profiles of **2.2**-**2.5**, and **2.7**, which were broad and consisted of more than one endotherm.

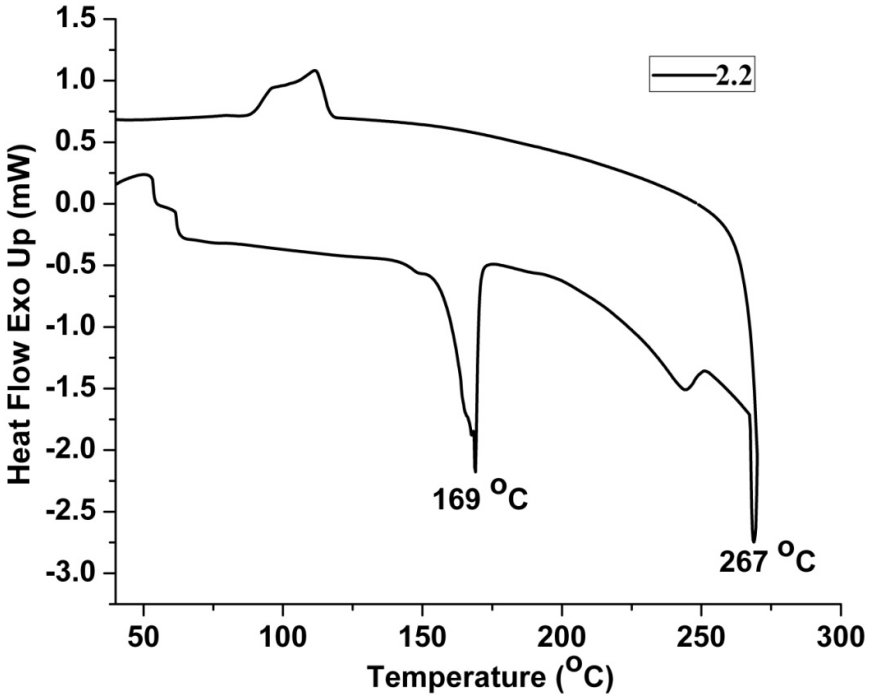

Figure 2.1: The DSC profile of the dicarbonate **2.2**. See Figures A68-A82 in Appendix II for DSC of other carbonates and thiocarbonates.

These DSC profiles suggested physical and/or chemical changes on heating solid carbonates and thiocarbonates. The PXRD pattern of the heated (below the melting point) samples of **2.4** matched quite well with the PXRD pattern of the cyclic carbonate **2.15** indicating the occurrence of cyclization in the crystalline state.

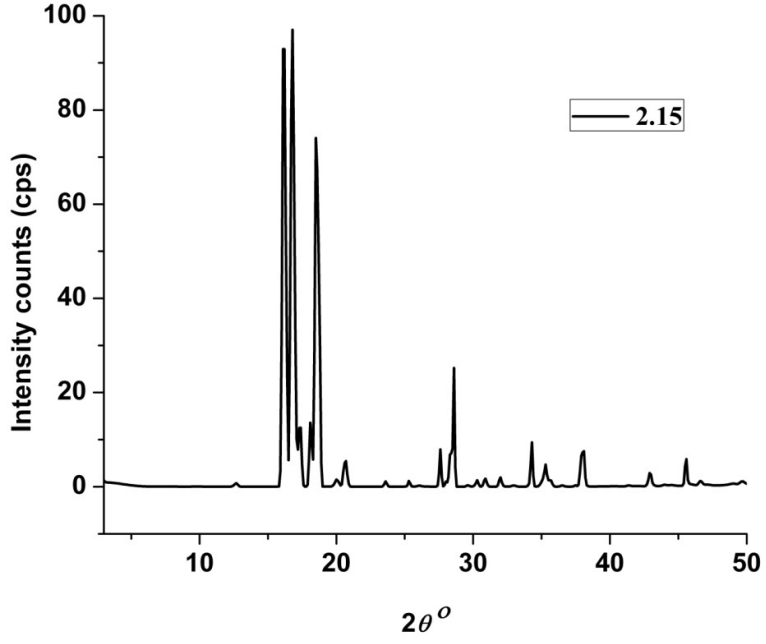

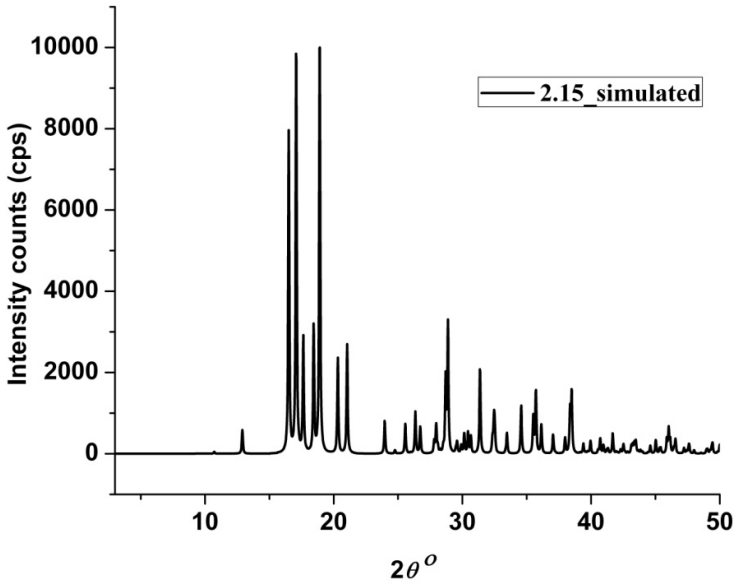

Figure 2.2: The PXRD profile of the product (**2.15**) before purification) obtained by heating **2.4** (top) and PXRD of **2.15** simulated (bottom) from single crystal X-ray diffraction data. (See Figure A83-A98 in Appendix II for PXRD of other carbonates and thiocarbonates).

All the carbonates and thiocarbonates except **2.3** reacted in the solid state below their respective melting point to yield the corresponding cyclic carbonates and thiocarbonates. This cyclization reaction occurred with the elimination of phenol. ^{1}H NMR spectrum of the mixture of products (before isolation of the cyclic carbonate or thiocarbonate) revealed signals due to the presence of phenol. However no attempt was made to isolate phenol, after the cyclization reaction. (Figures A28-A31, Appendix II).

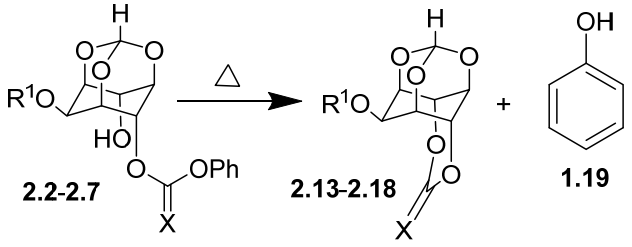

2.2, **2.13** X=O, R^1 = C_6H_5OC=O
2.3, **2.14** X=S, R^1 = C_6H_5OC=S
2.4, **2.15** X=O, R^1 = H
2.5, **2.16** X=S, R^1 = H
2.6, **2.17** X=O, R^1 = C_6H_5C=O
2.7, **2.18** X=S, R^1 = C_6H_5C=O

Scheme 2.3: Intramolecular cyclization reaction in carbonate and thiocarbonates.

Starting material, g, mmol (mp ^{o}C)	Conditions, time h (°C)	Product (yield %)
2.2, 0.05, 0.116, (168-170)	Solid, 48 (160-165)	**2.13** (91)
	Melt, 5 (220-230)	**2.13** (85)
2.2, 0.03, 0.07	Refluxing *p*-xylene, 48	**2.13** (55-60)
2.3, 0.05, 0.108, (94-102)	Solid, 48 (80-85)	None
	Melt, 1 (155-160)	**2.14** (77)
2.3, 0.03, 0.065	Refluxing *p*-xylene, 48	**2.14** (45-50)
2.4, 0.05, 0.154, (178-180)	Crystals, 48 (160-165)	**2.15** (85)
2.4, 0.02, 0.061	Melt, 5 (220-230)	**2.15** (83)
2.4, 0.03, 0.092	Refluxing *p*-xylene, 48	**2.15** (50-55)
2.5, 0.05, 0.147, (148-150)	Solid, 48 (130-131)	**2.16** (79)
	Melt, 1 (165-170)	**2.16** (83)
2.5, 0.03, 0.088,	Refluxing *p*-xylene, 48	**2.16** (50-55)
2.6, 0.02, 0.048, (166-167)	Crystals, 48 (158-160)	**2.17** (85)
	Melt, 1 (190)	**2.17** (87)
	Refluxing *p*-xylene, 48	**2.17** (55-60)
2.7, 0.02, 0.046, (162-164)	Crystals, 48 (155-157)	**2.18** (84)
	Melt, 1 (190)	**2.18** (82)
	Refluxing *p*-xylene, 48	**2.18** (45-50)

Table 2.1: Results on the thermal cyclization of carbonates and thiocarbonates derived from the triol **2.1**.

The yield of cyclized products were between 79% and 91% (Scheme 2.3, Table 2.1) at temperatures at least 5 ^{o}C below their melting points. Since both the starting carbonates and thiocarbonates as well as the resulting cyclic carbonates and thiocarbonates have higher melting points than the reaction temperature, involvement of molten phases during the reaction is unlikely. For instance an equimolar ground mixture of the thiocarbonate **2.5** (melting point 148-150 °C, reaction temperature 130-131 °C) and the product (cyclic thiocarbonate **2.16**), although showed signs of melting between 140-144 °C, did not melt completely till 290 °C. Based on the thermal analysis data and the PXRD data it was not possible to ascertain how the

reaction progresses in the solid state or the effect of the changes in the composition of the reaction mixture (in terms of relative proportion of the reactant and products) on the progress of the reaction. However, these factors are not a major concern since the cyclization reaction involved is an intramolecular reaction.

The thiocarbonate **2.3** failed to react below its melting point; the cyclization took place only in the molten state. The intramolecular cyclization reaction of other carbonates and thiocarbonates was also facile in the molten state (yield 77-87%) but relatively less facile in the solution state (yield of cyclic carbonate 45-60%). The occurrence of the cyclization reaction in fluid phases indicated that the topochemical control was not absolutely essential for the progress of the cyclization reaction. However, comparison of the yields in three different phases for the thiocarbonate **2.5** showed that the efficiency of cyclization was compromised by the intervention of the solvent. This can be concluded from the higher yield of **2.16** (79%) obtained in the solid state reaction at a lower temperature (130-131 °C, 48 h) as compared to the yield (50-55%) in the solution state reaction (bp of the solvent *p*-xylene, 138.4 °C, 48 h). Similarly, between the solid and the molten state reactions, although the difference in reaction temperature is about 30 °C the yields are similar. Hence, although these cyclization reactions are not strictly topochemically controlled, the molecular pre-organization in crystals appears to aid the cyclization reaction.

Earlier work in our laboratory had shown that racemic 2,4-di-*O*-benzoyl-*myo*-inositol orthoesters exhibited facile intermolecular acyl transfer reactivity in their crystals.[5,6] It is interesting to see that extension of the ester moiety by insertion of an oxygen atom (resulting in the corresponding carbonate and thiocarbonate derivative) resulted in intramolecular reaction in these molecular crystals. These cyclization reactions did not need the assistance of a base which is in contrast to the intermolecular acyl group migration reactions in molecular crystals of racemic 2,4-di-*O*-benzoyl-*myo*-inositol orthoesters, which required the presence of a base to initiate the reaction in the crystal lattice.[6] The cyclization reaction in the solution state was however hastened in the presence of a base (such as triethyl amine). This was apparent during the preparation of **2.6** and **2.7**, since longer reaction time and/or higher temperature (>45 °C) during the work-up procedure led to the formation of the corresponding cyclic carbonate **2.17** and thiocarbonate **2.18** respectively.

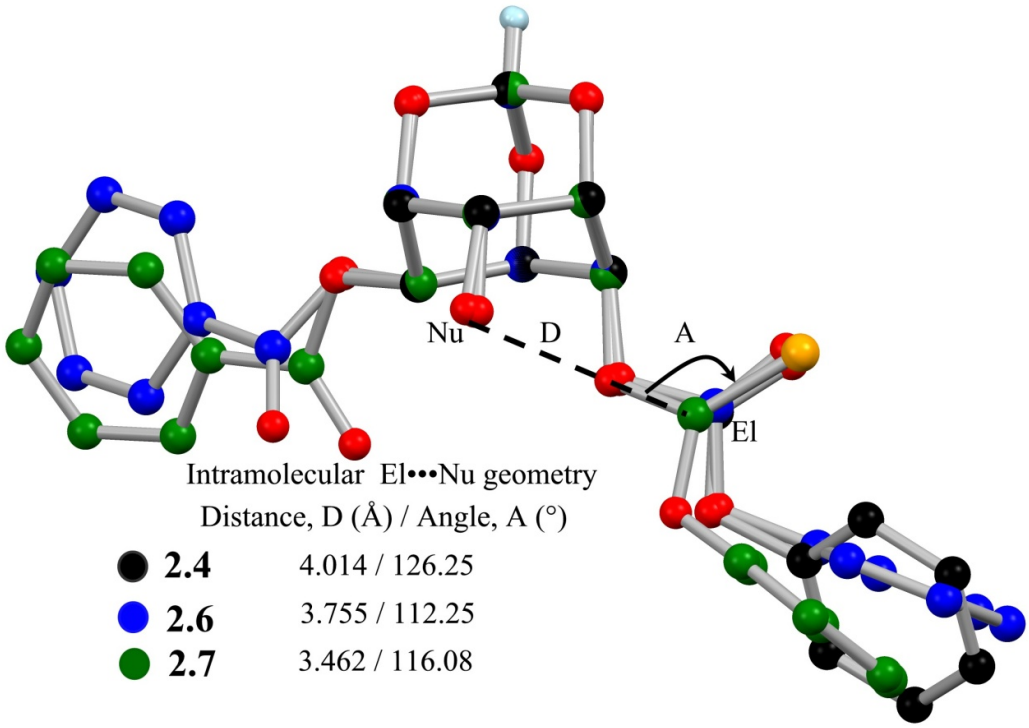

Figure 2.3: Overlap of molecules present in crystals (at 23 °C) of carbonates **2.4**, **2.6** and the thiocarbonate **2.7** revealing intramolecular El···Nu geometry. Hydrogen atoms are not shown for clarity.

The conformation of individual molecules (Figure 2.3) in crystals of **2.4**, **2.6** and **2.7** revealed the reason for the ease of their cyclization (Scheme 2.3). The geometrical parameters for the intramolecular El···Nu (O=C···OH or S=C···OH) interactions reveal proximity of the reacting groups in an orientation that facilitates cyclization. The X-ray diffraction analysis of a crystal of **2.4** at different temperatures (-173, 23, 80, 100 and 120 °C) revealed that the relative orientation of the El···Nu varied only slightly on heating (Figure 2.4).

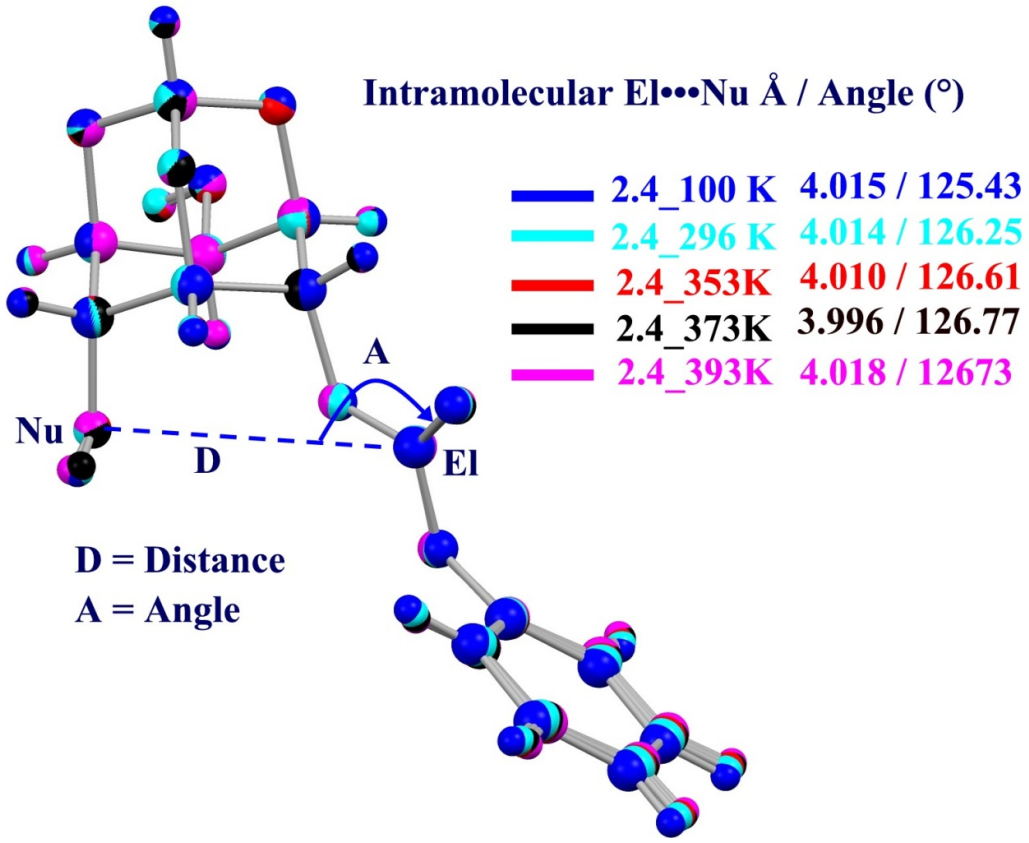

Figure 2.4: Structural overlay of molecules of **2.4** at different temperatures in their crystal shows that there is not much variation in the relative orientation of the nucleophile (OH) and the electrophile (C=O) within each molecule.

At higher temperature (140 °C) X-ray diffraction pattern was diffused due to high mosaicity of the crystal. The intramolecular geometry for the El···Nu interaction (Figure 2.3) is slightly different as compared to that reported in other molecular crystals that support intramolecular acyl transfer (Scheme 2.4)[7] and intramolecular cyclization in the solid state Scheme 2.5.[8]

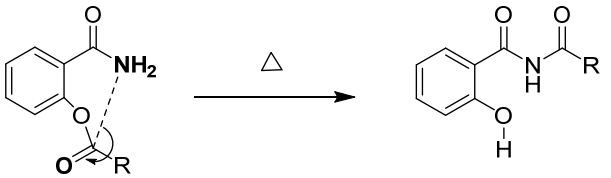

1.11 R = CH_3 t ~ 100 °C **1.14** R = CH_3
1.12 R = C_6H_5 t ~ 100 °C **1.15** R = C_6H_5
1.13 R = C_2H_5 t ~ 85 °C **1.16** R = C_2H_5

Compound	Distance Nu…El (Å)/ angle Nu…El (°)
1.11	3.274(6) / 101.7
1.12	3.528(3) / 116.1
1.13	3.34 / 110.6

Scheme 2.4: Intramolecular acyl transfer reaction in solid state.

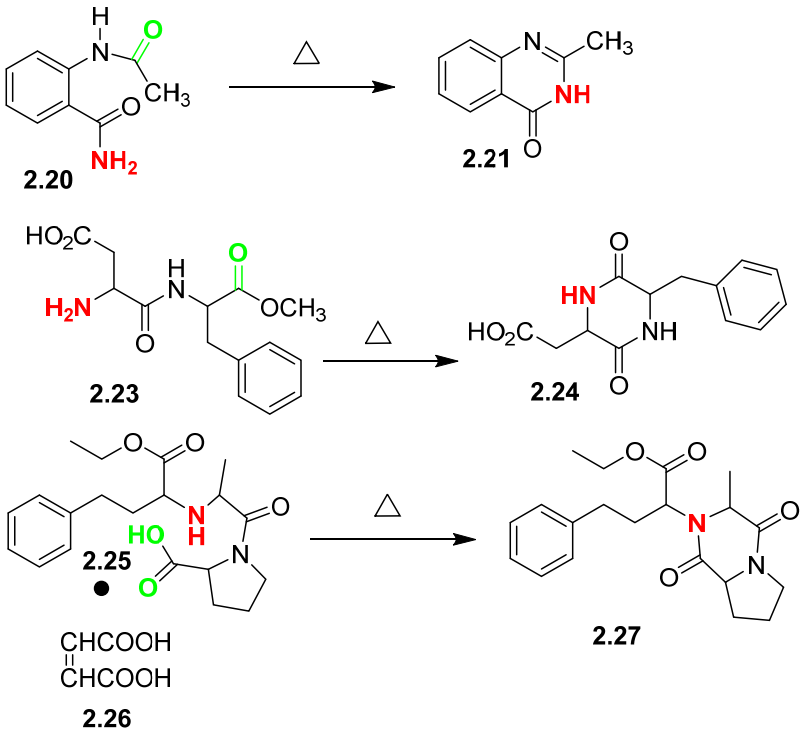

Scheme 2.5: Intramolecular cyclization reaction in solid state.

The increase in El···Nu distance (3.27 to 3.4- 4.1 Å) and angle (101 to 112-126°) observed between crystals of reactants shown in Scheme 2.4 and the carbonates **2.4**, **2.6** and **2.7** could be due to the rigid molecular frame of *myo*-inositol orthoformate. Further analysis of the crystal structures revealed that the relative geometry of the nearest nucleophile (OH) and the electrophile (C=O or C=S) in crystals of **2.4**, **2.6** and **2.7** was not suitable for intermolecular acyl group migration (Figure 2.5).

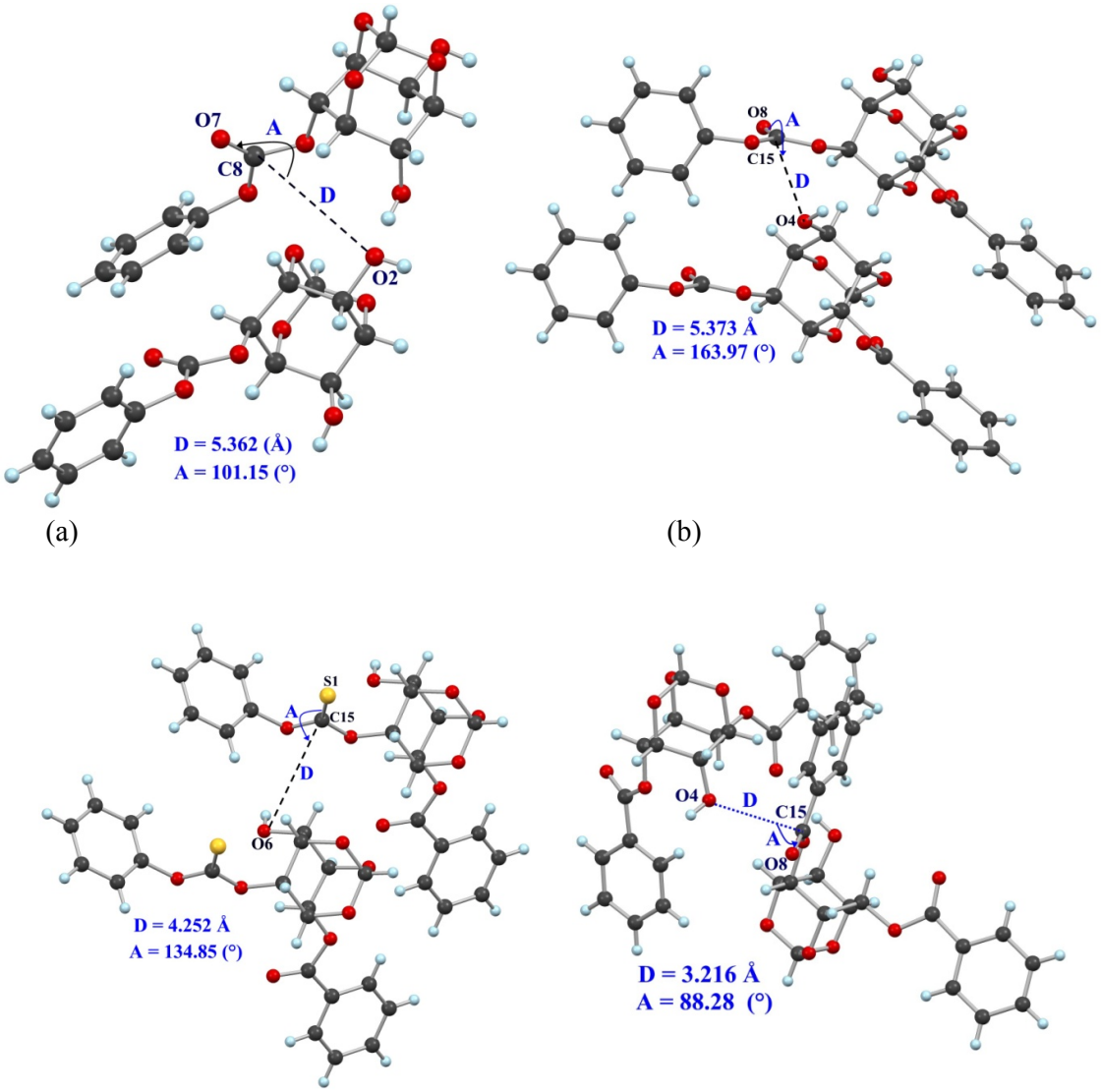

Compound	Intermolecular (Distance) El···Nu Å / Angle (°)
2.4 (Figure 2.5a)	5.362 / 101.15
2.6 (Figure 2.5b)	5.373 / 163.97
2.7 (Figure 2.5c)	4.252 / 134.85
1.21 (Figure 2.5d)	3.216 / 88.28

Figure 2.5: The intermolecular geometry (A= angle, D = distance) of the nucleophile (OH) and the electrophile (C=O or C=S) in crystals of (a) **2.4**, (b) **2.6**, (c) **2.7** at 296 K and (d) in crystals of racemic 2,4-di-O-benzoyl-*myo*-inositol-1,3,5-orthoformate **1.21** (given for comparison).

The intermolecular El···Nu geometry (Figure 2.5) was consistently worse than the corresponding intramolecular geometry (Figure 2.3). The intermolecular El···Nu parameters in crystals of **2.4** (5.362 Å, 101.15°), **2.6** (5.373 Å, 163.9°) and **2.7** (4.252 Å, 134.8°) were very different as compared to molecular crystals of racemic 2,4-di-*O*-benzoyl-*myo*-inositol-1,3,5-orthoformate (**1.21**) that support intermolecular acyl transfer (Figure 2.5).[2.5-6]

The lack of adequate examples of intramolecular acyl transfer reactions in the solid-state as described in this paper, precludes the determination of exact El···Nu parameters needed for the reaction to occur. However, from the data currently available on intra- and intermolecular solid-state reactions[7] (Scheme 2.4), it appears that an El···Nu distance of about 4Å could possibly be a limiting distance for a successful acyl transfer reaction in crystals. It is interesting to note that the topochemical postulate of Schmidt for [2+2] cycloaddition reactions proposed 4.2 Å as the limiting distance for the addition reaction to occur.[9] Hence (although it appears premature) it is tempting to speculate whether 4.2 Å could be the limiting distance needed for any covalent bond formation in the solid state.

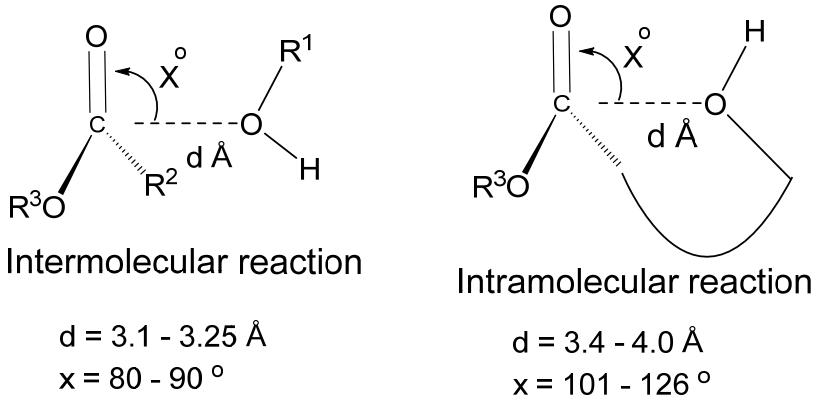

Scheme 2.6: Cartoon showing the range of El···Nu distance and angle required for intermolecular (left) and intramolecular (right) acyl transfer reactions.

A comparison of the structure and reactivity of the crystals of racemic 2,4-di-*O*-benzoyl-*myo*-inositol-1,3,5-orthoformate (**1.21**) [6a] and the corresponding carbonates **2.4**, **2.6** and the thiocarbonate **2.7**, reveal that, as expected, the discrete molecular packing facilitating a domino type of reaction required to bring about intermolecular acyl transfer in crystals of the former dibenzoate was not required for the intramolecular reaction (in **2.4**, **2.6** and **2.7**) leading to the formation of cyclic

carbonates and thiocarbonates **2.15**, **2.17** and **2.18**. However the El···Nu interactions do play a prominent role in both these reactions (Figure 2.3, Scheme 2.6). Whether the cyclization reaction proceeds in a step-wise manner with the involvement of a tetrahedral intermediate (**2.29**, Scheme 2.7) or in a single step through an S_N2 type of reaction (**2.31**, Scheme 2.7) is not entirely clear. Analogy with the mechanism of the corresponding solution state reactions would suggest the operation of the former (Path A) while adherence to the topochemical postulate which dictates that reactions in crystals can only occur with a minimum of atomic and molecular motion, would support the latter (Path B).[9]

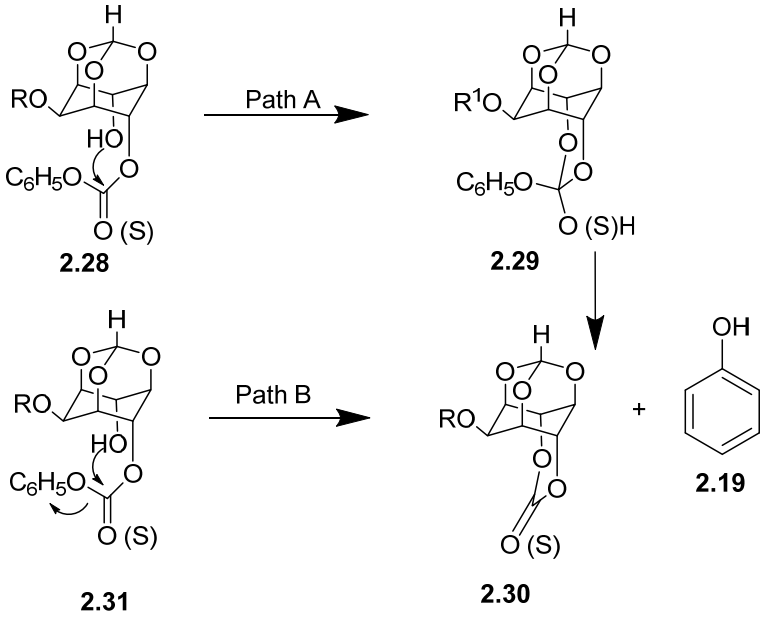

Scheme 2.7: The possible way of formation of cyclic carbonate or thiocarbonates from the *myo*-inositol orthoformate derived carbonates and thiocarbonates.

The structure overlay of the molecules (Figure 2.3) in crystals of **2.4**, **2.6** and **2.7** showed that the difference in orientation of the benzene rings of the C6-carbonate (or the C6-thiocarbonate) moiety and the C2-benzoate moiety in **2.6** and **2.7** was about 16^o and 30^o respectively. The difference in orientation of the benzene rings of the C6-carbonate (or the C6-thiocarbonate) moiety between **2.4** and **2.6** and between **2.4** and **2.7** was about 47^o and 43^o respectively. The conformation of the C4-hydroxyl group in molecules of **2.4**, **2.6** and **2.7** in all these crystals is more or less similar while the distance between the hydroxyl oxygen and the carbonyl (or the thiocarbonyl) carbon (O=C···O/ S=C···O) increased on going from the thiocarbonate **2.7** (3.46 Å / 116^o) to carbonates **2.6** (3.75 Å / 112^o) and **2.4** (4.01 Å / 126^o). These results show that the

orientational differences and variation in the geometrical parameters of the El···Nu interactions could be due to the engagement of carbonate or thiocarbonate part as well as the hydroxyl group in intermolecular interactions (Table A3, Appendix II). This is understandably so since the inositol orthoformate moiety is inherently rigid. Hence for this class of molecules their intramolecular reactivity could reveal their molecular conformation in the solid state.

From the foregoing discussion, equally good reactivity of the crystalline (**2.4**, **2.6**, **2.7**) and non-crystalline (**2.2**, **2.5**) carbonates and the thiocarbonates suggests that the individual molecules in all these carbonates and the thiocarbonates could have similar conformation. As evident from previous chapters, relative geometry of the El···Nu interaction is similar, in crystals exhibiting comparable intermolecular acyl transfer reactivity.[2] Hence, in the present context of intramolecular reaction, the relative geometry of the El···Nu interaction could have implications on the conformation of the individual molecules in the solid. The lack of reactivity of **2.3** in the solid state is most likely due to the lower reaction temperature (dictated by the lower melting point of **2.3**). This was evident since **2.3** failed to react in the molten state up to 110-115 °C although at this temperature the molecules of **2.3** have greater conformational freedom. Hence no inference about the conformation of the molecules of **2.3** in the solid state can be made due to its lack of reactivity.

We had also prepared the carbonate and thiocarbonate derivatives of *myo*-inositol orhoformate which were incapable of undergoing intramolecular cyclization reaction (Scheme 2.8). All these derivatives were obtained as crystalline solids. Details of crystal structure data, thermal analysis and PXRD are given in Appendix II.

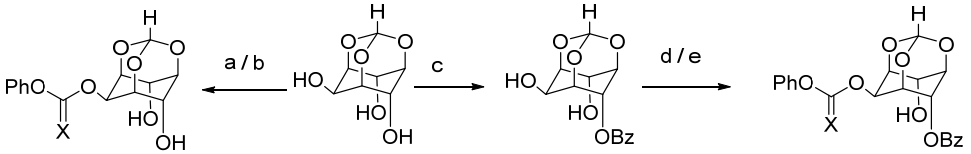

2.32 X=O
2.33 X=S

2.1

2.34

2.35 X=O
2.36 X=S

Scheme 2.8: (a) PhOCOCl, pyridine, DMF, -5 ^{o}C- rt, 2 h, 71%; (b) PhOCSCl, pyridine, DMF, -5 ^{o}C - rt, 2 h, 52%; (c) BzCl, Et_3N, DMF, 0^{o}C - rt, 8h, 48%; (d) PhOCOCl, pyridine, DMF, -5 - 0 ^{o}C, then rt, 6-7 h, 55%; (e) PhOCSCl, pyridine, DMF, -5 - 0 ^{o}C then rt, 10-12 h, 52%.

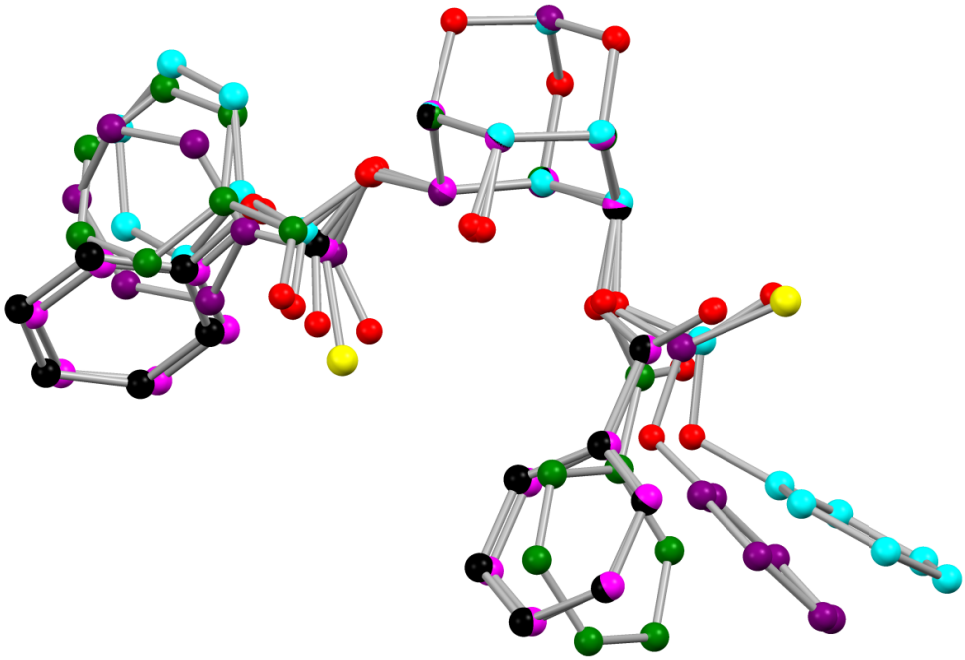

Figure 2.6: Structure overlay of the molecules in crystals of the carbonates **2.35** (black), **2.6** (cyan) and thio carbonates **2.36** (magenta), **2.7** (purple) with that of the primed molecule of the dibenzoate **1.21** (green).

Crystals of the all 2,4 disubstituted mixed (thio)carbonate and benzoate esters namely **2.6**, **2.7**, **2.35**, **2.36** belong to the monoclinic space group $P2_1/c$, just as the crystals of the racemic dibenzoate **1.21** did. The asymmetric unit of crystals of racemic **1.21** had two molecules while those of the carbonates and thiocarbonates have one molecule each. Superimposition of the molecules in all these crystals (Figure 2.6) revealed that the conformation of carbonates and thiocarbonates much deviated from that of the conformation of the dibenzoate **1.21**.

These carbonate and thiocarbonate derivatives (**2.35**, **2.36**) did not undergo any thermal induced reaction in the solid state. As expected, single crystal X-ray diffraction data of these derivatives revealed intermolecular El···Nu interactions (Figure 2.7, Table 2.2) unsuitable for acyl transfer reactions. The carbonate **2.35** as well as the thiocarbonate **2.36** did not exhibit acyl transfer reaction in their crystals or solid state when heated (140-145 ^{o}C, 72 h) in the presence of solid sodium carbonate. The TLC analysis after the reaction revealed the mixture of products and no attempt was made to isolate them.

Distance (Å) / Angle (°)	**2.35**	**2.36**
O6(Nu)···C15(El)	4.709	4.820
∠ O6(Nu)···C15-O9 (El) (**2.35**)	45.09	N/A
∠ O6(Nu)···C15-O8 (El) (**2.36**)	N/A	40.94
∠H6A-O6(Nu)···C15(El)	88.81	87.57
∠C6-O6(Nu)···C15 (El)	143.12	143.85

Table 2.2: The El···Nu geometrical parameters for compounds **2.35** and **2.36**.

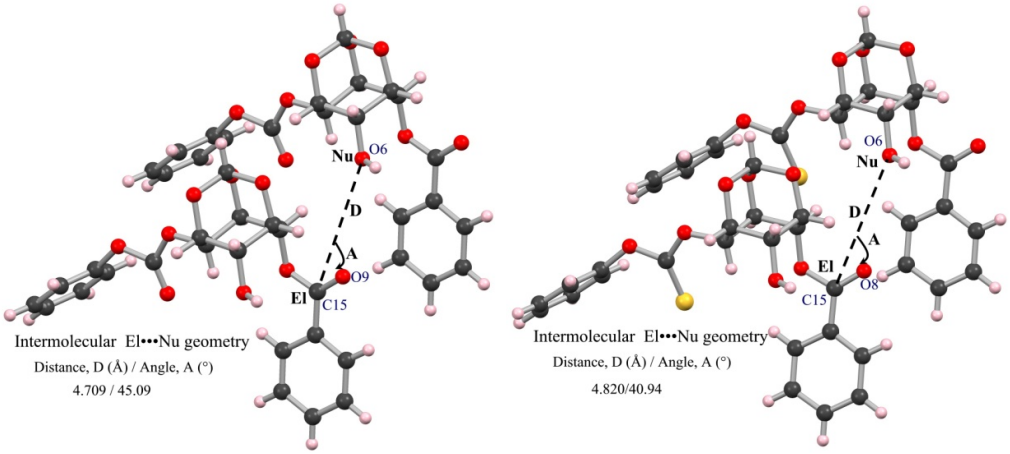

(a) (b)

Figure 2.7: Relative geometry of electrophile···nucleophile orientation in crystals of (a) **2.35** and (b) **2.36**.

Conclusions:

Racemic 4-*O*-phenoxycarbonyl and 4-*O*-phenoxythiocarbonyl derivatives of *myo*-inositol orthoformate undergo thermal intramolecular cyclization in the solid state to yield the corresponding 4,6-bridged carbonates and thiocarbonates resepctively. The thermal cyclization also occurs in the solution and molten states, but less efficiently, suggesting that these cyclization reactions are aided by molecular pre-organization, although not strictly topochemically controlled. Hence, the thermal cyclization of inositol orthoformate derived carbonates and thiocarbonates in the solid state provides convenient access to C4,C6-bridged *myo*-inositol derivatives. Crystal structures of two carbonates and a thiocarbonate clearly revealed that the relative orientation of the electrophile and the nucleophile in the crystal lattice facilitates the intramolecular cyclization reaction and forbids the intermolecular reaction. The correlation observed between chemical reactivity and the non-covalent interactions in the crystal of reactants provides a way to estimate the chemical stability of analogous molecules in the solid state. This could have potential applications in pharmaceutical solids and formulations, organic solid state devices as well as food additives.[8,10] The observed correlation between the conformation of molecules in their crystal and reactivity of these carbonates and the thiocarbonates suggest that the facile chemical reactivity in molecular crystals could provide clues on the probable conformation of closely related molecules in the solid state. These reactions constitute rare examples of chemical reactions involving acyl groups, in the solid state. The increased yield and facility of reactions in the solid state, as compared to the corresponding reactions in the solution state, coupled with greatly reduced use of solvents make solid state reactions potentially useful for the development of environmentally sustainable chemical reactions of the future.

Experimental Section:

The reagent phenyl chloroformate and phenyl chlorothionoformate directly used as such obtained from Sigma-Aldrich.

Preparation of carbonates and thiocarbonates: general procedure: A mixture of *myo*-inositol-1,3,5-orthoformate (**2.1** or its 2-benzoate **1.27**), dry pyridine (for **2.2** and **2.3**) or a mixture of dry DMF and triethylamine (TEA) was cooled (0 to -5 ^{o}C) and phenyl chloroformate (or phenyl chlorothionoformate) was added slowly. The reaction mixture was stirred at ambient temperature till TLC analysis showed the absence of the starting material (30 min to 2 h). The reaction mixture was decomposed by the addition of ice. The resulting mixture was concentrated under reduced pressure [below 45 ^{o}C to prevent the cyclization of the carbonate or the thiocarbonate] and the residue obtained was taken in ethyl acetate and washed with 2% HCl and subsequently with brine. The organic layer was dried over anhydrous sodium sulfate. The solvents were removed under reduced pressure and the product obtained was purified by column chromatography (silica gel 230–400 mesh) to isolate the corresponding carbonate or the thiocarbonate. The product was crystallized from a suitable solvent. See Table 2.3 for details. Characterization data for each product is given below.

Entry	Reactants (mmol)	Solvent (mL); time h	Product[a] (yield%) MP ^{o}C[b]
1	**2.1** (2.36), PhOCOCl (7.23)	Pyridine (15); 1	**2.2** (79) 168-170[c]
2	**2.1** (6.45), PhOCSCl (14.2)	Pyridine (20); 2	**2.3** (69) 94-102.
3	**2.1** (2.11), PhOCOCl (2.53)	TEA (2), DMF (8); 0.5	**2.4** (64) 178-180
4	**2.1** (1.05), PhOCSCl (1.27)	TEA (1), DMF (4); 0.5	**2.5** (66) 148-150
5	**1.27** (0.68), PhOCOCl (0.95)	TEA (0.4), DMF (5); 0.5	**2.6** (55) 166-167
6	**1.27** (1.02), PhOCSCl (1.35)	TEA (0.5), DMF (7); 0.5	**2.7** (52) 162-164

Table 2.3: Preparation of inositol orthoformate derived carbonates and the thiocarbonates.

[a]Eluent for column chromatography: ethyl acetate – light petroleum; 15:85 for **2.2**, **2.3**; 35:65 for **2.4**; 30:70 for **2.5**; 20:80 for **2.6** and **2.7**.

[b]solvent of crystallization: chloroform for **2.4**; ethyl acetate – light petroleum (1:4) for **2.6**, **2.7**; **2.3** crystallized as benzene solvate from a solution of benzene, in one of the trials; however, the melting point shown is for the solid sample obtained after chromatography; crystals of **2.2** and **2.5** could not be obtained from common solvents.

[c]2,4,6-tri-*O*-phenoxycarbonyl-*myo*-inositol-1,3,5-orthoformate (**2A**) was obtained as a minor product.

Racemic 2,4-di-*O*-phenoxycarbonyl-*myo*-inositol-1,3,5-orthoformate (2.2):

Data for **2.2:** TLC R_f : 0.3 in 1:4 ethyl acetate : light petroleum; **MP** = 168-170 ^oC; **IR** (Chloroform): $\bar{\nu}$ 1729, 1767, 3500 - 3400 cm^{-1}; **^{1}H NMR** ($CDCl_3$, 500 MHz): δ 2.57 (d, J = 6.7 Hz, 1 H, D_2O exchangeable, Ins OH), 4.50 - 4.53 (m, 1 H, Ins H), 4.62 (br. s, 1 H, Ins H), 4.65 - 4.72 (m, 2 H, Ins H), 5.27 (s, 1 H, Ins H), 5.55 (br. s, 1 H, Ins H), 5.63 (s, 1 H, Ins H), 7.17 (d, J = 7.6 Hz, 2 H, Ar H), 7.21 - 7.31 (m, 4 H, Ar H), 7.35 – 7.44 ppm (m, 4 H, Ar H); **^{13}C NMR** ($CDCl_3$, 126 MHz): δ 67.0, 67.2, 67.8, 68.7, 71.3, 71.6, 102.7, 120.7, 120.9, 126.3, 126.5, 129.6, 129.7, 150.7, 150.9, 151.8, 153.1 ppm; **Elemental analysis** calcd for $C_{21}H_{18}O_{10}$ (430.09): C, 58.61; H, 4.22 %; found, C, 58.54; H, 3.82 %.

Data for 2,4,6-tri-*O*-phenoxycarbonyl-*myo*-inositol-1,3,5-orthoformate (2.2A):

Data for **2.2A:** TLC R_f : 0.3 in 15:85 ethyl acetate : light petroleum; **MP** = 170-172 ^oC; **IR** (solid): $\bar{\nu}$ 1766, cm^{-1}; **^{1}H NMR** ($CDCl_3$, 200 MHz): δ 4.72- 4.77 (m, 2 H, Ins H), 5.02-5.10 (m, 1 H, Ins H), 5.30-5.34 (m, 1 H, Ins H), 5.55 (t, J = 4Hz, 2 H, Ins H), 5.69 (d, J = 1.1 Hz, 1 H, Ins H), 7.09 - 7.18 (m, 4 H, Ar H), 7.19 - 7.25 (m, 2 H, Ar H), 7.26 - 7.48 ppm (m, 9 H, Ar H); **^{13}C NMR** (Acetone-d_6, 50 MHz,): δ 66.6, 67.7, 69.2, 71.9, 103.7, 121.8, 121.9, 127.0, 127.1, 130.4, 151.9, 152.1, 153.0, 153.8 ppm; **Elemental analysis** calcd for $C_{28}H_{22}O_{12}$ (550.47): C, 61.09; H, 4.03 %; found, C, 61.40; H, 3.79 %.

Racemic 2,4-di-*O*-phenoxythiocarbonyl-*myo*-inositol-1,3,5-orthoformate (2.3):

Data for **2.3:** TLC R_f : 0.3 in 1:4 ethyl acetate : light petroleum; **MP** = 95-102 ^oC; **IR** (Chloroform): $\bar{\nu}$ 1731, 3600 - 3200 cm^{-1} ; **^{1}H NMR** ($CDCl_3$, 200 MHz): δ 2.57 (d, J = 6.8 Hz, 1 H, D_2O exchangeable, Ins OH), 4.60 – 4.72 (m, 2 H, Ins H), 4.75 (br. s, 1H, Ins H), 4.94 - 5.00 (m, 1 H, Ins H), 5.68 (d, J = 1.2 Hz, 1 H, Ins H), 5.74 – 5.79 (m, 1 H, Ins H), 6.04 – 6.11 (m, 1 H, Ins H), 7.05 – 7.22 (m, 4 H, Ar H), 7.29 – 7.52 ppm (m, 6 H, Ar H); **^{13}C NMR** ($CDCl_3$, 126 MHz): δ 67.4, 67.6, 67.9, 71.3, 71.7, 75.4,

102.8, 121.6, 121.8, 126.9, 127.0, 129.7, 129.8, 153.1, 153.3, 192.4(C=S), 194.2(C=S) ppm; **Elemental analysis** calcd for $C_{21}H_{18}O_8S_2$ (462.49): C, 54.54; H, 3.92 %; found, C, 54.26; H, 3.66%.

Racemic 4-*O*-phenoxyocarbonyl-*myo*-inositol-1,3,5-orthoformate (2.4):

Data for **2.4:** TLC R_f : 0.3 in 40:60 ethyl acetate : light petroleum; **MP** = 178-180 ^oC; **IR** (Chloroform): $\bar{\nu}$ 1757, 3500 - 3250 cm^{-1} ; **^{1}H NMR** (*Acetone-d_6*, 500 MHz): δ 4.12 (br. s, 1 H, Ins H), 4.17 (d, J = 7.9 Hz, 1 H, Ins H), 4.28 (br. s, 1 H, Ins H), 4.55 - 4.60 (m, 3 H, one H is D_2O exchangeable, Ins OH, Ins H), 4.97 (d, J = 3.7 Hz, 1 H, D_2O exchangeable, Ins OH), 5.32 (br. s, 1 H, Ins H), 5.49 (s, 1 H, Ins H), 7.22 (d, J = 7.9 Hz, 2 H, Ar H), 7.27 - 7.32 (m, 1 H, Ar H), 7.41 - 7.46 ppm (m, 2 H, Ar H); **^{13}C NMR** (*Acetone-d_6*, 50 MHz): δ 60.8 , 67.6, 69.1, 72.8, 73.2, 75.3, 103.7, 121.9, 126.9, 130.3, 152.1, 153.1 ppm; **Elemental analysis** calcd for $C_{14}H_{14}O_8$ (310.26): C, 54.20; H, 4.55 %; found, C, 54.04; H, 4.20 %.

Racemic 4-*O*-phenoxythiocarbonyl-*myo*-inositol-1,3,5-orthoformate (2.5):

Data for **2.5:** TLC R_f : 0.3 in 35:65 ethyl acetate : light petroleum; **MP** = 148-150 ^oC; **IR (**Nujol): $\bar{\nu}$ 1591, 1716 (weak), 3500 - 3200 cm^{-1}; **^{1}H NMR** ($CDCl_3$, 200 MHz): δ 2.42 (d, J = 7.6 Hz, 1 H, D_2O exchangeable, Ins OH), 3.20 (d, J = 11.9 Hz, 1 H, D_2O exchangeable, Ins OH), 4.08-4.17 (m, 1 H, Ins H), 4.23-4.30 (m, 1 H, Ins H), 4.46-4.52 (m, 1 H, Ins H), 4.60- 4.73 (m, 2 H, Ins H), 5.55 (d, J = 1.2 Hz, 1 H, Ins H), 6.02-6.08 (m, 1 H, Ins H), 7.06-7.14 (m, 2 H, Ar H), 7.29 - 7.35 (m, 1 H, Ar H), 7.40 - 7.47 ppm (m, 2 H, Ar H); **^{13}C NMR** ($CDCl_3$, 126 MHz): δ 60.8, 67.25, 67.3, 70.9, 74.2, 75.8, 103.0, 121.6, 127.0, 129.8, 153.1, 192.6 (C=S) ppm; **HRMS** [$C_{14}H_{14}O_7S$ + H]$^+$= 327.0533, Found = 327.0530.

Racemic 2-*O*-benzoyl-4-*O*-phenoxycarbonyl-*myo*-inositol-1,3,5-orthoformate (2.6):

Data for **2.6:** TLC R_f : 0.3 in 1:4 ethyl acetate : light petroleum; **MP** = 166-167 ^oC; **IR** (Nujol): $\bar{\nu}$ 1732, 3550 - 3450 cm^{-1}; **^{1}H NMR** ($CDCl_3$, 400 MHz): δ 2.80 (br. s, 1H, D_2O exchangeable, Ins OH), 4.46 -4.50 (m, 1H, Ins H), 4.60 - 4.67 (m, 2H, Ins H), 4.70 (br. s, 1H, Ins H), 5.54 – 5.58 (m, 2H, Ins H), 5.62 (br. s, 1H, Ins H), 7.18 - 7.22 (m, 2H, Ar H), 7.23 - 7.29 (m, 1H, Ar H), 7.36 - 7.42 (m, 2H, Ar H), 7.44 - 7.50 (m, 2H, Ar H), 7.57 - 7.63 (m, 1H, Ar H), 8.14 - 8.18 ppm (m, 2H, Ar H); **^{13}C NMR** ($CDCl_3$, 101 MHz): δ 64.3, 67.3, 68.0, 69.1, 71.7, 71.8, 102.8, 120.8, 126.5, 128.5,

129.3, 129.6, 130.0, 133.5, 150.7, 151.9, 166.1 ppm; **Elemental analysis** calcd for $C_{21}H_{18}O_9$ (414.37): C, 60.87; H, 4.38 %; found, C, 60.75; H, 4.26 %.

Racemic 2-*O*-benzoyl-4-*O*-phenoxythiocarbonyl-*myo*-inositol-1,3,5-orthoformate (2.7):

Data for **2.7:** TLC R_f : 0.3 in 1:4 ethyl acetate : light petroleum, **MP** = 162-164 ^oC; **IR** (Nujol): $\bar{\nu}$ 1720, 3500 - 3450 cm^{-1}; **^{1}H NMR** ($CDCl_3$, 500 MHz): δ 2.59 (d, J = 7 Hz, 1H, D_2O exchangeable, Ins OH), 4.47 - 4.52 (m, 1H, Ins H), 4.66 - 4.74 (m, 3H, Ins H), 5.50 - 5.54 (m, 1H, Ins H), 5.63 - 5.66 (m, 1H, Ins H), 6.07-6.1 (m, 1H, Ins H), 7.12 - 7.17 (m, 2H, Ar H), 7.30 - 7.35 (m, 1H, Ar H), 7.36 - 7.51 (m, 4H, Ar H), 7.56 - 7.64 (m, 1H, Ar H), 8.16 ppm (dd, J = 8.3, 1.2 Hz, 2H, Ar H); **^{13}C NMR** ($CDCl_3$, 125 MHz): δ 63.4, 67.4, 67.8, 68.6, 71.8, 75.6, 102.9, 121.6, 127.0, 128.5, 129.4, 129.8, 130.0, 133.5, 153.2, 166.0, 192.7(C=S) ppm; **Elemental analysis** calcd for $C_{21}H_{18}O_8S$ (430.43) C, 58.60; H, 4.22 %; found, C, 58.96; H, 4.35 %.

Thermal cyclization in the solid state: General procedure A. The required carbonate or the thiocarbonate was ground well to make fine powder. The powder was taken in a test tube filled with argon and heated 5-10 ^oC below its melting point for 48 h. The reaction assembly was cooled to room temp and the solid was washed with diethyl ether and crystallized from acetone. Condensation of phenol as a liquid on the upper, cooler parts of the reaction vessel could be observed in most experiments. No attempt was made to isolate phenol which was formed as a byproduct.

Thermal cyclization in the molten state: General procedure B. The required carbonate or the thiocarbonate was ground well to make a fine powder. The powder was taken in a test tube filled with argon and heated at a temperature 20-40 ^oC above its melting point for 1-5 h and then cooled to ambient temp. The solid obtained was washed with diethyl ether and crystallized from acetone.

Thermal cyclization in the solution state: General procedure C. The required carbonate or the thiocarbonate was dissolved in dry warm *p*-xylene (4 mL) and refluxed (in an atmosphere of argon) using an oil bath (140-145 ^oC) for 48 h. The solvent was then evaporated under reduced pressure. The residue was washed with diethyl ether and crystallized from acetone.

2-*O*-phenoxycarbonyl-*myo*-inositol-1,3,5-orthoformate 4,6-cyclic carbonate (2.13):

Data for **(2.13): MP** = 271-275 ^{o}C; **IR** (Solid): $\bar{\nu}$ 1751 cm^{-1}; **^{1}H NMR** (DMSO-d_6, 400 MHz): δ 4.81- 4.84 (m, 2 H, Ins H), 4.88- 4.90 (br. s, 1 H, Ins H), 4.97-5.02 (m, 1 H, Ins H), 5.25 – 5.32 (m, 2 H, Ins H), 5.88 (d, J = 1Hz, 1 H, Ins H), 7.30 - 7.36 (m, 3 H, Ar H), 7.43 - 7.50 ppm (m, 2 H, Ar H); **^{13}C NMR** (DMSO-d_6, 101 MHz): δ 58.9, 66.5, 68.4, 69.5, 101.2, 121.4, 126.7, 129.9, 145.0, 150.8, 152.5 ppm; **HRMS** cacld for $[C_{15}H_{12}O_9 + NH_4]^+$ = 354.0820; Found = 354.0815.

2-*O*-phenoxythiocarbonyl-*myo*-inositol-1,3,5-orthoformate 4,6-cyclic thiocarbonate (2.14):

Data for **(2.14): MP** = 268-270 ^{o}C; **IR** (Solid): $\bar{\nu}$ 1751 cm^{-1}; **^{1}H NMR** (DMSO-d_6, 400 MHz): δ 4.98 – 5.01 (m, 2 H, Ins H), 5.05 - 5.08 (m, 1 H, Ins H), 5.39 (br. s, 1 H, Ins H), 5.52 (t, J = 4.6 Hz, 2 H, Ins H), 5.96 (br s, 1 H, Ins H), 7.25-7.31 (m, 2 H, Ar H), 7.36 - 7.40 (m, 1 H, Ar H), 7.48 - 7.57 ppm (m, 2 H, Ar H); **^{13}C NMR** (DMSO-d_6, 126 MHz): δ 58.5, 67.7, 71.0, 71.1, 100.9, 121.7, 127.0, 129.9, 152.9, 185.1, 193.6 ppm; **HRMS** $[C_{15}H_{12}O_7S_2 + H]^+$ = 369.0097; Found = 369.0094.

***myo*-Inositol-1,3,5-orthoformate 4,6-cyclic carbonate (2.15):**

Data for **(2.15): MP** = 275-280 ^{o}C; **IR** (Solid): $\bar{\nu}$ 1765, 3550-3300 cm^{-1}; **^{1}H NMR** (*Acetone-d_6*, 500 MHz): δ 3.88 (d, J = 8.5 Hz, 1 H, Ins H), 4.46 - 4.51 (m, 2 H, Ins H), 4.83 - 4.86 (m, 1 H, Ins H), 4.93 (d, J = 8.8 Hz, 1 H, D_2O exchangeable, Ins OH), 5.14 (t, J = 4.7 Hz, 2 H. Ins H), 5.58 ppm (s, 1 H, Ins H); **^{13}C NMR** (Acetone-d_6, 126 MHz): δ 60.5, 60.8, 71.0, 72.6, 102.7, 145.7 ppm; **Elemental analysis** calcd for $C_8H_8O_7$ (216.14): C, 44.46; H, 3.73 %; found, C, 44.08; H, 3.57 %.

***myo*-Inositol-1,3,5-orthoformate 4,6-cyclic thiocarbonate (2.16):**

Data for **(2.16): MP** = 290 -295 ^{o}C; **IR** (Solid): $\bar{\nu}$ 1716, 3500 - 3350 cm^{-1}; **^{1}H NMR** (*Acetone-d_6*, 400 MHz): δ 3.78 - 3.83 (m, 1 H, Ins H), 4.50 – 4.55 (m, 2 H, Ins H), 4.86 - 4.93 (m, 1 H, Ins H), 5.00 (d, J = 8.6 Hz, 1 H, D_2O exchangeable, Ins OH), 5.29 - 5.34 (m, 2 H, Ins H), 5.61 ppm (d, J = 1.2 Hz, 1 H, Ins H); **^{13}C NMR** (*Acetone-d_6*, 101 MHz): δ 60.2, 61.1, 72.4, 72.7, 102.7, 186.6 ppm; **Elemental analysis** calcd for $C_8H_8O_6S$ (232.21): C, 41.38; H, 3.47; S, 13.81%; found, C, 41.51; H, 3.46 , S, 13.61%.

2-*O*-benzoyl-*myo*-inositol-1,3,5-orthoformate 4,6-cyclic carbonate (2.17):

Data for **(2.17): MP** = 280-285 ^{o}C; **IR** (Nujol): $\bar{\nu}$ 1725, 1773 cm^{-1}; **^{1}H NMR** (DMSO-d_6, 200 MHz): δ 4.78-4.87 (m, 2 H, Ins H), 5.00- 5.05 (m, 1 H, Ins H), 5.18 (br. s, 1 H, Ins H), 5.31 (t, J = 4.7 Hz, 2 H, Ins H), 5.92 (s, 1H, Ins H), 7.55 - 7.66 (m, 2 H, Ar H), 7.68 - 7.80 (m, 1 H, Ar H), 8.06 ppm (d, J = 7.1 Hz, 2 H, Ar H); **^{13}C NMR** (DMF-d_7, 126 MHz): δ 59.9, 63.4, 69.6, 70.3, 102.1, 129.2, 129.7, 129.9, 134.2, 145.5, 165.6 ppm; **Elemental analysis** calcd for $C_{15}H_{12}O_8$ (320.25): C, 56.26; H, 3.78%; found, C, 55.94; H, 3.86 %.

2-*O*-benzoyl-*myo*-inositol-1,3,5-orthoformate 4,6-cyclic thiocarbonate (2.18):

Data for **(2.18): MP** = 305-310 ^{o}C; **IR** (Nujol): $\bar{\nu}$ 1595, 1721cm^{-1}; **^{1}H NMR** (DMSO-d_6, 500 MHz): δ 4.87 (br. s, 2 H, Ins H), 5.04- 5.08 (m, 1 H, Ins H), 5.09 (br. s, 1 H, Ins H), 5.50 (t, J = 4.6 Hz, 2 H, Ins H), 5.95 (s, 1 H, Ins H), 7.57-7.66 (m, 2 H, Ar H), 7.71 - 7.78 (m, 1 H, Ar H), 8.05 ppm (d, J = 7.3 Hz, 2 H, Ar H); **^{13}C NMR** (DMF-d_7, 101 MHz): δ 59.6, 63.4, 69.4, 72.0, 102.1, 129.2, 129.6, 129.9, 134.3, 165.5, 186.2 ppm; **HRMS** calcd for $[C_{15}H_{12}O_7S + H]^+$ = 337.0376; Found = 337.0374.

Preparation of racemic 2-*O*-phenoxycarbonyl-*myo*-inositol-1,3,5-orthoformate (2.32):

myo-Inositol-1,3,5-orthoformate **2.1** (0.440 g, 2.31 mmol) and dry pyridine (5 mL) were dissolved in dry DMF (8 mL) and cooled. Phenyl chloroformate (0.4 mL, 3.23 mmol) was added slowly; the reaction mixture turned viscous and opaque in a few min. The reaction mixture was warmed to ambient temperature and stirred for 10 min when a clear solution was obtained. The reaction mixture was cooled (ice-water) and stirred for 1 h. TLC analysis indicated compete consumption of the starting material. Reaction mixture was decomposed by the addition of ice and concentrated under reduced pressure. The residue obtained was suspended in ethyl acetate and washed with 2% HCl followed by brine. The product obtained after removal of ethyl acetate under reduced pressure was purified by column chromatography (silica gel 230–400 mesh, eluent: 35:65 ethyl acetate: light petroleum) to get racemic 2-*O*-phenoxycarbonyl-*myo*-inositol 1,3,5- orthoformate (0.512 g, 71%) as a colorless solid. It was crystallized from chloroform.

Data for **2.32:**TLC R_f : 0.3 in 35:65 in ethyl acetate : light petroleum; **MP** = 196-197^{o}C, **IR** (Chloroform): $\bar{\nu}$ 1761, 3500 - 3100 cm^{-1} ; **^{1}H NMR** (Acetone-d_6, 500

MHz): δ 4.28 (br. s, 1 H, Ins H), 4.42 (br. s, 2 H, Ins H), 4.53 - 4.56 (m, 2 H, Ins H), 5.21 (d, J = 7 Hz, 2 H, D_2O Exchangeable, Ins OH), 5.31 (s, 1 H, Ins H), 5.52 (s, 1 H, Ins H), 7.28 - 7.34 (m, 3 H, Ar H), 7.43 - 7.50 ppm (m, 2 H, Ar H); **^{13}C NMR** (Acetone-d_6, 126 MHz): δ 68.5, 68.7, 69.9, 72.6, 103.2, 122.0, 126.9, 130.3, 152.2, 153.9 ppm; **Elemental analysis** calcd for $C_{14}H_{14}O_8$ (310.26); C, 54.20; H, 4.55; found, C, 54.22%; H, 4.64 %

Preparation of racemic 2-*O*-phenoxythiocarbonyl-*myo*-inositol-1,3,5-orthoformate (2.33):

The thiocarbonate **2.33** was prepared from *myo*-inositol-1,3,5-orthoformate **2.1** (0.237 g, 1.24 mmol), dry pyridine (2 mL) and dry DMF (3 mL) as above. The crude product obtained was purified by column chromatography (silica gel 230–400 mesh, eluent: 3:7 ethyl acetate: light peroleum) to get 2-phenylthiocarbonate **2.33** (0.212 g, 52%) as a colorless solid. Crystals of **2.33** were obtained from chloroform solution, by slow evaporation under ambient conditions.

Data for **2.33:** TLC R_f : 0.3 in 3:7 ethyl acetate : light petroleum; **MP** = 162-164^o C; **IR** (Chloroform): $\bar{\nu}$ 1758 (weak), 3450 - 3100 cm^{-1}; **^{1}H NMR** ($CDCl_3$, 200 MHz): δ 3.58 (d, J = 7.1 Hz, 2 H, D_2O exchangeable, Ins OH), 4.35 - 4.43 (m, 1 H, Ins H), 4.59 - 4.76 (m, 4 H, Ins H), 5.60 (d, J = 1.3 Hz, 1 H, Ins H), 5.82 – 5.87 (m, 1 H, Ins H), 7.12 - 7.21 (m, 2 H, Ar H), 7.28 - 7.37 (m, 1 H, Ar H), 7.39 - 7.51 ppm (m, 2 H, Ar H); **^{13}C NMR** ($CDCl_3$, 50 MHz): δ 68.1, 68.5, 71.3, 71.9, 102.4, 121.8, 126.8, 129.6, 153.3, 194.3(C=S) ppm; **Elemental analysis** calcd for $C_{14}H_{14}O_7S$ (326.05); C, 51.53; H, 4.32; found, C, 51.76; H, 4.42 %.

Preparation of the racemic 2-*O*-phenoxycarbonyl-4-*O*-benzoyl-*myo*-inositol-1,3,5- orthoformate (2.35):

Racemic 4-*O*-benzoyl-*myo*-inositol-1,3,5-orthoformate **2.34** (0.40 g, 1.36 mmol) was dissolved in dry DMF (10 mL) and pyridine (2.5 mL). To the cooled solution, phenyl chloroformate (0.24 mL, 1.9 mmol) was added drop-wise and stirred for 6-7 h at room temperature. The reaction mixture was decomposed by the addition of few pieces of ice and concentrated under reduced pressure. The residue was worked up with ethyl acetate and the extract was washed with brine. The crude product obtained after evaporation of the solvent under reduced pressure was purified by column chromatography (silica gel 230–400 mesh, eluent: 20 % ethyl acetate in light

petroleum) to get the carbonate **2.35** (0.312 g, 55%) as a colorless solid. It was crystallized from a mixture of ethyl acetate and light petroleum (1:4).

Data for **2.35:** TLC R_f : 0.3 in 1:4 ethyl acetate : light petroleum, **MP** = 185-186 ^oC, **IR** (Nujol): $\bar{\nu}$ 1703, 1755, 3500 - 3300 cm^{-1} ;**^{1}H NMR** ($CDCl_3$, 400 MHz): δ 2.50 (d, J = 4.7 Hz, 1H, D_2O Exchangeable, Ins OH), 4.52 (br. s, 1H, Ins H), 4.60 (br. s, 1H, Ins H), 4.64 (br. s, 1H, Ins H), 4.72 (br. s, 1H, Ins H), 5.37 (s, 1H, Ins H), 5.64 (s, 1H, Ins H), 5.81 (br. s, 1H, Ins H), 7.17 - 7.29 (m, 3H, Ar H), 7.34 - 7.47 (m, 4H, Ar H), 7.52 - 7.60 (m, 1H, Ar H), 8.00 ppm (d, J = 7.6 Hz, 2H, Ar H); **^{13}C NMR** ($CDCl_3$, 101 MHz): δ 67.2, 67.5, 68.3, 68.4, 69.2, 71.4, 102.9, 120.9, 126.3, 128.7, 128.8, 129.6, 129.8, 133.8, 150.9, 153.3, 165.0 ppm; **Elemental analysis** calcd for $C_{21}H_{18}O_9$ (414.37); C, 60.87; H, 4.38; O, 34.75; found, C, 60.82%; H, 4.38 %.

Preparation of racemic 2-*O*-phenoxythiocarbonyl-4-*O*-benzoyl-*myo*-inositol-1,3,5-orthoformate (2.36):

Racemic 4-*O*-benzoyl-*myo*-inositol-1,3,5-orthoformate **2.34** (0.456 g, 1.55 mmol) was dissolved in dry DMF (8 mL) and pyridine (4 mL). To the cooled solution, phenyl chlorothionoformate (0.28 mL, 2.01 mmol) was added drop-wise and stirred for 12-14 h at room temperature. The reaction mixture was decomposed by the addition of few pieces of ice and concentrated under reduced pressure. The residue was worked up with ethyl acetate and the extract was washed with brine. The crude product obtained after evaporation of the solvent under reduced pressure was purified by column chromatography (silica gel 230–400 mesh, eluent: 20 % ethyl acetatein light petroleum) to get the thiocarbonate **2.36** (0.344 g, 52%) as a colorless solid. Crystals of **2.36** were obtained from a mixture of light petroleum and ethyl acetate (1:4).

Data for **2.36:** TLC R_f : 0.35 in 1:4 ethyl acetate : light petroleum, **MP** = 184-186^oC, **IR** (Nujol): $\bar{\nu}$ 1705, 1759(weak), 3500-3400 cm^{-1} ; **^{1}H NMR** ($CDCl_3$, 500 MHz): δ 2.47 (d, J = 5.2 Hz, 1 H, D_2O Exchangeable, Ins OH), 4.61 - 4.66 (m, 2 H, Ins H), 4.74 - 4.80 (m, 2 H, Ins H), 5.68 (s, 1 H, Ins H), 5.82 (br. s, 1 H, Ins H), 5.99 (d, J = 1.2 Hz, 1 H, Ins H), 7.12-7.18 (m, 2 H, Ar H), 7.28 - 7.33 (m, 1 H, Ar H), 7.38-7.46 (m, 4 H, Ar H), 7.54 - 7.60 (m, 1 H, Ar H), 8.00- 8.08 ppm (m, 2 H, Ar H); **^{13}C NMR** ($CDCl_3$,126 MHz): δ 67.5, 68.45, 68.5, 68.9, 71.3, 72.1, 102.9, 121.8, 126.8, 128.6, 128.8, 129.6, 129.9, 133.7, 153.3, 165.0, 194.4 (C=S) ppm; **Element alanalysis** calcd for $C_{21}H_{18}O_8S$ (430.43); C, 58.60; H, 4.22; found, C, 58.49; H, 4.48 %.

DSC Analysis:

DSC analyses of the (thio) carbonates (**2.2-2.7**, **2.13**-**2.17**, **2.32-2.33**, **2.35-2.36**) were carried out on a Mettler (for **2.2**, **2.2A**, **2.3**, **2.4**, **2.5**, **2.6**, **2.7**, **2.15, 2.32-2.33**, **2.35-2.36**) or Waters (for **2.13**, **2.14**, **2.16** and **2.17**) DSC instrument. The solid (~3-4 mg) was placed on an aluminum pan (40 µl) and was analyzed using an empty pan as the reference. The heating rate was 5° (for **2.2**, **2.2A**, **2.3**, **2.4**, **2.5**, **2.6**, **2.7**, **2.15, 2.32-2.33**, **2.35-2.36**) or 10° (for **2.13**, **2.14**, **2.16** and **2.17**) C/min. Nitrogen gas was used for purging. See Appendix II for further details.

Powder X-ray Diffraction Studies:

The experimental Powder X-ray diffraction patterns were recorded on Rigaku Micromax-007HF instrument (High intensity microfocous rotating anode X-ray Generator) with R-axis detector IV++ at a continuous scanning rate of 2° 2θ/min using Cu Kα radiation (40 kV, 30 mA) with the intensity of the diffracted X-ray being collected at intervals of 0.1° 2θ. A nickel filter was used to remove Cu K$_\beta$ radiation. PXRD patterns of all the samples were recorded at room temperature. The PXRD pattern of a fresh sample of the racemic (thio)carbonate and of the solid obtained after heating it (below its melting point) for 48 h revealed the formation of the cyclic (thio)carbonate. See the Appendix II for details.

X-ray Crystallography:

Single crystal X-ray structures of **2.4**, **2.7**, **2.13-2.18**, **2.32**, **2.36** (Bruker SMART APEX II) and **2.3**, **2.6**, **2.33**, **2.35** (Bruker SMART APEX I) were determined by measuring X-ray diffraction intensity data on a single crystal X-ray CCD diffractometer having graphite-monochromatised (Mo-Kα = 0.71073 Å) radiation at room temperature or at 100K. The crystal structure of **2.4** was solved at five different temperatures (100 K, 296 K, 353 K, 373 K and 393 K) to investigate the effect of temperature on El···Nu geometry (see the Appendix II for details).

References:

[1] K. M. Sureshan, T. Murakami, T. Miyasou, Y. Watanabe, *J. Am. Chem. Soc.* **2004**, *126*, 9174-9175 and references cited therein.

[2] M. I. Tamboli, S. Krishnaswamy, M. S. Shashidhar, R. G. Gonnade, *Chem. Eur. J.* **2013**, *19*, 12867-12874 and references cited therein.

[3] (a) S. Ballereau, S. N. Poirier, G. Guillemette, B. Spiess, G. Schlewer, *J. Chem. Soc., Perkin Trans. 1* **1998**, 1859-1863; (b) T-H Kim, M. Giles, A. B. Holmes, *Chem. Commun.* **2000**, 2421-2422; (c) S. J. Angyal, *Carbohydr. Res*. **2000**, *325*, 313-320; (d) H-J Lee, T-H Kim, *Bull. Korean Chem. Soc*. **2006**, *27*, 359-360; (e) K. V. P. Pavan Kumar, K. C. Kumara Swamy, *Carbohydr. Res.* **2007**, *342*, 1182-1188; (f) D. Mansell, N. Veiga, J. Torres, L. L. Etchells, R. A. Bryce, C. Kremer, S. Freeman, *Tetrahedron* **2010**, *66*, 8949-8957.

[4] K. M. Sureshan, S. Devaraj, M. S. Shashidhar, *Tetrahedron* **2009**, *65*, 2703-2710 and references cited therein.

[5] T. Praveen, U. Samanta, T. Das, M. S. Shashidhar, P. Chakrabarti, *J. Am. Chem. Soc.* **1998**, *120,* 3842-3845.

[6] (a) M. P. Sarmah, R. G. Gonnade, M. S. Shashidhar, M. M. Bhadbhade, *Chem. Eur. J.* **2005**, *11*, 2103-2110; (b) C. Murali, M. S. Shashidhar, R. G. Gonnade, M. M. Bhadbhade, *Eur. J.Org. Chem.* **2007**, 1153-1159; (c) C. Murali, M. S. Shashidhar, R. G. Gonnade, M. M. Bhadbhade, *Chem. Eur. J.* **2009**, *15*, 261-269; (d) S. Krishnaswamy, M. S. Shashidhar, M. M. Bhadbhade, *CrystEngComm* **2011**, *13*, 3258-3264.

[7] K. Vyas, H. Manohar, *Mol. Cryst. Liq. Cryst.* **1986**, *137*, 37-43.

[8] (a) L. A. Errede, M.C. Etter, R. C. Williams, S. M. Darnauer, *J. Chem. Soc., Perkin Trans. 2* **1981**, 233-238; (b) M.C. Etter, *J. Chem. Soc., Perkin Trans. 2* **1983**, 115-121; (c) Y-D Cheng, S-Y Lin, *J. Agric. Food Chem.* **2000**, *48,* 631-635; (d) S-L Wang, S-Y Lin, T-F Chen, *Chem. Pharm. Bull.* **2001**, *49*, 402-406.

[9] (a) M. D. Cohen, G. M. Schmidt, F. I. Sonntag, *J. Chem. Soc.* **1964**, 1996-2000; (b) G. M. Schmidt, J. *Pure Appl. Chem.* **1971**, *27*, 647-678.

[10] (a) A. E. Troup, H. Mitchner, *J. Pharm. Sci.* **1964**, *53*, 375-379; (b) A. L. Jacobs, A. E. Dilatush, S. Weinstein, J. J. Windheuser, *J. Pharm. Sci*. **1966**, *55*, 893-895; (c) K. T. Koshy, A. E. Troup, R. N. Duvall, R. N. Conwell, L. L. Shankle, *J. Pharm. Sci*. **1967**, *56*, 1117-1121.

Appendix II given in Pen Drive, along with Thesis

List of the content in Appendix II

Chapter 3

Section 3A

Progress towards designing crystals capable of supporting intermolecular benzoyl group migration: polymorphism, reactivity, and crystal structure of racemates and enantiomers of *myo*-inositol orthoester dibenzoates.

Some of the results presented in this chapter are published:

M. I. Tamboli, V. Bahadur, R. G. Gonnade, M. S. Shashidhar, Correlation of the solid-state reactivities of racemic 2,4(6)-di–*O*–benzoyl-*myo*-inositol-1,3,5-orthoformate and its 4,4'–bipyridine cocrystal with their crystal structures, *Acta Cryst*. **2014**, *C70*, 1040-1045.

Introduction:

There has been a revival in interest in polymorphism – a phenomenon which manifests in the differences in the solid state structure and properties of small molecules - in the recent past.[1] Polymorphism of molecular crystals has been the subject of intense investigations due to its implications in topics as varied as understanding the origin of crystal structures and prediction of crystal structures to potency of bio-active compounds, herbicides, high energy materials, dyes and pigments, patentability and commercial aspects of drugs and APIs.[2] Relatively less conspicuous in the literature is the effect of polymorphic structures of small organic molecules on their chemical properties in the crystalline state.[3] This could be largely due to the major role of serendipity in the identification of crystalline solids capable of supporting chemical reactions in them. Hence, although there are instances of chemical reactions taking place in molecular crystals[4] and cocrystals[5] investigations on the polymorphism exhibited by these small molecules and its effect on the chemical reactions are scarce. We had reported the first instance of intermolecular benzoyl group transfer reactivity in crystals (Form **1.21I** crystals) of racemic **1.21**, more than a decade ago.[4c] This chapter presents results on the (pseudo)polymorphic behavior of racemic 2,4-di-*O*-benzoyl-*myo*-inositol-orthoformate **1.21** (Scheme 3.1). Although we suspected the existence of polymorphs of racemic **1.21**, based on the occasional variation in observed reactivity of racemic **1.21** in the crystalline state, isolating the polymorphic crystals suitable for X-ray diffraction analysis proved to be elusive. However our consistent efforts to capture the elusive polymorphs of racemic **1.21** yielded two new polymorphs (Forms **1.21II** and **1.21III** crystals) and one solvatomorph containing chloroform (Form **1.21IV** crystals). Whereas the solvatomorph Form **1.21IV**, after the escape of chloroform solvent from the crystal lattice exhibited comparable intermolecular benzoyl group transfer reactivity (Scheme 3.1) in the presence of solid sodium carbonate (as observed in Form **1.21I** crystals[4c]). The crystal structure analysis of the third polymorph (i.e. Form **1.21III** crystals) and the chloroform solvate (Form **1.21IV** crystals) revealed unfavorable molecular organization for the acyl transfer reaction and hence suggested them to be uncreative. We have demonstrated in Chapter 1 that an understanding of crystal structures that support acyl-transfer reactions can assist in the prediction of occurrence (or not) of similar reactions in other molecular crystals.[6]

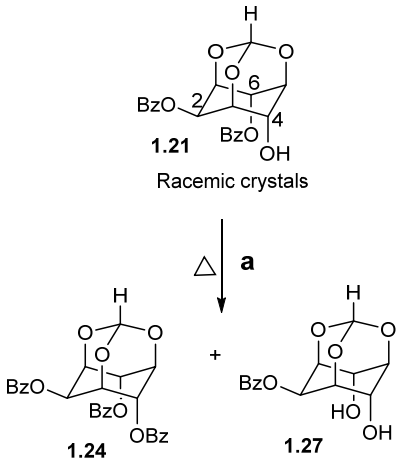

Scheme 3.1: Transesterification reaction in crystals of racemic **1.21** (a) Anhydrous Na_2CO_3.

Results and discussion:

Crystallization of the racemic dibenzoate **1.21** from common organic solvents gave Form **1.21I** crystals (reported earlier[4c]); but crystallization from chloroform - *n*-hexane mixture gave Form **1.21I** crystals along with smaller amount of Form **1.21II** or Form **1.21III** crystals in the same flask, depending on the solvent composition. Since Form **1.21I** crystals were obtained in all the crystallization attempt, their formation seems to be thermodynamically controlled whereas occasional formation of Forms **1.21II** and **1.21III** crystals appears to be driven by kinetic process. We also attempted the crystallization of racemic **1.21** in the presence of (-)-D-2,6-di-*O*-benzoyl-*myo*-inositol-1,3,5-orthobenzoate (**D-1.23**) hoping to improve the yield of Forms **1.21II** and **1.21III** crystals, since the structurally similar additives that mimic the conformation of a molecule in stable crystal structures can suppress the formation of stable polymorphs.[7] However, this experiment resulted in the formation of the chloroform solvate (Form **1.21IV**) of **1.21**. The Form **1.21IV** crystals turned opaque completely in a few days when stored at room temperature and open to atmosphere. The DSC and PXRD profiles of this opaque solid revealed sharp peaks, which suggested it to be polycrystalline in nature. These crystals were also not suitable for single crystal X-ray diffraction experiments. A comparison of the PXRD profile of this opaque solid with other polymorphs suggested it to be inhomogeneous (in terms of polymorphic composition). Although these crystals exhibited intermolecular benzoyl group transfer reaction in the presence of solid sodium carbonate, the yield

varied in range 20-40% of each of the tribenzoate **1.24** and monobenzoate **1.27** with different batches. This suggested that the conversion of Form **1.21IV** crystals to other crystal forms was neither specific nor consistent. Form **1.21II** and Form **1.21III** crystals were stable and did not exhibit any thermal phase transitions to Form **1.21I** crystals as revealed by their DSC and PXRD profiles. Crystal structure of Form **1.21I** and Form **1.21II** were similar[6] and Form **1.21II** crystals have all the required parameters for facile intermolecular benzoyl group transfer reaction (see below).

Structure of the polymorphs of the racemic dibenzoate 1.21:

Form **1.21I** crystals of **1.21** crystallized in monoclinic space group $P2_1/c$,[4c] while crystals of Form **1.21II** belong to triclinic space group *P*-1, both comprising two molecules in the asymmetric unit. Crystals of Form **1.21III** and the chloroform solvate, Form **1.21IV**, belong to monoclinic space group $P2_1/c$ and $P2_1/n$ respectively containing one molecule in the asymmetric unit. Molecules in all the polymorphs and chloroform solvate of **1.21** were superimposed to examine their conformational differences (Figure 3.1). Structure overlay of both molecules in the asymmetric unit of Form **1.21I** and Form **1.21II** crystals show similar conformation whereas molecules in Form **1.21III** and Form **1.21IV** crystals showed marked difference in conformation. The conformation of the C6-*O*-benzoyl group in Form **1.21III** and Form **1.21IV** has similar conformation; however conformation of the C2-*O*-benzoyl group revealed noticeable difference. The orientational differences of about 83.5° and 84.5° were observed in the conformations of C6-*O*-benzoyl groups in Form **1.21I** with respect to Form **1.21III** and Form **1.21IV** crystals respectively. Similarly, marked differences were also observed in the relative orientation of the equatorial C2-*O*-benzoyl groups in Form **1.21I**, Form **1.21III** and Form **1.21IV** crystals. The degree of difference between Form **1.21I** and Form **1.21III**, Form **1.21I** and Form **1.21IV**, and Form **1.21III** and Form **1.21IV** were 49.8°, 34.8° and 84.5° respectively.

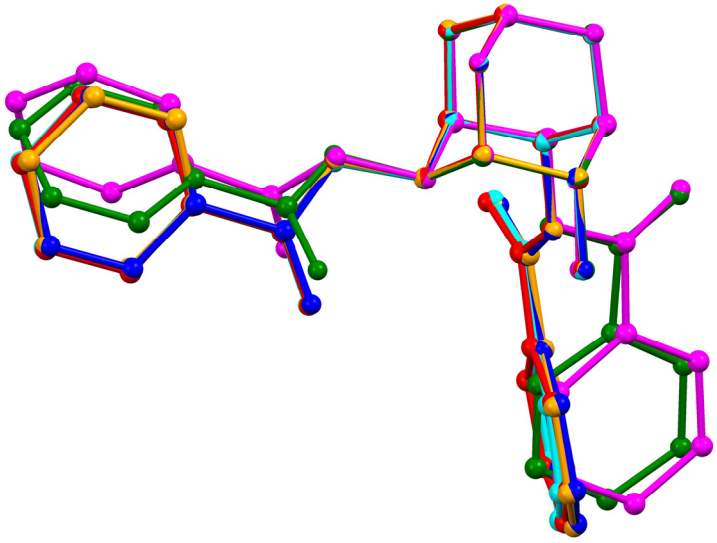

Figure 3.1: Structure overlay of molecules in the asymmetric unit of polymorphs of **1.21**. Form **1.21I** - unprimed molecule - cyan and primed molecule – blue; Form **1.21II** - unprimed molecule - red and primed molecule - orange); Form **1.21III** – magenta; Form **1.21IV** - green. ORTEPs of polymorphs and chloroform solvate of dibenzoate **1.21** are provided in Appendix III (Figure A11-A14, Appendix III).

Structure of Form 1.21I and Form 1.21II crystals of the dibenzoate 1.21.

Similar conformation of molecules in Form **1.21I** and Form **1.21II** crystals reflected in their grossly similar molecular packing. Molecules in Form **1.21I** and Form **1.21II** crystals generate similar helical assemblies through O-H···O (O4-H4*A*···O7, O6'-H6'*A*···O7' for Form **1.21I** and O4-H4A···O7, O4'-H4'A···O7' for Form **1.21II** crystals, entries 1, 2, 15, 16, Table A1, Appendix III) hydrogen bonding interactions (Figure 3.2).

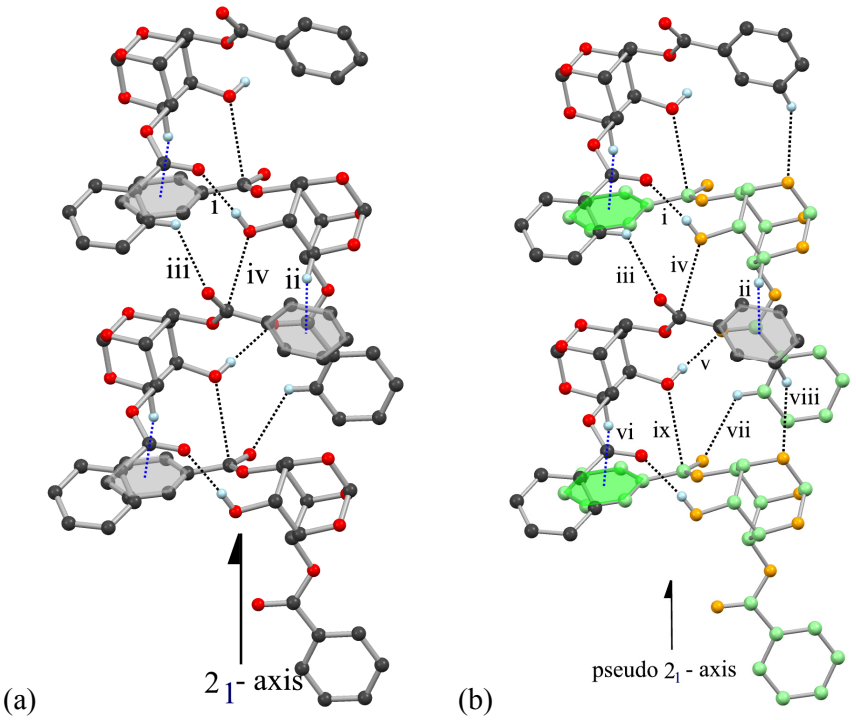

Figure 3.2: Comparison of the helical assemblies formed by molecules in (a) Form **1.21I** and (b) Form **1.21II** crystals. Gray and green molecules in (b) are symmetry independent however they have same configuration. Helical assembly in Form **1.21I** crystals is formed (by association of one of the molecule in the asymmetric unit) *via* (i) O4-H4*A*···O7 hydrogen bond and supplemented by (ii) C3-H3···πCg6, (iii) C10-H10···O8 and short (iv) H4*A*-O4···C15=O8 contact. In Form **1.21II** crystals the helical assembly is formed (by association of both the molecules in the asymmetric unit) through (i) O4'-H4'*A*···O7 and (v) O4-H4*A*···O7' supported by (ii) C3'-H3'···πCg6, (iii) C10-H10···O8, (iv) short H4'*A*-O4'···C15 = O8, (vi) C3-H3···πCg15, (vii) C10'-H10'···O8', (viii) C18-H18···O5' and short (ix) H4*A*-O4···C15' = O8' interactions.

Each helix in Form **1.21I** and Form **1.21II** crystals of racemic dibenzoate **1.21** is chiral due to the association of same enantiomers *via* hydrogen bonding interactions. Both symmetry independent molecules (both enantiomers) in Form **1.21I** crystals create their respective helical assemblies along the crystallographic 2_1-screw axis (Figure 3.2a and Figure 3.3a) however; the association is different in Form **1.21II** crystals. In Form **1.21II** crystals both symmetry independent (same enantiomer) molecules assemble alternately along non-crystallographic axis to generate the

composite helix (Figure 3.2b, Figure 3.3b). Both molecules unit-translate along the *a*-axis to form pseudo-two fold screw axis (two fold screw axis is not the symmetry element in triclinic system). It is worth to note that although the O···O distances in O-H···O hydrogen bonding interactions in both polymorphs are comparable, the H···O distances and the angles O-H···O show marked difference (Table A1, Appendix III). The H···O distances are short and angles O-H···O are linear in Form **1.21I** crystals while in Form **1.21II** crystals they follow opposite trend, the H···O distances are long and the angles O-H···O deviate from linearity. Molecules in the helix also get support from short and linear C-H···π, an interaction which ensures their tight binding along the helix. The geometry of the C-H···π interactions made by the C1'-H1'or C3-H3 in Form **1.21I** (C3'-H3', C3-H3 in Form **1.21II**) of the inositol ring with the phenyl ring of C6-O-benzoyl group of the next molecule along the helix is similar (entries 7, 8, 22 and 23, Table A1, Appendix III). The carbonyl oxygen atom O8 of the C6-*O*-benzoyl group in both polymorphs is also involved in supporting the helical architecture although through long and non-linear C10-H10···O8 and C10'-H10'···O8' (entries 11, 12, 26 and 27, Table A1, Appendix III) interactions made by the unit-translated molecules along the helical axis (Figure 3.2b). The helical assembly formed by primed molecules in Form **1.21I** crystals is further supplemented by C18'-H18'···O5' (entry 13, Table A1, Appendix III) interactions to provide the tight binding of the molecules along the helix. The helical assemblies in both polymorphs brings the electrophile (El, C=O) of the axial C6-*O*-benzoyl group of one molecule in proximity to the nucleophile (Nu, -OH) of the axial C4-hydroxyl group of the next molecule along the helix to create the short O···C=O contact of varying 'pre-organized' geometry. Therefore, in Form **1.21I** crystals, there are two types of El···Nu geometries along the two different helices formed by each enantiomer (primed and unprimed); i.e. one between the C6-*O*-benzoyl group and C4-hydroxyl group (in one helix) and other between C6'-*O*-benzoyl group and C4'-hydroxyl group. Similarly, in Form **1.21II** crystals also there are two types of El···Nu geometries however, both geometries are part of the single composite helix. The first geometry is between the C6-*O*-benzoyl group and C4'-hydroxyl group and the other between C6'-*O*-benzoyl group and C4-hydroxyl group.

The packing of these neighboring helices in both forms are also grossly similar (Figure 3.3). Helices in both crystal forms pack discretely in antiparallel fashion.

Neighboring helices in Form **1.21I** crystals are linked *via* C-H···O interactions namely C21-H21···O2', C21'-H21'···O2, C3'-H3'···O8 and C-H···π (C4-H4···Cg14) (Figure 3.3a, entries 5, 6, 14, 9, Table A1, Appendix III) to generate the discrete packing of helices on the *ab* plane. Similarly, neighboring helices in Form **1.21II** crystals are connected centrosymmetrically *via* C1-H1···O8, C1'-H1'···O8', C21-H21···O2 and C21'-H21'···O2' (Figure 3.3b, entries 20, 21, 28, 29, Table A1, Appendix III) to enable the distinct packing of helices along the *bc* diagonal.

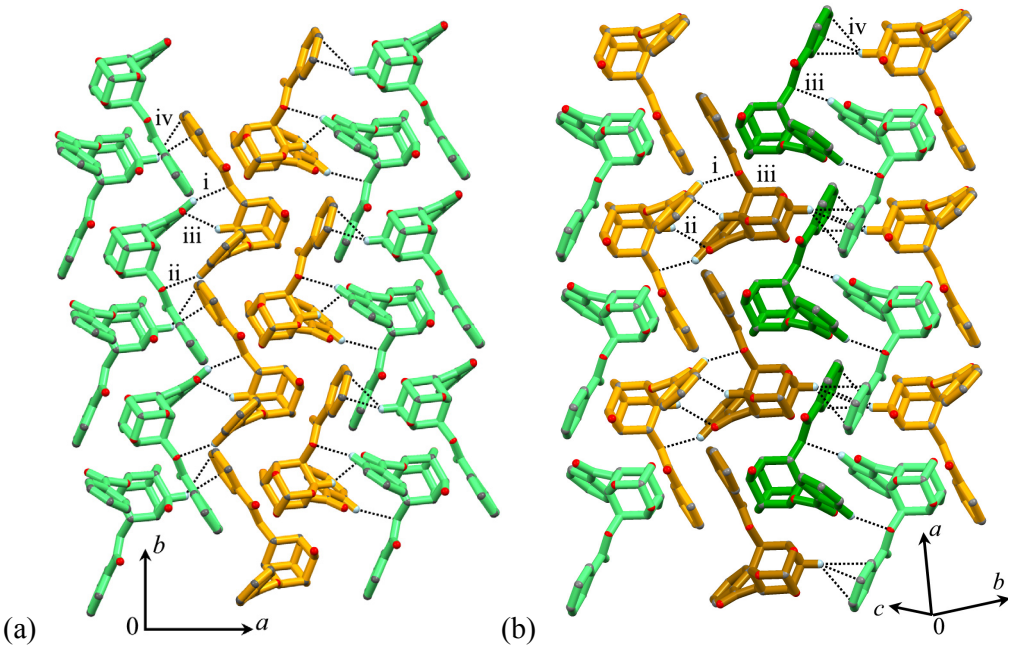

Figure 3.3: Packing of helices in Form **1.21I** (a) and Form **1.21II** (b) crystals of the racemic dibenzoate **1.21**. Discrete helices are seen in both polymorphs of **1.21**. The color scheme is used to distinguish the neighboring helices; in Form **1.21I** crystals unprimed and primed molecules are displayed as green and orange respectively, whereas in Form **1.21II** crystals, the unprimed and primed molecules are displayed orange and green respectively. The slight darker shade is used to just to distinguish the neighboring helices. In Form **1.21I** crystals the neighboring helices are linked via (i) C21-H21···O2', (ii) C21'-H21'···O2, (iii) C3'-H3'···O8 and (iv) C-H···π (C4-H4···Cg14) interactions whereas in Form **1.21II** crystals the adjacent helices are connected through (i) C21-H21···O2, (ii) C1-H1···O8, (iii) C21'-H21'···O2', and (iv) C-H···π (C4-H4···Cg14) interactions. Dotted lines in all the figures indicate C-H···O or C-H···π contacts.

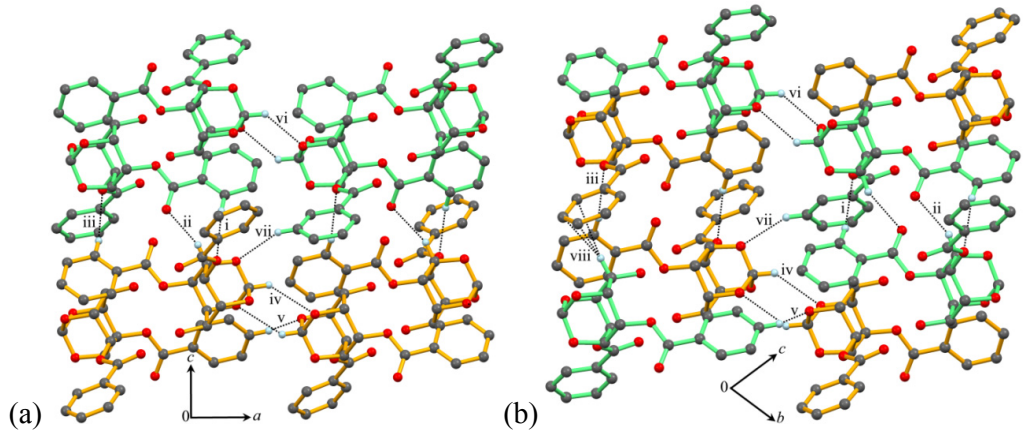

Figure 3.4: Association of dancing pairs through C-H…O interactions in (a) Form **1.21I** and (b) Form **1.21II** crystals of **1.21**. The color scheme is used to distinguish the different enantiomers. In Form **1.21I** crystals the adjacent dancing pairs are linked via (i) C21-H21···O2', (ii) C3'-H3'···O8, (iii) C21'-H21'···O2, (iv) C7'-H7'···O5', (v) C19-H19···O1', (vi)C7-H7···O3 and (vii) C13-H13···O3' contacts whereas in Form **1.21II** crystals the neighboring dancing pairs are connected through (i) C21-H21···O2, (ii) C1-H1···O8, (iii) C21'-H21'···O2', (iv) C7'-H7'···O5', (v) C19-H19···O3', (vi)C7-H7···O3, (vii) C13-H13···O1' and (viii) C4-H4···πCg14 interactions.

A view of the molecular organization down the helical axis in both polymorphs reveals a pair-wise association of molecules, similar to dancing pairs (Figure 3.4). The packing of these dancing pairs show bridging of adjacent helices. The overall packing of these dancing pairs is different in both forms. In Form **1.21I** crystals each dancing pair is formed by same enantiomer molecules related by crystallographic 2_1 axis whereas in Form **1.21II** crystals they are formed by same enantiomer molecules however both molecules are conformational isomers related by pseudo 2_1 axis. Neighboring helices in Form **1.21I** crystals are connected centrosymmetrically *via* C21'-H21'···O2, C21-H21···O2', C3'-H3'···O8 (entry 5, 6, and 14 and 9; Table A1, Appendix III) interactions along the *a*-axis whereas they are linked via C7'-H7'···O5', C7-H7···O3, C13-H13···O3' and C19'-H19'···O1'(entries 18, 17, 19 and 30; Table A1, Appendix III) interactions along the *c*-axis to generate the compact packing. In Form **1.21II** crystals the neighboring dancing pairs are associated *via* centrosymmetric C21-H21···O2, C21'-H21'···O2', C1-H1···O8, C13-H13···O1' and C4-H4···Cg14 (entries 20, 21, 24, 25 and 28; Table A1, Appendix III) interactions along the *bc* diagonal whereas along the direction normal to the *bc*

diagonal the adjacent pairs are joined *via* centrosymmetric C7'-H7'···O5', C7-H7···O3 and C19-H19···O3' (entries 17, 18 and 30; Table A1, Appendix III) interactions to generate the packing similar to Form **1.21I** crystals. The geometrical parameters of all these C-H···O interactions are similar in both forms (Table A1, Appendix III).

Structure of Form 1.21III crystals of the dibenzoate 1.21:

Structure of Form **1.21III** crystals (consisting of molecules of **1.21** which showed marked difference in conformation of C2-*O*- and C6-*O*-benzoyl groups as compared to molecules in Form **1.21I** and Form **1.21II** crystals) resembled the crystal structure of the 2,4-di-*O*-*p*-halobenzoyl analogs of **1.21**.[8] The striking difference in the conformation of C2-*O*-benzoyl group of **1.21** in Form **1.21III** crystals compared to the Forms **1.21I** and **1.21II** crystals precluded the helical association of molecules. Instead molecules in Form **1.21III** crystals generated a one-dimensional molecular string (by assembly of one of the enantiomers of **1.21**) along the *b*-axis (screw axis) *via* the stitching of the unit-translated molecules. Molecules along the 1D string are linked via the intermolecular O4-H4*A*···O1 (entry 31; Table A1, Appendix III) interactions engaging hydroxyl (O4-H4*A*) and oxygen atom O1 of the orthoformate bridge along with C-H···π contact made by C1-H1 of the inositol ring with the phenyl ring of the C6-O-benzoyl group. Both contacts mentioned above are short and almost linear in approach (entries 31 and 38; Table A1, Appendix III). The neighboring antiparallel 1D molecular string comprised of the other enantiomer of racemic **1.21** that weaved centrosymmetrically with the first one across the inversion center via bifurcated C5-H5···O8, C7-H7···O8 and C6-H6···O5 (entries 33, 35 and 33; Table A1, Appendix III) interactions (Figure 3.5a). The geometries of these interactions are similar. The 1D bilayers are associated through centrosymmetric C19-H19···O7 (entry 36; Table A2, Appendix III) contact and hydrophobic forces to create a 2D bilayer see Figure 3.5b. Along the third dimension these 2D bilayers are connected *via* three C-H···O interactions namely C3-H3···O3, C14-H14···O3 and C19-H19···O7 (entries 32, 37 and 36; Table A1, Appendix III) and a marginal C-H···π interactions (entry 39; Table A1, Appendix III) made by C20-H20 of the phenyl ring of the C6-*O*-benzoyl group with the phenyl ring of the C2-*O*-benzoyl group to generate the compact packing on the *ac* plane (Figure A19, Appendix III).

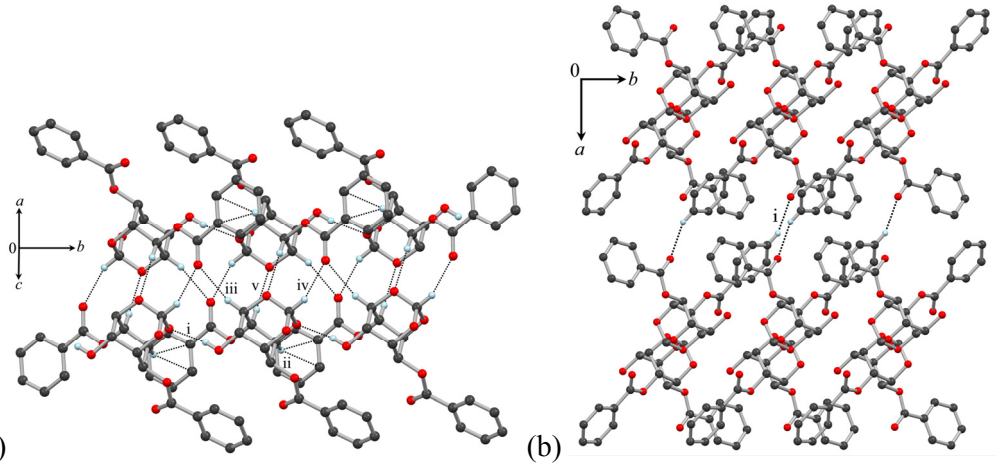

Figure 3.5: (a) Stitching of the 1D molecular strings formed via (i) O4-H4*A*···O1 hydrogen bond and (ii) C1-H1···π contact through (iii) C5-H5···O8 (iv) C7-H7···O8 and (v) C6-H6···O5 contacts to produce a bilayer structure. (b) Linking of the adjacent bilayers through weak (i) C19-H19···O7 contacts and other hydrophobic forces.

Structure of Form 1.21IV crystals of the dibenzoate 1.21:

Although the conformation of both benzoyl groups differ significantly in Form **1.21IV** crystals compared to Forms **1.21I** and **1.21II** crystals, molecules of **1.21** in chloroform solvate do generate helical assemblies along the crystallographic 2_1 screw axis similar to those present in Form **1.21I** and Form **1.21II** crystals. The successive molecules along the helix are linked *via* classical O-H···O=C hydrogen bonding interactions (entry 40, Table A1, Appendix III); the –OH group at the C-4 position donates its H atom to the carbonyl oxygen O7 of the equatorial C2-*O*- benzoyl group (Figure 3.6a). This is similar to the helical assembly observed in pseudopolymorphs of *p*-chloro and *p*-bromo-benzoyl analogs of racemic **1.21**.[9] The H···O distance is comparable with that observed in Form **1.21I** crystals but the O-H···O interaction is nonlinear. In addition to O-H···O some weak C-H···O contacts also hold the molecules together along the helix. The C5-H5 and C4-H4 of the inositol ring make C-H···O contacts respectively with the hydroxyl oxygen O4 and carbonyl oxygen O7 of the adjacent 2_1 screw related molecule along the helix (entries 43 and 44, Table A1, Appendix III). Additionally, along the helical assembly, the unit-translated molecules are linked via short and linear C11-H11···O1 (entry 46, Table A1, Appendix III) contacts. The helices are packed more compactly roughly normal to the *ac* diagonal *via* short but non-linear C7-H7···O1 and C11-H11···O3 (entries 45 and 46, Table A1,

Appendix III) interactions along with staggered aromatic πCg5···πCg5 (entry 49, Table A1, Appendix III) stacking interactions between the phenyl rings of the C*2*-O-*p*-halobenzoyl group leaving no accessible space for solvent inclusion along this direction (Figure A20, Appendix III). However, the arrangement of the neighboring helices along *ac* diagonal reveal their discrete packing similar to the Forms **1.21I** and **1.21II** crystals providing well guided channel (Figure 3.6b). The linking of the adjacent antiparallel helices along this direction is solely via weak hydrophobic forces which create a cavity of roughly dimension 7×9 Å^2 to accommodate the chloroform molecules in between the two orthoformate bridgeheads.

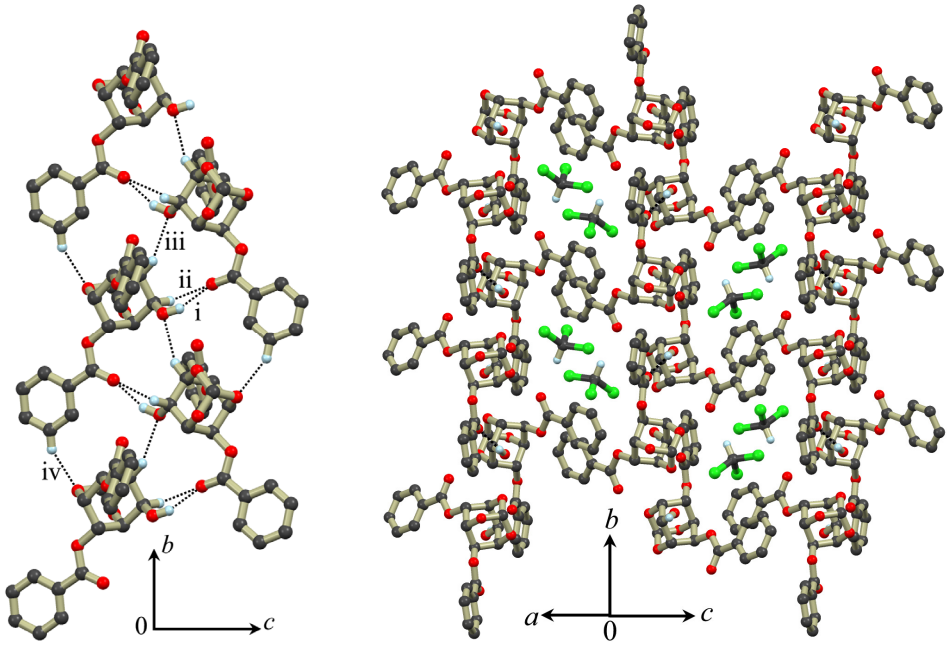

(a) (b)

Figure 3.6: (a) Helical assembly of molecules of **1.21** in Form **1.21IV** crystals generated through (i) O4-H4*A*···O7 hydrogen bonds. The helical chain is further supported by (ii) C4-H4···O7, (iii) C5-H5···O4 and (iv) C11-H11···O1 contacts. (b) The neighboring helical assemblies are loosely packed diagonal to the *ac* plane to create the accessible space for chloroform molecules.

The guest chloroform molecules occupy the open channel and interact with the host molecules (of racemic **1.21)** *via* C-H···O, C-H···Cl, C-Cl···O and C-Cl···π contacts. The C22–H22 of the chloroform molecule interacts with carbonyl oxygen atom O8 of the host to create C22-H22···O8 interaction (entry 47; Table A1, Appendix III); Cl2

interacts with ether oxygen O5 to generate C22-Cl2···O5 (entry 48; Table A1, Appendix III) halogen bonding contact; the inositol ring H atoms, H2 and H4 interact with chlorine atom Cl2 to form C2-H2···Cl2 (entry 41; Table A1, Appendix III) and C4-H4···Cl2 (entry 42; Table A1, Appendix III) interactions; the Cl3 atoms of chloroform is engaged with C-Cl···π (entry 50; Table A1, Appendix III) contact with the phenyl ring of the C2-O-benzoyl group (Figure 3.7). All these contacts are weak and are not sufficiently strong to hold the guest chloroform molecules in the crystal lattice under ambient conditions. Molecular packing viewed down the helical axis revealed that the chloroform molecules occupy the channel created in between the helix (Figure A21, Appendix III).

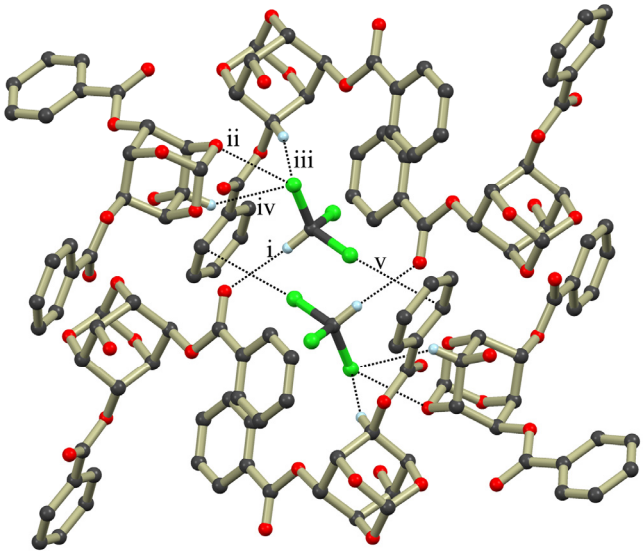

Figure 3.7: Host – guest interactions in Form **1.21IV** crystals, guest molecules interact with the host molecules *via* (i) C22-H22···O8, (ii) C22-Cl2···O5, (iii) C2-H2···Cl2, (iv) C4-H4···Cl2, and (v) C22-Cl3···πCg5 contacts.

The computation of lattice energies for polymorph and solvatomorph of racemic **1.21** using Coulomb-London-Pauli (**CLP**) models integrated into the computer program package **CLP** revealed the values of -165.0, -164.4, -143.3 and -114.7 kJ mol^{-1} for Form **1.21I**, Form **1.21II**, Form **1.21III** and Form **1.21IV** crystals respectively. The values of crystal densities 1.477 g cm^{-3} (Form **1.21I** and Form **1.21II**) and 1.474 g cm^{-3} (Form **1.21III**) are consistent with the calculated lattice energies. The lattice energy values indicate that the Form **1.21I** crystal is the most

stable whereas Form **1.21IV** crystal is the least stable; amongst the three polymorphs, Form **1.21III** is the least stable. This may explain the formation of only Form **1.21I** crystals in most of the crystallization trials. However, occasional appearance of only Form **1.21II** crystals from chloroform-*n*-hexane solution of racemic **1.21** cannot be accounted on the basis of lattice energies, since both Forms **1.21I** and **1.21II** have almost the same lattice energies. The lesser stability of Form **1.21IV** crystals could be because of the weak association between the host molecules that resulted in the fragile packing leading to the release of chloroform molecules from the crystal lattice.

In addition to the lattice energies, the CLP module also calculates intermolecular interaction energies to elucidate which molecular organizations contribute most to the overall lattice stabilization. The intermolecular interaction energies for short and linear O-H···O interactions involved in the formation of helical assembly of molecules in Forms **1.21I**, **1.21II** and **1.21IV** crystals and linear chain in Form **1.21III** crystals have values -74.2 kJ mol^{-1}, -70.7 kJ mol^{-1} (Form **1.21I** crystals), -72.2 kJ mol^{-1}, -69.6 kJ mol^{-1} (Form **1.21II** crystals), -80.3 kJ mol^{-1} (Form **1.21IV** crystals) and -49.4 kJ mol^{-1} (Form **1.21III** crystals). The O-H···O interactions energy values indicates that helical association of molecules is the most preferred organization and the linear chain assembly observed in Form **1.21III** crystals is least favored. However, this could be because of the involvement of more basic carbonyl oxygen as hydrogen bond acceptor in Forms **1.21I**, **1.21II** and **1.21IV** compared to less basic ether oxygen in Form **1.21III** crystals. The interactions energies for C-H···O interactions could not be computed in Forms **1.21I**, **1.21II** and **1.21IV** crystals because of their weak geometries, but energies for two short and linear C-H···O interactions namely C6-H6···O5 and C7-H7···O8 engaged in the stitching of the linear O-H···O assemblies in Form **1.21III** crystals could be estimated with interaction value -20.3 kJ/mol.

Intermolecular interactions in polymorphs of racemic **1.21**were quantified *via* Hirshfeld surface analysis[10] (Figure A22, Appendix III) and Fingerprint plots of the Hirshfeld surfaces (Figure A23, Appendix III) using *CrystalExplorer*[11]. The relative contribution of various non-covalent interactions show the differences in the structures of polymorphs of racemic **1.21** (Figure 3.8).

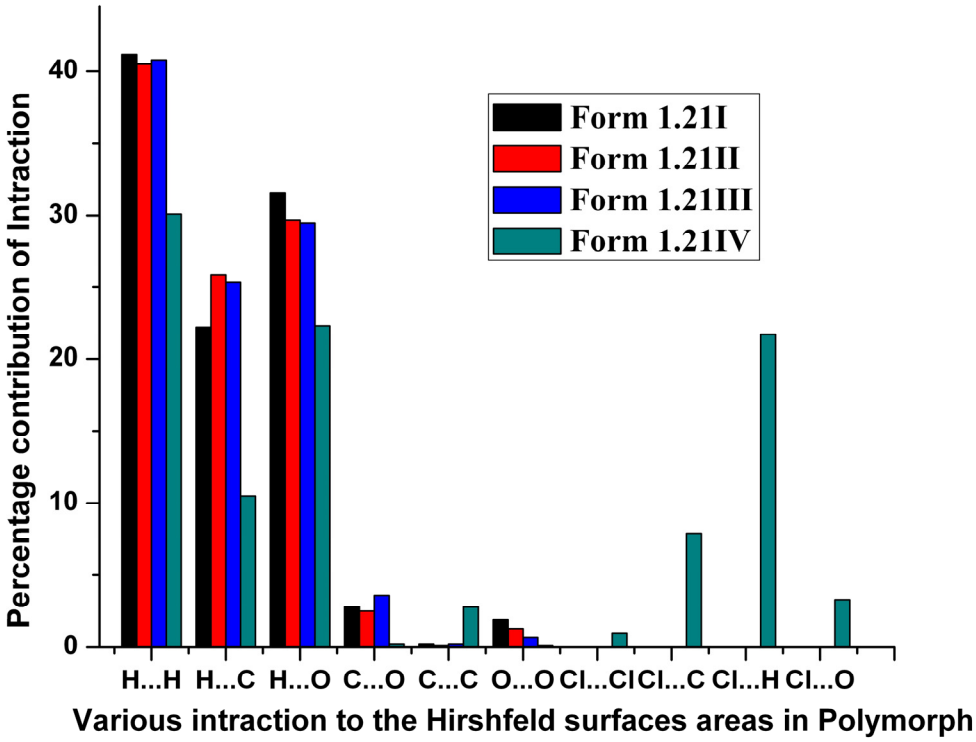

Figure 3.8: Contribution of various interactions to Hirshfeld surface areas in polymorph of **1.21**. Axis label: *X*-axis: Non-covalent interactions; *Y*-axis: % contribution of interactions.

Benzoyl transfer reactivity of polymorphs of racemic 1.21 in the light of their crystal structures:

Single crystal structure analysis of all the crystal forms of racemic **1.21** was carried out with an aim to understand the benzoyl transfer reactivity of racemic **1.21** in the solid state. Subsequent to reporting the first intermolecular benzoyl group transfer reaction in crystals of racemic **1.21**,[4c] we encountered samples of racemic **1.21** which did not exhibit the transesterification reaction with conversion exceeding 90%. We did realize that this could be due to the presence of polymorphic crystals of racemic **1.21**, since crystallization of these 'less reactive samples' gave crystalline solids that exhibited chemical conversions exceeding 90%. Our initial attempts to grow and isolate 'less reactive crystals' of **1.21** were not successful. Recently we were successful in obtaining crystal structure of several polymorphs as mentioned above and compare their structures. Among these polymorphs, Form **1.21II** and **1.21III** crystal have very poor reproducibility (or difficult to obtain) as compared to other forms. The isolation of polymorphs of racemic **1.21** was particularly strenuous since the unreactive polymorph and the pseudopolymorph were minor components in the solid and also were not very stable under crystallization conditions.

Distance (Å) / Angle (°)	**Form 1.21I**	**Form 1.21II**	**Form 1.21III**	**Form 1.21IV**
O4(Nu)…C15(El)	3.240/3.160	3.198/3.190	5.635/3.602*	4.698
∠ O4(Nu)···C15-O7(El)	91.49/88.95	90.16/90.70	11.86/136.99*	33.90
∠H4*A*-O4(Nu)···C15(El)	108.36/116.62	113.37/113.23	55.95/76.76*	84.64
∠C4-O4(Nu)···C15 (El)	114.44/119.31	118.40/114.80	92.36/173.80*	73.37

Table 3.1: Geometrical parameters for El···Nu interactions between neighboring molecules with the closest approach in the polymorphs and chloroform solvates of racemic **1.21**. * implies geometrical parameter of axial hydroxyl group with equatorial ester group. [Relative orientation of the molecules are shown in Figures A15-A18 (Appendix III)].

The helical association of molecules in Form **1.21I**[5b] and Form **1.21II** crystals places the C6-O-benzoyl (El) group and C4-hydroxyl group (Nu) suitable for the intermolecular benzoyl group transfer reaction (Table 3.1). Since these parameters are conducive for a facile intermolecular benzoyl transfer reaction, Form **1.21II** crystals of **1.21** supports transesterification reaction in the presence of solid sodium carbonate as revealed from the crystal structure analysis. The El···Nu geometry in Form **1.21III** and Form **1.21IV** crystals deviate from that observed in Form **1.21I** and **1.21II** crystals and hence are not expected to undergo transesterification below their melting points. The solid state benzoyl transfer reactivity of Form **1.21III** and Form **1.21IV** crystals of **1.21** could not be tested due to low yield (Form **1.21III**) and stability issues (Form **1.21IV**) associated with these forms. But, we had shown earlier that deviation from the geometrical parameters for El···Nu interaction led to loss of reactivity in molecular crystals.[5b] As mentioned earlier, the reactivity of opaque crystals obtained from Form **1.21IV** crystals was not consistently reproducible. Hence we can conclude that the reason for the occasional variation in transesterification reactivity of crystals of racemic **1.21** was due to the formation of the polymorphs whose structure does not support benzoyl transfer reaction.

Conclusions:

Racemic 2,4-di-*O*-benzoyl-*myo*-inositol-orthoformate (**1.21**) undergoes facile transesterification reaction in the crystalline state, in the presence of solid sodium carbonate. However, occasional difference in the reactivity of racemic **1.21** in the crystalline state prompted us to investigate its polymorphic behavior. This investigation yielded three polymorphs and one chloroform solvate of racemic **1.21**. Structures of all these crystal forms were solved. However, only the Form **1.21I** crystals and the chloroform solvate could be obtained reproducibly while formation and yield of Forms **1.21II** and **1.21III** were inconsistent in crystallization experiments. DSC and powder X-ray diffraction measurements revealed that the polymorphs did not undergo thermal phase change. The geometrical parameters of the nucleophile···electrophile (-HO···C=O) geometry along the helix in Forms **1.21I**, **1.21II** suggested facile acyl transfer reactivity, which was confirmed by experiment.

During routine preparation and crystallization steps (of racemic **1.21**), it is likely that the relative proportions of the polymorphs vary occasionally and lead to variation in the transesterification reactivity (in the solid state) and extent of conversion of

racemic **1.21** to the products. It is interesting to note that the structure of Form **1.21III** crystals of **1.21** is similar to that of the halobenzoates of *myo*-inositol orthoformate[8] while the structure of the solvated Form **1.21IV** is similar to the solvated crystals of the halobenzoates.[9] These comparisons suggest that the polymorphic crystals of the dibenzoate **1.21** reflect the crystal structure of its closely related analogs. In general, since polymorphic molecular crystals could have widely different reactivities, it can potentially be used as a handle to tune the reactivity of small molecules in the solid state, provided polymorphic behavior of the small molecule can be characterized and controlled.[3] These observations could be useful in engineering crystals and supramolecular assemblies with desired properties.

Experimental section:

Crystallization of racemic 2,4-di-*O*-benzoyl-*myo*-inositol 1,3,5-orthoformate (1.21):

Procedure A: Crystallization of racemic **1.21** from ethyl acetate, methanol, acetone, ethanol, chloroform, dichloromethane, acetonitrile 1,4-dioxane, THF, DMF, toluene, nitromethane usually gave hexagonal crystals (Form **1.21I**, Figure 3.9a) as reported earlier.[4c]

Procedure B: Racemic **1.21** (2.0 g) was dissolved in chloroform (20-25 mL) to obtain a clear solution. *n*-Hexane (20-25 mL) was added and the solution stored (open to atmosphere) under ambient conditions for 1-2 days. Form **1.21I** and occasionally Form **1.21II** crystals were obtained (Figure 3.9b), the quantity of former was always more compared to the latter. Form **1.21II** crystals (along with Form **1.21I**) could also be obtained by crystallization of racemic **1.21** from hot ethyl acetate in the presence of 5-10 mol % of 4, 4'- bipyridine. However, Form **1.21II** could not be obtained in all the crystallization experiments consistently.

Procedure C: Racemic **1.21** (2.0 g) was dissolved in chloroform (20-25 mL) and *n*-hexane (50-60 mL) was added till turbidity appeared. The mixture was warmed to obtain a clear solution. The resulting solution was stored (open to atmosphere) for 1-2 days under ambient conditions in beaker. Few clusters of shiny needle type crystals (Form **1.21III**) were deposited (0.010-0.015 g) along the sides of the beaker (Figure

3.9c). The yield of these crystals was always much less compared to Form **1.21I** crystals at the bottom of the beaker

Procedure D: Racemic **1.21** (2.0 g) and D-(-)2,6-di-*O*-benzoyl-*myo*-inositol-1,3,5-orthobenzoate (0.020 g, 1-2 mol %) see chapter 3B for details) were dissolved in chloroform (20-25 mL) and stored (open to atmosphere) for 1-2 days under ambient conditions in a beaker. Long needle shaped shiny crystals (Form **1.21IV**, Figure 3.9d) appeared (later shown to be chloroform solvate of racemic **1.21**) which were separated from the mother liquor by decantation. Form **1.21IV** crystals turned opaque on exposure to air (3-4 days, Figure 3.9e).

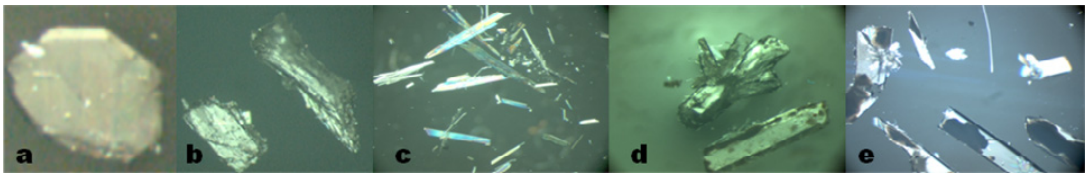

Figure 3.9: Photomicrograhs of crystals of **1.21** (a) Form **1.21I** crystals; (b) Form **1.21II** crystals; (c) Form **1.21III** crystals; (d) Form **1.21IV** crystals and (e) opaque crystals obtained by storing Form **1.21IV** crystals 3-4 days under ambient conditions.

Differential Scanning Calorimetry:

DSC analyses of all the polymorphs of racemic **1.21** were carried out on a Mettler DSC instrument. Crystals (~3-4 mg) were placed on an aluminium pan (40 µl) and were analyzed using an empty pan as the reference. The heating rate was 5° C/min, and nitrogen gas was used for purging. DSC analysis of the three polymorphs (Forms **1.21I - 1.21III**) revealed a single sharp endotherm corresponding to their melting between 175-180 ^{o}C (Figures 3.10, black, red and blue respectively), thus ruling out the possibility of structural phase changes before melting. The DSC profile of Form **1.21IV** crystals showed two endotherms; the first being broad centered at 70 ^{o}C (Figure 3.10, green) indicated the release of solvent molecules from the crystal lattice and the second endotherm peaked at 176 ^{o}C attributed to its melting. DSC of the opaque crystals obtained on storing Form **1.21IV** crystals after 4 days showed only the melting endotherm centered at 176 ^{o}C (Figure 3.10, magenta).

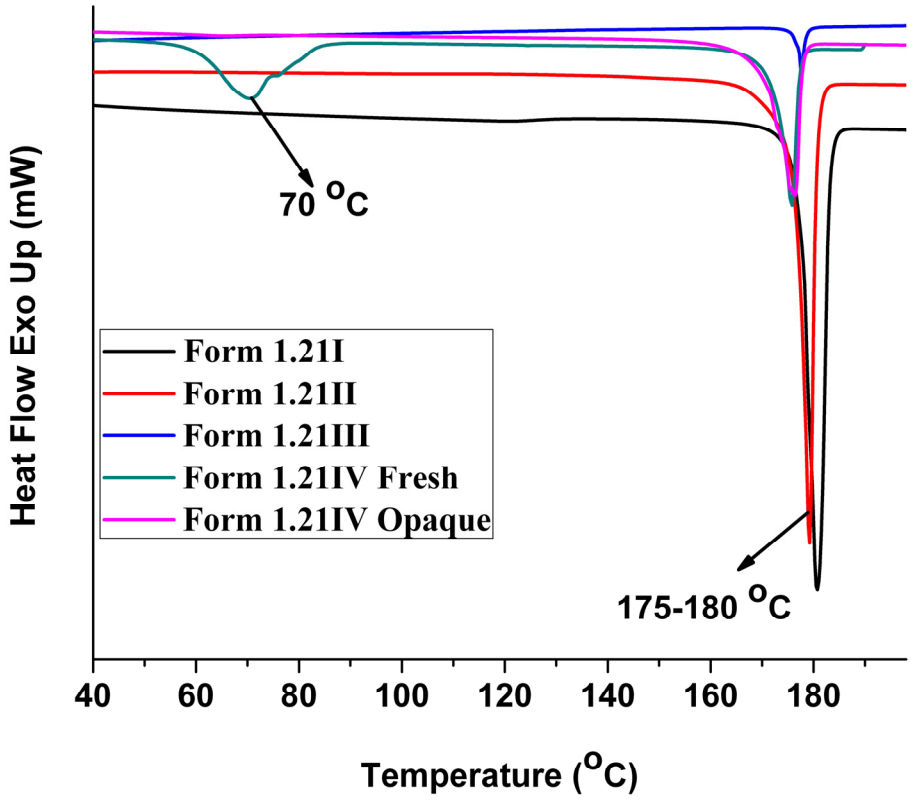

Figure 3.10: DSC profiles of polymorphs and the chloroform solvate of the racemic dibenzoate **1.21**.

Powder X-Ray Diffraction: The experimental PXRD patterns were recorded on Rigaku Micromax-007HF instrument (High intensity microfocous rotating anode X-ray Generator) with R-axis detector IV++ at a continuous scanning rate of 2° 2θ/min using Cu Kα radiation (40 kV, 30 mA) with the intensity of the diffracted X-ray being collected at intervals of 0.1° 2θ. A nickel filter was used to remove Cu K$_\beta$ radiation. The PXRD patterns of Form **1.21I** and Form **1.21II** crystals were similar where as PXRD of Form **1.21III** crystal were not recorded due very less yield (Figure 3.11). The powder X-ray diffraction analysis of freshly grown Form **1.21IV** could not be carried out due its instability on exposure to air. The PXRD patterns of the opaque crystals obtained by exposing Form **1.21IV** crystals to atmosphere under ambient conditions closely resembled that of reactive Form **1.21I** or Form **1.21II** crystals. This revealed the possible structural transformation of Form **1.21IV** crystals after the escape of the solvent (Figure 3.11).

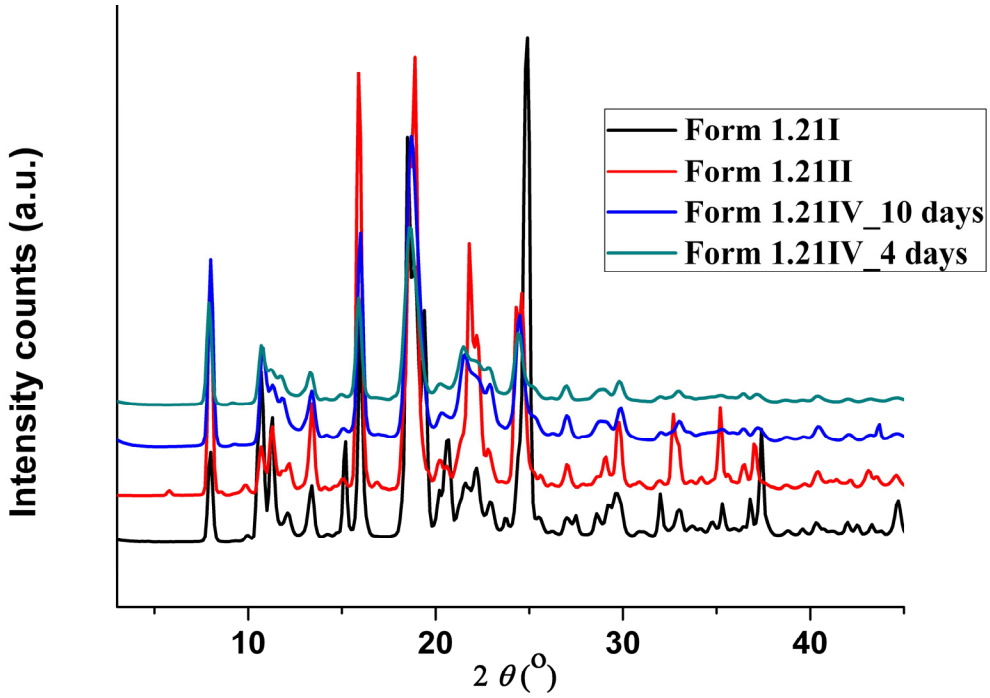

Figure 3.11: PXRD patterns of polymorphs of racemic **1.21** and its chloroform solvate.

X-ray Crystallography:

Single crystal X-ray structures of the polymorphs and chloroform solvate of racemic **1.21** were determined by measuring X-ray diffraction intensity data on a Bruker SMART APEX II single crystal X-ray CCD diffractometer. The data of unstable Form **1.21IV** crystal was carried out at 90K. See Table 3.2 for crystal data and appendix III for other details.

	Form 1.21I	**Form 1.21II**	**Form 1.21III**	**Form 1.21IV**
Formula	$C_{21}H_{18}O_8$	$C_{21}H_{18}O_8$	$C_{21}H_{18}O_8$	$C_{21}H_{18}O_8{\cdot}CHCl_3$
M_r	398.35	398.35	398.35	517.72
Crystal size, mm	0.54 x 0.34 x 0.27	0.54 x 0.34 x 0.17	0.37 x 0.04 x 0.02	0.48 x 0.24 x 0.11
Temp. (*K*) Morphology	100(2) K Hexagonal	100(2) K Block	90(2) K Needle	90(2) K Needle
Crystal system	Monoclinic	Triclinic	Monoclinic	monoclinic
space group	*P2₁/c*	*P*-1	*P2₁/c*	P*2₁/n*
a [Å]	16.3308(4)	9.7459(6)	14.1618(12)	12.5144(6)
b [Å]	9.7407(3)	13.9314(11)	6.4831(5)	9.8946(5)
c [Å] α [°]	22.5175(6) 90	14.0484(9) 71.666(4)	20.0743(16) 90	17.3365(9) 90
β[°] γ [°]	90.692(2) 90	83.050(5) 83.369(4)	103.063(4) 90	94.762(2) 90
V [Å^3]	3581.67(17)	1791.2(2)	1795.4(3)	2139.28(19)
Z, D_{calc} [g cm^{-3}]	8, 1.477	4, 1.477	4, 1.474	4, 1.607
F(000)	1664	832	832	1064
μ [mm^{-1}]	0.115	0.114	0.114	0.478
Ab.correction T_{min} T_{max}	multi-scan 0.9407 0.9697	multi-scan 0.9408 0.9808	multi-scan 0.9586 0.9978	multi-scan 0.8039 0.9488
$2\theta_{max}$	50.10	50.10	50.48	54.00
reflns. collected	25370	11294	13090	18291
Unique reflns.	6324	5927	3244	4665
Observed reflns.	4677	4245	2858	4305
h, k, l (min, max)	(-19, 19), (-11, 11), (-26, 26)	(-11, 11), (-15, 12), (-16, 15)	(-16, 16), (-7, 7), (-24, 23)	(-15, 15), (-11, 12), (-21, 22)
R_{int}	0.0640	0.0350	0.0482	0.0294
No. of para	525	525	264	299
R_1 [I>2σ(I)]	0.0723	0.0606	0.0782	0.0329
wR_2 [I>2σ(I)]	0.1682	0.1386	0.1358	0.0809
R_1 (all data)	0.1013	0.0911	0.0904	0.0360
WR_2 (all data)	0.1844	0.1542	0.1402	0.0831
goodness-of-fit	1.083	1.061	1.293	1.022
$\Delta\rho_{max}$,$\Delta\rho_{min}$(eÅ^{-3})	0.414, -0.386	0.438, -0.1542	0.316, -0.385	0.450, -0.308
CCDC no.	1426889	1426973	993300	993301

Table 3.2: Crystallographic information table for polymorphs and chloroform solvate of the racemic dibenzoate **1.21**.

Transesterification in Form 1.21II crystals of racemic 1.21:

Freshly grown Form **1.21II** crystals (0.100 g, 0.25 mmol) of racemic **1.21** was subjected to intermolecular benzoyl group transfer reaction in the presence of solid sodium carbonate (0.212 g, 2 mmol) as reported earlier[4c] to obtain 2,4,6-tri-*O*-benzoyl-*myo*-inositol-1,3,5-orthoformate (0.054 g, 43%) **1.24** and 2-*O*-benzoyl-*myo*-inositol-1,3,5-orthoformate (0.032 g, 44%) **1.27**. The two products were isolated by column chromatography (silica gel 100-200 mesh, eluent 10% ethyl acetate in light petroleum and 30% ethyl acetate in light petroleum respectively).

Transesterification in opaque crystals obtained from Form 1.21IV crystals of racemic 1.21:

The solid obtained after exposing Form **1.21IV** crystals (0.050 g, 0.125 mmol) of racemic **1.21** to atmosphere (4-5 days) was subjected to intermolecular benzoyl group transfer reaction in the presence of solid sodium carbonate (0.106 g, 1 mmol) as reported earlier[4c] to obtain the tribenzoate **1.24** and the monobenzoate **1.27** along with minor amount of orthoformate **2.1**, other unidentified products. The major products (**1.24** and **1.27**) were isolated by column chromatography (silica gel 100-200 mesh, eluent 10% ethyl acetate in light petroleum and 30% ethyl acetate in light petroleum respectively). However, the benzoyl transfer reactivity in as above, was inconsistent. The individual yields of the tribenzoate **1.24** and the monobenzoate **1.27** varied between 20 - 40% in different batches.

References:

[1] (a) J. D. Dunitz, J. Bernstein, *Acc. Chem. Res*. **1995**, *28*, 193–200; (b) H. G. Brittain, *Polymorphism in Pharmaceutical Soilds*, Marcel Dekker Inc., New York, **1999**; (c) J. A. R. P. Sarma, G. R. Desiraju, *in Crystal Engineering: Polymorphism and Pseudopolyorphism in Organic Crystals: A Cambridge Structural Database Study, eds*. Seddon, S. R.; Zaworotko, M. J. Kluwer, Norwell, MA, USA, **1999**, p. 325; (d) J. Bernstein, *Polymorphism in Molecular Crystals*, Oxford University Press, Oxford, UK, **2002**; (e) A. J. Cruz-Cabeza, J. Bernstein, *Chem. Rev.* **2014**, *114*, 2170-2191; (f) P. T. Jeremiah, A. E. O'Connor, M. Alexander, B. Elena, J. P. C. Joseph, A. L. Geoffrey, L. S. W. Henry, M. Jonathan, S. Martin, J. B. Alexander *Cryst. Growth Des*. **2015**, *15*, 115 –123; (g) D. H. O. Iain, C. Isabelle, E. Stephen, P. A. F. Francesca, R. L. Alistair, M. Jacques, G. M. William, J. P. Timothy, R. P. Colin, I. S. Ronald, *CrystEngComm*, **2009**, *11*, 359–366; (h) N. Pancĉe, Y. Nobuhiro; M. R. Wael,; B. Joel, *Chem. Comm*. **2013**, *49*, 1948 – 1950; (i) R. D. Gautam, *Cryst. Growth Des*. **2008**, *8*, 3 – 5.

[2] (a) W. C. McCrone, *Anal. Chem.* **1950**, *22*, 1225–1226; (b) T. B.Brill, R. J. Karpowicz, *J. Phys. Chem.* **1982**, *86*, 4260–4265; (c) G. W. Stockton, R. Godfrey, P. Hitchcock, R. Mendelsohn, P. C. Mowery, S. Rajanand, A. F. Walker, *J. Chem. Soc. Perkin Trans. 2*, **1998**, 2061–2071; (d) C. P. Price, A. L. Grzesiak, J. W. Kampf, A. J. Matzger, *Cryst. Growth Des*. **2003**, *3*, 1021–1025; (e) P. Vishweshwar, J. A. McMahon, M. Oliveira, M. L. Peterson, M. J. Zaworotko, *J. Am. Chem. Soc.* **2005**, *127*, 16802–16803; (f) R. Hilfiker, *Polymorphism in the Pharmaecutical Industry*, Wiley-VCH, Weinheim, Germany, **2006**; (g) F. P. A. Fabbiani, C. R. Pulham, *Chem. Soc. Rev*. **2006**, *35*, 932–942; (h) C. Näther, I. Jeβ, *Angew. Chem. Int. Ed.* **2006**, *45*, 6381–6383; (i) E. F. Paulus, F. J. J. Leusen, M. U. Schmidt, *CrystEngComm*, **2007**, *9*, 131–143; (j) A. D. Bond, R. Boese, G. R. Desiraju, *Angew. Chem., Int. Ed. Engl.* **2007**, *46*, 615–617; (k) Z. A. Dreger, Y. M. Gupta, *J. Phys. Chem. A,* **2010**, *114*, 8099–8105; (l) S. Seethalekshmi, T. N. Guru Row, *Cryst. Growth Des*. **2012**, *12*, 4283–4289; (m) S. H. Thorat; M. V. Patwadkar; R. G. Gonnade; R. Vaidhyanathan *CrystEngComm*, **2014**, *16*, 8638–8641; (n) M. I. Tamboli,; S. Krishnaswamy, R.

G. Gonnade, M. S. Shashidhar, *Cryst. Growth Des.* **2014**, *14*, 4985- 4996; (o) L. Geng-Geng, X. Jiu-Xu, F. Kai, Z. Qing-Hua, W. Ji-Huai, D. Jing-Cao, *Dalton Trans*, **2013**, 42, 16268-16271; (p) Y. Fan, Y. Zhao, L. Ye, B. Li, G. Yang, Y. Wang, *Cryst. Growth Des*. **2009**, *9*, 1421-1430; (q) Y. Fan, W. Song, D. Yu, K. Ye, J. Zhang, Y. Wang, *CrystEngComm* **2009**, *11*, 1716-1722.

[3] (a) M. D. Cohen, G. M. Schmidt, F. I. Sonntag, *J. Chem. Soc.* **1964**, 1996-2013; (b) Y. Matsuda, M. Mihara, *J. Pharm. Pharmacol*. **1994**, *46*, 162-167; (c) R. S. Gopalan, G. U. Kulkarni, *Proc. Indian Acad. Sci.* (*Chem. Sci.*), **2001**,*113* 307–324; (d) H. Shinya, T. Shinji, T. Fumino, U. Hidehiro, *Angew. Chem., Int. Ed. Engl.* **2006**, *45*, 6013–6016; (e) C. Murali, M. S. Shashidhar, R. G. Gonnade, M. M. Bhadbhade, *Chem. Eur. J*. **2009**, *15*, 261–269; (f) S. Krishnaswamy, M. S. Shashidhar, M. M. Bhadbhade, *CrystEngComm*, **2011**, *13*, 3258-3264; (g) C. Xiaoming, L. Tonglei, R. M. Kenneth, R. B. Stephen, *Mol. Cryst. Liq. Cryst*, **2002**, *381*, 121-131; (h) K. K. Goutam, J. V. Jagadese, *Chem. Soc. Rev*. **2013**, *42*, 1755–1775; (h) B. Kumar, S. Ramkinkar, *Chem. Soc. Rev.* **2013**, *42*, 950-967.

[4] A. Pathigooala, R. G. Gonnade, K. M. Sureshan, *Angew. Chem. Int. Ed. Engl*. **2012**, 51, 4362-4366; (b) A. Pathigoolla, K. M. Sureshan, *Angew. Chem. Int. Ed. Engl*. **2013**, *52*, 8671- 8675; (c) T. Praveen, U. Samanta, T. Das, M. S. Shashidhar, P. Chakrabarti, *J. Am. Chem. Soc.* **1998**, *120*, 3842-3845 and references cited therein. (d) B. K. Ruth, N. D. Eileen; C. E. Margaret; C. P. Iain; Y.C. David, *J. Am. Chem. Soc*. **1980**, *102*, 7709 –7714; (e) S. Ryo, K-O Kazuhiko, I. Tatsuro, K. Keiji, *J. Am. Chem. Soc*. **2000**, *122*, 10282 –10288; (f) B. Dario, D. Daniela, L. G. Stefano, M. Lucia, P. Marco, G. Fabrizia, *Top Curr Chem* **2005**, *254*, 71–94.

[5] (a) J. H. Kim, S. V. Lindeman, J. K. Kochi, *J. Am. Chem. Soc*., **2001**, *123*, 4951-4959; (b) M. P. Sarmah, R. G. Gonnade, M. S. Shashidhar, M. M. Bhadbhade, *Chem. Eur. J.* **2005**, *11*, 2103-2110; (c) L. R. MacGillivray, G. S. Papaefstathiou, T. Friščić, T. D. Hamilton, D-K. Bučar, Q. Chu, D. B.Varshney, I. G. Georgiev, *Acc. Chem. Res.* **2008**, *41*, 280- 291; (d) M. L. Cheney, G. J. McManus, J. A. Perman, Z. Wang, M. J. Zaworotko, *Cryst. Growth Des*. **2007**, *7*, 616 – 617; (e) S-L. Zheng, O. Pham, M. L. Christophe, V. Velde, M. Gembicky, P. Coppens, *Chem. Comm*. **2008**, 2538- 2540; (f) M. Khan, V. Enkelmann, G. Brunklaus,

Cryst. Growth Des. **2009**, *9*, 2354- 2362; (g) D. S. Khorasani, M. A. Botes, M. A. Fernandes, D. C. Levendis, *CrystEnggComm* **2015**, *17*, 8933-8945.

[6] M. I. Tamboli, S. Krishnaswamy, M. S. Shashidhar, R. G. Gonnade, *Chem. Eur. J.* **2013**, *19*, 12867–12874.

[7] (a) R. J. Davey, N. Blagden, G. D. Potts, R. Docherty *J. Am. Chem. Soc*. **1997**, *119*, 1767–1772; (b) C. H. Gu, K. Chatterjee; Jr. V. Young, D. J. W. Grant, *Cryst. Growth Des*, **2002**, *235*, 471– 481; (c) C. Murali, M. S. Shashidhar, R. G. Gonnade, M. M. Bhadbhade, *Chem. Eur. J.* **2009**, *15*, 261 – 269.

[8] R. G. Gonnade, M. M. Bhadbhade, M. S. Shashidhar, *CrystEnggComm,* **2008**, *10*, 288- 296.

[9] S. Krishnaswamy, R. G. Gonnade, M. S. Shashidhar, M. M. Bhadbhade, *CrystEngComm*, **2010**, *12*, 4184–4197.

[10] (a) J. J. McKinnon, M. A. Spackman, A. S. Mitchell, *Acta Crystallogr. Sect. B* **2004**, *B60*, 627−668; (b) J. J. McKinnon, D. Jayatilaka, M. A. Spackman, *Chem. Commun*. **2007**, 3814−3816; (c) M. A. Spackman, D. Jayatilaka, *CrystEngComm*. **2009**, *11*, 19−32.

[11] S. K. Wolff, D. J. Grimwood, J. J. McKinnon, D. Jayatilaka, M. A. Packman, **2007**. *Crystal Explorer. University of Western Australia, Perth, Australia.*http://hirshfeldsurface.net/CrystalExplorer.

Chapter 3

Section 3B

Progress towards designing crystals capable of supporting intermolecular benzoyl group migration: polymorphism, reactivity, and crystal structure of enantiomeric *myo*-inositol orthoester dibenzoates.

Introduction:

Study of chemical reactions of small organic molecules in the solution state over the last hundred years or more resulted in a firm basis for the development of synthetic organic chemistry. A sizable portion of these reactions in the past few decades dealt with chiral or non-racemic compounds. Solvents essentially largely help to prevent the non-covalent interactions (homomolecular and heteromolecular interactions that do not lead to product formation) between reactant molecules and appear to aid the rate of product formation. This thought is supported by the fact that many reactions are relatively more facile in the solution state as compared to the corresponding reaction in the solid state. However, this indiscriminate prevention of intermolecular interactions between the reactant molecules, even when they are favorable for the progress of a reaction, could in fact hamper the rates of reactions in solutions. Reports on facile reactions in the solid state (as compared to the corresponding reactions in the solution state), especially reactions in molecular crystals are examples of such situations.[1] Generally reactions that are relatively more facile in the solid state also exhibit better product selectivity, including regio- and stereo-selectivity, as compared to the corresponding solution state reaction.[2] In solution state reactions, often the rate and the selectivity can be varied by the use of different solvents (classical solvent effects) for the same reaction, which amounts to changing the environment of the reacting molecules.

In solid state reactions (especially in the crystalline state) a change of environment of reacting molecules can in principle be achieved by the use of polymorphs, pseudopolymorphs and cocrystals. Polymorphism of molecular crystals has been the subject of intense investigations[3] due to its implications in topics as varied as understanding the origin of formation of crystals and prediction of crystal structures to potency of bio-active compounds, herbicides, high energy materials, patentability and commercial aspects of drugs and APIs.[4] Relatively less conspicuous in the literature is the effect of polymorphic structures of crystals of small organic molecules on their chemical properties in the crystalline state.[5] This could be largely due to the major role of serendipity in the identification of crystalline solids capable of supporting chemical reactions in them. Hence, although there are several instances of chemical reactions taking place in molecular crystals [6] and cocrystals,[7] investigations on the polymorphism exhibited by these small molecules are scarce. A special case of cocrystals is of crystalline racemates (1:1 cocrystals of

enantiomers). But there appear to be no known example of a racemate and one of its enantiomers exhibiting similar chemical reaction in their crystals. We encountered such an opportunity during the investigation of polymorphism and intermolecular benzoyl group transfer reaction in crystals of dibenzoates of *myo*-inositol orthoesters (Scheme 3.2).[5e-f, 6c,7b, 7g, 8]

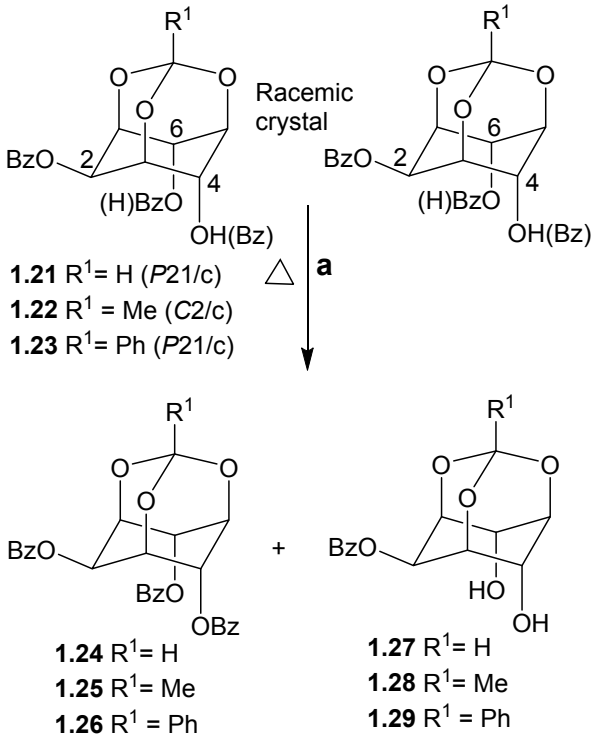

Scheme 3.2: Acyl group migration in the racemic 2,4(6)-di-*O*-benzoyl-*myo*-inositol-orthoester (a) Anhydrous Na_2CO_3. (Atom labels shown in brackets generate enantiomers of the structures shown).

In line with the aspects mentioned above, the first part of this chapter presented results on the polymorphic and pseudo polymorphic structures of racemic 2,4-di-*O*-benzoyl-*myo*-inositol-orthoformate **1.21**. We could also obtain cocrystals of the reacemic benzoate **1.21** with 4,4'-bipyridine; the presence of the latter in the crystal completely prevented the benzoyl transfer reactivity between molecules of **1.21**.

Crystals of racemic dibenzoates of *myo*-inositol orthoesters had structures that supported facile benzoyl group transfer reaction in them (Scheme 3.2). Each helix (which functioned as a reaction channel) in these crystals consisted of one of the enantiomers of these dibenzoates, which clearly established that the reaction in the

crystalline racemate occurred between molecules having the same absolute configuration (Figure 3.12, Scheme 3.3).

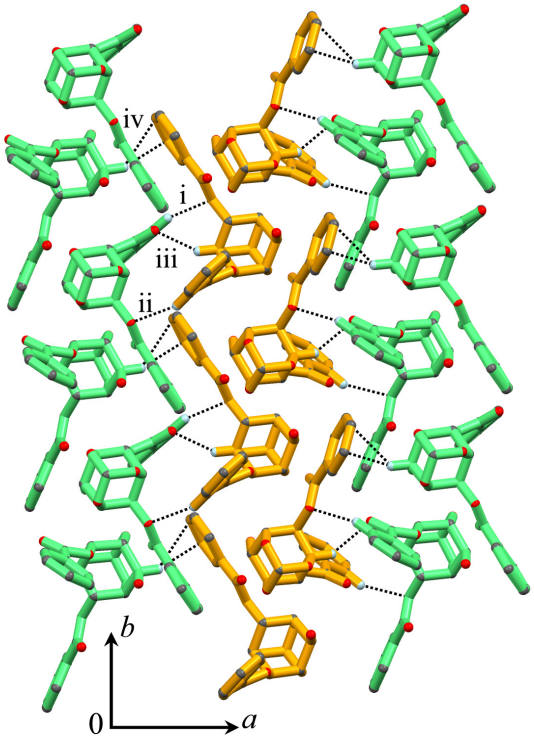

Figure 3.12: Packing of helices in crystals of dibenzoate **1.21**. Discrete helices consist of a single enantiomer of **1.21**. The color scheme is used to distinguish the neighboring helices made of opposite enantiomers.

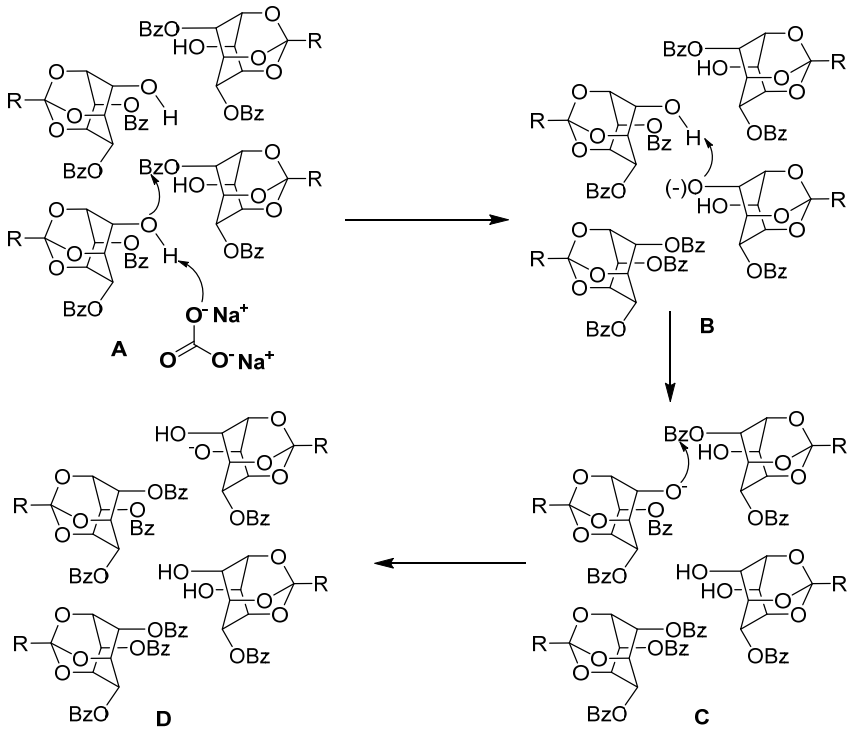

Scheme 3.3: Plausible mechanism for the benzoyl group transfer in crystals of reactive dibenzoate orthoesters.

Hence it was of interest to see if these enantiomers formed chiral crystals on their own, having structure similar to the corresponding racemate, that supported benzoyl group transfer reaction, or whether presence of the opposite enantiomer in the crystal lattice was absolutely essential to stabilize the structure required to facilitate the benzoyl group transfer reaction. Accordingly, the work described in this part pertains to the preparation of enantiomeric dibenzoates of *myo*-inositol orthoesters and a comparison of their crystal structure and reactivity with those of the corresponding racemates.

Results and Discussion:

Cocrystallization of racemic 2,4-di-*O*-benzoyl-*myo*-inostiol orthoformate with 4,4'-bipyridine:

Investigation of the crystal structure of the racemic dibenzoate (**1.21**) revealed that the facile reaction in the crystalline state was due to pre-organization of the electrophile (C=O) and the nucleophile (-OH) with the required geometry for nucleophilic addition and the helical assembly of the molecules which allowed a domino type of reaction.[5e,7b] We were curious to see whether the inclusion of a base in crystals of

the racemic dibenzoate would augment or hinder the benzoyl-transfer reactivity of the molecules. We chose symmetrical 4,4'-bipyridine (**3.1**) as the cocrystal builder, since it is known to form cocrystals with molecules containing -OH or -COOH functional groups.[9] We also attempted cocrystallization of **1.21** with other nitrogenous bases (adenine, guanine, cytosine, thymine and uracil) in different solvents (ethanol, methanol, acetone, *iso*-propanol and acetonitrile, and mixtures of these solvents), but no cocrystals were obtained.

Cocrystal **1.21•3.1** consisted of equimolar amounts of the dibenzoate **1.21** and 4,4'-bipyridine **3.1**, as revealed by ^{1}H NMR spectroscopy and single-crystal X-ray diffraction analysis. Cocrystals **1.21•3.1** were stable under ambient conditions for several months, as revealed by their melting point and X-ray powder diffraction patterns (Figure A28, see Appnedix III). The DSC profile of **1.21•3.1** revealed that it was stable up to the melting point and that there was no phase change prior to melting of the cocrystals (Figure A27, see Appnedix III). When heated, either in the presence or absence of sodium carbonate, **1.21•3.1** failed to undergo a benzoyl-transfer reaction, in contrast with the crystals of racemic dibenzoate **1.21** (Scheme 3.2).

Although the crystal structure of racemic dibenzoate (**1.21**) had been reported previously,[6c,7b] it was re-determined here (Table A2, see Appnedix III) for the sake of comparison with the cocrystal **1.21•3.1** (Table A2, see Appnedix III). The overlap of the dibenzoate molecules in crystals of **1.21** and **1.21•3.1** revealed major conformational differences in the orientation of the two benzoyl groups (Figure 3.13).

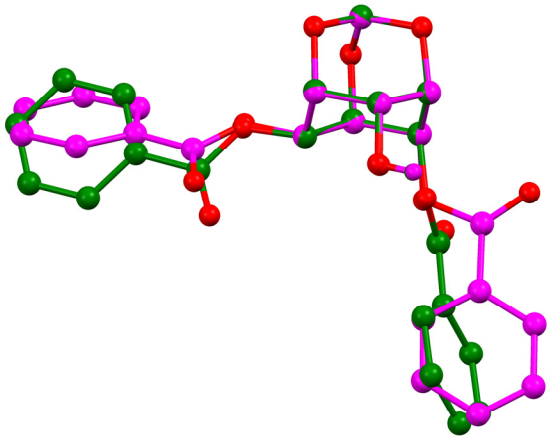

Figure 3.13: The molecular overlap of the dibenzoate molecules in crystal of **1.21** (green) and cocrystal **1.21•3.1** (magenta).

A comparison of the crystal structures of the dibenzoate **1.21** and the cocrystal **1.21•3.1** revealed distinctly different arrangements of the molecules (Figures 3.14). The presence of bipyridine molecules in cocrystal **1.21•3.1** breaks the O-H···O-linked helical assembly of dibenzoate molecules by interacting with their -OH group through O-H···N hydrogen-bonding interactions. The -OH group of the dibenzoate molecule forms a hydrogen bond with one of the N atoms (N2) of bipyridine, while the other N atom (N1) is involved in C-H···N interactions with an aromatic C-H group of the axial benzoyl group resulting in an alternating arrangement of dibenzoate and bipyridine molecules forming a chain (Figure 3.14).

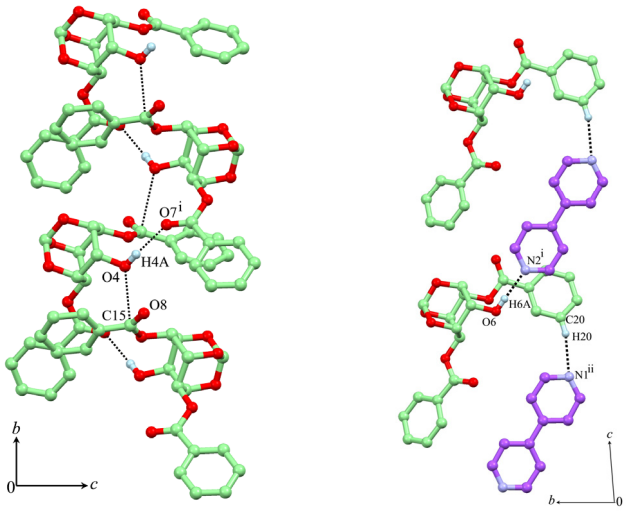

Figure 3.14: Helical assembly of molecules through O-H···O interactions in crystals of **1.21** (left) and association of molecules of **1.21** with bipyridine in cocrystals **1.21•3.1** through O-H···N interactions (right).

A bipyridine molecule occupies the position of the dibenzoate molecule between the two unit-translated molecules and disrupts the helical chain (Figures 3.14b). The unit-translated neighbouring chains, comprising molecules of the dibenzoate **1.21** and bipyridine, are loosely connected along the *b*-axis via van der Waals forces, generating a two-dimensional sheet structure in the *bc*-plane (Figure 3.15b).

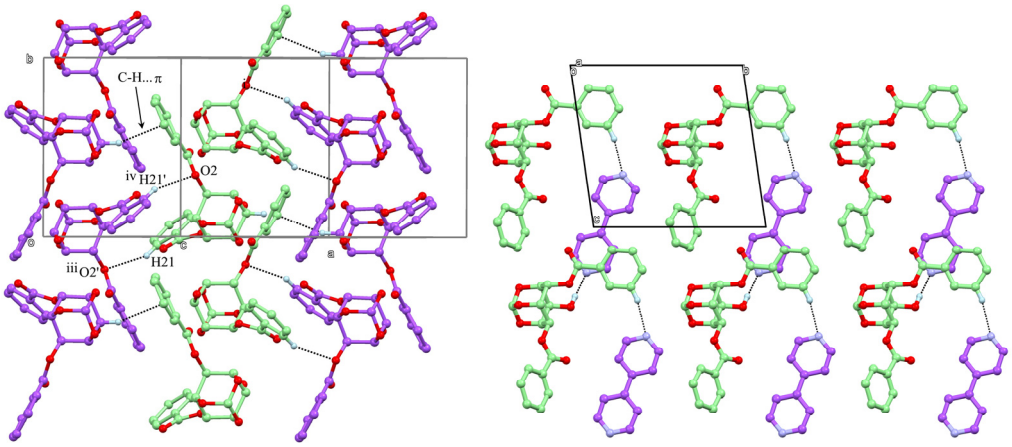

(a) (b)

Figure 3.15: (a) Molecular packing showing the discrete layer of helices in **1.21** and (b) molecular packing in **1.21•3.1** showing the two dimensional sheet generated by weak association between dibenzoate and bipyridine molecules.

The presence of the bipyridine molecules in the cocrystal prevents the juxtaposition of dibenzoate molecules, resulting in the prevention of the intermolecular benzoyl-group transfer between the dibenzoate molecules. An optimistic view of this aspect is that cocrystallization can be a method to decrease the ease of chemical reactions between molecules in a crystal and thereby increase the stability of constituent molecules of a reactive crystal.

Preparation, crystallization and benzoyl group transfer reactivity in crystals of enantiomeric dibenzoates of *myo*-inostiol orthoesters:

The chiral dibenzoates **D-1.21**, **D-1.22** and **D-1.23** were prepared from the corresponding dicamphanates, **3.6**, **3.5** and **dia3.2** (see chapter 4 for details on the preparation of these diastereomers and elaboration on the representation and conventions for the nomenclature of chiral inositol derivatives) as shown in Scheme 3.4. The allyl ether in the dibenzoates **D-3.4**, **D-3.9** and **D-3.10** was cleaved using Pd $(OH)_2$ /C in refluxing *iso*-propanol[10] without noticeable racemization of the dibenzoates **D-1.21** and **D-1.23**; but the dibenzoate **D-1.22** was obtained in 88% enantiomeric purity. The latter on crystallization from chloroform - light petroleum or ethyl acetate - light petroleum, gave crystals of **D-1.22** which were enantiomerically pure as revealed by HPLC analysis.

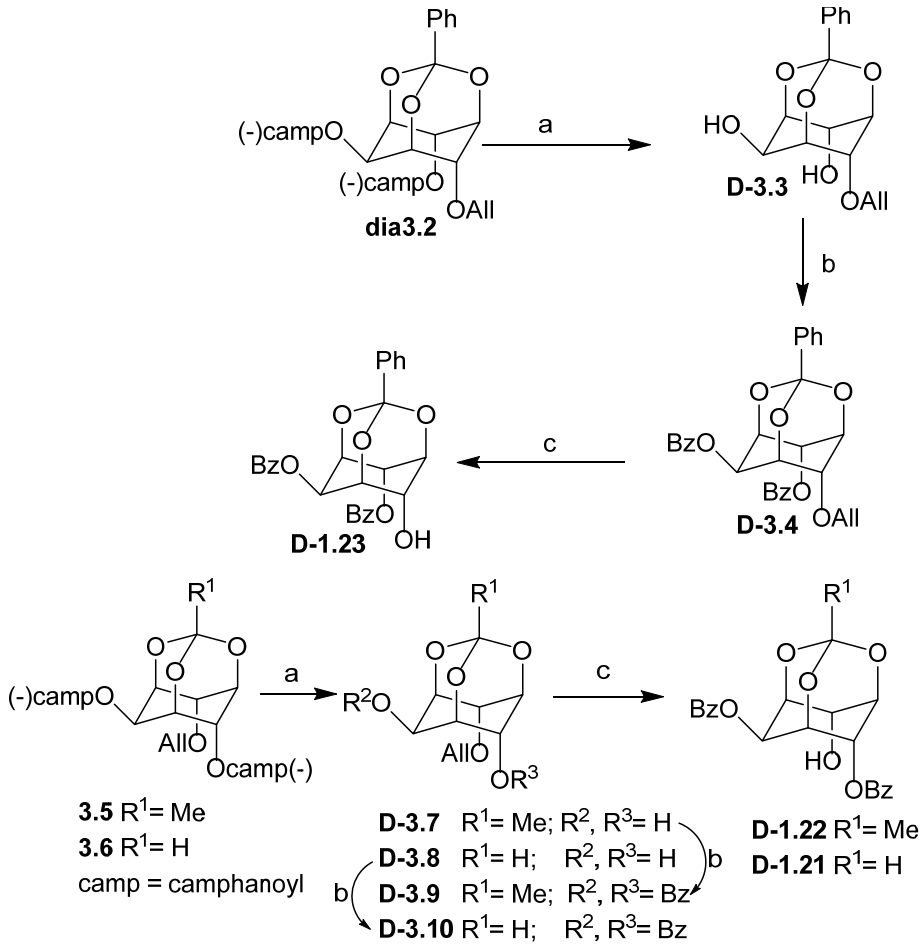

Scheme 3.4: (a) *Iso*-butyl amine, MeOH, DCM reflux, 8-10 h; (b) Pyridine, DMAP, benzoyl chloride, 0^{o}C - RT; (c) Pd $(OH)_2$ / C, *Iso*-propanol, reflux.

The chiral D-2,6-di-*O*-benzoyl-*myo*-inositol orthobenzoate **D-1.23** showed interesting polymorphic behavior depending on the solvent and conditions of crystallization. The orthobenzoate **D-1.23** on crystallization from chloroform and *n*-pentane (or acetone – light petroleum) mixture gave two polymorphs, concomitantly. Long plates (Form- **D-1.23I**, appeared to be the thermodynamic form since these crystals were formed at the bottom of the flask, well below the surface of the solvent) and very few irregular shaped crystals (From **D-1.23II**, appeared to be a kinetic form since these crystals were formed at the periphery – due to evaporation of the solvent at the surface). Form **D-1.23I** crystals were also obtained from a saturated solution in 15-20:85-80 ethyl acetate: light petroleum (bp. 60-80 ^{o}C).

DSC profiles of Form **D-1.23I** crystals of the orthobenzoate **D-1.23** and orthoacetate **D-1.22**, orthoformate **D-1.21** (Figures 3.16a, 3.17 and 3.18) showed one sharp endotherm revealing that they did not undergo thermal phase transition before

melting. Whereas the DSC profile of the Form **D-1.23II** crystals of **D-1.23** showed two endothermic peaks at 146 and 168 °C (Figure 3.16b). The peak at 146 °C was followed by an exotherm (although not very prominent) indicating phase transitions, before the final melting endotherm at 168 °C. These observations suggested melting of Form **D-1.23II** crystals followed by formation of a solid phase between 140 and 150 °C.

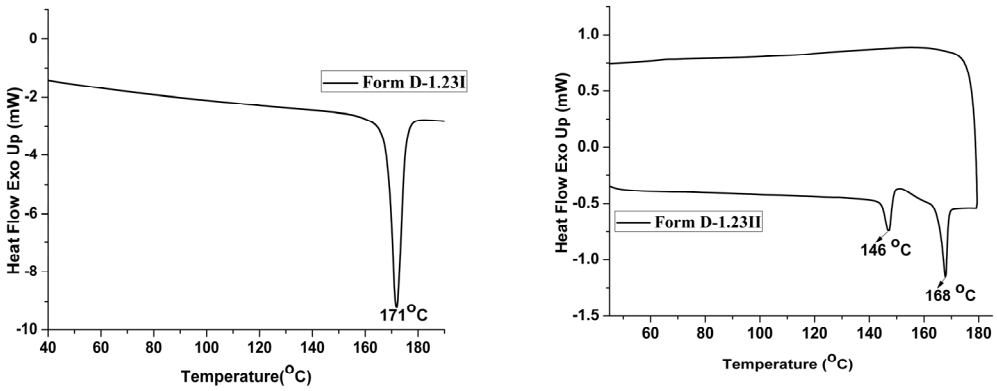

(a) (b)

Figure 3.16: DSC of the (a) Form **D-1.23I** crystals and (b) Form **D-1.23II** of the orthobenzoate **D-1.23**.

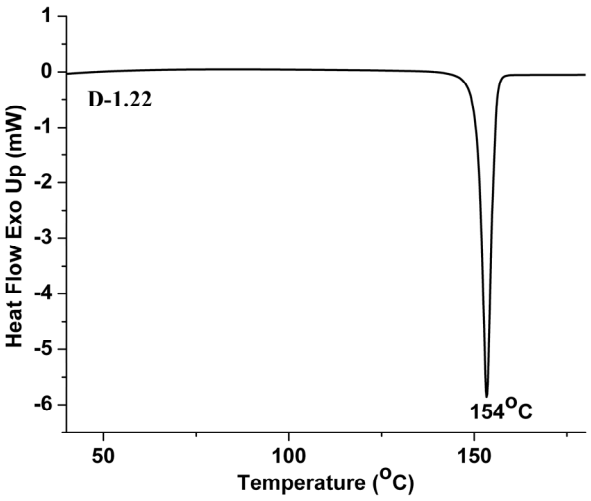

Figure 3.17: DSC of crystals of the orthoacetate **D-1.22**.

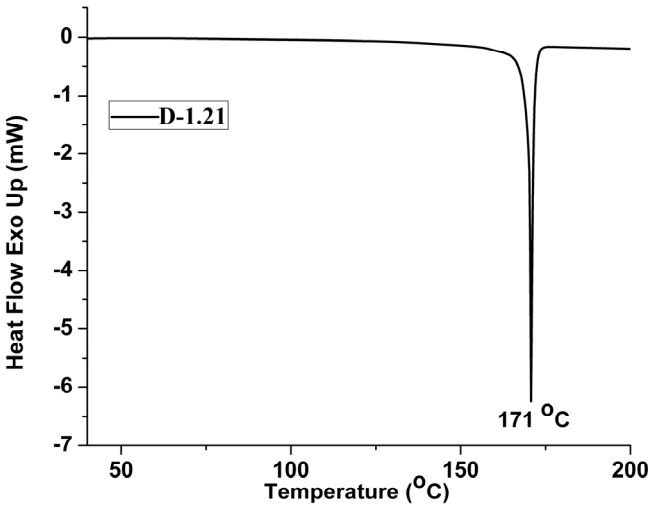

Figure 3.18: DSC of crystals of the orthoformate **D-1.21**.

These DSC results prompted us to investigate the effect of heat on Form **D-1.23II** crystals of **D-1.23** by hot stage microscopy. Form **D-1.23II** crystals of **D-1.23** on heating showed changes on their surface around 139-142 ^{o}C and began melting beyond this temperature (143-146 ^{o}C). Further heating resulted in the formation of plate like crystals (referred to as Form **D-1.23III** in the rest of this chapter) and the newly formed crystals melted in the range 164-168 ^{o}C (Figure 3.19). Cooling of this molten mass to room temperature did not result in solid formation. Thus, HSM studies clearly showed the melting of From **D-1.23II** crystals followed by the formation of a different solid phase as suggested by thermal analysis (Figure 3.16b). The plate like Form **D-1.23III** crystals formed from Form **D-1.23II** crystals was not suitable for single crystal X-ray diffraction analysis. The PXRD patterns of Form **D-1.23I**, Form **D-1.23II** and Form **D-1.23III** crystals (obtained after heating Form **D-1.23II** crystal at 150-152 ^{o}C for 12 h) of **D-1.23** are shown in Figure 3.20.

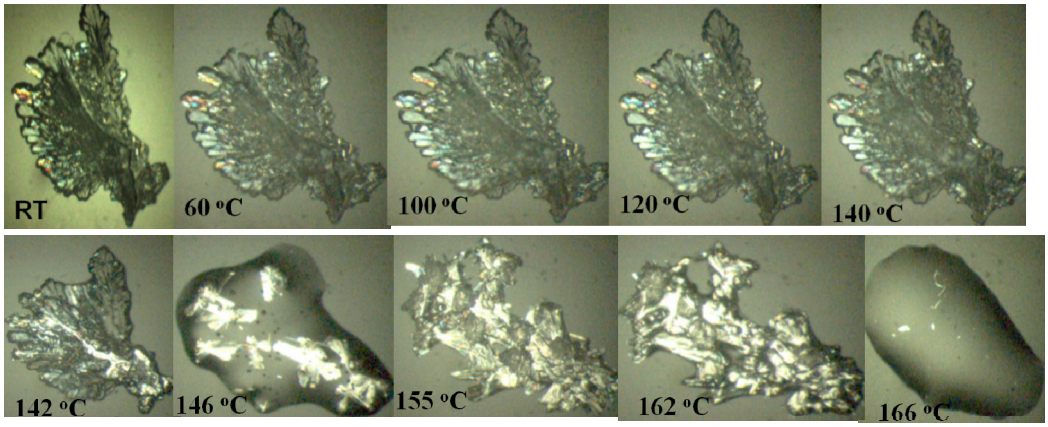

Figure 3.19: Thermal response of the Form **D-1.23II** crystal of **D-1.23**.

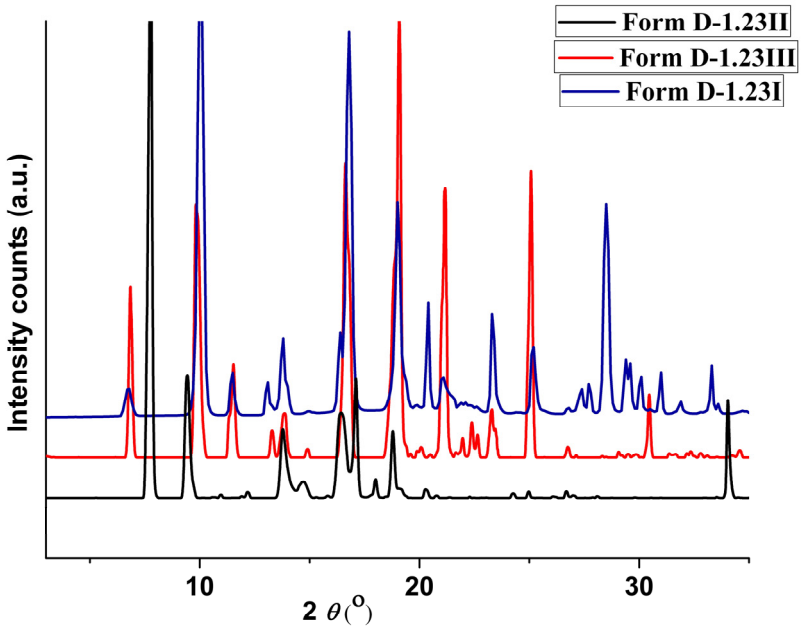

Figure 3.20: PXRD profile of the Form **D-1.23I** (blue), Form **D-1.23II** (black) and Form **D-1.23III** (red) crystals of **D-1.23**.

Although PXRD profiles of Form **D-1.23I** and Form **D-1.23III** crystals appeared similar, there are differences which preclude us from concluding that they are structurally same. Hence we conclude that the Form **D-1.23III** crystals either have structure different from Form **D-1.23I** and Form **D-1.23II** crystals or consist of more than one solid form.

The orthoacetate **D-1.22** on crystallization from a mixture of ethyl acetate and light petroleum or chloroform and light petroleum gave block shaped crystals. The orthoformate **D-1.21** on crystallization from chloroform and *n*-pentane mixture gave

thin fibrous needle shaped crystals as reported.[5e] The enantiomeric purity of crystals of **D-1.21**, **D-1.22** and **D-1.23** was at least 99% as determined by chiral HPLC analysis. The DSC profiles of crystals of **D-1.21** and **D-1.22** ruled out phase transitions before melting. A comparison of the PXRD patterns of the crystals with the simulated PXRD pattern from the single crystal diffraction data excluded the presence of polymorphs.

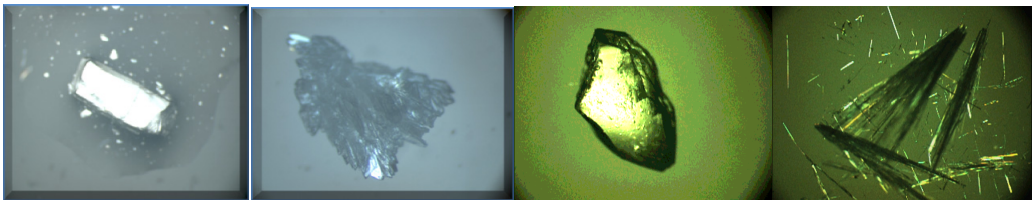

(a) (b) (c) (d)

Figure 3.21: Photograph of crystals of (a) Form **D-1.23I** (b) Form **D-1.23II** (c) **D-1.22** and (d) **D-1.21**.

It was interesting to note that the chiral di-*O*-benzoate orthoester crystals had lower melting point compared to the corresponding racemate. All the racemic 2,4-di-*O*-dibenzoate orthoesters underwent facile intermolecular acyl group migration reaction in the presence of the anhydrous sodium carbonate in the solid state. The enantiomeric dibenzoates of orthoformate **D-1.21** and orthoacetate **D-1.22** were not reactive in their crystals. The enantiomeric orthobenzoate **D-1.23** produced one reactive crystal form (Form **D-1.23I**) and one unreactive crystal form (Form **D-1.23II**). These differences could be rationalized based on their crystal structures.

As predicted from the crystal structures (see below), Form **D-1.23I** crystals underwent facile intermolecular benzoyl group transfer reaction to give the corresponding tribenzoate and the diol in excellent yield (Form **D-1.23I** + Na_2CO_3 → **1.26** + **1.29**). The reactivity of crystals of Form **D-1.23I** was comparable to the reactivity exhibited by racemic **1.23**. The crystal structure revealed that the relative orientation of the El and Nu was not conducive for acyl-transfer reaction in Form **D-1.23II** crystals. As expected (from their crystal structures) crystals of the orthoacetate **D-1.22** and the orthoformate **D-1.21** did not exhibit good inter molecular benzoyl transfer reactivity.

Comparison of the crystal structures of Form D-1.23I and Form D-1.23II crystals of the orthobenzoate with the racemate 1.23 and its implications:

The chiral dibenzoates of *myo*-inositol orthoestesters (orthoformate **D-1.21**- thin needles, orthoacetate **D-1.22**- blocks and orthobenzoate **D-1.23**- long plates [Form **D-1.23I**], irregular shaped crystals [Form **D-1.23II**]) (Figure 3.21) were suitable for single crystal X-ray diffraction analysis. The chiral D-2,4-dibenzoate of the orthoformate **D-1.21** crystallized in the orthorhombic crystal system (space group $P2_12_12_1$) and the analogous orthoacetate **D-1.22** crystallized in the monoclinic crystal system (space group $P2_1$); both these crystals contained one molecule in the asymmetric unit. Chiral orthobenzoate **D-1.23** produced two polymorphs. The Form **D-1.23I** crystals belonged to orthorhombic crystal system (space group $P2_12_12_1$, Z' = 1) while Form **D-1.23II** crystals belonged to the trigonal crystal system (space group $P3_2$, Z' = 2).

The structure overlay of the molecules (Figure 3.22a) in dimorphs of the orthobenzoate **D-1.23** crystals of Form **D-1.23I** and Form **D-1.23II** (unprimed) showed that significant difference in conformation of the benzene ring of C6-benzoate moiety (~ 60 °) and the phenyl ring of the orthobenzoate group (~ 71°); the difference in orientation between C2-benzoate moiety was ~ 24°. The conformation of the C4-hydroxyl group of molecules in both crystals was similar. Both the molecules in the asymmetric unit of Form **D-1.23II** crystals have very similar conformation (Figure 3.22b). Hence the dimorphism of the orthobenzoate **D-1.23** is an example of conformational polymorphism. A comparison of the conformation of the molecules in crystals of racemic orthobrnzoate **1.23** and the enantiomer **D-1.23** (Figure 3.23) revealed significant differences in conformation of molecules between those present in the racemate and Form **D-1.23II** crystals (Figure 3.23b).

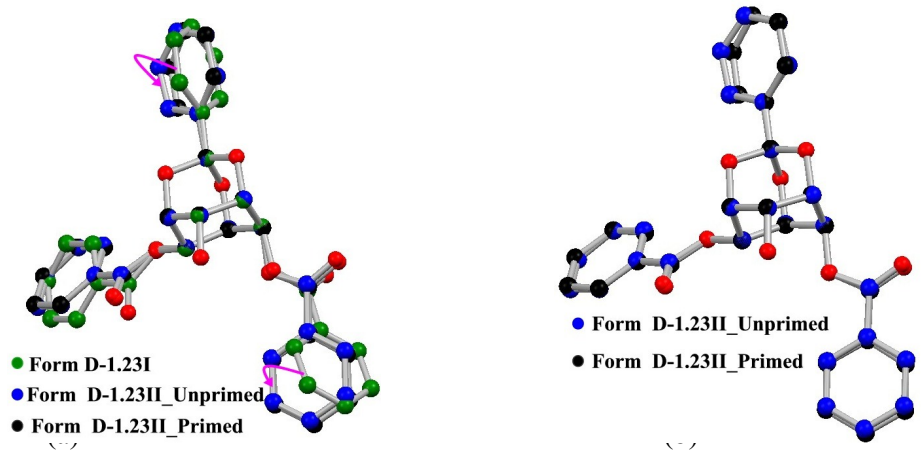

Figure 3.22: (a) Structure overlay of molecules in asymmetric unit of Form **D-1.23I** and Form **D-1.23II** (b) Structure overlays of the both the molecules in the asymmetric unit of Form **D-1.23II**.

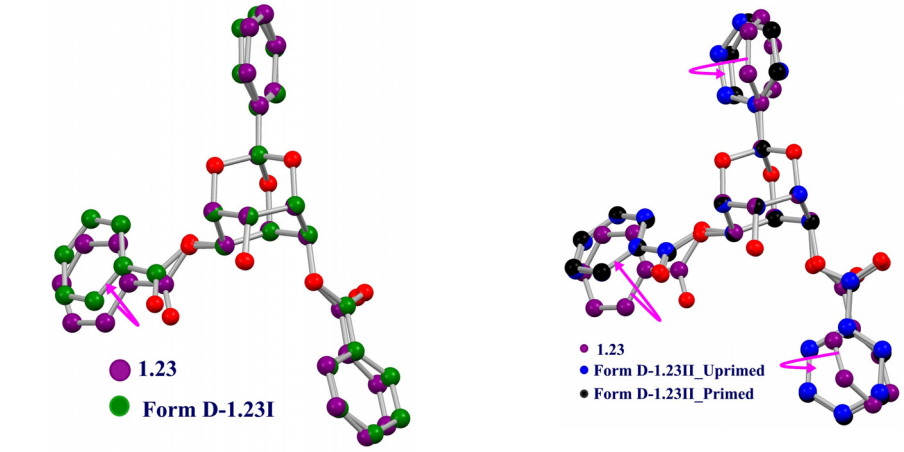

(a) (b)

Figure 3.23: (a) Structure overlay of molecules in crystals of Form **D-1.23I** and Form **D-1.23II** of **D-1.23** with racemic **1.23**.

Form **D-1.23I** crystals of D-2,6-di-*O*-benzoyl-*myo*-inositol-1,3,5-orthobenzoate (**D-1.23**) crystallized in the orthorhombic $P2_12_12_1$ crystal system containing one molecule in the asymmetric unit. Like racemic orthobenzoate **1.23**, moleucles in **D-1.23** also formed the helical architecture through conventional O-H···O (O4-H4*A*···O7) hydrogen bonding interactions across the crystallographic 2_1-screw axis (*a*-axis). The helical orgnization places the electrophile (El, C=O) and nucleophile (Nu, -OH) in proximity to generate short El···Nu contact (3.196 Å) with approximately perpendicular (83.00°) approach of Nu to El (Figure 3.24a, Table 3.3). The helical

assembly is supplementated by weak C-H···O (C5-H5···O4 and C6-H6···O4) and C-H···π(C3-H3···Cg) interactions (Figure 3.25a). The neighboring halices along the *b*-axis are loosely connected via bifurcated weak C-H···O interaction (C12-H12···O8 and C13-H13···O8) to generate the discrete packing. Conversely, in racemic benzoate **1.23** the adjoining helices are linked strongly *via* short and linear C-H···O interactions namely C1-H1···O8 and C23-H23···O2. The significant difference between the Form **D-1.23I** and racemic banzoate **1.23** is that in Form **D-1.23I** the adjacent helices are arranged in parallel mode whereas in racemic benzoate they are packed in anti-parallel fashion (Figure 3.26).

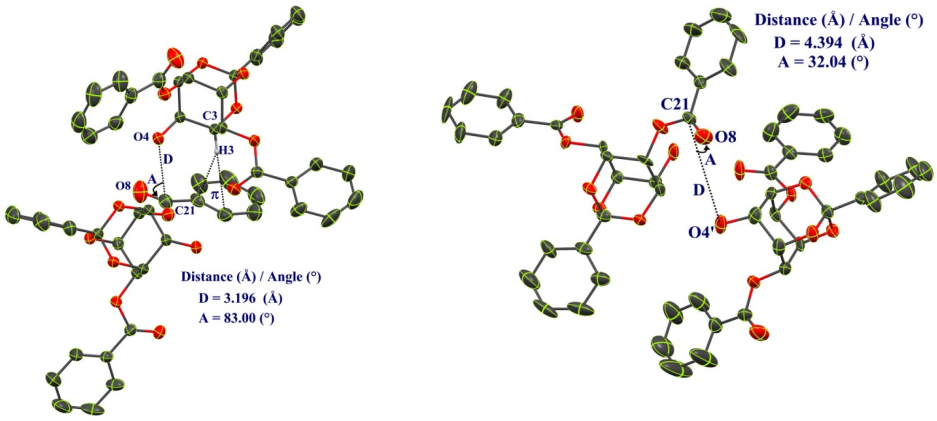

(a) Form **D-1.23I** (b) Form **D-1.23II**

Figure 3.24: Relative orientation of the reacting molecules in dimorphs of **D-1.23**.

Distance(Å) / Angle(°)	**Form D-1.23I**	**Form D-1.23II**	**1.23**
OH(Nu)··· O=C(El)	3.196	4.612 / 4.394	3.1442(2)
∠O(Nu)···C=O(El)	83.00	36.28 / 32.04	85.6(1)
∠H-O(Nu)···C(El)	105.65	127.34 / 128.76	113(1)
∠C-O(Nu)···C (El)	99.66	92.75 / 95.99	111.1(1)

Table 3.3: Geometrical parameters for El···Nu interaction between reacting molecules in the chiral and racemic crystals of the orthobenzoate **1.23**.

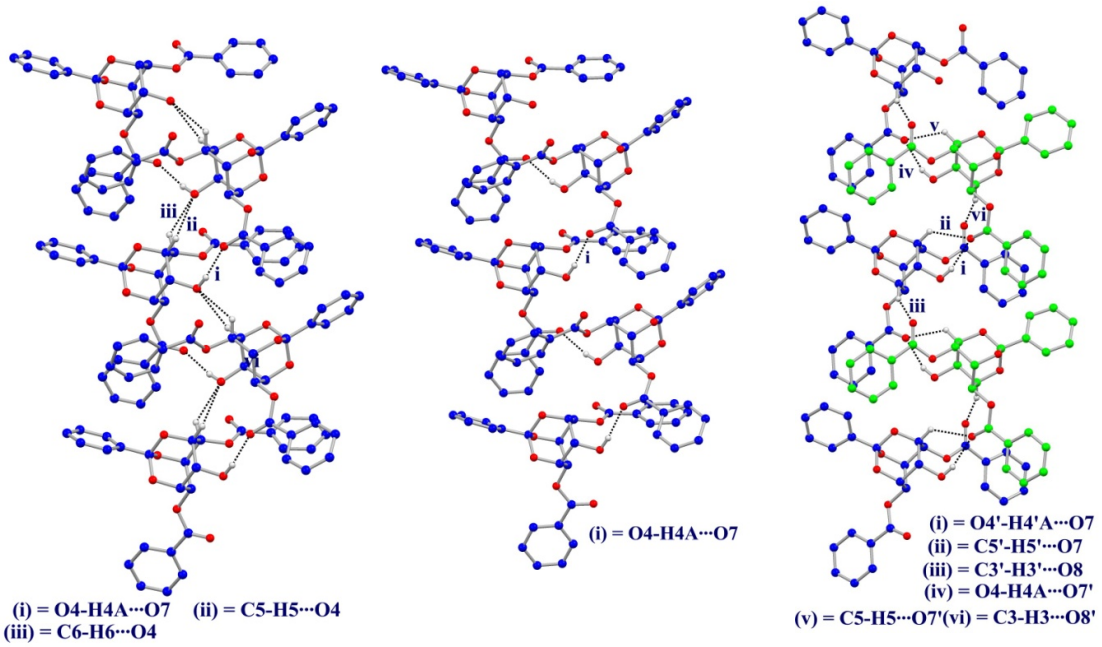

(a) Form **D-1.23I** (b) **1.23** (c) Form **D-1.23II**

Figure 3.25: Helical assembly of molecules in dimorphs of chiral **D-1.23** and the crystalline recemate **1.23** *via* O-H···O hydrogen bonding.

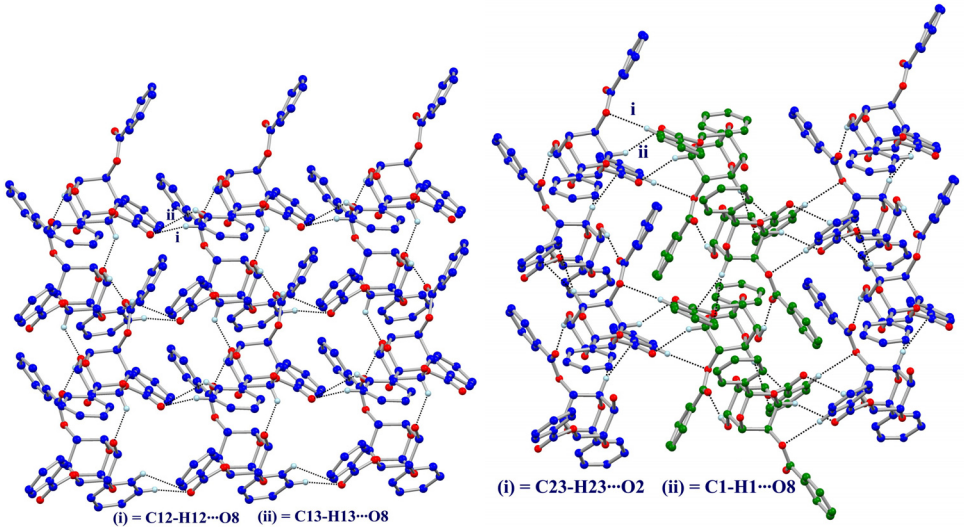

Figure 3.26: Packing of helices in crystals of Form **D-1.23I** (left), and its racemates **1.23** (right) (different colour of helices represent different enantiomer).

The Form **D-1.23II** crystals belong to the trigonal $P3_2$ crystal system containing two molecules in the asymmetric unit. The molecules are labeled as unprimed and primed.

Both molecules generate the composite helical assembly along the *a*-axis comprising an alternate arrangement of two symmetry independent molecules through conventional O-H···O hydrogen bonding interactions. Along the helical assembly the hydroxyl group (O4-H4*A*) of the unprimed molecules donates H-atom to the carbonyl oxygen O7' of the primed molecules and *visa-versa* to generate the O4-H4*A*···O7' and O4'-H4'*A*···O7 hydrogen bonding interactions. The helical assembly is further supported by short and non-linear C-H···O interactions namely C5-H5···O7', C5'-H5'···O7, C3-H3···O8', C3'-H3'···O8. However, the helical arrangement does not juxtapose the El and Nu of both molecules in the reactive geometry as observed in Form **D-1.23I** crystals (Table 3.3 and Figure 3.24b). The electrophile (C=O) and the nucleophile (OH) are 4.394 Å apart and the angle of approach of the nucleophile to the electrophile was found to be 32.04°. The adjacent helices along the *c*-axis are loosely connected via van der Waals forces and are related by 3_1 operations i.e. each helix is rotated by 120° in clockwise direction and translated by 1/3 of the *c*-axis (Figure 3.27). Hence, there is clear difference in the organization of helices in Form **D-1.23I** and Form **D-1.23II** crystals. The neighboring helices are closely packed to generate mixed helical arrangements through C25-H25···O3. These differences in the crystal structure indicate that Form **D-1.23II** crystals do not facilitate intermolecular benzoyl transfer reaction.

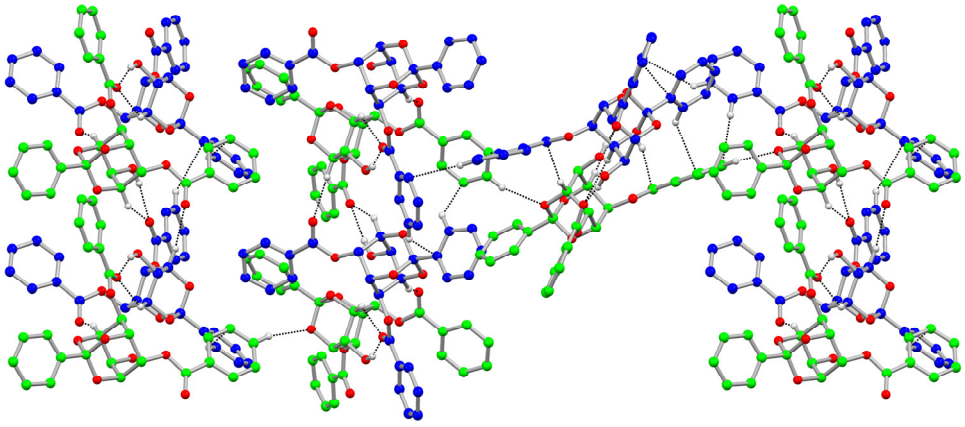

Figure 3.27: Packing of helices in crystals of Form **D-1.23II** revealing that the neighbouring helices are not discrete.

The estimation of the packing energies from room temperature data of racemic **1.23**, Form **D-1.23I** and Form **D-1.23II** crystals gave values of -239.7 kJ/mol, -221.00

kJ/mol and -211.65 kJ/mol respectively. It suggests that racemic crystals are more stable while Form **D-1.23II** crystals are least stable.

Comparison of the crystal structures of the orthoacetate (D-1.22) with the racemate (1.22) and its consequence:

Molecules in crystals of D-2,4-di-*O*-benzoyl-*myo*-inositol-1,3,5-orthoacetate **D-1.22** crystallized in monoclinic crystal system having space group $P2_1$. The structure overlay of the molecules in (the reactive) crystal of racemic **1.22**[7b] with chiral **D-1.22** showed significant differences in the conformation of the equatorial 2-benzoate group (by ~42°) while difference in the orientation of 4-benzoate is marginal (Figure 3.28). The packing energy differences between the reactive racemic crystals (-215.41 KJ/ mole) and the chiral crystals (-195.59 KJ/ mole) at room temperature were found to be ~20 KJ/ mole.

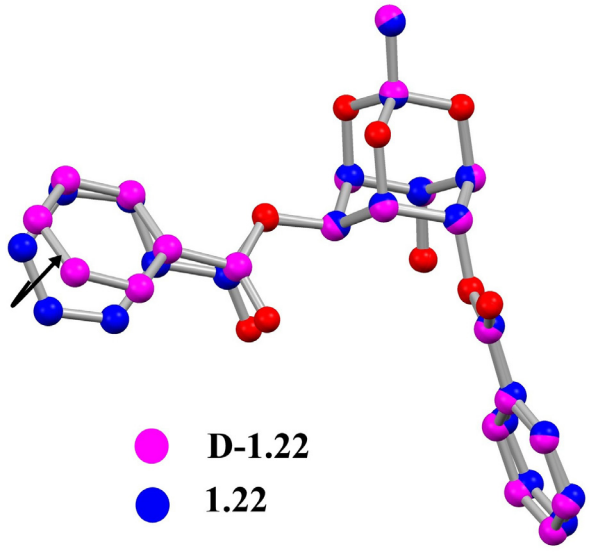

Figure 3.28: Structure overlay of the molecules in crystals of **D-1.22** (magenta) and in reactive crystals of the racemate **1.22** (blue).

The molecules of **D-1.22** assemble along *a*-axis forming 1D homochiral chain through intermolecular O-H···O hydrogen bonding interactions involving C6-OH and the oxygen O3 of the orthoacetate; also this 1D chain supported by C21-H21···O7 interaction (Figure 3.29). This homochiral assembly doesn't bring the C6-OH group (nucleophile - Nu) and the C=O (electrophile - El) of the 2-*O*-benzoyl group in close proximity to generate the short El···Nu interaction and deviates from the required

parameter for the facile acyl group migration. The electrophile (C=O) and the nucleophile (Nu) are 3.523 Å apart and the angle of approach of the nucleophile to the electrophile was 132.16°. The 1D chiral homo layer chain formed bilayer through the weak C-H···π interaction along *c*-axis Figure 3.30 (left).

The helical assembly in crystals of **D-1.22** is formed by weak but linear C-H···O contact between the aromatic hydrogen of the 4-benzoate with the oxygen O1 of the orthoester namely C18-H18···O1. The successive molecules along the helical assembly are rotated by 180° and translated along the *b*-axis by half value of the *b*-axis length (crystallographic 2_1-screw axis). The helices are interlinked by weak C-H···π interaction shown in Figure 3.30 (right). This helical assembly also prevents the close approach of the C6-OH group (nucleophile - Nu) and the C=O (electrophile - El) of the 4-*O*-benzoyl group (O=C···OH = 6.303 Å, 14.69°).

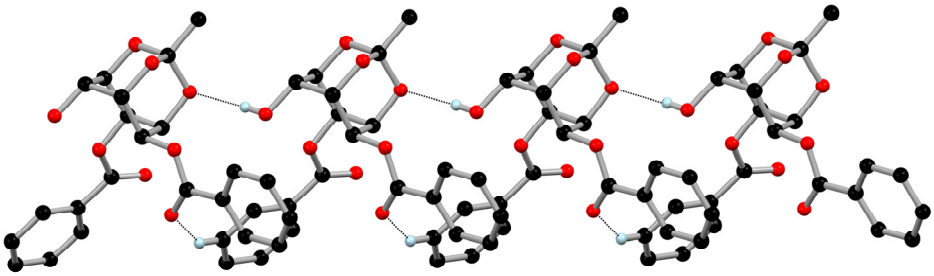

Figure 3.29: Formation of the 1D homochiral chain through O-H···O hydrogen bonding and 1D chain supported by C21-H21···O7 interaction in **D-1.22**.

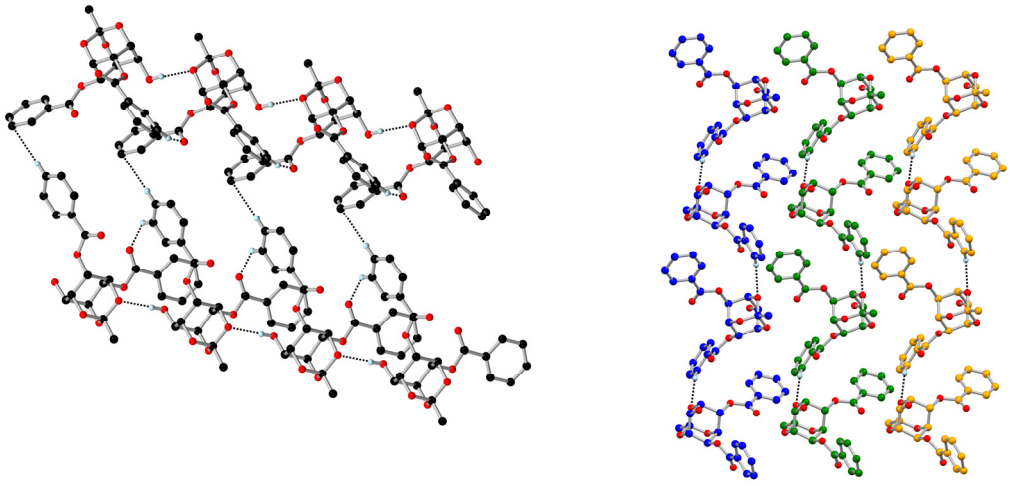

Figure 3.30: Formation of the bilayers through C-H···π interaction in the crystals of **D-1.22** (left), Packing of the helices in crystals of **D-1.22** (right).

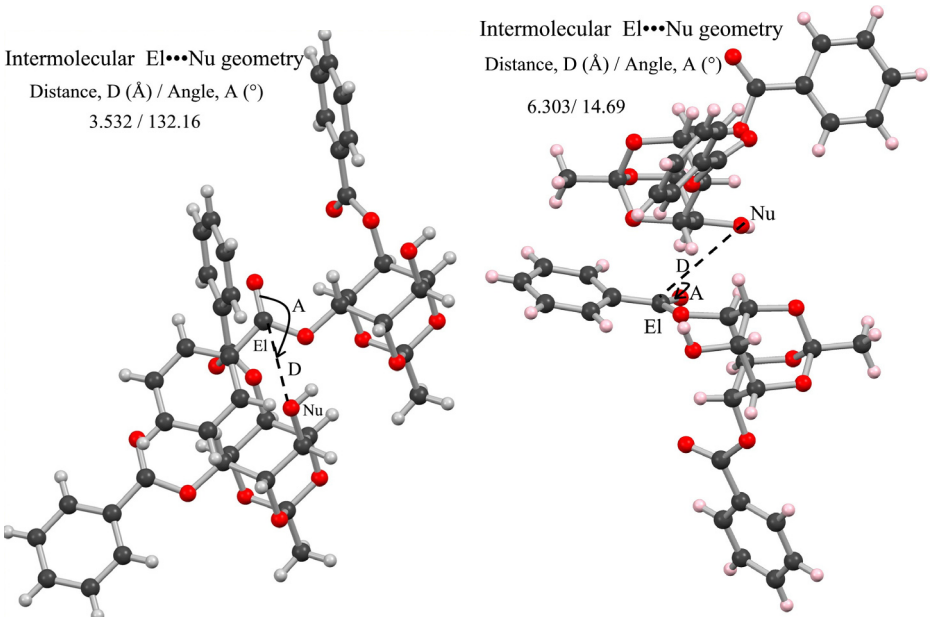

(a) (b)

Figure 3.31: (a) Relative orientation of the neighboring molecules in crystal of **D-1.22** with closest intermolecular contact between the C6-OH and 2-*O*-benzoyl C=O group (distance O7=C9···O6-H6A = 3.523Å and angle O6···C9=O7 = 132.16°); (b) Relative orientation of the neighboring molecules in crystal of **D-1.22** with closest contact between the C6-OH and 4-*O*-benzoyl C=O group (distance O8=C16···O6-H6A = 6.306Å and angle O6···C21=O8 = 14.69°).

Since the El···Nu interactions deviate from those required for efficient benzoyl group transfer (Figure 3.31), heating the crystals in the presence of a base gives a mixture of products.

Comparison of the crystal structures of orthoformate D-1.21 and racemic 1.21 and its consequence:

A comparison of the crystal structures of racemic-2,4-di-*O*-benzoyl-*myo*-inositol-1,3,5-orthoformate **1.21**, with the chiral of D-2,4-di-*O*-benzoyl-*myo*-inositol-1,3,5-orthoformate (**D-1.21**) was carried out to account for the lack of reactivity of the chiral crystals. The packing energy of the racemic (-209.9 KJ/ mole) as well as the chiral (-211.36 KJ/ mole) crystals at room temperature were found to be more or less similar. The structure overlay of the molecules in crystal of racemic **1.21** and **D-1.21**

showed significant differences in the conformation of the axial benzoate group by (~70^{o}) where as the marginal difference were found with equatorial benzoate group (~7^{o}) (Figure A64, Appendix III). Perhaps as a result, in chiral crystals of **D-1.21**, ($P2_12_12_1$) these molecules assembled in a helical fashion *via* hydrogen bonding between the C6-OH hydroxyl group of and the carbonyl oxygen of the C4-axial benzoate of neighboring molecule through (O6-H6A···O8) interaction, whereas in the its racemate equatorial benzoate groups of neighboring molecule involved in the helixes formation (Figure A66-A67, Appendix III). This helical assembly generated in chiral crystals precludes the orientation of the C6-OH group (nucleophile - Nu) and the C=O (electrophile - El) of the 4-*O*-benzoyl group (Figure A65, Appendix III) in a manner required (El···Nu distance and angle ~3.2 Å and ~90^{o} respectively) for the acyl transfer reaction. These observations are in accordance with the earlier published work C. Murali's thesis[7h] and paper[7b] but is described here for the same of completeness (For details See Appendix III).

Conclusion:

Comparison of the structure and intermolecular benzoyl group transfer reactivity of crystals of racemic and the corresponding enantiomeric di-*O*-benzoyl-*myo*-inositol-1,3,5-orthoesters suggests that the racemate and the enantiomers can have comparable structure and reactivity in the solid state. The results reported here perhaps constitute the first example of such an investigation. These results could be of significance in identifying chiral crystal systems capable of supporting chemical reactions in their constituent molecules. The results reported here could also be of relevance and use to those interested in molecular cocrystals and their properties.

Experimental Section:

General conditions: See Chapter 4 for the preparation of **3.2**, **3.5** and **3.6**.

Optical rotation was measured (in mentioned solvent) using 589 nm on JASCO (P-2000) Polarimeter.

Preparation of cocrystals 1.21•3.1:

The racemic dibenzoate (**1.21**, 0.400 g, 1 mmol)[11] and 4,4'-bipyridine (**3.1**, 0.156 g, 1 mmol) were dissolved in warm ethyl acetate (20 mL). The solution was stored (open to the atmosphere) at room temperature for 3-4 days, after which time 1:1 cocrystals **1.21•3.1** around (0.450 - 0.500 g) were obtained. **MP** = 130-131 ^{o}C; **IR** (Nujol):$\bar{\nu}$ 1721, 3200-3459 cm^{-1}; **^{1}H NMR** ($CDCl_3$, 400 MHz): δ 4.01-4.15 (m, 1H, D_2O exchangeable), 4.51 (m, 1H), 4.60-4.65 (m, 2H), 4.76 (m, 1H), 5.66 (d, *J* = 1.2 Hz, 1H), 5.73 (s, 1H), 5.81-5.85 (m, 1H), 7.42- 7.50 (m, 4H), 7.50-7.54 (m, 4H), 7.55-7.63 (m, 2H), 8.05-8.10 (m, 2H), 8.14-8.19 (m, 2H), 8.67-8.75 ppm (m, 4H); **^{13}C NMR** ($CDCl_3$, 101 MHz): δ 63.9, 67.2, 68.5, 68.8, 69.7, 72.0, 103.0, 121.5, 128.5, 128.6, 129.0, 129.5, 129.9, 133.4, 133.6, 145.6, 150.5, 165.2, 166.1 ppm.

Preparation of (-)-D-4-*O*-allyl-*myo*-inositol-1, 3, 5-orthobenzoate (D-3.3):

A mixture of the dicamphanate **dia3.2** (2.125 g, 3.187 mmol), methanol (20 mL), dichloromethane (20 mL) and *iso*-butyl amine (15 mL) was refluxed overnight, in an inert atmosphere. The solvent was removed under reduced pressure and the gummy residue was worked up as usual. The residue was dissolved in ethyl acetate and washed with water, 2% HCl, saturated sodium bicarbonate solution and brine. The organic layer was dried over anhydrous sodium sulphate and concentrated under reduced pressure to obtain a gum. The crude product was purified by column chromatography (silica gel, 100-200 mesh, eluent 25:75 ethyl acetate : light petroleum) to get (-)-D-4-*O*-allyl-*myo*-inositol-1,3,5-orthobenzoate (**D-3.3**, 0.94 g, 96%) as a gum.

Data for **D-3.3:** TLC R_f **:** 0.45 (40:60 ethyl acetate : light petroleum); $[\alpha]_D^{28}$= -8 ($CHCl_3$, c = 1.1) **IR** ($CDCl_3$):$\bar{\nu}$ 3200-3600 cm^{-1}; **^{1}H NMR** ($CDCl_3$, 400 MHz): δ 3.45 - 3.65 (br. s, 1 H, D_2O exchangeable), 3.7- 3.75 (m, 1 H, D_2O exchangeable) 4.01 - 4.19 (m, 3 H), 4.32 - 4.50 (m, 4 H), 4.54 (br. s, 1 H), 5.24 - 5.35 (m, 2 H), 5.75-5.90 (m, 1 H), 7.31 - 7.44 (m, 3 H), 7.59 - 7.75 ppm (m, 2 H); **^{13}C NMR** ($CDCl_3$, 101 MHz): δ 59.6, 67.5, 68.0, 71.6 (CH_2), 73.3, 73.8, 75.8, 107.2, 119.2 (CH_2), 125.1,

127.8 , 129.4, 132.6, 136.5 ppm. **Elemental analysis:** calculated for $C_{16}H_{18}O_6$ (306.31): C, 62.74; H, 5.92; found, C, 62.64; H, 6.02.

Preparation of (-)-D-2,6-di-*O*-benzoyl-4-*O*-allyl-*myo*-inositol-1,3,5-orthobenzoate (D-3.4):

The diol **(-)-D-3.3** (0.700 g, 2.285 mmol) and DMAP (0.085 g) were dissolved in pyridine (10 mL) and cooled with ice. Benzoyl chloride (1 mL) was added and stirred overnight (12 h) while the reaction mixture warmed to room temperature. Pieces of ice were added to hydrolyze the unreacted benzoyl chloride. The reaction mixture was concentrated under reduced pressure and the residue was worked up as usual. The crude product was purified by column chromatography (silica gel 100-200 mesh, eluent 15:85 ethyl acetate: light petroleum) to get (-)-D-2,6-di-*O*-benzoyl-4-*O*-allyl-*myo*-inositol-1,3,5-orthobenzoate as a gum (**D-3.4**, 1.058 g, 90%).

Data for **D-3.4:** TLC R_f **:** 0.45 (20:80 ethyl acetate : pet ether); $[\alpha]^{28}_D$= -26 ($CHCl_3$, c = 0.46); **IR** (Neat)**:** $\bar{\nu}$ 1720 cm^{-1}; **^{1}H NMR** ($CDCl_3$, 400 MHz): δ 4.02 - 4.22 (m, 2 H), 4.48 - 4.63 (m, 1 H), 4.81 - 5.01 (m, 3 H), 5.13 - 5.31 (m, 2 H), 5.75 - 5.92 (m, 2 H), 5.97 - 6.04 (m, 1 H), 7.39 - 7.54 (m, 7 H), 7.55 - 7.68 (m, 2 H), 7.77 - 7.93 (m, 2 H), 8.14 - 8.33 ppm (m, 4 H); **^{13}C NMR** ($CDCl_3$, 101 MHz): δ 63.2, 67.8, 68.1, 70.85 (CH_2), 71.3, 73.1, 107.8, 117.8 (CH_2), 125.2, 127.9, 128.3, 129.0, 129.4, 129.7, 129.8, 133.2, 133.3, 133.4, 136.6, 165.1, 165.9 ppm; **HRMS** $[C_{30}H_{26}O_8+H]^+$ = 515.1700; found = 515.1700.

Preparation of (-)-D-2,6-di-*O*-benzoyl-*myo*-inositol-1,3,5-orthobenzoate (D-1.23).

The allyl ether **D-3.4** (0.620 g, 1.24 mmol), 20% $Pd(OH)_2/C$ (0.844 g) and *iso*-propanol (15 mL) were mixed and refluxed for 3-4 h. TLC analysis showed that most of starting material had been consumed. The reaction mixture was filtered through Celite, washed with ethyl acetate (25 mL) and methanol (25 mL) and the filtrate was concentrated under reduced pressure to a gum. The dibenzoate **D-1.23** (gum, 0.388 g, 66%) was isolated by column chromatography (silica gel 100-200 mesh, eluent 20:80 ethyl acetate: light petroleum).

Data for **D-1.23:** TLC R_f **:** 0.40 (20:80 ethyl acetate : light petroleum); $[\alpha]^{28}_D$= - 51 ($CHCl_3$, c = 1.2); **IR** ($CDCl_3$)**:** $\bar{\nu}$ 1724, 3200-3600 cm^{-1}; **^{1}H NMR** ($CDCl_3$, 400 MHz): δ 2.65 (d, *J* = 5.50 Hz, 1 H, D_2O exchangeable), 4.64 - 4.70 (m, 1 H), 4.72 - 4.80 (m, 2 H), 4.82 - 4.88 (m, 1 H), 5.72 - 5.76 (m, 1 H), 5.93 - 5.99 (m, 1 H), 7.38 - 7.50 (m, 7 H), 7.56 - 7.63 (m, 2 H), 7.71 - 7.78 (m, 2 H), 8.06 - 8.12 (m, 2 H), 8.14 - 8.21 ppm

(m, 2 H); **^{13}C NMR** ($CDCl_3$, 101 MHz): δ 62.9, 67.4, 68.5, 69.4, 71.1, 73.2, 107.7, 125.4, 128.1, 128.5, 128.7, 128.9, 129.5, 129.8, 129.9, 129.95, 133.5, 133.7, 136.6, 165.2, 166.2 ppm; **Elemental analysis c**alculated for $C_{27}H_{22}O_8$ (474.46): C, 68.35; H, 4.67; found C, 68.24; H, 4.62.

A comparison of the chiral HPLC profile of the dibenzoate **D-1.23** with its racemate **1.23** revealed that the enantiomeric purity of **D-1.23** crystals was at least 99%.

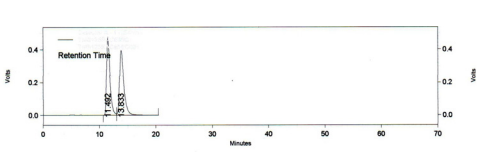

Detector A - 1 (254nm)

Retention Time	C Area	Area %
11.492	20024662	48.267
13.833	21462353	51.733
Totals	41487015	100.000

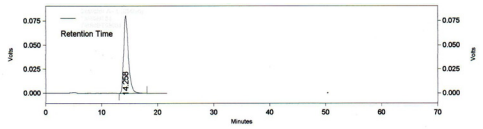

Detector A - 1 (254nm)

Retention Time	C Area	Area %
14.258	4681575	100.000
Totals	4681575	100.000

Figure 3.32: HPLC of racemic **1.23** and **D-1.23** crystal. [Column Chiraacel OD-H (250 × 4.6mm), mobile phase 20:80 *iso*-propanol-n-hexane, wavelength 254 nm, Flow rate 0.7 mL/min, concentration 1mg/mL, injection volume 5μL].

Crystallization of D-1.23: Crystallization of **D-1.23** from a saturated solution in 15-20:85-80 v/v ethyl acetate: light petroleum (bp. 60-80 ^{o}C) gave long plates (Form **D-1.23I**, MP =168 °C). Crystallization from chloroform and *n*-pentane mixture (1:4 v/v) gave long plates (Form **D-1.23I**, appeared to be the thermodynamic form since these crystals were formed at the bottom of the flask, well below the surface of the solvent) and concomitantly, a few irregular shaped crystals (From **D-1.23II**, MP = 145 °C and solidify and finally melt at 168 °C) appeared to be a kinetic form since these crystals were formed at the periphery – due to evaporation of the solvent at the surface. The Form **D-1.23II** crystals also obtained from the saturated solution of acetone in pet ether along with Form **D-1.23I** crystal. In most of the trials Form **D-1.23I** crystals were obtained exclusively. No attempt was made to reproduce Form **D-1.23II** crystals.

Transesterification of (-)-D-2,6-di-*O*-benzoyl-*myo*-inositol-1,3,5-orthobenzoate (D-1.23) in the solid state:

(a) In Form D-1.23I crystals: Form **D-1.23I** crystals of **D-1.23** (0.060 g, 0.125 mmol) and solid sodium carbonate (0.106 g, 1 mmol) were ground together using mortar and pestle and the mixture heated in a sealed tube in an atmosphere of argon, at 140 ^{o}C for 60 h. The reaction mixture was cooled to room temperature and extracted with chloroform (20 mL). The solid was allowed to settle and the supernatant liquid was decanted. The solid residue was extracted with methanol (20 mL). The solid was allowed to settle and the supernatant liquid was decanted. The solid residue was extracted with 1:1 chloroform - methanol mixture (20 mL). The combined extract was evaporated under reduced pressure and the residue was chromatographed (silica gel 100-200 mesh, 10% ethyl acetate in light petroleum) to obtain the tribenzoate **1.26** (0.033 g, ~43%, mp. 221-222 ^{o}C, Lit mp. 225-226 ^{o}C[8a] and the diol **1.29** (0.019 g, ~44%, mp. 185-187 ^{o}C, Lit. mp. 185-187 ^{o}C. 50% ethyl acetate in light petroleum.[8a] The structure of **1.26** and **1.29** was confirmed by a comparison of their H^1 NMR spectra with those of authentic samples. [8a]

(b) In Form D-1.23II crystals. Form **D-1.23II** crystals of **D-1.23** (0.020 g, 0.041 mmol) and solid sodium carbonate (0.035 g, 0.33 mmol) were ground together using mortar and pestle and the mixture heated in a sealed tube in an atmosphere of argon, at 130 ^{o}C for 60 h. The reaction mixture was cooled to room temperature and extracted with chloroform (10 mL). The solid was allowed to settle and the supernatant liquid was decanted. The solid residue was extracted with methanol (10 mL). The solid was allowed to settle and the supernatant liquid was decanted. The solid residue was extracted with 1:1 chloroform - methanol mixture (10 mL). The combined extract was evaporated under reduced pressure. TLC analysis of the reveals the presence of the major spot for dibenzoate along with minor impurities. The ^{1}H NMR of the combined extract suggesting the presence of the dibenzoate as major compound.

(c) in solution. A mixture of the dibenzoate **D-1.23** (0.070 g, 0.15 mmol), di-*iso*-propylethylamine (0.15 mL, 1.2 mmol) and dry DMF (3 mL) was stirred at 140 ^{o}C for 70 h. The residue obtained after removal of the solvent was chromatographed (silica gel 100-200 mesh) to obtain the tribenzoate **1.26** (0.016 g, 18%, eluent, 1/9 ethyl

acetate/light petroleum), the dibenzoate **D-1.23** (0.040 g, 57%, 1/4 ethyl acetate/ light petroleum, v/v) and the diol **1.29** (0.08 g, 14%, 1/1 ethyl acetate/ light petroleum, v/v). The ratio of the enantiomers present in the recovered dibenzoate was 1:1.3 (by chiral HPLC).

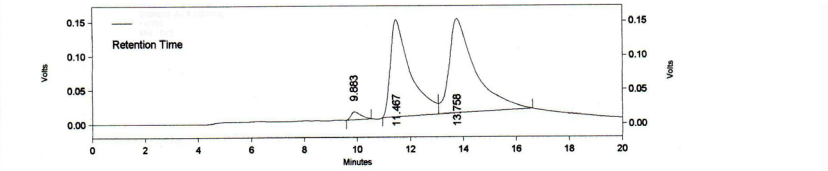

Detector A - 1 (254nm)

Retention Time	C Area	Area %
9.883	294649	1.720
11.467	7351679	42.912
13.758	9485593	55.368
Totals	17131921	100.000

Figure 3.33: HPLC analysis of the recovered dibenzoate. Column Chiraacel OD-H (250 × 4.6mm), mobile phase 20:80 *iso*-propanol-n-hexane, wavelength 254nm, Flow rate 0.7 mL/min, concentration 1mg/mL, injection volume 5µL).

(d) In the molten state. Form **D-1.23I** crystals of (-)-D-2,6-di-*O*-benzoyl-*myo*-inositol-1,3,5-orthobenzoate (**D-1.23**, 0.030 g, 0.0625 mmol) and solid sodium carbonate (0.053 g, 0.5 mmol) were ground together using mortar and pestle and the mixture heated in a sealed tube in an atmosphere of argon at 180 ^{o}C for 12 h. The TLC analysis of the reaction mixture showed the presence of several products including the dibenzoate. No attempt was made to separate these products.

Preparation of (+)-D-6-*O*-allyl-*myo*-inositol-1,3,5-orthoacetate (D-3.7):

A mixture of the dicamphanate **3.5** (2.000 g, 3.307mmol), MeOH (20 mL), dichloromethane (20 mL) and *iso*-butyl amine (15 mL) were used to prepare **D-3.7** (as in the preparation of **D-3.3**). The product was purified by column chromatography (silica gel, 100-200 mesh, eluent 3:7 ethyl acetate:light petroleum, v/v) to get (+)- D-4-*O*-allyl *myo*-inositol-1,3,5-orthoacetate D-**3.7** (0.774 g, 96%) as a gum. See Chapter 4 for the preparation of **3.5**.

Data for **D-3.7:** TLC R_f**:** 0.4 (1:1 ethyl acetate : light petroleum, v/v); $[\alpha]^{28}_{D}$ = +33 ($CHCl_3$, c = 0.23); **IR** (Neat)**:** $\bar{\nu}$ 3350-3600 cm^{-1}; **^{1}H NMR** ($CDCl_3$, 500 MHz): δ

1.45 (s, 3 H), 3.3 (br. s, 1H, D_2O exchangeable), 3.66 (d, J = 7.63 Hz, 1 H, D_2O exchangeable), 4.00 (s,1 H), 4.09 – 4.36 (m, 6H), 4.42 (br. s, 1 H), 5.26 - 5.35 (m, 2 H), 5.82 - 5.92 ppm (m, 1 H); **^{13}C NMR** ($CDCl_3$, 126 MHz): δ 24.1, 59.7, 67.4, 67.6, 71.8 (CH_2), 72.7, 74.0, 75.2, 108.6, 119.4 (CH_2), 132.7 ppm; **Elemental analysis** calculated for $C_{11}H_{16}O_6$ (244.24): C, 54.09; H, 6.60; found C, 54.26; H, 6.42.

Preparation of (+)-D-2,4-di-*O*-benzoyl-6-*O*-allyl *myo*-inositol-1,3,5-orthoacetate (D-3.9). The diol (+)-**D-3.7** (0.700 g, 2.86 mmol), DMAP (0.100 g), pyridine (10 mL) and benzoyl chloride (1 mL) were used to prepare the dibenzoate **D-3.9** (as in the preparation of **D-3.4**). The gummy **D-3.9** (1.24 g, 93%) obtained was dissolved in hot *iso*-propanol (20-25 mL) and the solution was stored under ambient conditions (4-6 h) when needle shaped crystal were obtained.

Data for **D-3.9:** TLC R_f **:** 0.5 (30:70 ethyl acetate : pet ether); $[\alpha]^{28}_D$ = + 37 (DCM, c = 0.66); **MP** = 122-124 ^oC; **IR** (solid)**:** $\bar{\nu}$ 1717 cm^{-1}, **^{1}H NMR** ($CDCl_3$, 400 MHz): δ 1.56 (s, 3 H), 4.02 - 4.10 (m, 2 H), 4.34 - 4.39 (m, 1 H), 4.54 - 4.61 (m, 2 H), 4.64 – 4.69 (m, 1 H), 5.07 - 5.21 (m, 2 H), 5.56 - 5.60 (m, 1 H), 5.70 - 5.82 (m, 2 H), 7.41 - 7.52 (m, 4 H), 7.55 - 7.64 (m, 2 H), 8.05 -8.09 (m, 2 H), 8.14 - 8.19 ppm (m, 2 H); **^{13}C NMR** ($CDCl_3$, 101 MHz): δ 24.2, 63.4, 67.3, 68.2, 70.3, 70.8, 71.1 (CH_2), 73.2, 109.2, 118.1 (CH_2), 128.4, 129.2, 129.7, 129.9, 130,133.4, 133.5, 133.6, 165.5, 166.2 ppm; **Elemental analysis** calculated for $C_{25}H_{24}O_8$ (452.46): C, 66.37; H, 5.35; found C, 66.23; H, 5.21.

Preparation of (+)-D-2,4-di-*O*-benzoyl-*myo*-inositol-1,3,5-orthoacetate (D-1.22): The allyl ether **D-3.9** (1.1 g, 2.42 mmol), 20% $Pd(OH)_2/C$ (0.848 g) and *iso*-propanol (10 mL) were used to cleave the allyl ether (as in the preparation of **D-1.23**) to obtain a (gum, 0.812 g, 81%, enantiomeric 94:6 by HPLC).

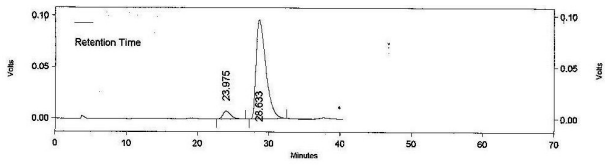

Detector A - 1 (254nm)

Retention Time	C Area	Area %
23.975	570152	5.880
28.633	9126783	94.120
Totals	9696935	100.000

Figure 3.34: HPLC analysis of the gummy dibenzoate **D-1.22** before crystalization.

The gum (0.700 g) was dissolved in chloroform (5-10 mL) and diluted with light petroleum (60 mL). The resulting mixture was warmed on water bath and stored under ambient conditions when **D-1.22** crystallized as plates (3-4 days).

Data for **D-1.22**: TLC R_f **:** 0.40 (30:70 ethyl acetate : light petroleum); $[\alpha]^{28}_{D}$ = + 55.3 ($CHCl_3$, c = 1.3); **MP** = 147-149 °C; **IR** (solid)**:** $\bar{\nu}$ 1714, 3400-3500 cm^{-1}; **^{1}H NMR** ($CDCl_3$, 400 MHz): δ 1.56 (s, 3 H), 2.55 (d, 1 H, *J* = 8.7 Hz, D_2O exchangeable), 4.48 - 4.65 (m, 1 H), 4.66 - 4.72 (m, 1 H), 5.61 (s, 1 H), 5.76 - 5.82 (m, 1 H), 7.40 - 7.55 (m, 4 H), 7.5 - 7.62 (m, 2 H), 8.04 (d, *J* = 7.6 Hz, 2 H), 8.14 ppm (d, *J* = 7.6 Hz, 2 H); **^{13}C NMR** ($CDCl_3$, 101 MHz): δ 24.1, 62.9, 67.4, 68.6, 68.7, 70.3, 72.5, 109.0, 128.5, 128.7, 129.0, 129.6, 129.9, 130.0, 133.4, 133.7, 165.2, 166.2 ppm; **Elemental analysis** calculated for $C_{22}H_{20}O_8$ (412.39):C, 64.08; H, 4.89; found, C, 64.11; H, 5.03.

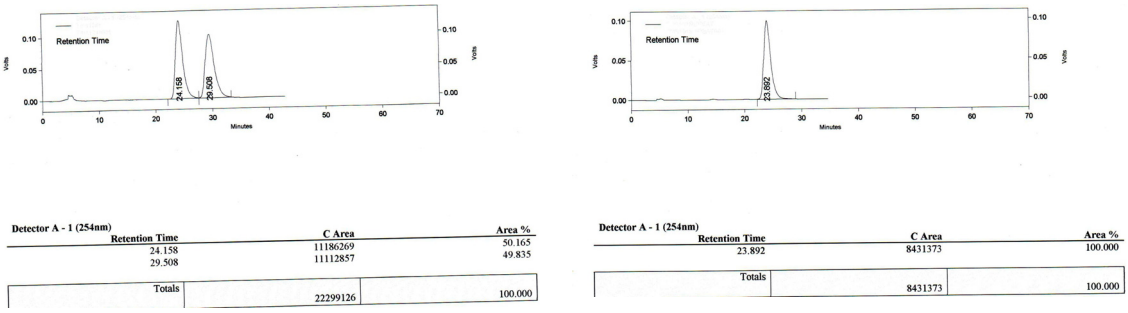

Detector A - 1 (254nm) Retention Time	C Area	Area %
24.158	11186269	50.165
29.508	11112857	49.835
Totals	22299126	100.000

Detector A - 1 (254nm) Retention Time	C Area	Area %
23.892	8431373	100.000
Totals	8431373	100.000

Figure 3.35: A comparison of the chiral HPLC profile of the dibenzoate **D-1.22** with its racemate revealed that the enantiomeric purity of **D-1.22** crystals was more than 99%. Chiral HPLC [Column Chiraacel OD-H (250 × 4.6mm), mobile phase 5:95 *iso*-propanol:n-hexane, wavelength 254nm, Flow rate 0.7 mL/min, concentration 1mg/mL, injection volume 5µL].

Reaction of (+)-D-2,4-di-*O*-benzoyl-*myo*-inositol-1,3,5-orthoacetate (D-1.22) in the solid state:

Freshly grown crystals of **(+)-**D-2,4-di-*O*-benzoyl-*myo*-inositol-1,3,5-orthoacetate (**D-1.22**) (0.103 g, 0.125 mmol) and solid sodium carbonate (0.212 g, 2 mmol) were ground together using mortar and pestle and the mixture heated in a sealed tube in an atmosphere of argon, at 125 °C for 72 h. The TLC analysis showed a mixture of products along with the starting material. No attempt was made to separate these products.

Preparation of (+)-6-*O*-allyl-*myo*-inositol-1,3,5-orthoformate (D-3.8): The dicamphanate **3.6** (1.100 g, 1.85 mmol), methanol (15 mL), dichloromethane (15 mL) and *iso*-butyl amine (10 mL) were used (as in procedure for **D-3.3**) to obtain crude **D-3.8**. The crude product was purified by column chromatography (silica gel, 100-200 mesh, eluent 2:3 ethyl acetate:light petroleum, v/v) to get (+)-D-6-*O*-allyl-*myo*-inositol-1,3,5-orthoformate (**D-3.8**, 0.408 g, 96%) as a gum. See Chapter 4 for the preparation of **3.6**.

Data for **D-3.8:** TLC R_f**:** 0.35 (40:60 ethyl acetate : light petroleum); $[\alpha]^{28}_{D}$= + 8.5 ($CHCl_3$, c = 1.4); **IR** ($CHCl_3$)**:** $\bar{\nu}$ 3478 cm^{-1}; **^{1}H NMR** ($CDCl_3$, 500 MHz): δ 3.61 (br. s, 1 H, D_2O exchangeable), 3.70 - 3.78 (m, 1 H, D_2O, exchangeable), 4.06 (br. s, 1 H), 4.10 - 4.19 (m, 2 H), 4.21- 4.23 (m, 1 H), 4.27 - 4.33 (m, 2 H), 4.36 - 4.40 (m, 1 H), 4.42 - 4.50 (m, 1 H), 5.27 - 5.36 (m, 2 H), 5.47 (s, 1 H), 5.83 - 5.93 ppm (m, 1 H); **^{13}C NMR** ($CDCl_3$, 126 MHz): δ 60.4, 67.2, 67.7, 71.8 (CH_2), 72.1, 74.1, 74.6, 102.6, 119.3(CH_2), 132.6 ppm; **HRMS** $[C_{10}H_{14}O_6 + H]^+$ = 231.0863; found = 231.0864.

Preparation of (+)-D-2,4-di-*O*-benzoyl-6-*O*-allyl-*myo*-inositol-1,3,5-orthoformate (D-3.10):

The diol (+)-**D-3.9** (0.250 g, 1.08 mmol) was benzoylated using DMAP (0.050 g), pyridine (6 mL) and benzoyl chloride (0.5 mL) to obtain **D-3.10** as a colorless solid (0.435 g, 91%).

Data for **D-3.10:** TLC R_f**:** 0.5 (20:80; ethyl acetate : pet ether); $[\alpha]^{28}_{D}$ = + 40 ($CHCl_3$, c = 0.35), **MP** = 95-97 ^oC; **IR** (Solid)**:** $\bar{\nu}$ 1713 cm^{-1}; **^{1}H NMR** ($CDCl_3$, 500 MHz): δ 3.99 - 4.14 (m, 2 H), 4.40 (br. s, 1 H), 4.58 (br. s, 2 H), 4.73 (br. s, 1 H), 5.09 – 5.22 (m, 1 H), 5.62- 5.68 (m, 2 H), 5.72 - 5.82 (m, 2 H), 7.42- 7.50 (m, 4 H), 7.55 – 7.63 (m, 2 H), 8.07 (d, *J* = 7.66 Hz, 2 H), 8.17 ppm (d, *J* = 7.66 Hz, 2 H); **^{13}C NMR** ($CDCl_3$, 126 MHz): δ 64.2, 67.2, 68.2, 69.7, 70.2, 71.1 (CH_2), 73.4, 103.2, 118.2 (CH_2), 128.5, 129.1, 129.6, 129.9, 130.1, 133.5, 133.5, 165.3, 166.2 ppm; **Elemental analysis** calculated for $C_{34}H_{36}O_{14}$ (438.43): C, 65.75; H, 5.06; found C, 65.94; H, 4.89.

Preparation of (+)-D-2,4-di-*O*-benzoyl-*myo*-inositol-1,3,5-orthoformate (D-1.21):

The allyl ether **D-3.10** (0.280 g, 0.63 mmol), 20% $Pd(OH)_2/C$ (0.180 g) and *iso*-propanol (5 mL) were mixed and refluxed for 24 h. The reaction mixture was processed as in the procedure for **D-3.5** to isolate **D-1.21** as a solid (0.195 g, 77 %). **D-1.21** (0.170 g) was dissolved in chloroform (3 mL) and diluted with light petroleum (15 mL). The turbid solution was warmed to obtain a clear solution and stored under ambient conditions (7-8 h) to obtain fibrous crystals.

Data for **D-1.21:** TLC R_f **:** 0.40 (30:70 ethyl acetate : light petroleum); $[\alpha]^{28}_D$= + 60.4 ($CHCl_3$, c = 1.1), Reported from lit[5e] $[\alpha]^{22}_D$ = + 66.0 ($CHCl_3$, c = 1); **MP** = 165 -167 °C (Lit mp 162 - 164 °C.[5e] These crystals did not undergo benzoyl transfer reaction in agreement with earlier report.[5e]

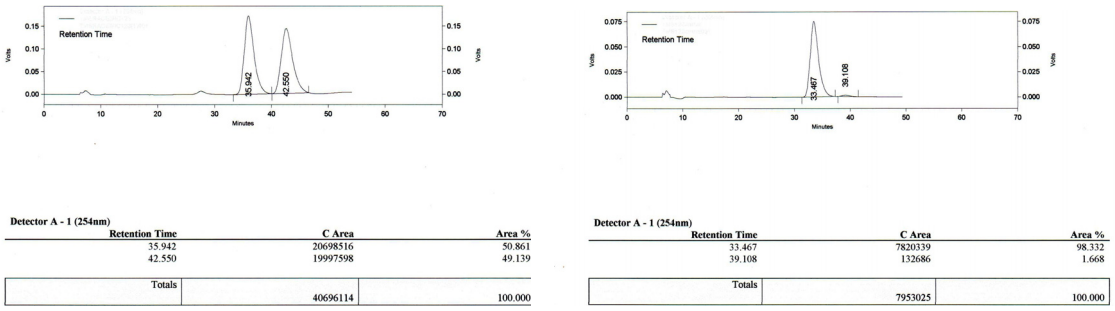

Detector A - 1 (254nm)

Retention Time	C Area	Area %
35.942	20698516	50.861
42.550	19997598	49.139
Totals	40696114	100.000

Detector A - 1 (254nm)

Retention Time	C Area	Area %
33.467	7820339	98.332
39.108	132686	1.668
Totals	7953025	100.000

Figure 3.36: A comparison of the chiral HPLC profile of the dibenzoate **D-1.21**with its racemate revealed that the enantioeric purity of **1.21** crystal at least 98%. [Column Chiracel OD-H (250 × 4.6mm), mobile phase 5:95 EtOH-n-hexane, wavelength 254 nm, Flow rate 0.5 mL/min, concentration 1mg/mL, injection volume 5µL].

DSC analysis:

DSC analyses of the Cocrystal **1.21•3.1** and all chiral di-benzoate orthoesters (Form **D-1.23I** of the orthobenzoate **D-1.23** and orthoacetate **D-1.22**, orthoformate **D-1.21**) were carried out on a Mettler or Waters (Cocrystal **1.21•3.1**, Form **D-1.23II** of the orthobenzoate **D-1.23**) DSC instrument. The solid (~3-4 mg) was placed on an aluminum pan (40 µl) and was analyzed using an empty pan as the reference. The heating rate was 5° (Form **D-1.23I** of the orthobenzoate **D-1.23** and orthoacetate **D-**

1.22, orthoformate **D-1.21**) or 10° (Form **D-1.23II** of the orthobenzoate **D-1.23**) C/min. Nitrogen gas was used for purging.

PXRD analysis:

The Powder X-ray diffraction patterns were recorded on Rigaku Micromax-007HF instrument (High intensity microfocous rotating anode X-ray Generator) with R-axis detector IV++ at a continuous scanning rate of 2° 2θ/min using Cu Kα radiation (40 kV, 30 mA) with the intensity of the diffracted X-ray being collected at intervals of 0.1° 2θ. A nickel filter was used to remove Cu K$_\beta$ radiation. PXRD pattern of crystals of the orthobenzoate **D-1.23 (**Form **D-1.23I**), orthoacetate **D-1.22** and orthoformate **D-1.21** and (separate) ground mixture of these crystals with sodium carbonate were recorded to see if any phase change occurred during grinding with sodium carbonate. The results from PXRD revealed that the dibenzoates **D-1.23**, **D-1.22**, and **D-1.21** did not undergo phase change on grinding with sodium carbonate, at room temperature (Figure A61-A63, See Appendix III).

X-ray Crystallography:

Single crystal X-ray structures of **D-1.23** (Form **D-1.23I**, **D-3.9**, **D-1.22**, **D-1.21** were determined at room temperature (Form **D-1.23I** at 413K, and Form **D-1.23II** at 200K) by measuring X-ray diffraction intensity data on a Bruker SMART APEX II single crystal X-ray CCD diffractometer having graphite-monochromatised (Mo-Kα = 0.71073 Å) radiation. The X-ray generator was operated at 50 kV and 30 mA. (See Tables A3 and A4 in Appendix III for crystal data and geometrical parameters of intermolecular interactions, ORTEP).

References:

[1] (a) V. Ramamurthy, K. Venkatesan, *Chem. Rev.* **1987**, *87,* 433-481; (b) Y. Ohashi, *Reactivity in Molecular Crystals*, WILEY -VCH, Weinheim, **1993**; (c) H. Kanazawa, Y. Ohashi, *Mol. Cryst. Liq. Cryst.* **1996**, *277*, 45-54; (d) A. E. Keating, M. A. Garcia-Garibay, *Mol. Supramol. Photochem*. **1998**, *2,* 195-248; (e) Braga, F. Grepioni, *Angew. Chem. Int. Ed.* **2004**, *43,* 4002-4011; (f) A. E. Troup, H. Mitchner, *J. Pharm. Sci.* **1964**, *53,* 375-379; (h) K. Tanaka, F. Toda*, Chem. Rev.* **2000**, *100*, 1025-1074.

[2] (a) G. M. J. Schmidt, *J. Chem. Soc.* **1964**, 2014-2021; (b) L. R. MacGillivray, G. S. Papaefstathiou, T. Friščić, D. B. Varshney, T. D. Hamilton, *Top. Curr. Chem.* **2004**, *248,* 201-221; (c) J. Yang, M. B. Dewal, S. Profeta, Jr. M. D. Smith, Y. Li, L. S. Shimizu, *J. Am. Chem. Soc.* **2008**, *130,* 612-621; (d) L. R. MacGillivray, G. S. Papaefstathiou, T. Friščić, T. D. Hamilton, D-K. Buĉar, Q. Chu, D. B. Varshney, I. G. Georgiev, *Acc. Chem. Res.* **2008**, *41,* 280-291; (e) M. H. Mir, L. L. Koh, G. K. Tan, J. J. Vittal, *Angew. Chem. Int. Ed.* **2010**, *49,* 390-393; (f) R. Sekiya, K. Kiyo-oka, T. Imakubo, K. Kobayashi, *J. Am. Chem. Soc.* **2000**, *122,* 10282-10288; (g) S. Kohmoto, Y. Ono, H. Masu, K. Yamaguchi, K. Kishikawa, Y. Yamamoto, *Organic Lett.* **2001**, *3*, 4153-4155.

[3] (a) J. D. Dunitz, J. Bernstein, *Acc. Chem. Res*. **1995**, *28*, 193–200; (b) H. G. Brittain, *Polymorphism in Pharmaceutical Soilds*, Marcel Dekker Inc., New York, **1999**; (c) J. A. R. P. Sarma, G. R. Desiraju, *in Crystal Engineering: Polymorphism and Pseudopolyorphism in Organic Crystals: A Cambridge Structural Database Study, eds*. Seddon, S. R.; Zaworotko, M. J. Kluwer, Norwell, MA, USA, **1999**, p. 325; (d) J. Bernstein, *Polymorphism in Molecular Crystals*, Oxford University Press, Oxford, UK, **2002**; (e) A. J. Cruz-Cabeza, J. Bernstein, *Chem. Rev.* **2014**, *114*, 2170-2191.

[4] (a) W. C. McCrone, *Anal. Chem.* **1950**, *22*, 1225–1226; (b) T. B. Brill, R. J. Karpowicz, *J. Phys. Chem.* **1982**, *86*, 4260–4265; (c) G. W. Stockton, R. Godfrey, P. Hitchcock, R. Mendelsohn, P. C. Mowery, S. Rajanand, A. F. Walker, *J. Chem. Soc., Perkin Trans. 2*, **1998**, 2061–2071; (d) C. P. Price, A. L. Grzesiak, J. W. Kampf, A. J. Matzger, *Cryst. Growth Des*. **2003**, *3*, 1021–1025; (e) P. Vishweshwar, J. A. McMahon, M. Oliveira, M. L. Peterson, M. J. Zaworotko, *J. Am. Chem. Soc.* **2005**, *127*, 16802–16803; (f) R. Hilfiker,

Polymorphism in the Pharmaecutical Industry, Wiley-VCH, Weinheim, Germany, **2006**; (g) F. P. A. Fabbiani, C. R. Pulham, *Chem. Soc. Rev*. **2006**, *35*, 932–942; (h) C. Näther, I. Jeβ, *Angew. Chem. Int. Ed.* **2006**, *45*, 6381–6383; (i) E. F. Paulus, F. J. J. Leusen, M. U. Schmidt, *CrystEngComm*, **2007**, *9*, 131–143. (j) A. D. Bond, R. Boese, G. R. Desiraju, *Angew. Chem., Int. Ed. Engl.* **2007**, *46*, 615–617; (k) S. H. Thorat; M. V. Patwadkar; R. G. Gonnade, R. Vaidhyanathan, *CrystEngComm*, **2014**, *16*, 8638–8641 (l) L. Geng-Geng, X. Jiu-Xu, F. Kai, Z. Qing-Hua, W. Ji-Huai, D. Jing-Cao, *Dalton Trans*, **2013**, 42, 16268-16271; (m) Y. Fan, Y. Zhao, L. Ye, B. Li, G. Yang, Y. Wang, *Cryst. Growth Des*. **2009**, *9*, 1421-1430 (n) Y. Fan, W. Song, D. Yu, K. Ye, J. Zhang, Y. Wang, *CrystEngComm* **2009**, *11*, 1716-1722.

[5] (a) M. D. Cohen, G. M. Schmidt, F. I. Sonntag, *J. Chem. Soc.* **1964**, 1996-2013; (b) Y. Matsuda, M. Mihara, *J. Pharm. Pharmacol*. **1994**, *46*, 162-167; (c) R. S. Gopalan, G. U. Kulkarni, *Proc. Indian Acad. Sci.* (*Chem. Sci.*), **2001**, *113* 307–324; (d) H. Shinya, T. Shinji, T. Fumino, U. Hidehiro, *Angew. Chem., Int. Ed. Engl.* **2006**, *45*, 6013–6016; (e) C. Murali, M. S. Shashidhar, R. G. Gonnade, M. M. Bhadbhade, *Chem. Eur. J*. **2009**, *15*, 261–269; (f) S. Krishnaswamy, M. S. Shashidhar, M. M. Bhadbhade, *CrystEngComm*, **2011**, *13*, 3258-3264; (g) C. Xiaoming, L. Tonglei, R. M. Kenneth, R. B. Stephen, *Mol. Cryst. Liq. Cryst*, **2002**, *381*, 121-131; (h) K. K. Goutam, J. V. Jagadese, *Chem. Soc. Rev*. **2013**, *42*, 1755–1775; (h) B. Kumar, S. Ramkinkar, *Chem. Soc. Rev.* **2013**, *42*, 950-967.

[6] A. Pathigooala, R. G. Gonnade, K. M. Sureshan, *Angew. Chem. Int. Ed. Engl*. **2012**, 51, 4362-4366; (b) A. Pathigoolla, K. M. Sureshan, *Angew. Chem. Int. Ed. Engl*. **2013**, *52*, 8671- 8675; (c) T. Praveen, U. Samanta, T. Das, M. S. Shashidhar, P. Chakrabarti, *J. Am. Chem. Soc.* **1998**, *120*, 3842-3845 and references cited therein. (d) B. K. Ruth, N. D. Eileen; C. E. Margaret; C. P. Iain; Y.C. David, *J. Am. Chem. Soc*. **1980**, *102*, 7709 –7714; (e) S. Ryo, K-O Kazuhiko, I. Tatsuro, K. Keiji, *J. Am. Chem. Soc*. **2000**, *122*, 10282 –10288; (f) B. Dario, D. Daniela, L. G. Stefano, M. Lucia, P. Marco, G. Fabrizia, *Top Curr Chem* **2005**, *254*, 71–94.

[7] (a) J. H. Kim, S. V. Lindeman, J. K. Kochi, *J. Am. Chem. Soc*. **2001**, *123*, 4951-4959; (b) M. P Sarmah, R. G. Gonnade, M. S. Shashidhar, M. M. Bhadbhade,

Chem. Eur. J. **2005**, *11*, 2103-2110; (c) M. L.Cheney, G. J. McManus, J. A. Perman, Z. Wang, M. J. Zaworotko, *Cryst. Growth Des*. **2007**, *7*, 616 – 617 (d) S-L. Zheng, O. Pham, M. L. Christophe, V. Velde, M. Gembicky, P. Coppens, *Chem. Comm*. **2008**, 2538- 2540; (e) M. Khan, V. Enkelmann, G. Brunklaus, *Cryst. Growth Des.* **2009**, *9*, 2354- 2362; (f) D. S. Khorasani, M. A. Botes, M. A. Fernandes, D. C. Levendis, *CrystEnggComm* **2015**, *17*, 8933-8945; (g) M. I. Tamboli, S. Krishnaswamy, M. S. Shashidhar, R. G. Gonnade, *Chem. Eur. J*. **2013**, *19*, 12867–12874; (h) C. Murali, Ph. D Thesis, Univ. of Pune*,* **2008**.

[8] (a) C. Murali, M. S. Shashidhar, R. G. Gonnade, and M. M. Bhadbhade, *Eur. J. Org. Chem.* **2007**, 1153-1159; (b) S. Krishnaswamy, R. G. Gonnade, M. S. Shashidhar, M. M. Bhadbhade, *CrystEngComm*, **2010**, *12*, 4184–4197.

[9] F. H. Allen, *Acta Cryst.* **2002**, *B58*, 380-388.

[10] M. Alson, M. S. Shashidhar, *Tetrahedron,* **2012**, *68*, 9769-9776.

[11]T. Das and M. S. Shahsibhar, *Carbohydr. Res.* **1998**, *308*, 165-168.

Appendix III given in Pen Drive, along with Thesis

List of the content in Appendix III

Chapter 4

Separation of diastereomeric dicamphanates of racemic 4-*O*-allyl-*myo*-inositol-1,3,5-orthoesters on gram scale by crystallization.

Introduction:

Since the discovery of the relationship between intracellular concentration of phosphoinositols and the release of calcium ions from intracellular sources, the chemistry and biology associated with naturally occurring inositol derivatives has expanded into a contemporary area of research with brisk activity.[1] Initial synthetic efforts targeted towards the synthesis of inositol derivatives were focused on the delineation of the relative reactivity of the inositol hydroxyl groups leading to the synthesis of suitably protected inositol derivatives as precursors for phosphoinositols and their analogs.[2] With advances towards mapping of the various steps involved in the *myo*-inositol cycle and the realization of the importance of glycoinositols, the focus shifted to the synthesis of chiral inositol derivatives. The known approaches for the preparation of chiral inositol derivatives include (a) use of chiral pool molecules (such as mannitol, glucose, galactose, quinic acid, cyclohexadiene diol) as starting materials[3] See Chart 4.1.

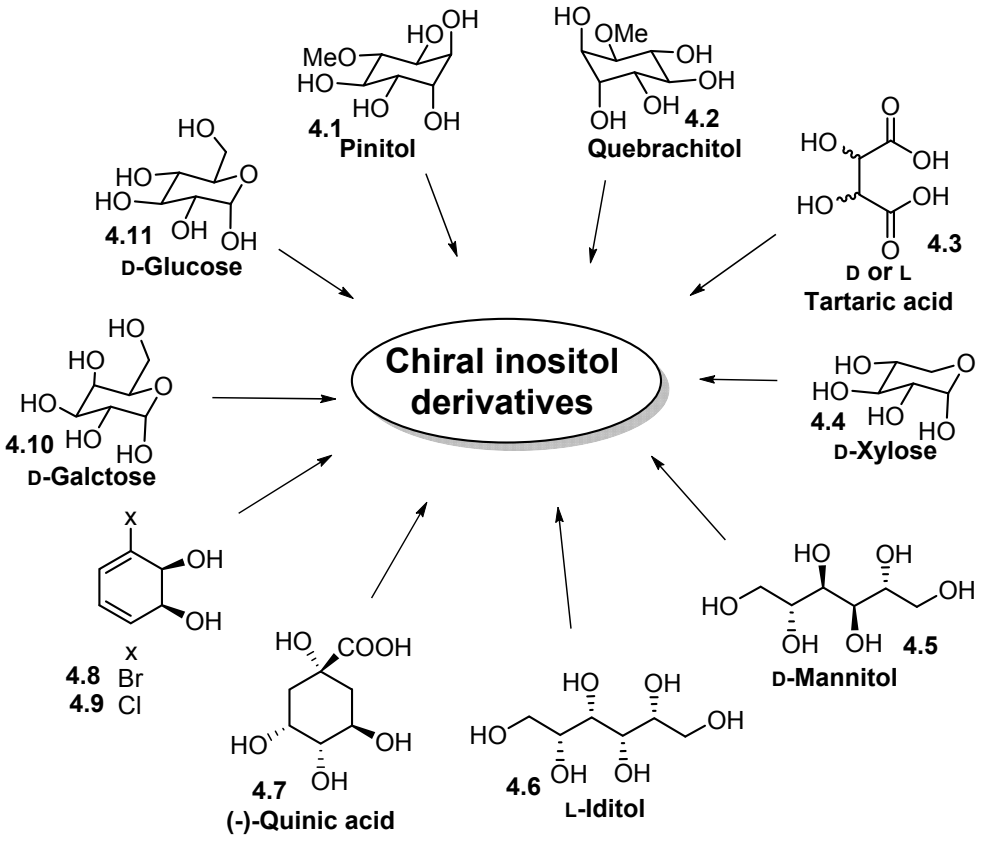

Chart 4.1: Chiral starting material used for the preparation of chiral inositol derivatives.

(b) Classical resolution of racemic inositol derivatives *via* conversion to separable diastereomers (top of scheme 4.1); (c) desymmterization of symmetric *meso*-derivatives of inositol (bottom of scheme 4.1).

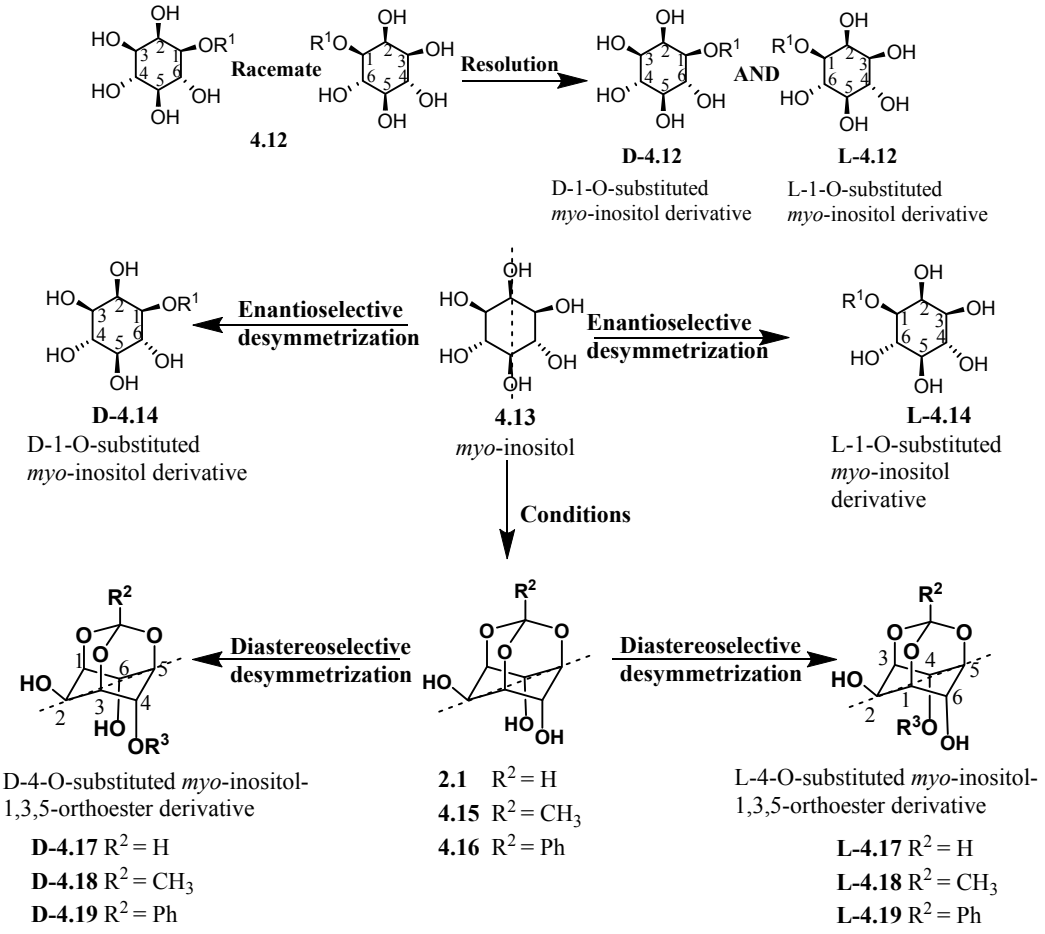

Scheme 4.1: Possible ways of obtaining chiral inositol derivatives from *myo*-inositol

Selected examples of these approaches from the literature are shown in charts 4.1 – 4.5 and schemes 4.2 – 4.5 below.

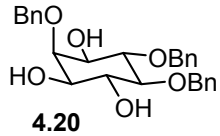

4.20

Chem. Commun. **1997**, 1633–1634

Org. Biomol. Chem. **2010**, *8*, 66–76

Org. Biomol. Chem. **2010**, *8*, 66–76

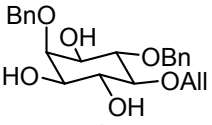

4.21

J. Chem. Soc., Perkin Trans. 1 **1999**, 923–935

Tetrahedron Asymm. **2009**, *20*, 2809–2813

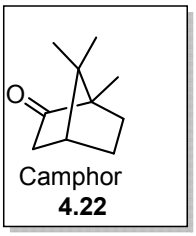

4.22

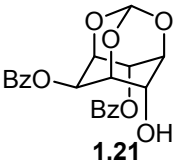

1.21

Eur. J. Org. Chem. **2003**, 1035–1041.

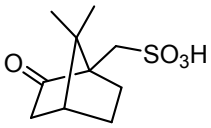

4.23

Chart 4.2: Inositol derivatives resolved using camphor or camphor sulfonic acid.

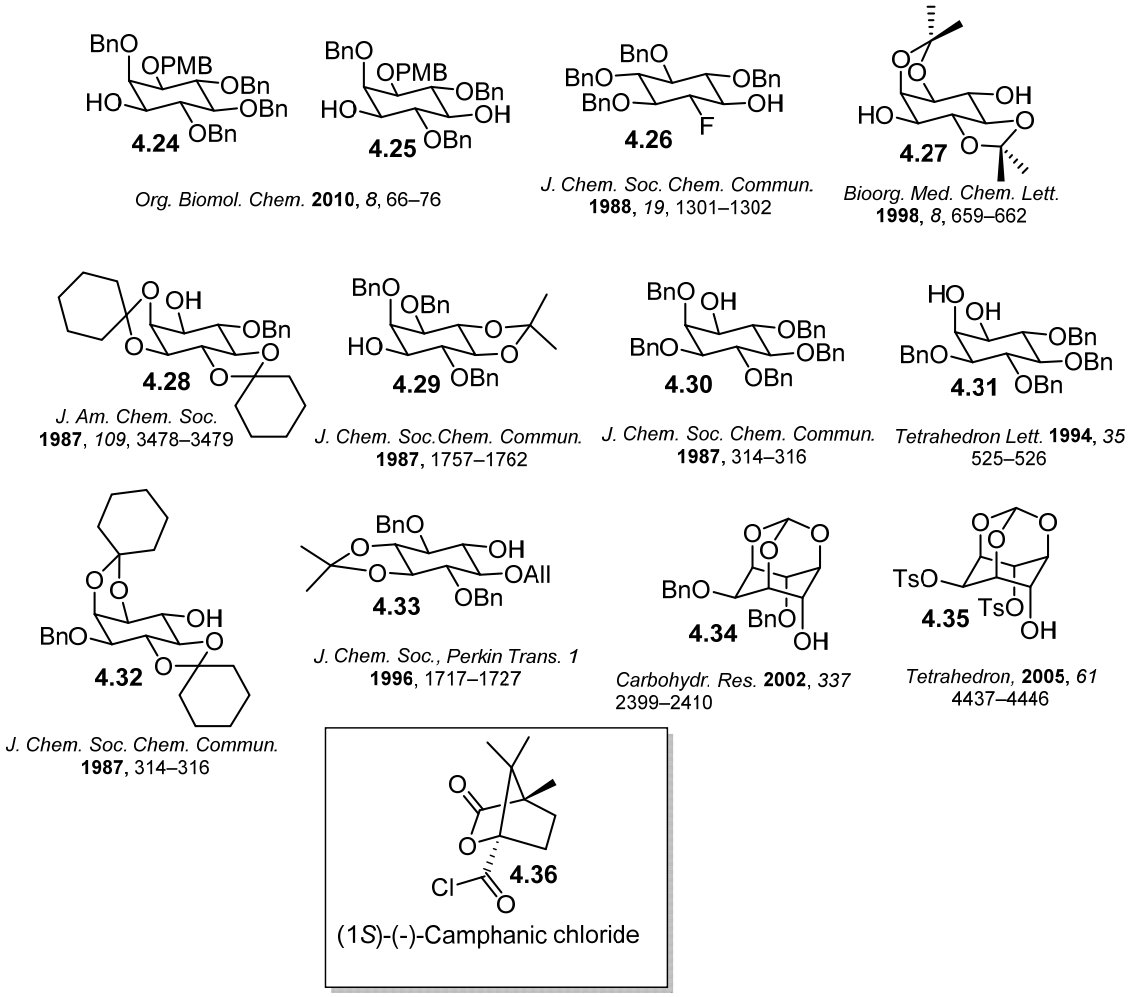

Chart 4.3: Inositol derivatives resolved using (1*S*)-(-)-camphanic chloride.

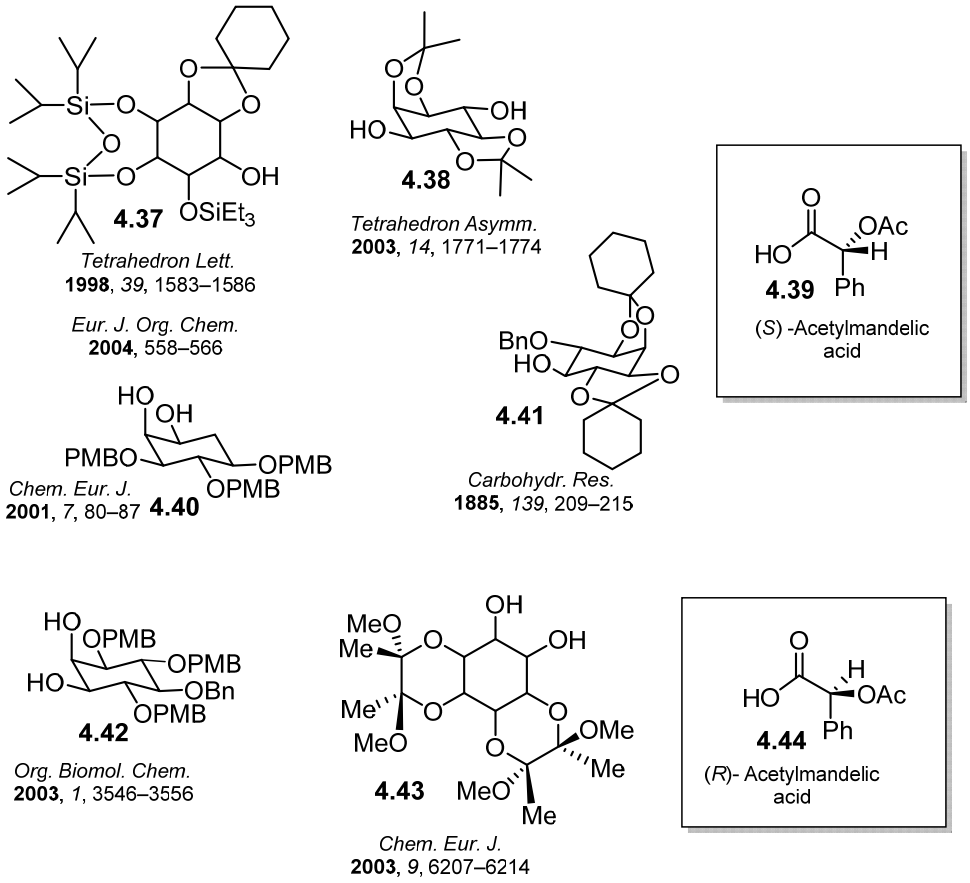

Chart 4.4: Inositol derivatives resolved using acetylmandelic acid.

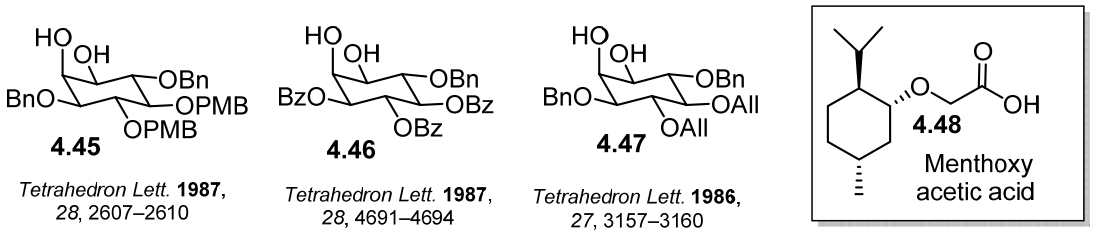

Chart 4.5: Inositol derivatives resolved using menthoxy acetic acid.

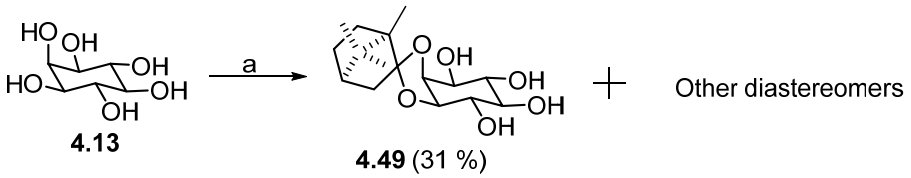

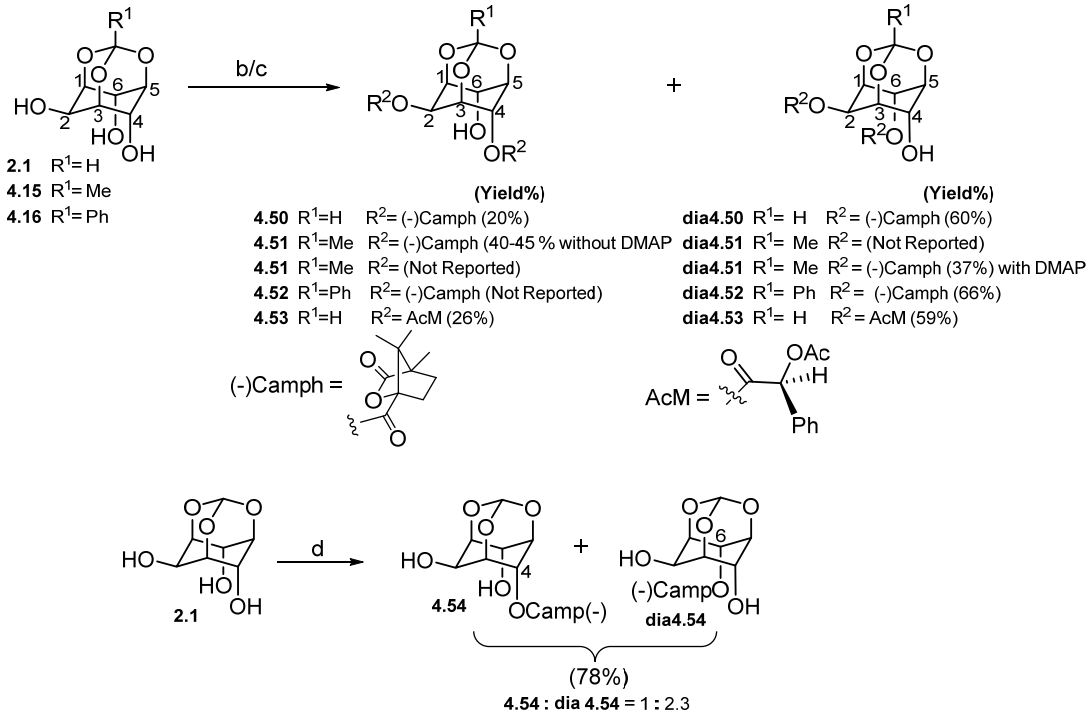

Scheme 4.2: (a) DMSO, D-camphor dimethyl acetal, followed by crystallization in MeOH.[4a] (b) (1*S*)-(-)-camphanic acid chloride (2.0 equiv), CH_2Cl_2, Et_3N, DMAP, 0 °C - rt;[4b-4d] (c) (*S*)-(+)-*O*-acetylmandeloyl chloride (2.1 equiv), pyridine, 0 °C, 2 h;[4e] (d) (1*S*)-(-)-camphanic anhydride,1 mol% $Yb(OTf)_3$, 1,4-dioxane, 40 °C, 3 days, 78%.[4f]

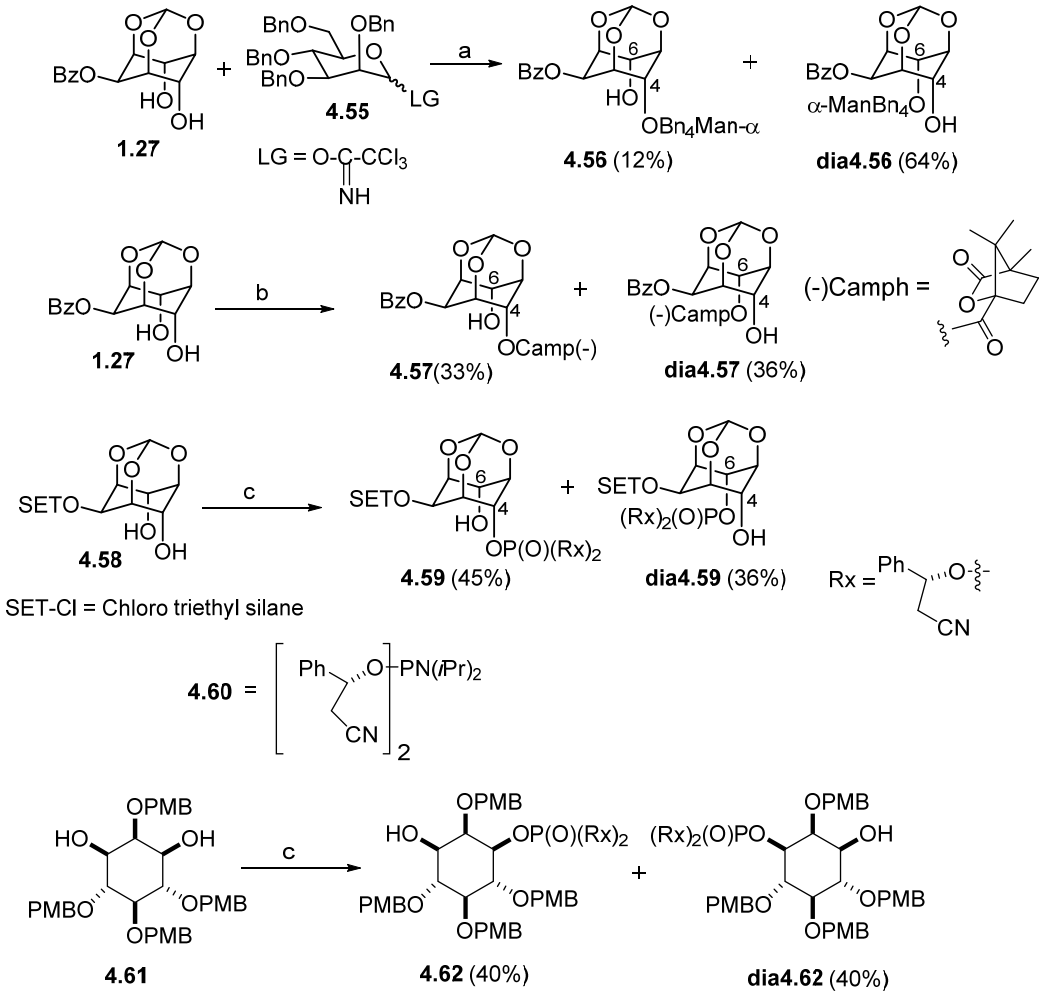

Scheme 4.3: (a) –78 to –20 °C, $BF_3.OEt_2$;[5a] (b) (1*S*)-(-)-camphanic acid chloride (1.2 equiv), Pyridine;[5b] (c) 3 equiv **4.58**, 1 equiv **4.60**, 5-(*p*-F-phenyl)1H-tetrazole in MeCN, then 0°C, *m*-CPBA.[5c]

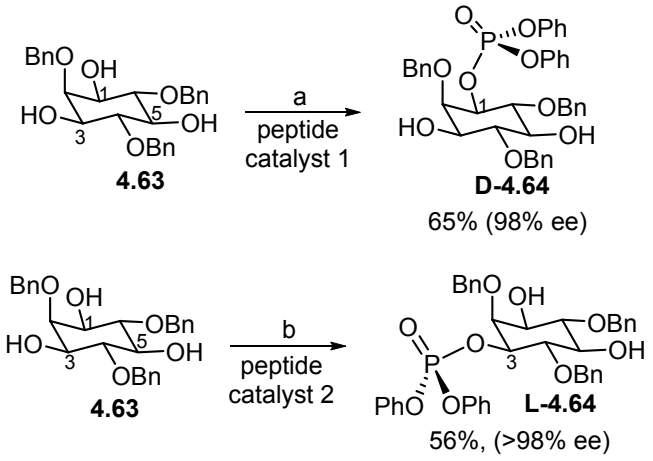

Scheme 4.4: (a) Cl-P=O $(OPh)_2$, peptide catalyst 1 (2 mol%), Et_3N, toluene, 0 °C, 65%, (98% ee); (b) Cl-P=O $(OPh)_2$, peptide catalyst 2 (2.5 mol%), Et_3N, toluene, 0 °C, 56%, (>98% ee).[6]

The progress in this area of synthetic organic chemistry was augmented by the attempts at using naturally occurring *myo*-inositol as a starting material for the synthesis of natural products other than phosphoinsitols[7] (Scheme 4.5).

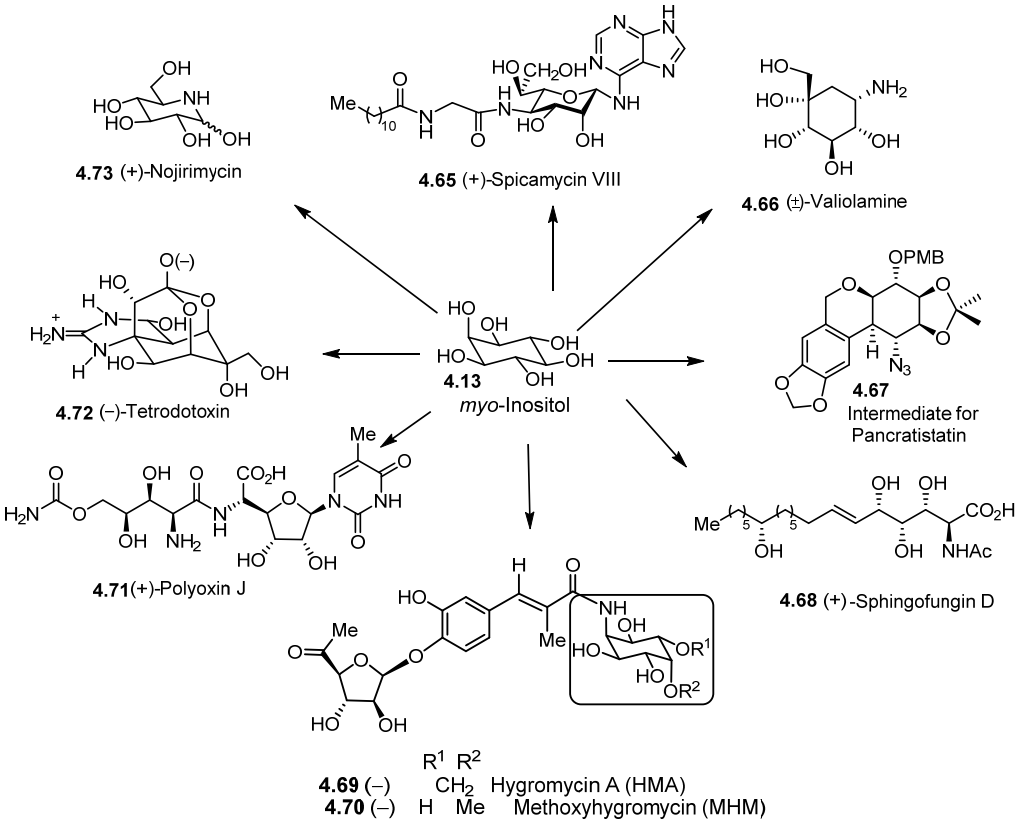

Scheme 4.5: Natural products synthesized from *myo*-inositol.

Development of practical methods for the preparation of chiral *myo*-inositol derivatives is a topic of current interest [1-7] and challenge since all the hydroxyl groups of *myo*-inositol are secondary; consequently the differences in their reactivity are subtle. As *myo*-inositol has the *meso*-configuration, generation of chiral *myo*-inositol derivatives necessarily involves the destruction of its symmetry. Orthoesters of *myo*-inositol have been extensively used as early intermediates for the synthesis of phosphoinositols, cyclitols and their derivatives, metal complexing agents and natural products containing the cyclitol moiety.[4,5] Considerable efforts have been invested in obtaining chiral *myo*-inositol derivatives from these rigid symmetric triols.[4,5] However most of these methods involve tedious chromatographic separation of diastereomeric derivatives and/ or provide chiral *myo*-inositol derivatives in small amounts.

More relevant to the work described in this thesis, we needed chiral inositol derivatives that could easily be converted to the chiral dibenzoates of *myo*-inositol orthoesters described in the previous [chapter 3B]. Although chiral orthoformate dibenzoate had earlier been prepared in our group[8] the synthetic scheme (scheme 4.6) seemed quite lengthy in view of the requirement to prepare dibenzoates of all the three orthoesters (described in the previous chapter 3B).

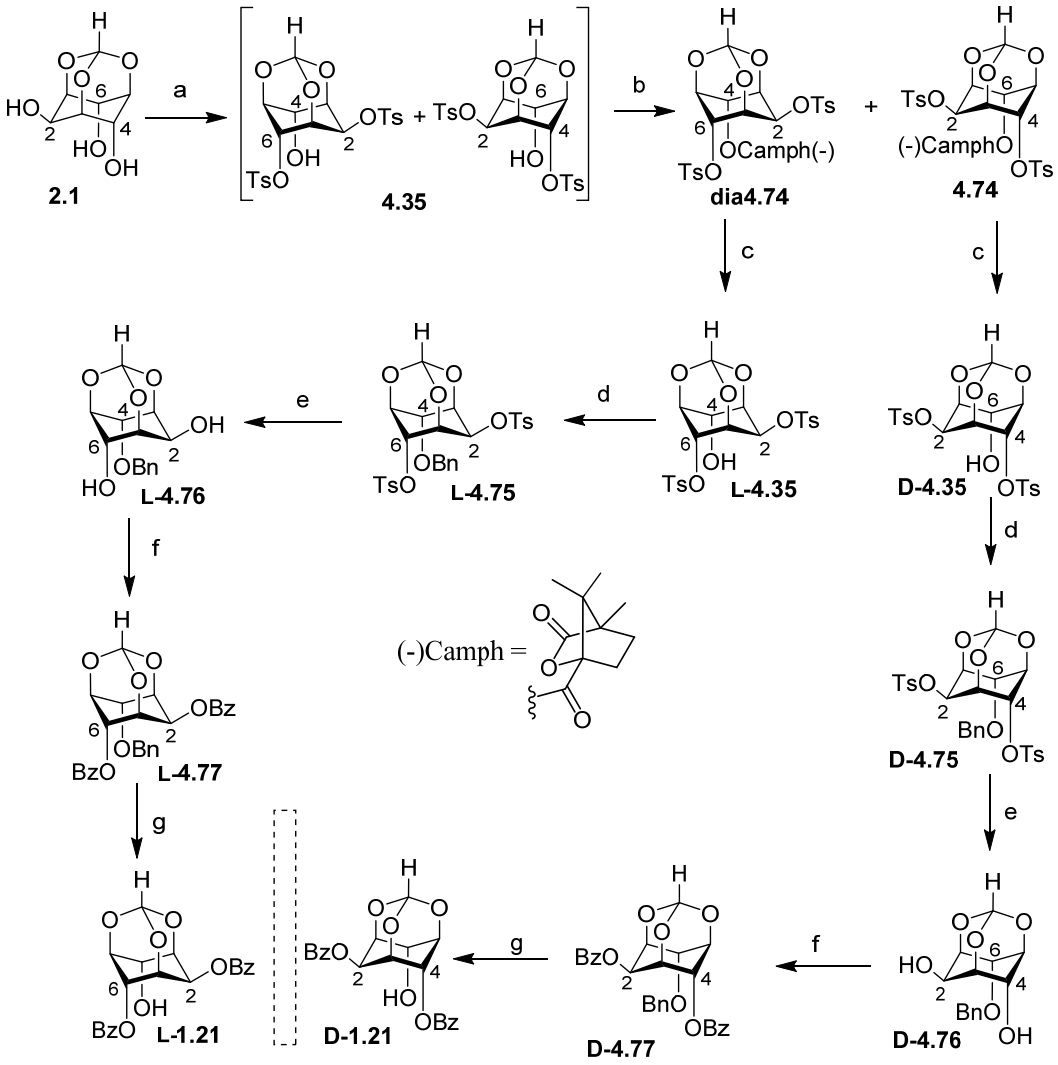

Scheme 4.6: (a) TsCl, pyridine, 80 ºC, 48 h; (b) (1*S*)-(-)-camphanic acid chloride, pyridine, DMAP, 90 ºC, 10 h; (c) *i*-BuNH_2, DCM-MeOH, reflux, 8 h; (d) BnBr, DMF, NaH, 30 min, rt; (e) NaOMe, MeOH, reflux, 12 h; (f) BzCl, pyridine, rt, 20 h; (g) H_2 (55 psi), $Pd(OH)_2$-C, MeOH - EtOAc, rt, 6 h. Reproduced from ref [8].

Although diastereoemric dicamphantes of all the three orthoesters have been reported [4] and initially looked suitable for the preparation of the corresponding enantiomeric dibenzoate (Scheme 4.7), closer scrutiny of the reports[4] and S. W. Garrett thesis[4h] suggested possibility of intramolecular acyl migration between the C4- and C-6 hydroxyl groups leading to interconversion of diastereomeric dicamphantes.

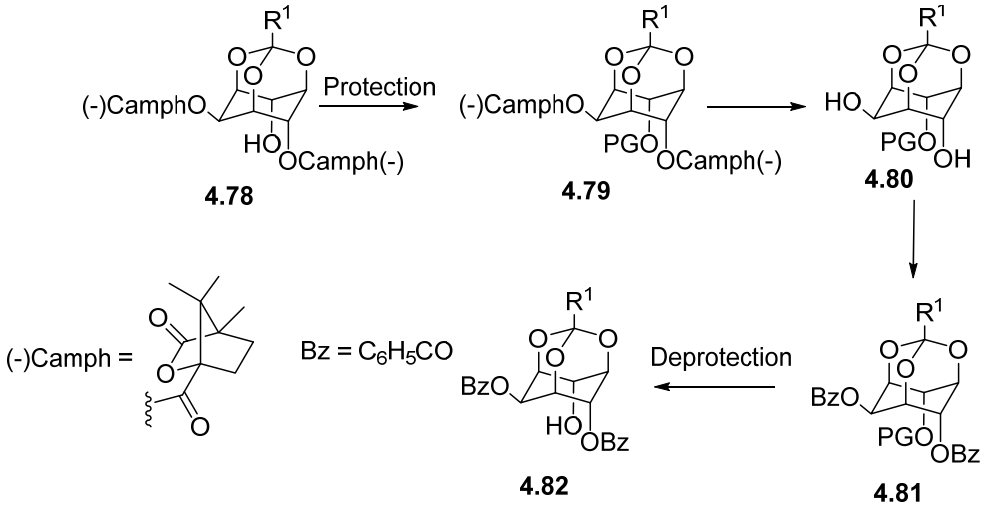

Scheme 4.7: A possible route for the preparation of enantiomeric dibenzoates of *myo*-inositol orthoesters from the known dicamphanates.

The suspicion that the diastereomeric dicamphanates could be prone to intramolecular acyl migration between the (C4 and C6) two axial hydroxyl groups arose since the relative yield of the reported[4c] and S. W. Garrett thesis[4h] individual diastereomeric orthoacetates varied considerably depending on the base (triethylamine or pyridine) used during the acylation of *myo*-inositol orthoacetate with camphanoyl chloride (Scheme 4.8).

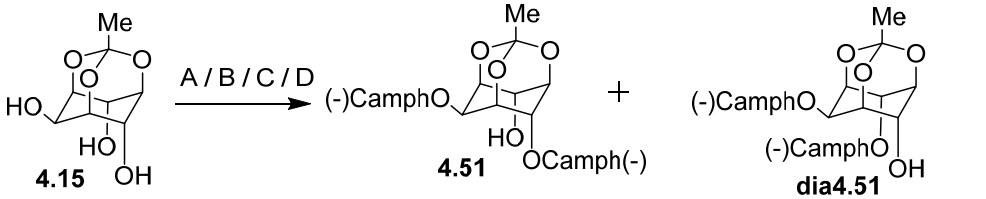

Conditions A	Not Reported	37 % after crystalization
Conditions B	40-45 % after crystalization	Not Reported
Conditions C	24%	34%
Conditions D	37%	20%

Scheme 4.8: (A) (1*S*)-(–)camphanoyl chloride, DMAP, DCM, 0 ^{o}C then rt, 2 h; (B) excluding DMAP from condition A ; (C) Triethyl amine, DMAP (100 mg), DCM ,(1*S*)-(–) camphanoyl chloride, 0 ^{o}C then rt, 2 h and (D) Pyridine, DMAP (50 mg), DCM ,(1*S*)-(–) camphanoyl chloride, 0 ^{o}C then rt, 1 h. Reproduced from reference [4c] and S. W. Garrett thesis.[4h]

Such acyl migration during the conversion of diastereomeric dicamphanates to the corresponding enantiomeric dibenzoates could adversely affect the purity of the

enantiomeric dibenzoates. Hence we attempted to prepare diastereomeric dicamphanates of *myo*-inositol orthoesters in which one of the axial hydroxyl groups is protected (to prevent intramolecular acyl migration). We chose the allyl group for the protection of the axial hydroxyl group since allyl ethers can be cleaved, in the presence of esters (under almost neutral conditions), using palladium (II) hydroxide.[9] A plausible synthetic scheme for the preparation of enantiomeric dibenzoates is shown in Scheme 4.9.

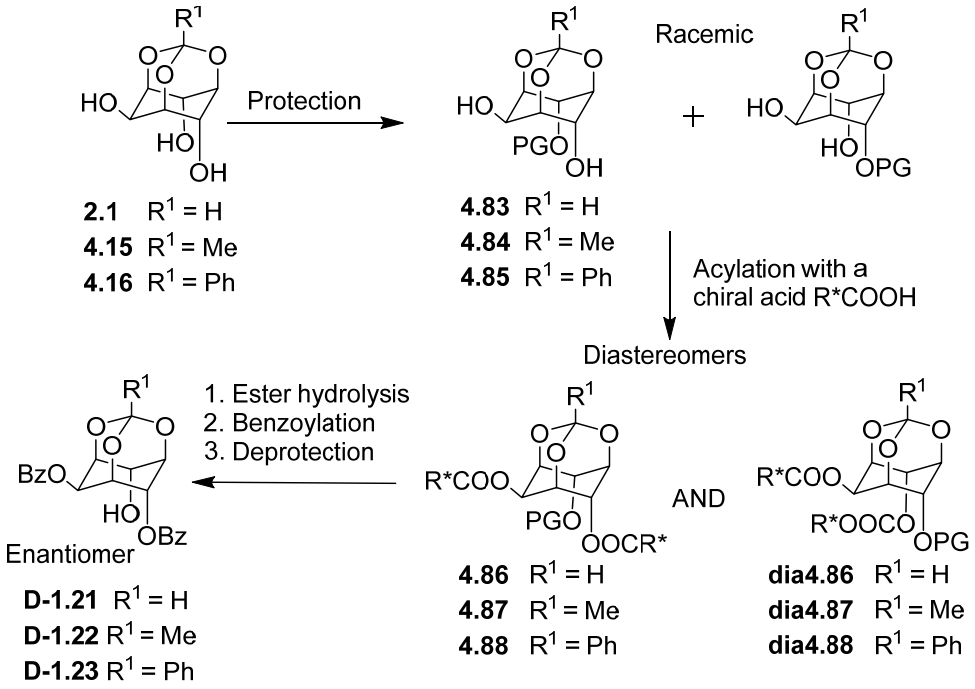

Scheme 4.9: A possible route for the preparation of enantiomeric dibenzoates of *myo*-inositol orthoesters from the corresponding *myo*-inositol orthoester.

Incidentally, development of practical methods for the preparation of chiral *myo*-inositol orthoester derivatives (starting from *myo*-inositol) as planned (Scheme 4.9) could also provide early intermediates for the synthesis of cyclitol derivatives including natural products. Accordingly, the present chapter presents the details on the preparation and separation of diastereomeric dicamphanates of racemic 4-allyl-*myo*-inositol-1,3,5-orthoesters (on gram scale) by crystallization as well as establishment of their configuration by conversion to diastereomeric dicamphanates of known configuration. Realization of the results described in this chapter was greatly aided by our past experience with crystallization and crystal structures of inositol derivatives.[10] Crystallization, although an enigmatic process, is perhaps the oldest method of separation and purification of organic compounds and provides

synthetic intermediates ranging from milligram to kilogram scale in a short time. Crystallization as a method of separation and purification is also environmentally sustainable since solvents used can be recovered and recycled. Before we present details of the work a short note on the nomenclature of *myo*-inositol derivatives is given below.

Structure and nomenclature of *myo*-inositol and its derivatives:

Inositols are hexa hydroxyl cyclohexanes; *myo*-Inositol (**4.13**), is the most abundantly available inositol in nature, among the nine known isomeric inositols (Chart 4.6). Inositols are also referred to as cyclitols; the latter is a general term used to describe poly hydroxyl cyclohexanes having at least four hydroxyl groups.

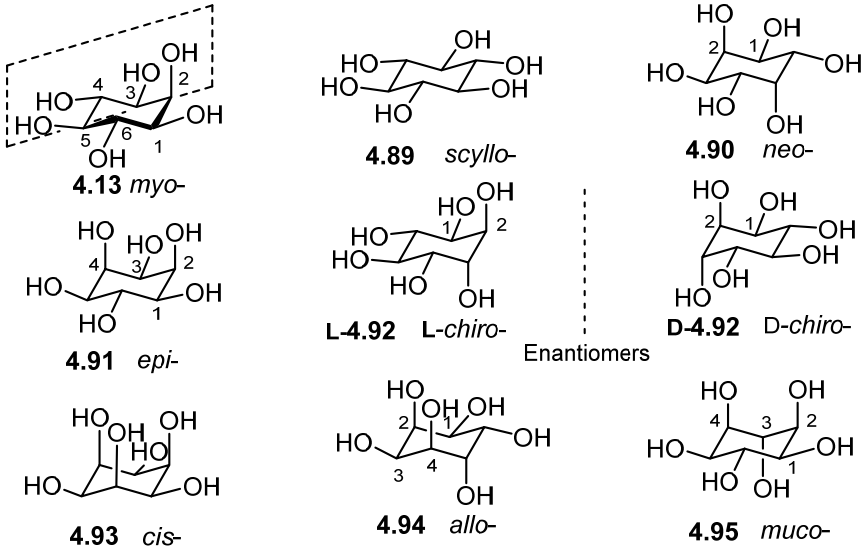

Chart 4.6: Nine isomeric inositols reported in the literature.

myo-Inositol is a *meso*-isomer with five equatorial hydroxyl groups and an axial hydroxyl group. There is a plane of symmetry passing through two carbon atoms (**4.13**, as shown in Chart 4.6). The carbon bearing the axial hydroxyl group is designated as C2 and the other ring carbons can be numbered from C1 to C6 starting from a C1 atom and proceeding around the ring in anticlockwise (**D-4.92**, Chart 4.7) or clockwise (**L-4.92**) fashion. According to convention,[11] anti-clockwise numbering in an unsymmetrically substituted *myo*-inositol leads to the configurational D-prefix and clockwise numbering gives the substituted *myo*-inositol an L-prefix (Chart 4.7). An IUBAC recommendation allowing all biologically relevant compounds to be denoted as D-isomers has also been proposed.[12] In this thesis to maintain uniformity,

ring carbon atoms of all the inositol derivatives are numbered in an anticlock-wise fashion.

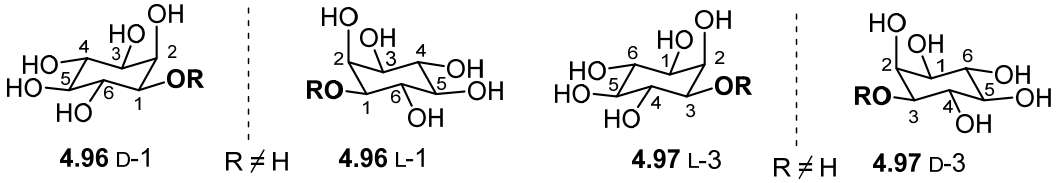

Chart 4.7: Numbering in unsymmetrical *myo*-inositol derivatives.

Although, many of the unsymmetrically substituted *myo*-inositol derivatives reported in this thesis are racemic, for clarity and simplicity they are represented in schemes by only one enantiomer. Optically inactive (*racemic*, *meso*) synthetic derivatives of inositol (other than phosphates) are numbered without prefixes, while optically active derivatives are numbered with a suitable prefix (**D** or **L**). Convention for numbering of structures in schemes in this thesis is shown in Scheme 4.10 using the dibenzoate derivative of *myo*-inositol orthoformate as an example; racemic 2,4-di-*O*-benzoyl-*myo*-inositol 1,3,5-orthoformate – **1.21**; D-2,4-di-*O*-benzoyl-*myo*-inositol orthoformate – **D-1.21** and its enantiomer L-2,4-di-*O*-benzoyl-*myo*-inositol 1,3,5-orthoformate – **L-4.30**. Diasteroisomers are numbered with same number but with a prefix **dia** to one of the diastereomers. For example: the *meso* triol **2.1** on esterification with 1*S*-(–)camphanoyl chloride forms diastereomeric mixture of the corresponding camphanate esters which are numbered as **4.50** and **dia 4.50**.

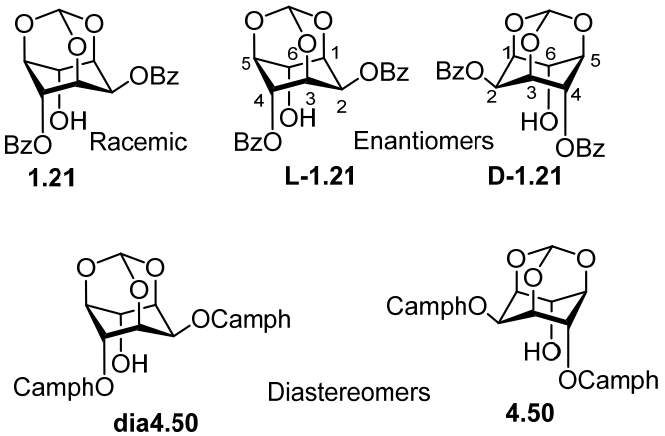

Scheme 4.10: Convention for numbering of structures in schemes in this thesis.

Results and Discussion

The racemic 4-*O*-allyl ethers of *myo*-inositol-1,3,5 orthoesters were prepared by the allylation of the corresponding triol in the presence of sodium hydride. Chelation assisted regioselective *O*-alkylation of these triols is well precedented in the literature [13] (Scheme 4.11).

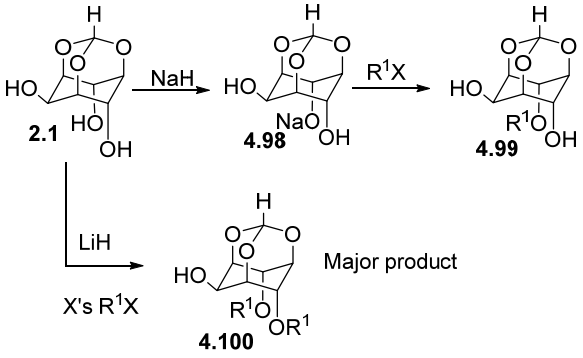

Scheme 4.11: Regioselective *O*-alkylation of the triol **2.1**.

These racemic 4-*O*-allyl ethers were acylated with (-) camphanic acid chloride to obtain a 1:1 mixture of the corresponding diastereoemric dicamphanate; the mixture of diastereomers was isolated by rapid column chromatography (Scheme 4.12).

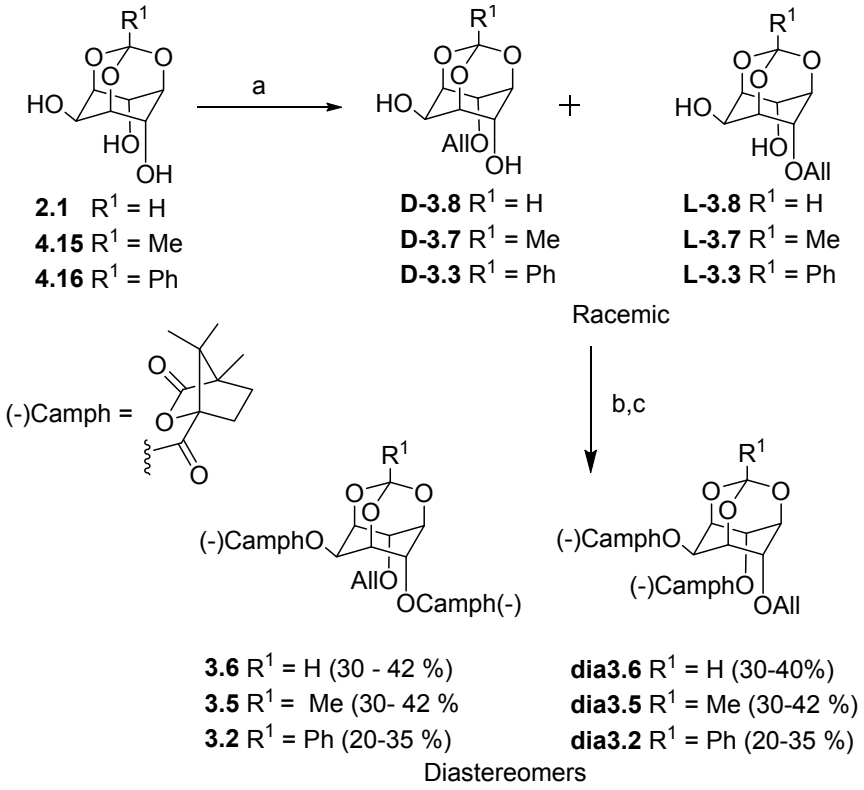

Scheme 4.12: (a) NaH, AllBr, DMF, 0 ^{o}C- rt, 8 h, 65 -70 %; (b) (1*S*)-(-) camphanoyl chloride, Et_3N, DMAP, pyridine, DCM reflux, for 2 days, 90-96 %; (c) crystallization from *n*-pentane/ methanol (for R^1 = H) or ethanol (for R^1 = Me) or *iso*-propanol (for R^1 = Ph); Diastereomeric purity of the dicamphanates was at least 95% after two crystallizations.

The experiments which culminated in the separation of diastereomeric dicamphanates by crystallization and the establishment of the configuration of the individual diastereomers is described below.

Crystallization behavior of diastereomeric dicamphanates of *myo*-inositol orthoformate:

The mixture of diastereomeric orthoformates were initially isolated on a small scale (0.200 g) by flash column chromatography. The gummy mixture was triturated with *n*-pentane to obtain a solid. Drop-wise addition of methanol (to the solid-pentane mixture) with warming resulted in a clear solution, which on standing at room temperature for 1 to 2 h deposited very fine needles (Figure 4.1) of one of the diastereomers (later identified as the more polar **3.6**). These crystals (of **3.6**) were subsequently used as seed crystals to separate **3.6** from the mixture of diastereoisomers on 20 gram scale.

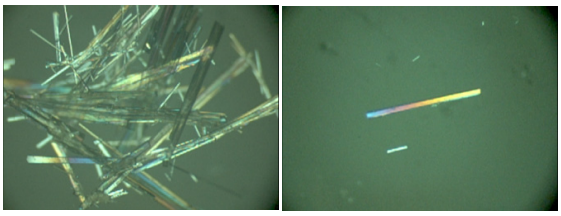

Figure 4.1: Crystals of **3.6** obtained (left) by crystallization of a mixture of **dia3.6** and **3.6** from *n*-pentane – methanol (1:9 v/v); A single crystal of **3.6** (right).

The mother liquor (after the removal of **3.6**) on standing deposited a crystalline mass of **dia3.6** contaminated with **3.6** (Figure 4.2).

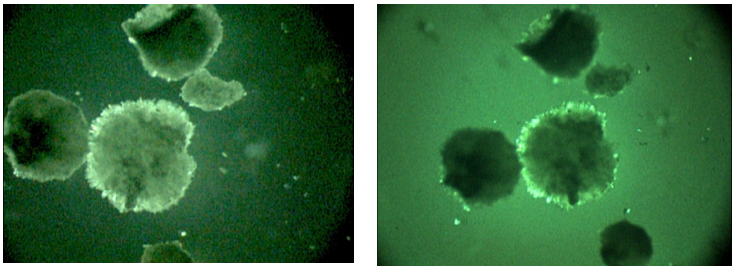

Figure 4.2: Crystalline mass of **dia3.6** obtained after the removal of **3.6** from a mixture of **dia3.6** and **3.6**; these solids have trace amount of **3.6** as impurity.

These crystallization experiments suggested that dicamphanate orthoformate diastereomers do not cocrystallize unlike inositol derived diastereomeric camphorsulfonates. Earlier work in our laboratory had revealed that diastereomeric camphorsulfonates **4.101** and **4.102** (Chart 4.8) obtained from the racemic dibenzoate **1.21** cocrystallized in the ratio 1:1.[14]

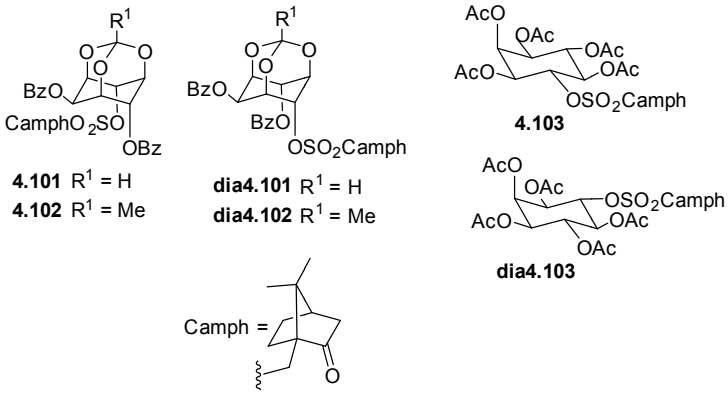

Chart 4.8: Diastereomeric *myo*-inositol derivatives which form cocrystals.

The separated crystalline diastereomers **3.6** and **dia3.6** obtained were used as seed crystals to separate the two diastereomeric orthoformates on multi-gram scale (see experimental section for details). The configuration of the individual allyl ether was established by conversion to the respective known dicamphanate [4a] **4.50** and **dia4.50** (Scheme 4.13). This procedure showed **3.6** and **dia3.6** to be D-2,4-di-*O*-[(-)-ω-camphanoyl]-6-*O*-allyl-*myo*-inositol-1,3,5-orthoformate and D-2,6-di-*O*-[(-)-ω-camphanoyl]-4-*O*-allyl-*myo*-inositol-1,3,5-orthoformate respectively.

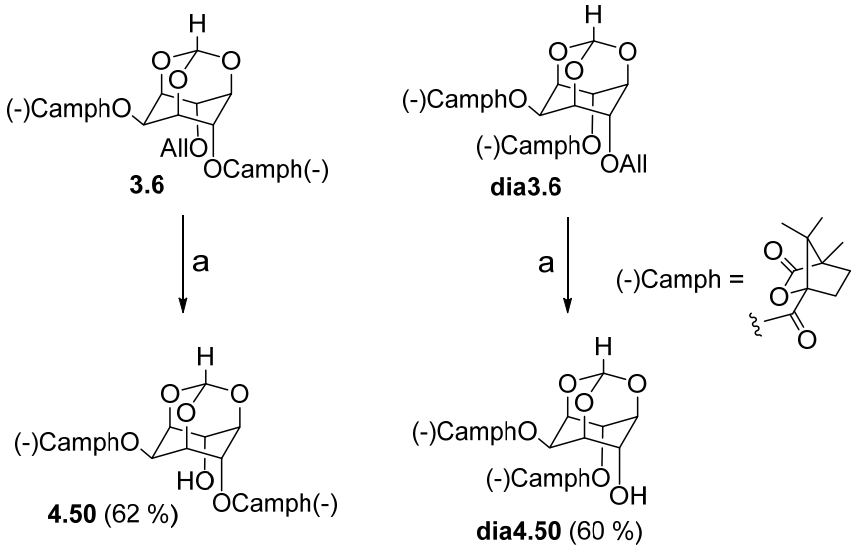

Scheme 4.13: Determination of the absolute configuration of diastereomeric allyl ethers by conversion to compounds of known configuration. (a) *Iso*-Propanol, Pd $(OH)_2$\C, Reflux, 24-30h.

The allyl ether in both the diastereomers were cleaved using palladium (II) hydroxide, a procedure that we had developed earlier.[9] It is interesting to note that the conditions of cleavage of allyl ethers did not lead to intramolecular migration of the camphanoyl moiety between the C4 (6)- and C6(4)-hydroxyl groups (which amount to inter-conversion of the diastereomers **4.50** and **dia4.50**).

Crystal structure of the orthoformate 3.6: The more polar diastereomer **3.6** crystallized in the orthorhombic space group $P2_12_12_1$ with one molecule in the asymmetric unit. Neighboring molecules along the *a*-axis are assembled helically across the 2_1-screw axis through short and linear C7-H7···O1 (entry 1, 2.32 Å, 175°) and long non-linear C13-H13*B*···O1 (entry 2, 2.70 Å, 131°) interactions (Figure 4.3).

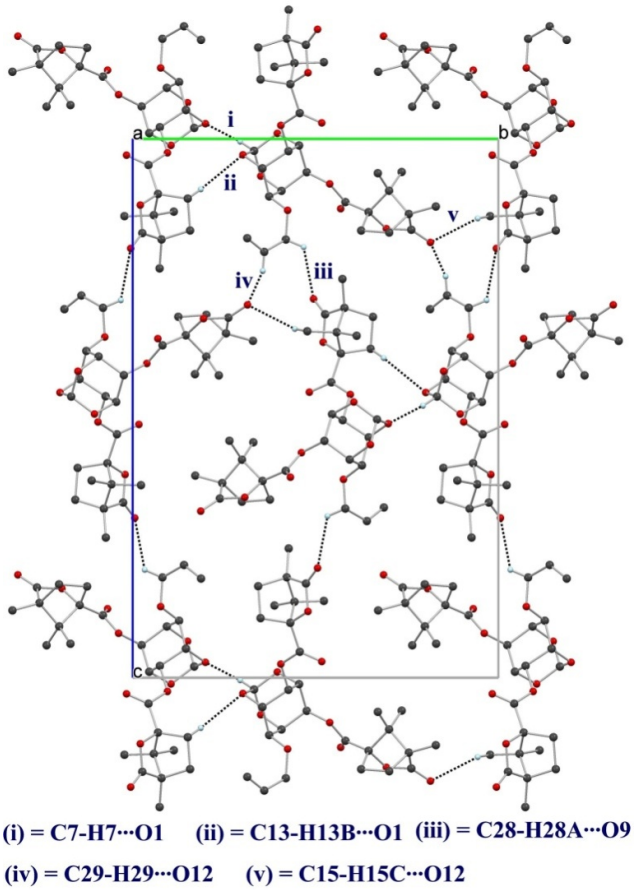

Figure 4.3: View of molecular packing in crystals of **3.6** on the *bc* plane showing flat helical association of molecules through C-H· · ·O interactions.

The helical organization brings the unit-translated molecules of the helix in proximity along the *a*-axis to generate six C-H···O interactions (entries 4-9, Table A2, Appendix IV) of varying strength and a short dipolar O···C=O (3.075 Å, 88.35°) contact between the orthoester ether oxygen (O3) and the C2-equatorial ester carbonyl carbon (C8=O7). This O···C=O contact is categorized as type III motif,[15] since approach of the ether oxygen is perpendicular to the plane of the carbonyl group (Figure 4.4).

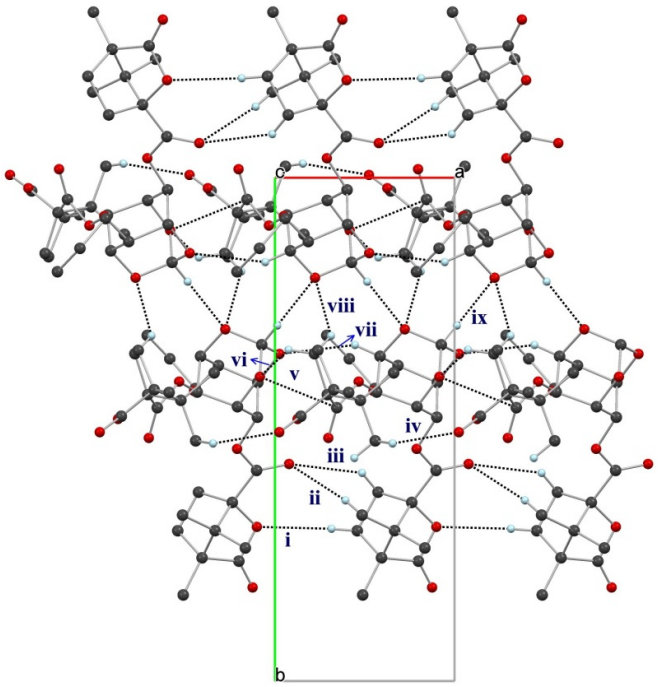

Figure 4.4: Molecular packing in crystals of **3.6** viewed down the *c*-axis revealing compact packing through C-H···O interactions.

The adjacent helices along the *c*-axis are stitched via short but non-linear C15-H15*C*···O12 contact (entry 3, Table A2, Appendix IV) to generate the 2D arrangement. Molecular packing viewed down the *a*-axis revealed helical arrangement of the molecules along the *b*- and *c*-axes via C29-H29···O12 (entry 10, Table A2, Appendix IV) and C28-H28*A*···O9 (entry 11, Table A2, Appendix IV) contacts respectively (Figure 4.3).

Crystal structure of dia3.6: Crystals of **dia3.6** belong to the monoclinic $P2_1$ space group containing one molecule in the asymmetric unit. The helical assembly in crystals of **dia3.6** is formed by the C27-H27*C*···O9 contact around the crystallographic 2_1-screw axis (*b*-axis). However, one can also envisage another helical assembly that is generated *via* C17-H17*A*···O5 interaction again around the *b*-axis (Figure 4.5).

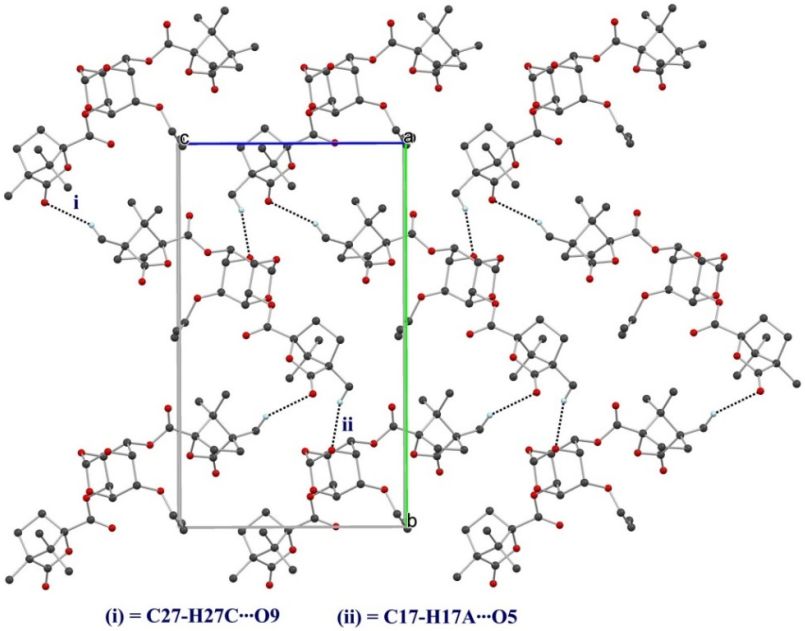

Figure 4.5: Molecular packing in crystals of **dia3.6** in the *bc*-plane showing helix formation via C-H···O interactions.

Molecular packing viewed down the helical axis (*b*-axis) revealed linking of the unit translated molecules to generate the 1D molecular-string along the *a*-axis via moderate C-H···O interactions namely C13-H13*A*···O3, C16-H16*A*···O9, C28-H28*B*···O12 and C23-H23*B*···O12. The neighboring strings along the *c*-axis are loosely connected via a rather long and non-linear C12-H12*B*···O12 interaction to create the 2D sheet on the *ac* plane (Figure 4.6).

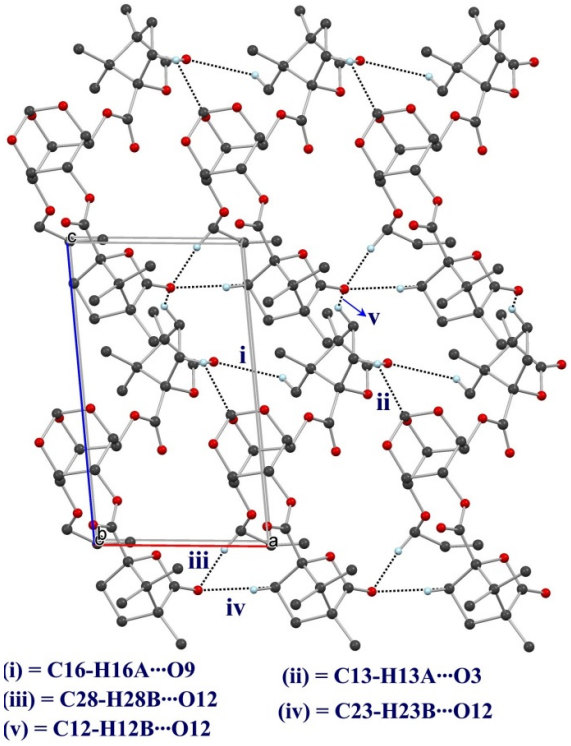

Figure 4.6: Molecular packing in crystals of **dia3.6** in the *ac* plane revealing 2D sheet formation.

We had earlier noticed that derivatives of *myo*-inositol orthoesters with comparable molecular structures exhibited similarities in their crystal structures.[10] The racemic dibenzoates of *myo*-inositol orthoesters in fact crystallized as isomorphs and two of these cocrystallized in closely related space group.[10a,10d-10e] Hence we suspected that the crystallization behavior of orthoacetate and orthobenzoate analogs of **3.6 / dia3.6** could be similar to that of **3.6 / dia3.6**, allowing their separation by crystallization. Although these orthoesters are structurally similar, difference in substitution (H, methyl, phenyl) at the apical orthoester position makes a world of difference during the hydrolytic and the reductive cleavage of these orthoesters. Hydrolysis of the (tri-*O*-substituted)-*myo*-inositol orthoformate yields the corresponding inositol triol **4.107**, while the corresponding orthoacetate and orthobenzoate yield the corresponding acetate and benzoate diols (**4.108-4.111**, Scheme 4.14).

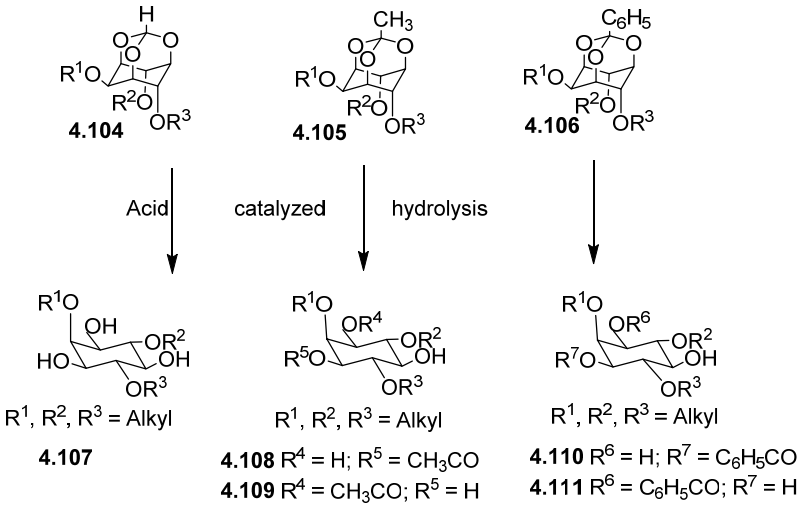

Scheme 4.14: Acid catalyzed hydrolysis of the *myo*-inositol orthoesters.

The reductive cleavage of *myo*-insitol orthoformate and orthoacetate yield the corresponding 1,3-bridged methylidene and the ethylidene acetals respectively. Similar reduction of the orthobenzoate on the other hand yields the corresponding 1,3-bridged benzylidene acetal (amenable to hydrogenolytic cleavage) which can further be reduced to the corresponding benzyl ether (Scheme 4.15).

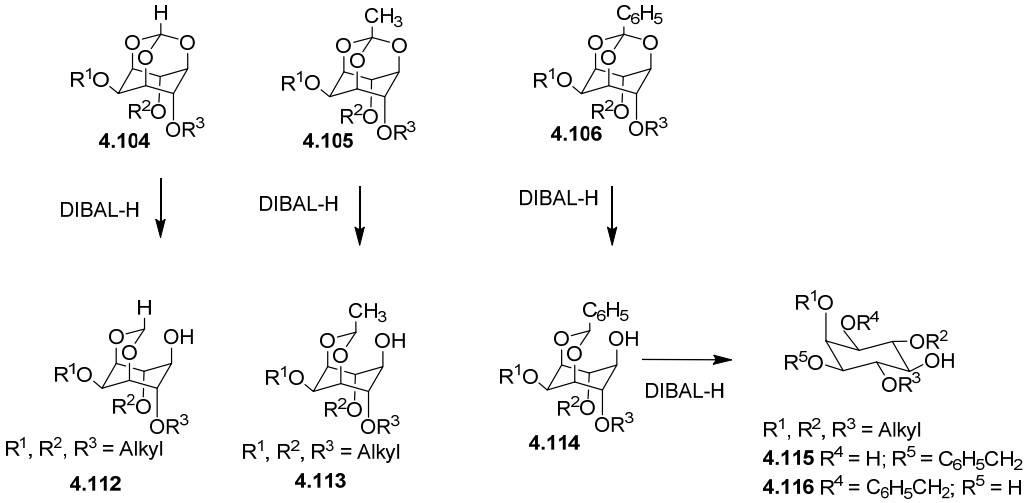

Scheme 4.15: The reductive cleavage of *myo*-insitol orthoesters.

These differences in product formation can be exploited for the synthesis of different cyclitol derivatives.[16] Hence we prepared racemic 4-*O*-allyl ethers of *myo*-inositol orthoacetate and *myo*-inositol orthobenzoate and investigated the crystallization behavior of their diastereomeric dicamphanates.

Crystallization behavior of diastereomeric dicamphanates of *myo*-inositol orthobenzoate:

A small quantity (0.20 g) of the mixture of diastereomeric orthobenzoate allyl ethers (**3.2**, **dia3.2**) was isolated by filter column chromatography in order to remove other impurities present in the crude product. Contrary to our expectations, attempts to separate the individual diastereomers by crystallization were not successful. Hence the two diastereomers (**3.2**, **dia3.2**) were separated by flash column chromatography. The less polar diastereomer **dia3.2** could be crystallized from diethyl ether or DMF. Attempts at crystallization of the more polar **3.2** from common solvents failed; gummy mass was obtained in all the experiments. The crystals of **dia3.2** obtained from diethyl ether were subsequently used as seed crystals to separate the mixture of diastereoisomers (previously isolated by filter column chromatography) on 10 gram scale. The gummy diastereomeric mixture (**3.2**, **dia3.2**, 10 g) was dissolved in warm *iso*-propanol (150-200 mL). Seed crystals of the less polar **dia3.2** were added and the flask was stored (open to atmosphere) at room temperature (30-35 ^{o}C) for 7-15 days. Block type crystals (Scheme 4.12) that separated were filtered (2.0-3.5 g). The configuration of the less polar diastereomer **dia3.2** was established by converting it to the known dicamphanate[4c] **dia4.52** (Scheme 4.16). This procedure also showed the orthobenzoates **3.2** and **dia3.2** to be D-2,4-di-*O*-[(-)-ω-camphanoyl]-6-*O*-allyl-*myo*-inositol-1,3,5-orthobenzoate and D-2,6-di-*O*-[(-)-ω-camphanoyl]-4-*O*-allyl-*myo*-inositol-1,3,5- orthobenzoate respectively.

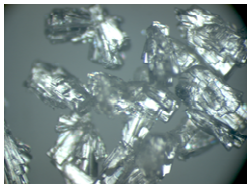

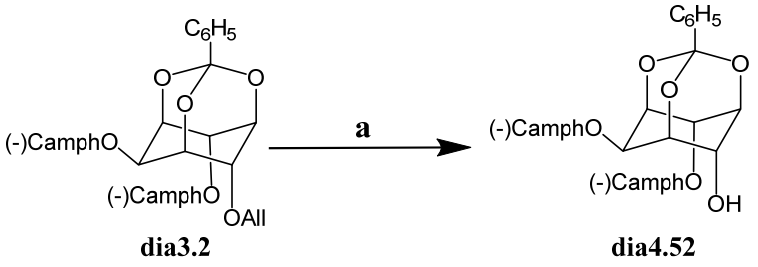

dia3.2 **dia4.52**

Scheme 4.16: Determination of the absolute configuration of the orthobenzoate **dia3.2** by converting to the known dicamphanate **dia4.52**. (a) *Iso*-Propanol, Pd $(OH)_2$\C, Reflux, 24-30h.

A solution of the residue obtained from the mother liquor in *iso*-propanol, on stirring at 45 ^{o}C for 12 h and then kept at ambient temperature for 24 h deposited **3.2** as a solid. This solid on precipitation from methanol or ethanol gave **3.2** of about 94% purity (6% being **dia3.2**).

Crystal structure of dia3.2: Crystals of **dia3.2** belong to orthorhombic $P2_12_12_1$ space group containing one molecule in the asymmetric unit. The helical assembly of molecules is formed by the short but non-linear C18-H18B···O9 contact around crystallographic 2_1-screw axis (*b*-axis). The helical architecture places the unit-translated molecule of the helix in close association to create C1-H1···O8, C3-H3···O10, C21-H21B···O9, C22-H22B···O1 and C34-H34B···O10 interactions (Figure 4.7).

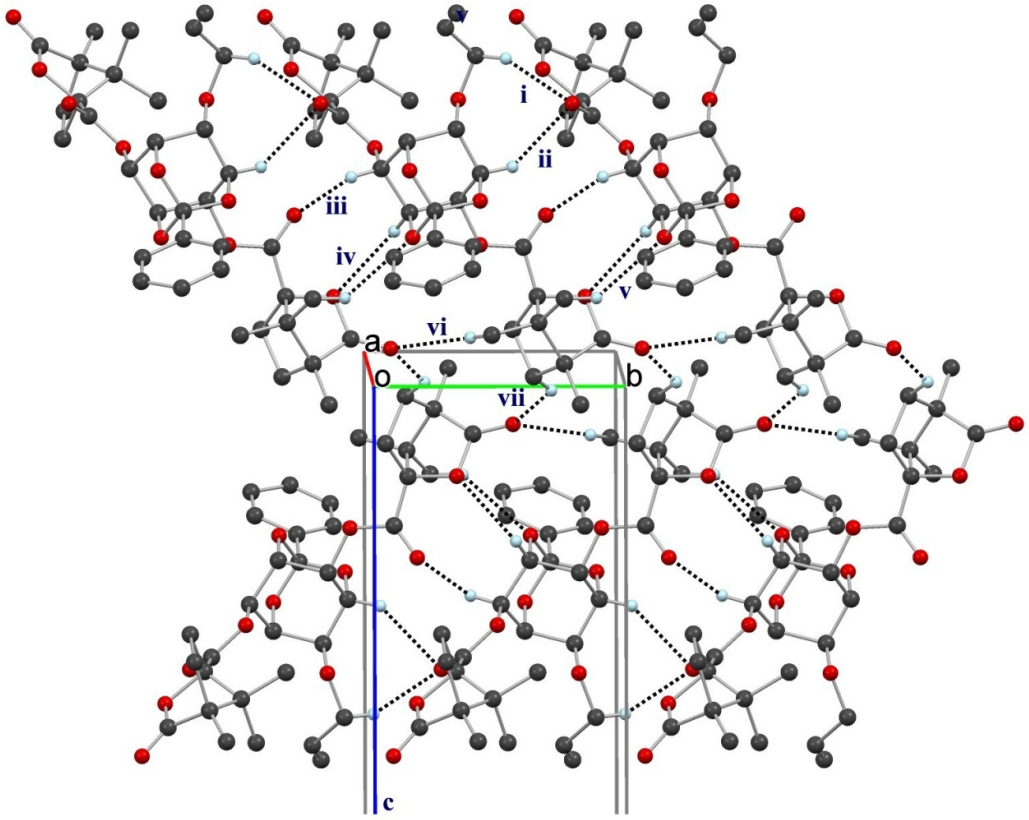

Figure 4.7: View of the molecular packing in crystals of **dia3.2** down the *a*-axis showing networking of helices along the *b*-axis via several C-H···O interactions. The neighboring helices along the *c*-axis are loosely held by hydrophobic forces.

The adjacent parallel helical assemblies along the *c*-axis are loosely connected by van der Waals forces due to the close proximity of the methyl groups of the camphanate moieties. A view of molecular packing down the *c*-axis revealed linking

of the neighbouring helices along the *a*-axis *via* short and linear C28-H28A···O5 contacts to generate discrete packing (Figure 4.8).

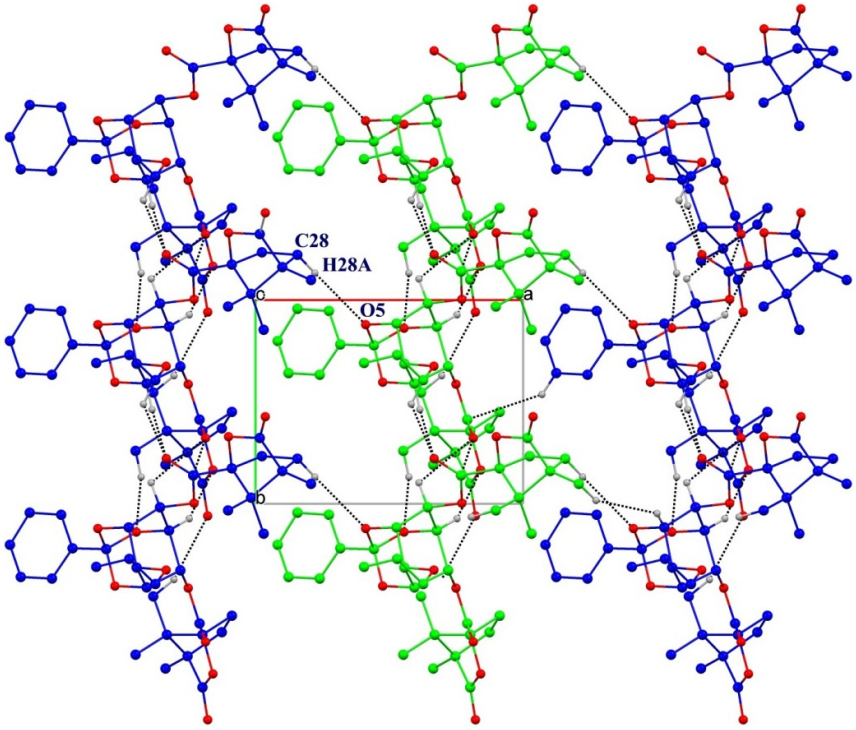

Figure 4.8: The view of molecular packing in crystals of **dia3.2** on the *ab* plane revealed interlinking of the neighboring helices along the *a*-axis via C28-H28A···O5 contacts.

Crystallization behavior of diastereomeric allyl ethers of *myo*-inositol orthoacetate:

First a small quantity (0.20 g) of the diastereomeric mixture of orthoacetate allyl ethers (**3.5**, **dia3.5**) was isolated by column chromatography. Attempts to separate the two diastereomers (**3.5**, **dia3.5**) by crystallization (as in the case of the corresponding orthoformates) from several solvents failed (acetone, ethanol, methanol, 1,4-dioxane, benzene, toluene, *iso*-propanol, diethyl ether, ethyl acetate, dichloromethane, chloroform). Hence a small quantity of the mixture of diastereomeric allyl ethers (0.20 g) was enriched by flash column chromatography. Both the diastereomers were obtained in about 80% purity (20% being the other diastereomer) as revealed by ^{1}H NMR spectroscopy. The enriched samples were crystallized from hot absolute ethanol when crystals of the diastereomer present in larger proportion were obtained. The purity of both the crystalline diastereomers (above 98 %) was estimated by HPLC.

The crystals of the individual diastereomers **3.5** (Figure 4.9) and **dia3.5** (Figure 4.10) obtained from ethanol were subsequently used as seed crystals to separate the mixture of the diastereoisomers on larger scale as described in the experimental section.

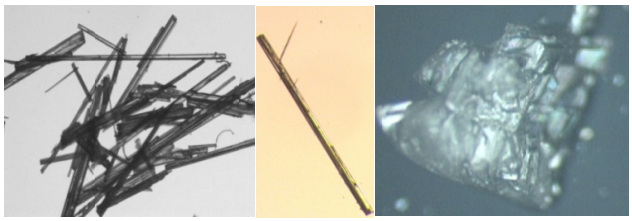

Figure 4.9: Crystals of ethanol solvate of **3.5**. In some crystallization experiments blocks (right) of **3.5** were obtained.

Figure 4.10: Crystals of **dia3.5** from ethanol.

The configuration of the diastereomeric orthoacetates was established by comparison of single crystal X-ray diffraction data of diastereomeric orthoformates and orthoacetates (Figure 4.11). The configuration of the diastereomeric orthoacetates could be established by this process since dicamphanates of orthoacetates and orthoformates only differ at the orthoester position, which has no bearing on the configuration of the molecule.

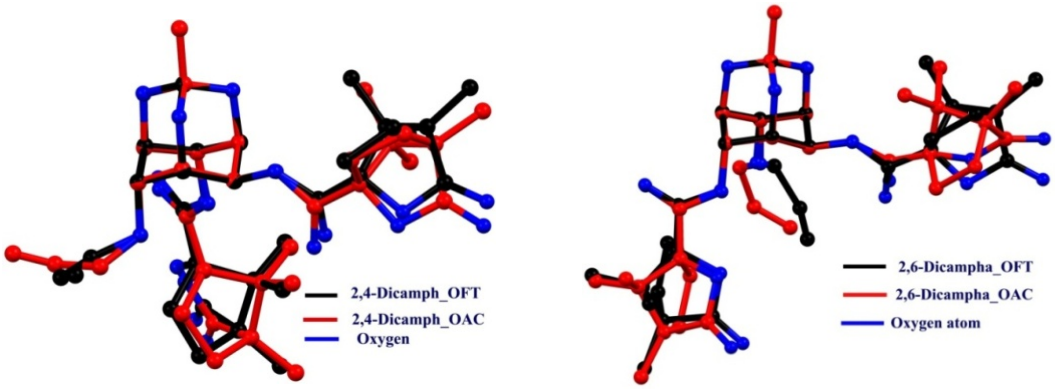

Figure 4.11: Molecular structural overlay of one of the molecules (primed) in the asymmetric unit of a crystal of 2,4-dicamphanate orthoacetate **3.5** (red) with that of the orthoformate **3.6** [black] (left). Molecular structural overlay of one of the molecules in the asymmetric unit of a crystal of 2,6-dicamphanate orthoacetate **dia3.5** [red] with that of the orthoformate **dia3.6** [black] (right).

Hence the less polar isomer **dia3.5** was found to be D-2,6-di-*O*-[(-)-ω-camphanoyl]-4-*O*-allyl-*myo*-inositol-1,3,5-orthoacetate and the more polar isomer **3.5** was found to be D-2,4-di-*O*-[(-)-ω-camphanoyl]-6-*O*-allyl-*myo*-inositol-1,3,5-orthoacetate. This assignment was confirmed by the conversion of the diastereomer **dia3.5** to the known L-2,4-di-*O*-benzyl-*myo*-insoitol (Scheme 4.17).[17, 18d]

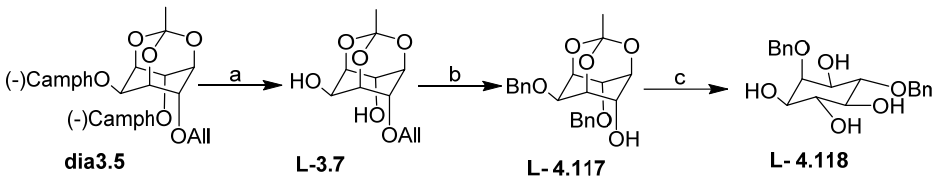

Scheme 4.17: Synthesis of (-)-L-2,4-di-*O*-benzyl-*myo*-inositol. (a) *Iso*-Butyl amine, methanol, DCM, reflux, 10-12 h, 96%; (b) (i) dry DMF, NaH, BnBr, ice-cold – rt, 14h; (ii) $Pd(OH)_2$\C, *iso*-propanol, reflux, 4-5 h, 91% (for two steps); (c) MeOH, 5 M HCl, reflux, 16 h, 93%.

It is pertinent to compare the yield and purity of L-2,4-di-*O*-benzyl-*myo*-inositol that we obtained from the orthoacetate dicamphanate with the methods reported earlier,[4d-

[4e, 17-18] although our aim in preparing the dibenzyl ether here was to establish the configuration of the orthoacetate dicamphanates. The yield of L-2,4-di-*O*-benzyl-*myo*-inositol in the present work was about 22% starting from *myo*-inositol; the proportion of D/L isomers was 95/5. The yield in other methods previously reported in the literature was between 3 and 46% see table 4.1, but most of these methods involved column chromatography for the separation of diastereomers and are not suitable to obtain larger amounts of the chiral dibenzyl ether **L-4.118**. In the present work the synthetic sequence involved seven steps and no chromatographic separation of the diastereomers. In two of the previous reports [4d-4e] yield of one of the diastereomeric ester derivative (of *myo*-inositol orthoester) obtained was higher than the other, leading to better yield (as compared to present work) of L-2,4-di-*O*-benzyl-*myo*-inositol. We suspect that the formation of unequal amounts of diastereomeric esters was a result of intramolecular acyl group migration between the C4- and C6-hydroxyl groups.

Entry	Key Intermediate	D (Yield)	L (Yield)	Reference
1	*myo*-inositol 1,3,5-orthoformate	(27)	27	18d
2	*myo*-inositol 1,3,5-orthoformate	(13)	12	17
3	*myo*-inositol 1,3,5-orthoformate	(14)	15	17
4	1,2;4,5-di-*O*-cyclohexylidene *myo*-inositol		3	18a
5	1,3,5-tri-*O*-benzoyl-*myo*-inositol		8	18b
6	(-)-2,3;4,5-di-*O*-cyclohexylidene-*myo*-inosito		1 7	18c
7	*myo*-inositol 1,3,5-orthoformate	39	37	18e
8	*myo*-inositol 1,3,5-orthoformate		39 (From 59% less polar diasteisomer)	4e
9	*myo*-inositol 1,3,5-orthobenzoate		46 (From 66% less polar diasteisomer)	4d
10	***myo*-inositol 1,3,5-orthoacetate**		~22 %(94.5:5.5) Purity by HPLC	Present work

Table 4.1: A comparison of the overall yield of D- and L-2,4-di-*O*-benzyl *myo*-inositol reported in the literature with present work. All yields are calculated from *myo*-inositol as the starting material.

Our initial attempts to cleave the allyl ether in the orthoacetate diastereomer **dia3.5**, exclusively to the corresponding known dicamphanate to establish the configuration of the diastereomer **dia3.5** (as done in the case of diastereomeric orthoformate and orthobenzoate allyl ethers) was inconclusive. The melting point of the known dicamphanate diastereomer **dia4.51** was reported to be 228-231 ^{o}C, while the sample we obtained by allyl ether cleavage of the diastereomer **dia3.5** was 234-240 ^{o}C. Similarly, the melting point of the known dicamphanate diastereomer **4.51** was reported to be 201-204 ^{o}C, while the sample we obtained by allyl ether cleavage of the diastereomer **3.5** was 212-215 ^{o}C. This could be due to the intramolecular migration of the camphanoyl moiety between the C4 - and C6 - hydroxyl groups in the orthoacetate diastereomers, subsequent to the cleavage of the allyl group. Our analysis of the single crystal X-ray diffraction data of the dicamphanate **4.51** indeed revealed a good El···Nu geometry for the intramolecular acyl group transfer to the free hydroxyl group (scheme 4.18).

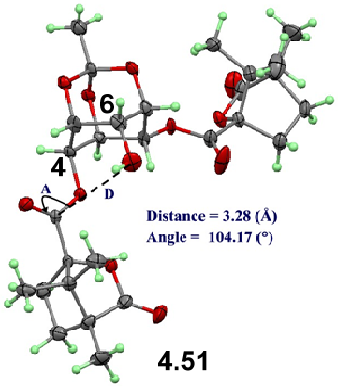

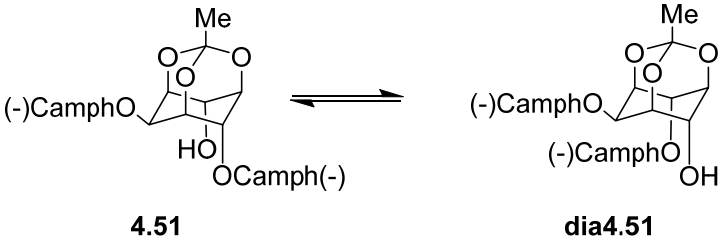

Compound	**Intramolecular El···Nu Distance (Å)**	**El···Nu Angle (°)**
4.51	3.28 [H-O6···C19=O10]	104.17 [∠O6···C19=O10]
dia4.51	3.691 [H-O4···C19=O10]	108.80 [∠O4···C19=O10]

Scheme 4.18: Intramolecular acyl group transfer in diastereomeric orthoacetate dicamphanates.

Crystal structure of the ethanol solvate of 3.5: Crystals of the ethanol solvate of **3.5** belong to the chiral triclinic *P*1 space group containing two molecules (labeled as primed and unprimed) in the asymmetric unit along with a molecule of ethanol. A comparison of the conformation of both symmetry independent molecules revealed

significant difference in the orientation of allyl groups (Figure A72, Appendix IV). Molecular packing on the *bc*-plane revealed unit translated (primed) molecules along the *b*-axis connected to each other via short and moderately linear C6'-H6'···O9' contact to generate a molecular string. The neighbouring parallel molecular string along the *c*-axis is created by (unprimed) molecules, although they are not linked to each other directly, unlike primed molecules. The parallel molecular strings of primed and unprimed molecules are joined together *via* C13'-H13E···O11, C26'-H26D···O9, C28'-H28C···O9 and C13-H13B···O11' contacts. Ethanol molecule interacts with primed and unprimed molecules via C32-H32A···O12', O13-H14G···O8 and O13-H14G···O7 contacts (Figure 4.12).

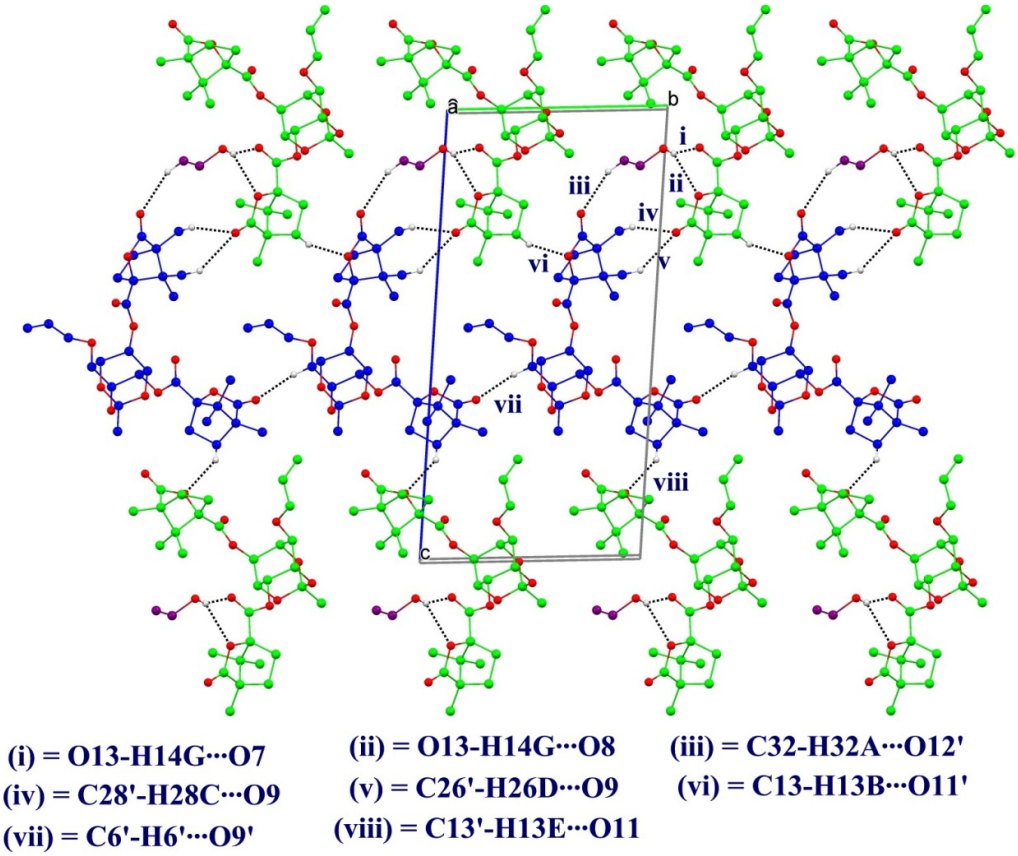

Figure 4.12: Molecular packing in crystals of ethanol solvate of **3.5** in the *bc* plane.

Molecular packing viewed down the *b*-axis revealed a columnar assembly of both primed and unprimed molecules along the *a*-axis. Along the column, unit-translated

umprimed molecules are linked *via* C24-H24B···O10, C23-H23A···O10, C4-H4···O7, C17-H17C···O9 contacts and a type III short dipolar O3···C9=O7 contact. Similarly, the unit-translated primed molecules are also stitched along the column through C4'-H4'···O7', C24'-H24E···O10', C14'-H14E···O3' and C16'-H16F···O7' interactions. The adjacent parallel columns of primed and unprimed molecules are connected *via* C13-H13B···O11' and C13'-H13E···O11 contacts. The extended columnar assembly on the *ac* plane generates the 2D layered arrangement wherein ethanol molecules are interacting with top and bottom layer of the 2D sheet *via* C3-H3···O13 and C27-H27A···O13 hydrogen bonding interactions (Figure 4.13).

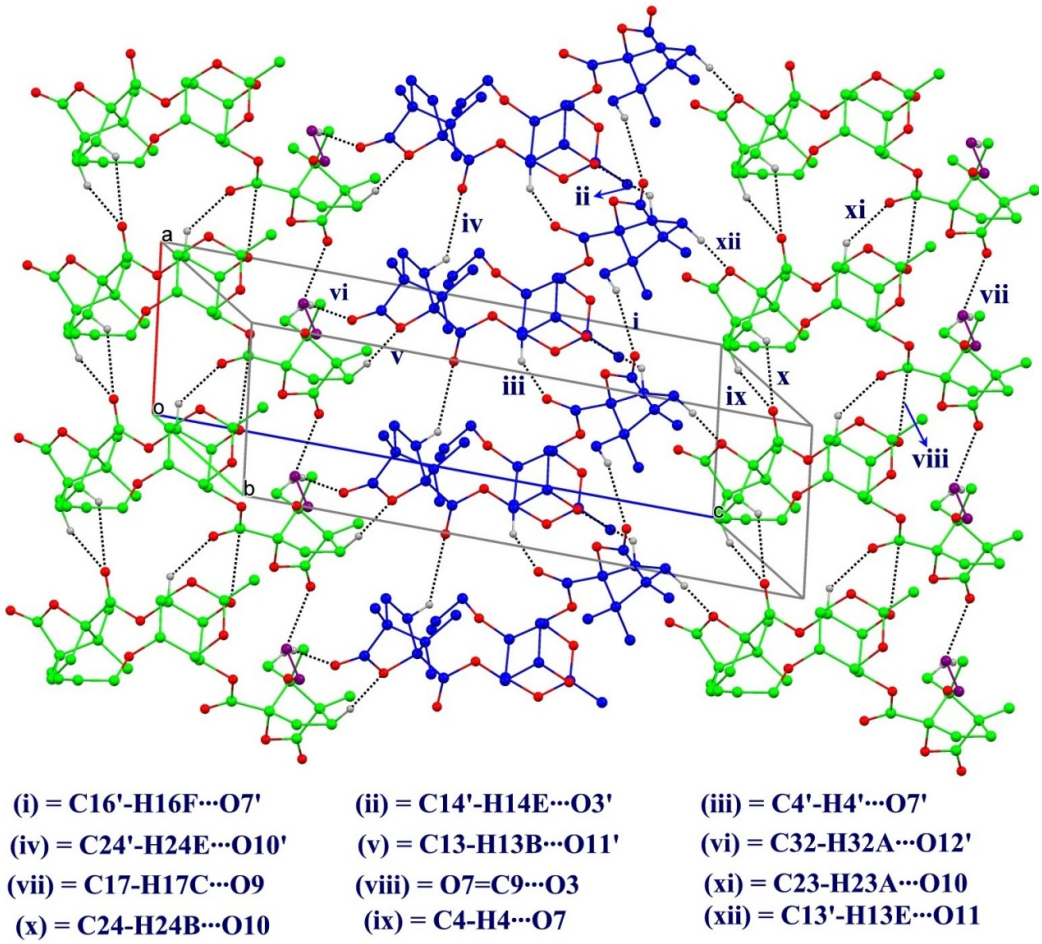

Figure 4.13: Molecular packing in ethanol solvated crystals of **3.5** viewed down the *b*-axis (*ac* plane) reveals the columnar assembly of both primed and unprimed molecules, along the *a*-axis.

Crystal structure of the orthoacetate dia3.5: The orthoacetate **dia3.5** crystallized in monoclinic $P2_1$ space group containing one molecule in the asymmetric unit. Adjoining molecules along the *b*-axis are assembled helically across the 2_1-screw axis through short and linear C23-H23A···O10, bifurcated C29-H29B···O12, C24-H24B···O12 and C28-H28B···O7 interactions. The helical organization brings the unit-translated molecules of the helix in proximity along the *b*-axis to generate the C13-H13B···O5 interactions. The neighboring parallel helices bring the orthoester bridge in close association to create short and linear C4-H4···O1 and C6-H6···O3 interactions (Figure 4.14).

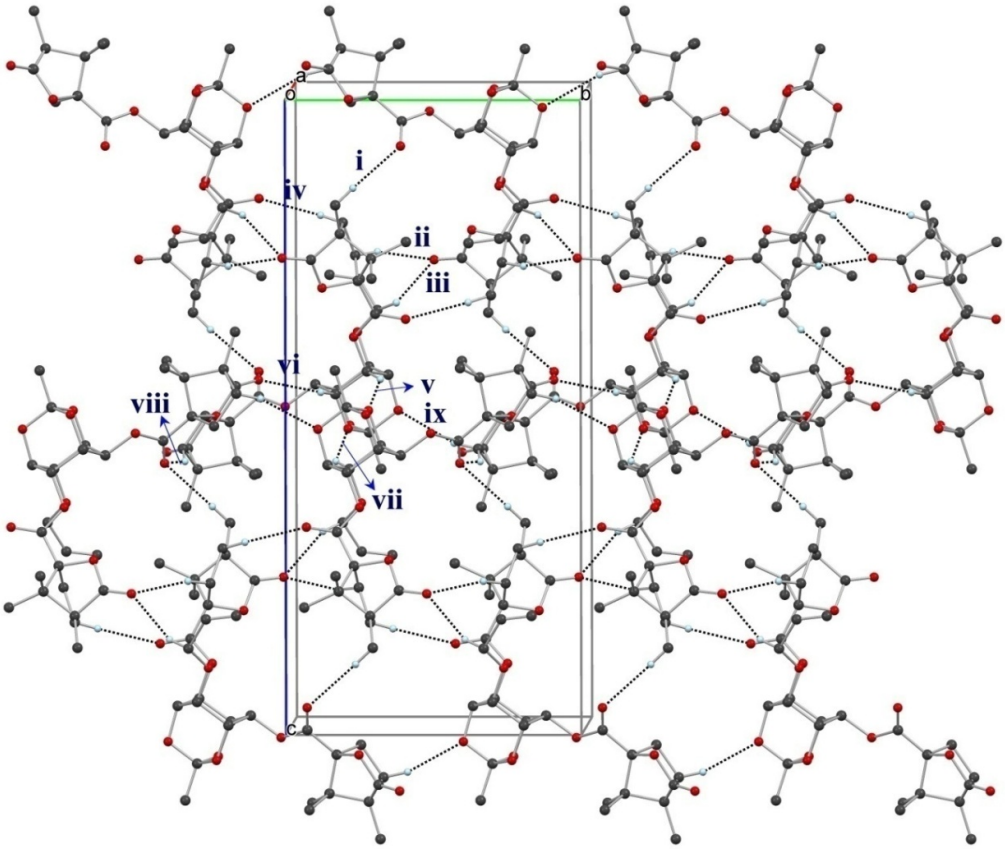

Figure 4.14: Helical assembly of molecules along the 2_1-screw axis (*b*-axis) in a crystal of **dia3.5**.

Arrangement of molecules viewed down the *c*-axis display helical assembly of molecules related by 2_1-screw axis through short and linear C1-H1···O9, C13-H13A···O7 and C14-H14B···O8 interactions. The neighboring parallel helices along the *b*-axis are joined *via* unit translated C13-H13B···O5 and 2_1-screw related C4-H4···O1 and C6-H6···O3 interactions to generate intercalated packing of helices (Figure 4.15).

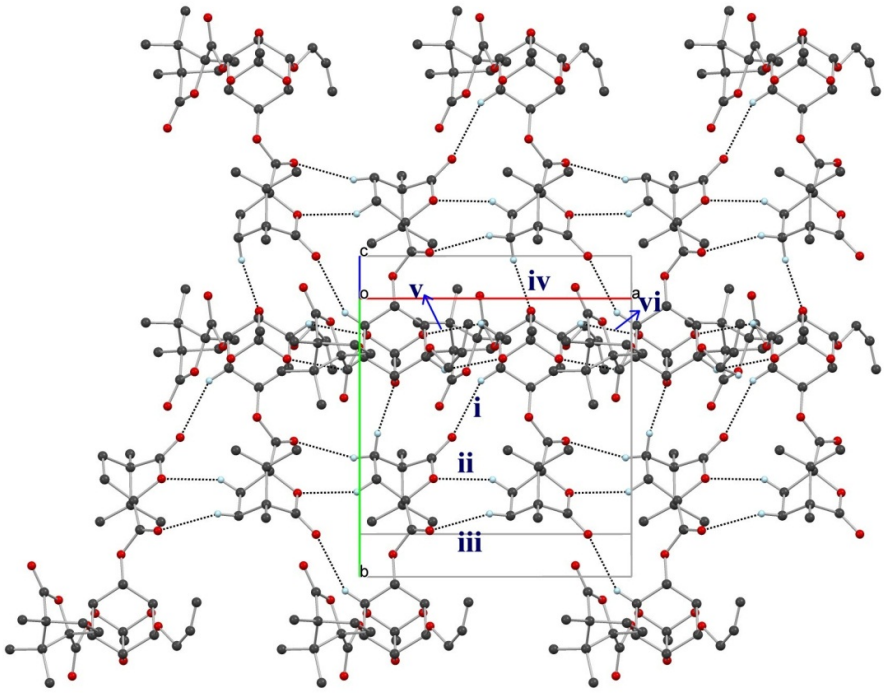

Figure 4.15: Arrangement of molecules viewed down the *c*-axis in crystals of **dia3.5**.

Comparison of physical properties of diastereomeric allyl ethers. The melting point of the diastereomeric orthoformates **3.6** and **dia3.6** were not very different (the difference in melting points was ~ 2-3 °C); the difference in melting points between the diastereomeric orthobenzoates **3.2** and **dia3.2** was 10-15 °C; but that between diastereomeric orthoacetates **3.5** and **dia3.5** was considerable (45 °C). This difference could be due to the fact that **3.5** crystallized as an ethanol solvate. The ethanol molecules remained in the lattice till the melting of the crystal which suggested strong association between the molecules of ethanol and molecules of **3.5**. The orthoacetate **3.5** failed to form a solid in the absence of ethanol, even when cooled to -20 °C. A

comparison of the calculated densities of the diastereomeric pairs reveal that the crystals are more or less equally dense (**3.6** =1.339; **dia3.6** =1.368; **3.5** =1.300; **dia3.5** =1.269; **dia3.2** =1.284) and it is unlikely that this factor had contribution in their separation by crystallization. We determined the solubility of diastereomeric orthoformates **3.6** and **dia3.6** since the difference in their melting points was not considerable, but were separable by crystallization. Surprisingly, the difference in their solubility in methanol (**3.6** = 41 mg/mL; **dia3.6** = 131 mg/mL at room temperature) was considerable.

Crystal structure of five of the six dicamphanates could be solved; the orthobenzoate dicamphanate **3.2** did not form good crystals. Crystal structure of all the dicamphanates are dominated by CH···O interactions since there is no other functional group in these molecules capable of stronger non-covalent interactions. Crystals of the orthoacetate **3.5** is an exception since it crystallized as an ethanol solvate, but the structure as expected is dominated by CH···O interactions. The lattice energy (**3.6** = -235.47 KJ/mole; **dia3.6** = -240.87 KJ/mole) values for diastereomeric orthoformate crystals were not very different. It is interesting to note that we did not observe the formation of cocrystals of these diastereomeric pairs which suggested that the non-covalent interactions between the molecules of a given diastereomeric dicamphanate is stronger than that between two different diastereomeric orthoesters. This is unlike diastereomeric inositol derived camphorsulfonates which cocrystallized and had to be separated chromatographically.[14b-14d] The factors mentioned above appear to have contributed to the separation of diasteremeric dicamphanates during their crystallization.

Conclusions:

We have developed a convenient and practical method for the preparation of chiral protected *myo*-inositol derivatives without involving laborious chromatographic methods of purification. The chiral diastereomeric derivatives could be obtained in gram quantities and the methods are amenable to further scale-up due to the simple procedures involved. It is interesting to note that the separation procedures could be evolved due to the knowledge of the crystal structures of inositol derivatives of comparable molecular structure. The procedures developed for the separation of diastereomeric *myo*-inositol orthoesters helped us to greatly shorten the scheme for the preparation of enantiomeric dibenzoates (of chapter 3B). Since all these chiral

inositol derivatives have the orthoester bridge, they can be converted to a host of synthetically useful chiral inostol derivatives, as the transformation of similar racemic *myo*-inositol orthoesters (via partial or complete cleavage of the orthoester) to other protected inositol derivatives is well established.[16] We are hopeful that the results presented here fills in the lacuna in using the abundantly available *myo*-inositol as a starting material for the synthesis of chiral natural products and their analogs.

General methods: Racemic 4-*O*-allyl-*myo*-inositol-1,3,5-orthoformate,[19] *myo*-inositol-1,3,5-orthobenzoate,[20] *myo*-inositol-1,3,5-orthoacetate[4c] and (1*S*)-(-)-camphanic acid chloride[21] and racemic 2,4-di-O-benzyl-*myo*-inositol[18d] (**4.118**) were prepared according to reported procedures. Usual workup implies decomposition of the reaction mixture by the careful addition of ice or water and removal of the solvent under reduced pressure. The residue obtained was extracted into a suitable solvent (such as ethyl acetate or dichloromethane) and washed with water, dilute hydrochloric acid (if appropriate), saturated sodium bicarbonate (if appropriate) and then with brine. The organic layer was dried over anhydrous sodium sulphate and the solvent was removed under reduced pressure.

Experimental section:

Acylation of racemic 4-*O*-allyl-*myo*-inositol-1,3,5-orthoformate with camphanic acid chloride. Procedure A. (on small scale):

The racemic allyl ether **3.8** (0.300 g, 1.3 mmol) was dissolved in a mixture of dry dichloromethane (5 mL), dry triethylamine (3 mL), dry pyridine (3 mL) and DMAP (0. 050 g) and cooled in an ice-bath. (1*S*)(-)-camphanic acid chloride (0.702 g, 3.25 mmol) was added and the reaction mixture refluxed for 48 h in an inert atmosphere. It was then cooled to ambient temperature and worked up as usual using dichloromethane (200 mL),washed with water, dilute hydrochloric acid, saturated sodium bicarbonate and then with brine. The crude product was column chromatographed (silica gel 100-200 mesh, eluent, 30 % ethyl acetate in light petroleum) to isolate the mixture of diastereoisomers (0.705 g, 92%) as a gum. Although TLC (3:7 ethyl acetate: light petroleum, 3 runs) showed two spots [R_f (**dia3.6**) = 0.35, R_f (**3.6**) = 0.27] they could not be separated by column chromatography.

Data for the mixture of diastereomers **dia3.6** and **3.6: IR** (Neat): $\bar{\nu}$ 1746, 1781 cm^{-1}; **^{1}H NMR** ($CDCl_3$, 200 MHz): δ 0.93 - 1.04 (m, 6 H), 1.05 - 1.17 (m, 12 H), 1.67 - 1.81 (m, 2 H), 1.84 - 2.00 (m, 2 H), 2.02 - 2.20 (m, 2 H), 2.31 - 2.62 (m, 2 H), 4.03 - 4.18 (m, 2 H), 4.30 - 4.49 (m, 3 H), 4.60 - 4.65 (m, 1 H), 5.21 - 5.40 (m, 3 H), 5.50 - 5.65 (m, 2 H), 5.75 - 6.02 ppm (m, 1 H); **^{13}C NMR** ($CDCl_3$, 50 MHz): δ 9.55, 9.58, 16.48, 16.54, 16.57, 16.67, 16.83, 28.69 (CH_2), 28.76(CH_2), 28.87(CH_2), 28.91(CH_2), 30.5(CH_2), 30.7(CH_2), 54.10 , 54.23, 54.32, 54.36, 54.7, 64.8, 67.0, 67.2, 68.4, 68.6, 68.7, 69.2, 69.24, 69.6, 71.2(CH_2), 71.5(CH_2), 72.6,72.8, 90.6 , 90.7, 90.79, 90.82, 102.9, 118.8(CH_2), 118.9 (CH_2), 133.4, 133.5, 166.1, 166.6, 166.83, 166.89, 177.55, 177.57, 177.7 ppm; **Elemental analysis** calculated for $C_{30}H_{38}O_{12}$ (590.62): C, 61.01%; H, 6.49%; found, C, 60.89%; H, 6.13%.

Separation of diastereomers: The mixture of diasteroisomers (0.7 g) obtained above as a gum, was triturated with *n*-pentane (25 mL) to obtain a solid suspension. Drop-wise addition of methanol (3-5 mL) with warming resulted in a clear solution, which on standing at room temperature for 1 to 2 h deposited very fine needles (bunch of fibers) of one of the diastereomer (later identified as the more polar **3.6**) which were filtered (0.29 g).

Data for the crystalline diastereomer **3.6:**

MP = 143-147 ^oC; $[\propto]^{rt}_D$ = + 9.81 [$CHCl_3$, c=1.0]; **IR** (Nujol): $\bar{\nu}$ = 1756, 1788 cm^{-1}; **^{1}H NMR** ($CDCl_3$, 500 MHz): δ 0.99 - 1.16 (5s, 18 H), 1.64 - 1.79 (m, 2 H), 1.85 - 2.16 (m, 4 H), 2.37 - 2.47 (m, 1 H), 2.48 - 2.57 (m, 1 H), 4.04 - 4.15 (m, 2 H), 4.31 - 4.42 (m, 3 H), 4.61 - 4.65 (m, 1 H), 5.23 - 5.37 (m, 3 H), 5.52 - 5.64 (m, 2 H), 5.82 - 5.95 ppm (m, 1 H); **^{13}C NMR** ($CDCl_3$,101 MHz): δ 9.62, 9.68, 16.63, 16.68, 16.8, 16.9, 28.84 (CH_2), 29.0 (CH_2), 30.6(CH_2), 30.63(CH_2), 54.2, 54.5, 54.8, 64.84, 67.04, 68.5, 68.8, 69.7, 71.6 (CH_2), 72.9, 90.77, 90.86, 103.0, 119.1 (CH_2), 133.4, 166.1, 167.0, 177.63, 177.66 ppm; **Elemental analysis** calculated for $C_{30}H_{38}O_{12}$ (590.62): C, 61.01%; H, 6.49%; found, C, 61.25%; H, 6.61%.

The mother liquor was evaporated under reduced pressure to obtain a gum. The gum was triturated with *n*-pentane (20 mL) to obtain a solid. Drop-wise addition of methanol (3 mL) with warming resulted in a clear solution, which on standing at room temperature for 4 to 5 or (some time one week) days deposited a colorless amorphous solid (later identified as the less polar **dia3.6**) which was filtered (0.26 g). Attempts to obtain good quality crystals of **dia3.6** from other solvents failed. The diastereomers

dia3.6 could also be separated by crystallization of left residue after first crystallization, from ethanol.

Data for the diastereomer **dia3.6:**

MP =138-142 ^{0}C; $[\alpha]^{rt}_{D}$= - 20.20 [$CHCl_3$, c =1.0]; **IR** (Nujol)**:** $\bar{\nu}$ =1746, 1788 cm^{-1}; **^{1}H NMR** ($CDCl_3$, 200 MHz): δ 1.0 -1.15 (6s, 18 H), 1.63 - 1.80 (m, 2 H), 1.80 - 2.01 (m, 2 H), 2.03 - 2.21 (m, 2 H), 2.30 - 2.61 (m, 2 H), 4.08 - 4.16 (m, 2 H), 4.33 - 4.48 (m, 3 H), 4.58 - 4.65 (m, 1 H), 5.20 - 5.40 (m, 3 H), 5.50 - 5.61 (m, 2 H), 5.78 - 6.04 ppm (m, 1 H); **^{13}C NMR** ($CDCl_3$, 50 MHz): δ 9.6, 16.53, 16.63, 16.73, 28.7(CH_2), 28.9(CH_2), 30.6(CH_2), 30.8(CH_2), 54.3, 54.4, 54.8, 64.8, 67.3, 68.7, 69.24, 69.28, 71.3(CH_2), 72.7, 90.6, 90.9, 103.0, 118.9(CH_2), 133.5, 166.6, 166.9, 177.8 ppm.

Elemental analysis calculated for $C_{30}H_{38}O_{12}$ (590.62): C, 61.01%; H, 6.49%; found, C, 61.06%; H, 6.21%.

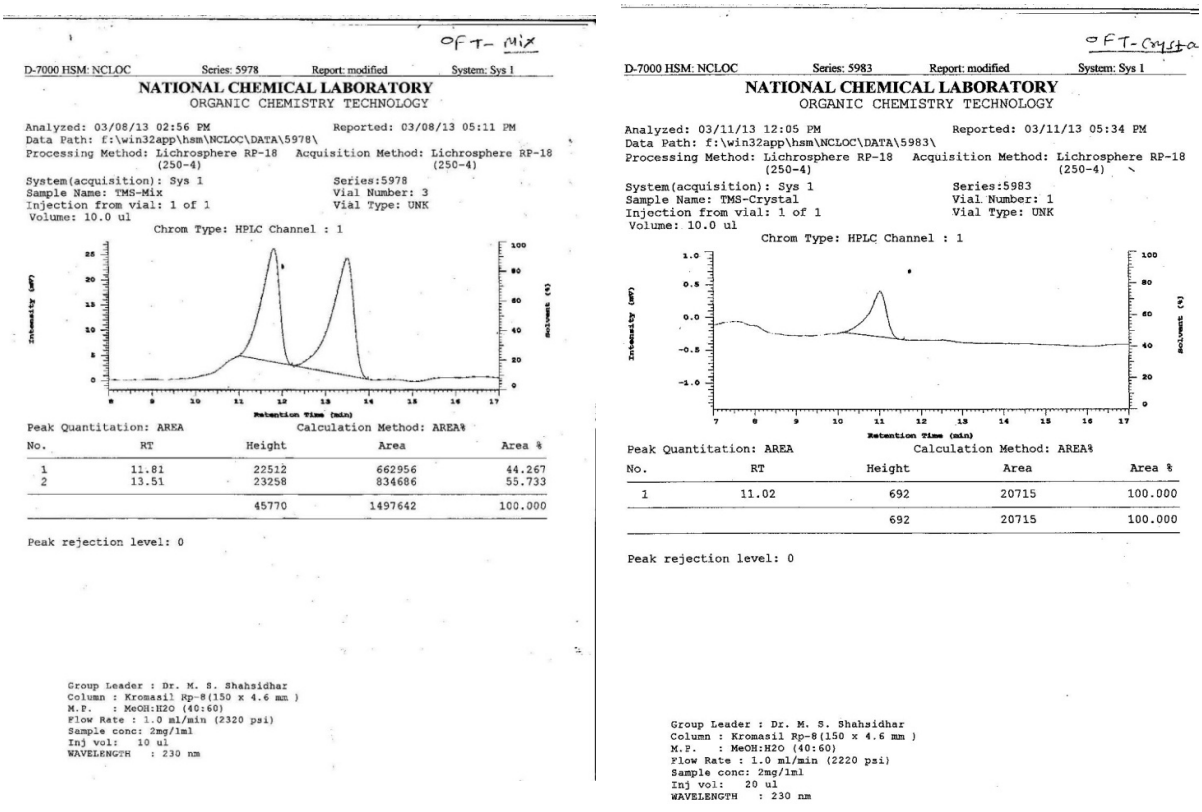

Figure 4.16: HPLC analysis of the diasteriomeric mixture **3.6**, **dia3.6** (Left), crystals of **3.6** (Right) which appeared within 2 h.

Acylation of racemic 4-*O*-allyl-*myo*-inositol-1,3,5-orthoformate with camphanic acid chloride. Procedure B. (on larger scale):

The racemic allyl ether **3.8** (3.000 g, 13.00 mmol) was dissolved in a mixture of dry dichloromethane (20 mL), dry triethylamine (20 mL), dry pyridine (20 mL) and DMAP (0.500 g) and cooled in an ice-bath. (1*S*) (-) camphanic acid chloride (7.02 g, 32.5 mmol, 2.5 eq) was added and the reaction mixture refluxed for 48 h in an inert atmosphere. The reaction mixture was worked up using dichloromethane (1 L) as in procedure A. The crude product was column chromatographed (silica gel 100-200 mesh, 30 % ethyl acetate in petroleum ether) to isolate the mixture of diastereoisomers (7.28 g, 95%).

A diasteriomeric mixture of allyl ethers (gum, 20 g) was taken in a two liter round bottomed flask, and triturated with *n*-pentane (500-600 mL) to obtain a solid. Methanol (60-70 mL) was then added and the mixture was slightly warmed to obtain a clear solution. The crystalline diastereomer (**3.6**) obtained in procedure A was used for seeding and the solution stored at room temperature. Crystals (6-8 g, 30-40 %) were deposited in 2-3 hour. (In some experiments the pentane – methanol solution was kept in fridge, instead of storing at room temperature. Crystals of **3.6** appeared after 30 min). Crystals were separated by filtration. The mother liquor was concentrated under reduced pressure and the residue was dissolved in methanol (25-30 mL) and diluted with n-pentane (pentane-250-300 mL) and stored at ambient temperature (in a 2 liter conical flask). After 6-7 days an amorphous solid was obtained (approx. 6 g) which was filtered. HPLC analysis of this powder showed that it was the less polar diastereomer **dia3.6**. The mother liquor was concentrated under reduced pressure and the residue was dissolved in methanol (5-10 mL) and diluted with pentane (60-70 mL) and stored at ambient temperature (in a 500 mL conical flask). After 1-2 h crystals of **3.6** was obtained (1 g) which was filtered. By this repetitive crystallization total yield of the more polar diastereomer **3.6** was about 30-42% and that of the less polar diastereomer **dia3.6** was 30-40%. Purity of both the diastereomers was determined by HPLC analysis (Appendix IV, Figures A51-A53). One of crystallization experiment good quality crystals of the less polar diastereomers **dia3.6** was obtained in ethanol.

Cleavage of the allyl ether in 3.6:

The crystalline diastereomer **3.6** (0.118 g, 0.2 mmol) was dissolved in *iso*-propanol (6 mL) and refluxed (24 h) after the addition of 20% Pd $(OH)_2$ /C (0.070 g 0.1 mmol). The reaction mixture was filtered through Celite, and concentrated under reduced pressure. The solid residue was column chromatographed (silica gel 100-200 mesh, eluent 7:3 ethyl acetate: light petroleum) to isolate the known D-2,4-di-*O*-camphonyl-*myo*-inositol-1,3,5-orthoformate as a solid (**4.50**, 0.068 g, 62%). Hence **3.6** is D-2,4-di-*O*-camphonoyl-6-*O*-allyl-*myo*-inositol-1,3,5-orthoformate.

Data for **4.50: MP:** 285 (charred) ^oC; Lit. [4b] >270 (charred); $[\propto]^{rt}_D$= +6 [DMF, c=1] Lit. [4b]; $[\propto]^{28}_D$= +7.5 [DMF, c=1].

Cleavage of the allyl ether in dia3.6:

Allyl ether in the diastereomer **dia3.6** (0.118 g, 0.2 mmol) was cleaved with 20% Pd $(OH)_2$ /C (0.070 g 0.1 mmol) in *iso*-propanol (6 mL) as above, to isolate the known D-2,6-di-*O*-camphonyl-*myo*-inositol-1,3,5-orthoformate as a solid (**dia4.50**, 0.066 g, 60%). Hence **dia3.6** is 1D-2,6-di-*O*-camphonyl-4-*O*-allyl-*myo*-inositol-1,3,5-orthoformate. Data for **dia4.50: MP:** >256 ^oC; Lit. [4b] >235 ^oC; $[\propto]^{rt}_D$= -16.6 [$CHCl_3$, c=1] Lit. [4b]; $[\propto]^{28}_D$= -15.5 [$CHCl_3$, c=1].

Preparation of racemic 4-*O*-allyl-*myo*-inositol-1,3,5-orthobenzoate (3.3):

myo-Inositol-1,3,5-orthobenzoate **4.16** (6.5 g, 18.79 mmol) was dissolved in dry DMF (120 mL), and the solution was cooled in an ice bath. To the cold solution, sodium hydride (0.752 g, 18.79 mmol, 1 eq.) was added with stirring. The mixture was warmed to room temperature and allyl bromide (1.94 mL, 22.54 mmol, 1.2 eq.) was added with stirring. The reaction mixture was stirred for 12 h. The reaction mixture was worked up as usual. The crude product was purified by column chromatography (silica gel 100-200 mesh, eluent 25:75 ethyl acetate: light petroleum) to get racemic 4-*O*-allyl *myo*-inositol-1,3,5-orthobenzoate as a gum (5.1 g, 89%).

Data for the allyl ether **3.3:** TLC R_f : 0.4 (40:60 ethyl acetate : light petroleum); **IR** (neat)**:** $\bar{\nu}$ 3300 - 3600 cm^{-1} ; **^{1}H NMR** ($CDCl_3$, 200 MHz): δ 3.17 (d, *J* = 12.0 Hz, 1H, D_2O Exchangeable.), 3.74 (d, *J* = 10.2 Hz, 1 H, D_2O Exchangeable), 4.06 - 4.28 (m, 3 H), 4.38 - 4.68 (m, 5 H), 5.26 - 5.44 (m, 3 H), 5.80 – 6.00 (m, 1 H), 7.32 - 7.44 (m, 3 H), 7.52 - 7.74 ppm (m, 2 H); **^{13}C NMR**($CDCl_3$, 50 MHz): δ 59.5, 67.4, 68.0, 71.5 (CH_2), 73.2, 73.7, 75.7, 107.1, 119.0 (CH_2), 125.1, 127.7, 129.4, 132.6, 136.5 ppm; **Elemental analysis** calcd for $C_{16}H_{18}O_6$ (306.11): C, 62.74%; H, 5.92%; found, C, 62.78%; H, 6.00 %

Acylation of racemic 4-*O*-allyl-*myo*-inositol-1,3,5-orthobenzoate (3.3) with (1*S*)-(–)-camphanic chloride. Procedure C. (on small scale):

The racemic allyl ether **3.3** (0.5 g, 1.63 mmol), dry dichloromethane (5 mL), triethylamine (3 mL), DMAP (0. 070 g), pyridine (3 mL) and (1*S*)-(–)-camphanic acid chloride (0.880 g, 4.08 mmol) were refluxed (oil bath temperature 80–85 ^{o}C) for 48 h in an atmosphere of argon. The reaction mixture was cooled and worked up as usual in dichloromethane (200 mL). The crude product was column chromatographed (silica gel 100-200 mesh, 20:80 ethyl acetate: light petroleum) to isolate the mixture of diastereoisomers (1.1 g, 93%).

Data for mixture of diastereomers **dia3.2** and **3.2:** TLC R_f **(dia3.2):** 0.5, R_f **(3.2)**: 0.45 (20:80 ethyl acetate : light petroleum, 6 elutions); **IR** ($CDCl_3$)**:** $\bar{\nu}$ 1756, 1790 cm^{-1}; **^{1}H NMR** ($CDCl_3$, 200 MHz): δ 0.97 - 1.04 (m, 6 H) 1.06 – 1.14 (m, 12 H), 1.67 - 1.8 (m, 2 H) 1.86 - 2.20 (m, 4 H), 2.36 – 2.59 (m, 2 H), 4.10 – 4.18 (m, 2 H), 4.43 - 4.50 (m, 1 H), 4.55 – 4.64 (m, 2 H), 4.72 – 4.8 (m, 1 H), 5.20 - 5.45 (m, 3 H), 5.63 - 5.77 (m, 1 H) 5.8 – 6.05 (m, 1 H) 7.33 - 7.41 (m, 3 H) 7.57 - 7.64 ppm (m, 2 H); **^{13}C NMR** ($CDCl_3$, 50 MHz): δ 9.6, 16.56, 16.63, 16.67, 16.72, 16.9, 28.76 (CH_2), 28.83 (CH_2), 28.92 (CH_2), 28.96 (CH_2), 30.5 (CH_2), 30.6 (CH_2), 30.8 (CH_2), 54.2, 54.3, 54.4, 54.8, 64.1, 67.8, 68.1, 68.8, 69.3, 70.0, 70.1, 70.7, 71.0,71.4 (CH_2), 71.7 (CH_2), 72.6, 72.8, 90.7, 90.8, 90.87, 90.93, 107.9, 119.0 (CH_2), 119.1(CH_2), 125.2, 128.0, 129.8, 133.44, 133.57, 136.15, 136.22, 166.2, 166.7, 166.9, 167.0, 177.63, 177.79 ppm; **Elemental analysis** calculated for $C_{36}H_{42}O_{12}$ (666.72): C, 64.85%; H, 6.35%; found, C, 64.69%; H, 6.23%.

Flash column chromatography (silica gel, 230-400 mesh; 10-12% ethyl acetate in petroleum ether) of the mixture of diastereoisomers (0.40 g) gave two gums enriched with one of the diastereomer. Less polar fraction (0.13 g) (mixture of **dia3.2** and **3.2** ratio 85:15 by HPLC), more polar fraction (0.16 g) (mixture of **3.2** and **dia3.2** ratio 80:20 by HPLC) (For HPLC, see Appendix IV, Figures A54). The enriched less polar diastereomer was dissolved in diethyl ether (0.1 g in 10-15 mL) or in DMF (0.015 g in 1 mL) by warming and the solution was allowed to stand at rt. for 2-3 days (10-15 days in case of DMF) when crystals were obtained (after the complete evaporation of ether; but not in DMF). These crystals were used as seed crystals for larger scale separation.

Data for crystals of the less polar diastereomer **dia3.2:** **MP** = 134-135 ^{o}C; $[\propto]^{rt}{}_{D}$= -25.3 [$CHCl_3$, c=1.1]; **IR** ($CHCl_3$)**:** $\bar{\nu}$ 1791, 1756 cm^{-1}; **^{1}H NMR** ($CDCl_3$, 200 MHz): δ 1.01 (s, 3H), 1.03 (s, 3H), 1.09 (s, 3H), 1.10 (s, 3H), 1.12 (br. s, 6H), 1.62 – 1.80 (m, 2H) 1.82 - 2.22 (m, 4 H), 2.31 - 2.58 (m, 2 H), 4.13 – 4.20 (m, 2H), 4.42 - 4.50 (m, 1 H), 4.58 – 4.66 (m, 2 H), 4.72 – 4.80 (m, 1 H), 5.23 - 5.41 (m, 3 H), 5.62 - 5.73 (m, 1 H), 5.82 - 6.03 (m, 1 H), 7.31 - 7.43 (m, 3 H), 7.54 - 7.65 ppm (m, 2 H); **^{13}C NMR** ($CDCl_3$, 101 MHz): δ 9.67, 9.7, 16.6, 16.7, 16.8, 28.8 (CH_2), 29.0 (CH_2), 30.5 (CH_2), 30.8 (CH_2), 54.36, 54.41, 54.8, 64.1, 68.1, 69.3, 70.1, 70.7, 71.4 (CH_2), 72.6, 90.7, 91.0, 107.9, 119.1 (CH_2), 125.2, 128.1, 129.8, 133.6, 136.2, 166.8, 166.9, 177.82, 177.84 ppm; **Elemental analysis** calculated for $C_{36}H_{42}O_{12}$ (666.72): C, 64.85; H, 6.35; found, C, 64.58%; H, 6.47%.

Acylation of racemic 4-*O*-allyl-*myo*-inositol-1,3,5-orthobenzoate (3.3) with (1*S*)-(–)-camphanic chloride. Procedure D. (on larger scale):

The racemic allyl ether **3.3** (5.0 g, 16.28 mmol), dry dichloromethane (30 mL), triethylamine (30 mL), DMAP (0.700 g), pyridine (30 mL) and (1*S*)-(–)-camphanic acid chloride (8.79 g, 40.79 mmol) were refluxed (80 ^{o}C – 85 ^{o}C) for 48 h in an inert atmosphere. The reaction mixture was cooled, concentrated and worked up as usual in dichloromethane (1 L). The crude product was column chromatographed (silica gel 100-200 mesh, 20:80 ethyl acetate: light petroleum) to isolate the mixture of diastereoisomers (10.96 g, 91%).

Crystallization Method D1: The mixture of diastereomers obtained above (3 g) was dissolved in warm *iso*-propanol (15-20 mL) and stored at 30-35 ^{o}C (at lower temperatures a solid or a gummy solid precipitates) for 7-10 days. Crystals of the less polar diastereomer (**dia3.2**) were deposited (1 g, 33%). Its purity (>97 %) and structure were confirmed by HPLC (For HPLC, see Appendix IV, Figures A55) and NMR spectroscopy.

Method D2: The gummy diastereomeric mixture (10 g) was taken in a 2 liter round bottom flask, and dissolved in warm *iso*-propanol (150-200 mL) and the solution was allowed to attain ambient temperature. Seed crystals of the less polar diastereomer **dia 3.2** were added and the flask was stored (open to atmosphere) at room temperature (30-35 ^{o}C) for 7-15 days. Block type crystals that separated were filtered (2.0-3.5 g, 20-35%) (For HPLC, see Appendix IV, Figures A56-A57).

The mother liquor was concentrated under reduced pressure and the residue was dissolved in *iso*-propanol (50-55 mL) in a 500 mL conical flask and stirred overnight at 45 ^{o}C. Then the solution was kept at room temp for 1 day when a solid was precipitated. It was filtered (through ordinary filter paper) and dried in air (2.3 g, 23%). The ratio of the two diastereomers present was found to be 70:30 by ^{1}H NMR spectroscopy. The solid was divided into three portions (approx. 0.6 g each). One portion was dissolved in warm methanol (20 mL); second portion was dissolved in warm ethanol (20 mL); third portion was dissolved in warm dioxane (20 mL). All the three solutions were left to stand open to atmosphere (2-3 days) at ambient tempr. Ethanol and methanol solutions deposited a powder. HPLC analysis revealed the relative ratio of the two diastereomers **3.2 : dia3.2** to be 94**:**06 (For HPLC, see Appendix IV, A58-A59).

Data for amorphous diastereomer **3.2** (obtained from ethanol)**:** **MP** = 145-151 ^{o}C; $[\propto]^{rt}{}_{D}$ = -1.3 [$CHCl_3$, c = 0.72]; **IR** ($CHCl_3$)**:** $\bar{\nu}$ 1790, 1758 cm^{-1}; **^{1}H NMR** ($CDCl_3$, 500 MHz): δ 1.00 (s, 3H), 1.01 (s, 3H), 1.11 (s, 3H), 1.12-1.15 (2s, 9H), 1.67 – 1.75 (m, 2H), 1.88 - 2.00 (m, 2 H), 2.02 - 2.14 (m, 2 H), 2.44 - 2.56 (m, 2 H), 4.10 – 4.18 (m, 2H), 4.46 (br. s, 1 H), 4.58 (br. s, 2 H), 4.76 (br. s, 1 H), 5.25 - 5.38 (m, 3 H), 5.68 - 5.74 (m, 1 H), 5.85 - 5.97 (m, 1 H), 7.33 - 7.43 (m, 3 H), 7.54 - 7.63 ppm (m, 2 H); **^{13}C NMR** ($CDCl_3$, 126 MHz): δ 9.63, 9.64, 16.64, 16.69, 16.73, 16.94, 28.85 (CH_2), 29.0 (CH_2), 30.56 (CH_2), 30.65 (CH_2), 54.21, 54.44, 54.76, 54.79, 64.1, 67.8, 68.8, 70.0, 71.0, 71.7 (CH_2), 72.8, 90.8, 90.9, 107.9, 119.1 (CH_2), 125.2, 128.1, 129.8, 133.5, 136.2, 166.2, 167.0, 177.66, 177.67 ppm.

Cleavage of the allyl group in dia3.2:

Crystals of **dia3.2** (0.100 g, 0.15 mmol) were dissolved in *iso*-propanol (3 mL); 20% $Pd(OH)_2$ /C (0.048 g, 0.068 mmol, ~0.5 eq.) was added and refluxed for 24 h. The reaction mixture was filtered through Celite, and concentrated under reduced pressure to obtain a solid. The solid was purified by column chromatography (silica gel 100-200 mesh, eluent 70:30 ethyl acetate: light petroleum) to get the known D-2,6-di-*O*-camphanoyl-*myo*-inositol-1,3,5-orthobenzoate as a solid (0.066 g, 61%). **Data: MP** = 246-247 ^{o}C; Lit. [4d] 238-240; $[\propto]^{20}{}_{D}$= -17 [DMF, c=1]; Lit. [4d] $[\propto]^{20}{}_{D}$= -19.4 [DMF, c=0.9].

Preparation of racemic 4-*O*-allyl-*myo*-inositol-1,3,5-orthoacetate from *myo*-inositol-1,3,5-orthoacetate:

myo-Inositol-1,3,5-orthoacetate **4.15** (2.212 g, 10.84 mmol) was dissolved in dry DMF (30 mL). To the ice cooled solution, sodium hydride was added (0.434 g, 10.84 mmol) with stirring. After 10-15 min allyl bromide (1.3 mL, 13.01mmol) was added with stirring. The reaction mixture was stirred overnight (8 -10 h) and quenched by the addition of ice, and DMF was removed under reduced pressure. The workup was carried out as usual. The crude product was purified by column chromatography (100-200 mesh silica gel, eluent 20:80 ethyl acetate: light petroleum) to obtain racemic 4-*O*-allyl-*myo*-inositol-1,3,5-orthoacetate **3.7** as a gum (1.900 g, 72%).

Data for **3.7:** R_f = 0.4 (1:1 ethyl acetate : light petroleum); **IR** ($CHCl_3$)**:** $\bar{\nu}$ 3200 – 3500 cm^{-1}; **^{1}H NMR** ($CDCl_3$, 200 MHz): δ 1.45 (s, 3 H), 3.26 (d, *J* = 11.6 Hz, 1 H D_2O exchangeable), 3.66 (d, *J* = 10.1 Hz, 1 H, D_2O exchangeable), 3.95 - 4.05 (m, 1 H), 4.11 - 4.51 (m, 7 H), 5.24 - 5.40 (m, 2 H), 5.77 - 6.00 ppm (m, 1 H); **^{13}C NMR** ($CDCl_3$, 101 MHz): δ 24.1, 59.7, 67.3, 67.6, 71.8 (CH_2), 72.7, 73.9, 75.2, 108.6, 119.4 (CH_2), 132.7 ppm; **HRMS** $[C_{11}H_{16}O_6 + H]^+$ = 245.1020, found = 245.1019.

Acylation of racemic 4-*O*-allyl-*myo*-inositol-1,3,5-orthoacetate (3.7) with (1*S*)-(–)-camphanic chloride. Procedure E. (on small scale):

The racemic orthoacetate allyl ether **3.7** (1.7 g, 6.96 mmol), dry dichloromethane (10 mL), triethylamine (10 mL), DMAP (0. 250 g), pyridine (10 mL) and (1*S*)-(–)-camphanic acid chloride (3.77 g, 17.4 mmol, 2.5eq.) were refluxed (80–85 ^oC) for 48h in an inert atmosphere. The reaction mixture was cooled, concentrated and worked up in dichloromethane (500 mL) as usual. The product was purified by column chromatography (silica gel 60-120 mesh, eluent: 20:80 ethyl acetate: light petroleum) to obtain the mixture of diastereomers as a gum (4 g, 95%).

Data for mixture of **dia3.5** and **3.5:** R_f **dia3.5** = 0.45; **R** $_f$ **3.5** = 0.4 (15:85 ethyl acetate: light petroleum, five runs) **IR** ($CHCl_3$)**:** $\bar{\nu}$ 1756, 1790 cm^{-1}; **^{1}H NMR** ($CDCl_3$, 200 MHz): δ 0.94 - 1.03 (3s, 6 H), 1.04 - 1.18 (5s, 12 H), 1.45 (s, 3 H), 1.60 - 1.79 (m, 2 H), 1.80 - 2.21 (m, 4 H), 2.29 - 2.62 (m, 2 H), 4.00 - 4.16 (m, 2 H), 4.25 - 4.48 (m, 3 H), 4.50 – 4.60 (m, 1 H), 5.15 - 5.38 (m, 3 H), 5.43 - 5.60 (m, 1 H), 5.75 - 6.02 ppm (m, 1 H); **^{13}C NMR** ($CDCl_3$, 101 MHz): δ 9.6, 9.65, 9.67, 16.54 , 16.63,16.65, 16.89 , 24.0 , 28.74 (CH_2), 28.81 (CH_2), 28.9 (CH_2), 29.0 (CH_2), 30.48 (CH_2), 30.52 (CH_2), 30.56 (CH_2), 30.8 (CH_2), 54.16 , 54.26, 54.39, 54.45, 54.75, 64.0, 67.0, 67.3, 68.7, 69.0, 69.3, 69.7, 70.1, 71.3 (CH_2), 71.6 (CH_2), 72.5, 72.7, 90.7 , 90.8, 90.86, 90.92, 109.1, 118.88 (CH_2), 118.96 (CH_2), 133.5, 133.6, 166.2, 166.7, 166.8,

166.9, 177.64, 177.68, 177.8, 177.85 ppm; **Elemental analysis** calculated for $C_{31}H_{40}O_{12}$ (604.65): C, 61.58%; H, 6.67%; found, C, 61.45%; H, 6.64%.

The diastereomeric mixture (0.500 g) was column chromatographed (silica gel 230-400 mesh, 10:90 ethyl acetate: light petroleum) to obtain enriched (about 80:20 as revealed by ^{1}H NMR spectroscopy) mixture of diastereoisomers **A** (0.150 g) and **B** (0.110 g). The enriched sample **A** (0.120 g) was crystallized from hot absolute ethanol (5 mL) when pure (less polar) diastereomer **dia3.5** was obtained (0.070 g, 58 %). A similar crystallization procedure (in ethanol) with **B** (0.100 g) provided the other (more polar) diastereomer **3.5** (0.045 g, 45%). The crystals of the individual diastereomer **dia3.5** and **3.5** obtained from ethanol (For HPLC see Appendix IV, A60) were subsequently used as seed crystals to separate the mixture of the diastereoisomers on larger scale.

Acylation of racemic 4-*O*-allyl-*myo*-inositol-1,3,5-orthoacetate (3.7) with (1*S*)-(–)-camphanic chloride. Procedure F (on larger scale):

To a cooled mixture of the racemic 4-allyl ether **3.7** (5**.**100 g, 20.88 mmol), dry dichloromethane (30 mL), dry triethylamine (25 mL), dry pyridine (25 mL) and DMAP (0.750 g) (1*S*)(-) camphanic acid chloride (11.31 g, 52.2 mmol, 2.5 eq) was added and the mixture refluxed for nearly 48 h in an argon atmosphere. After usual workup and chromatography a mixture of diastereomers (12.0 g, 95%) was isolated by column chromatography (silica gel 60-120 mesh, eluent: 20:80 ethyl acetate: light petroleum).

Crystallization procedure F1: The mixture of diastereomers **dia3.5** and **3.5** (gum, 12.0 g) obtained as above was taken in a 1 L round bottom flask and dissolved in ethanol (90-120 mL) by warming. Seed crystals of **3.5** were added and the flask was stored at room temperature (open to atmosphere) for 1-3 days when very thin needles or blocks of **3.5** (more polar diastereomer) appeared. These crystals were filtered (4 - 5 g, 34 - 42 %). [Storage of the ethanol solution (as above) for longer period of time resulted in the deposition of an amorphous solid **dia3.5** on crystals of **3.5** that had appeared previously.] The mother liquor was concentrated to a gum and dissolved in warm ethanol (50-70 mL) and the clear solution was allowed to attain room temperature. The seed crystals of the less polar diastereomer **dia3.5** (obtained on 0.2 g scale as above) were added and stored (open to atmosphere) at room temperature for 5-8 days when the less polar diastereomer **dia3.5** appeared as fibrous thin needle shaped crystals or a solid (3.5 - 4 g, 30 - 34%). Thus by repetitive crystallization using

the two diastereomers as seed crystals, the two diastereomeric orthoacetates **dia3.5** and **3.5** could be separated efficiently (For HPLC, see Appendix IV, A61-A64).

Data for **3.5: MP** = 115 ^{o}C (Crystals from ethanol **3.5 :** EtOH = 1:0.5); $[\alpha]^{rt}_{D}$= + 6.8 [$CHCl_3$, c=1.0]; **IR** (Nujol) = $\bar{\nu}$ 1750, 1792 cm^{-1}; **^{1}H NMR** ($CDCl_3$, 400 MHz): δ 0.99 (s, 3 H), 1.00 (m, 3 H), 1.09 (m, 3 H), 1.11 (m, 3 H), 1.14 (s, 6H), 1.24 (t, *J* = 7 Hz, 2 H, Ethanol) 1.45 (s, 3 H), 1.64 – 1.77 (m, 2 H), 1.86 - 2.15 (m, 4 H), 2.37 - 2.54 (m, 2 H), 3.71 (q, *J* = 7.1 Hz,1 H, Ethanol), 4.02 - 4.13 (m, 2 H), 4.29 (br. s, 1 H), 4.35 – 4.39 (m, 2 H), 4.55 (br. s, 1 H), 5.20 (s, 1 H), 5.23 - 5.35 (m, 2 H), 5.53 – 5.58 (m, 1 H), 5.80 - 6.00 (m, 1 H) ppm; **^{13}C NMR** ($CDCl_3$, 101 MHz): δ 9.64, 9.68, 16.58, 16.63, 16.69, 16.94, 18.4 (CH_3, Ethanol), 24.0, 28.9 (CH_2), 29.0 (CH_2), 30.57 (CH_2), 30.62 (CH_2), 54.2, 54.5, 54.8, 58.5 (CH_2, Ethanol), 64.1, 67.0, 68.8, 69.1, 70.2, 71.6 (CH_2), 72.8, 90.8, 90.9, 109.1, 119.0 (CH_2), 133.5, 166.2, 167.0, 177.66, 177.70 ppm; **Elemental analysis** calculated for $C_{31}H_{40}O_{12}$ (604.65)+0.5 C_2H_5OH: C, 61.23%; H, 6.91%; found, C, 60.95%; H, 6.91%.

Data for **dia3.5: MP** = 160 ^{o}C (crystals from ethanol); **IR** (Nujol)**:** $\bar{\nu}$ 1745, 1789 cm^{-1}; $[\alpha]^{rt}_{D}$= -19.28 [$CHCl_3$, c=1.0]; **^{1}H NMR** ($CDCl_3$, 500 MHz): δ 1.00 (s, 3 H), 1.01 (s, 3 H), 1.07 (s, 3 H), 1.11 (s, 3 H), 1.12 (s, 3 H), 1.14 (br. s, 3 H), 1.45 (s, 3 H), 1.65 - 1.77 (m, 2 H), 1.87 - 2.00 (m, 2 H), 2.01 - 2.15 (m, 2 H), 2.35 - 2.45 (m, 1 H), 2.46 – 2.55 (m, 1H) 4.06 - 4.15 (m, 2 H), 4.29 (br. s, 1 H), 4.39 – 4.46 (m, 2 H), 4.55 (br. s, 1 H), 5.18 (s, 1 H), 5.23 - 5.35 (m, 2 H), 5.46 - 5.52 (m, 1 H), 5.84 - 5.95 ppm (m, 1 H); **^{13}C NMR** ($CDCl_3$, 126 MHz): δ 9.68, 9.74, 16.6, 16.7, 24.1, 28.8 (CH_2), 29.0 (CH_2), 30.6 (CH_2) , 30.8 (CH_2), 54.3, 54.5, 54.8, 64.1, 67.4, 69.34, 69.35, 69.8, 71.3 (CH_2), 72.6, 90.7, 91.0, 109.2, 118.9 (CH_2) , 133.7, 166.8, 166.9, 177.86, 177.91 ppm; **Elemental analysis** calculated for $C_{31}H_{40}O_{12}$ (604.65): C, 61.58%; H, 6.67%; found, C, 61.56%; H, 6.76%.

Preparation of (-)-L- 6-*O*-allyl-*myo*-inositol-1,3,5-orthoacetate (L-3.7):

A mixture of the powdery dicamphanate **dia3.5 (**diastereomeric ratio **dia3.5: 3.5** = **95:5**, 0.900 g, 1.49 mmol), MeOH (20 mL), dichloromethane (20 mL) and *iso*-butyl amine (10 mL) was refluxed overnight (10-12 h), in an inert atmosphere. The solvent was removed under reduced pressure and the gummy residue was dissolved in ethyl acetate and worked up as usual. The product was purified by column chromatography (silica gel, 100-200 mesh, eluent 3:7 ethyl acetate: light petroleum) to get (-)-L-6-*O*-allyl-*myo*-inositol-1,3,5-orthoacetate **L-3.7** (0.348 g, 96%) as a gum.

Data **L-3.7:** R $_f$**:** 0.4 (50:50 ethyl acetate : light petroleum); $[\alpha]^{26}_D$= - 25.7 ($CHCl_3$, c= 3.3), **IR** (Neat)**:** $\bar{\nu}$ 3450-3550 cm^{-1}; **^{1}H NMR** ($CDCl_3$, 400 MHz): δ 1.45 (s, 3H), 3.36 (br. s, 1 H, D_2O exchangeable), 3.66 (br. s, 1 H, D_2O exchangeable), 4.0 (s, 1 H), 4.09 - 4.18 (m, 2 H), 4.20-4.23 (m, 1 H), 4.24-4.26 (m, 1 H), 4.27 - 4.31 (m, 1 H), 4.32 - 4.36 (m, 1 H), 4.42 (br. s, 1 H), 5.27 - 5.35 (m, 2 H), 5.82 - 5.94 ppm (m, 1 H); **^{13}C NMR** ($CDCl_3$, 101 MHz): δ 24.0, 59.6, 67.3, 67.5, 71.7 (CH_2), 72.7, 73.9, 75.2, 108.5, 119.3 (CH_2), 132.7 ppm; **HRMS** $[C_{11}H_{16}O_6+ H]^+$ = (245.1020), found = 245.1022.

Preparation of (-)-L-2,4-di-*O*-benzyl-*myo*-inositol-1,3,5-orthoacetate (L-4.117): The allyl diol **L-3.7** (0.080 g, 0.32 mmol), was dissolved in the dry DMF (4 mL). To the cold solution sodium hydride (0.070 g, 1.74 mmol) were added and the reaction mixture was stirred for 10-15 minutes. To this mixture benzyl bromide (0.2 mL, 1.74 mmol) was added drop-wise. The reaction mixture was stirred for 14 h at room temperature. The reaction mixture was decomposed by the addition of few pieces of ice and DMF was removed under reduced pressure. The residue was worked up as usual using ethyl acetate. The product obtained was used in the next step without purification.

The crude product was dissolved in the *iso*-propanol (3 mL) and refluxed for 4-5 h after the addition of 20 % palladium hydroxide (0.070 g, 0.1 mmol). The reaction mixture was filtered through Celite and the Celite was washed methanol and ethyl acetate. The filtrate was concentrated under reduced pressure. The residue was column chromatographed (silica gel 60-120 mesh, eluent, 15-20% ethyl acetate in light petroleum) to isolate (-)-L-2,4-di-*O*-benzyl-*myo*-inositol orthoacetate as a gum **L-4.117** (0.112 g, 91%).

Data for **L-4.117:** R *f* = 0.35 (20% ethyl acetate pet ether); $[\alpha]^{25}_D$= **-** 1.1 ($CHCl_3$, c= 1.0); **IR** ($CHCl_3$)**:** $\bar{\nu}$ 3450-3550 cm^{-1}; **^{1}H NMR** ($CDCl_3$, 400 MHz): δ 1.46 (s, 3 H), 3.51 (d, *J* = 9.8 Hz, 1 H, D_2O exchangeable), 3.81 (s, 1 H), 4.16-4.20 (m, 1 H), 4.24 - 4.28 (m, 1 H), 4.29 - 4.32 (m, 1 H), 4.33 - 4.36 (m, 1 H), 4.36 - 4.40 (m, 1 H), 4.41 - 4.51 (m, 2 H), 4.59 - 4.67 (m, 1 H), 4.72 - 4.79 (m, 1 H), 7.12 - 7.19 (m, 2 H), 7.31 - 7.44 ppm (m, 8 H); **^{13}C NMR** ($CDCl_3$, 101 MHz): δ 24.1, 64.9, 67.7, 67.9, 70.5, 71.0 (CH_2), 72.66 (CH_2), 72.67, 74.3, 108.4, 127.86, 127.92, 128.4, 128.6, 128.7, 135.9, 137.6 ppm.; **HRMS** $[C_{22}H_{24}O_6+ H]^+$ = (385.1646), found =385.1649.

Preparation of (-) L-2,4-di-*O*-benzyl-*myo*-inositol (L-4.118): (-)-L-2,4-di-*O*-benzyl *myo*-inositol orthoacetate **L-4.117** (0.06 g, 0.156 mmol) was dissolved in a mixture

of MeOH (3 mL) and 5M HCL (1 mL) and refluxed for 16 h. The solvent were removed under reduced pressure and the crude product were purified by column chromatography to isolate the known [17] (-)-L-2,4-di-*O*-benzyl-*myo*-inositol as a solid (0.052 g, 93%); **MP** =140-142^{o}C (crystals obtained from the *iso*-propanol); Lit. [17] 145 ^{o}C; HPLC analysis showed the enantiomeric ratio to be 95:5. R*f* = 0.3 (ethyl acetate), Found $[\alpha]^{25}_{D}$ = -27.0 (89 ee% (EtOH, c= 0.5); Lit. [17] $[\alpha]^{25}_{D}$ = -29.2 (EtOH, c= 0.5); **HRMS** $[C_{20}H_{24}O_6 + Na]^+$ = (383.1465), found = 383.1666. HPLC profile was compared with that of the known ref racemic debenzyl ether (see Figure in Appendix IV, Figure A65-A66).

X-ray Crystallography:

Single crystal X-ray structures of all the compound were (Bruker SMART APEX II) determined by measuring X-ray diffraction intensity data on a single crystal X-ray CCD diffractometer having graphite-monochromatised (Mo-Kα = 0.71073 Å) radiation at room temperature for compound. The X-ray generator was operated at 50 kV and 30 mA. For details see the appendix IV.

DSC Analysis:

DSC analyses of the ethanol solvate **3.5** was carried out on a Waters DSC instrument. The solvated crystals (~3-4 mg) were placed on an aluminum pan (40 µl) and was analyzed using an empty pan as the reference. The heating rate was 5° (C/min). Nitrogen gas was used for purging. The DSC profile of ethanol solvate of **3.5** showed one endothermic peak correponding to melting at 116 ^{o}C in first heating cycle. Cooling and second heating cycle did not show any crystalization or melting. This implies that in the ethanol solvated crystals of **3.5** loses ethanol on melting.

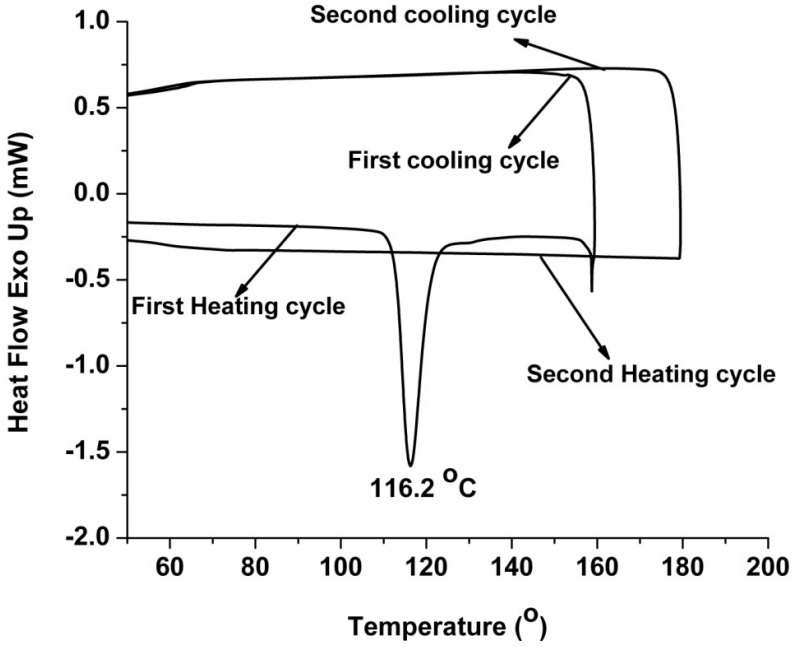

Figure 4.17: DSC profile of the ethanol solvated crystals of **3.5**.

References:

[1] (a) *Cell Signalling*, Hancock, J. T. Oxford University Press, New Delhi, India, **2005**; (b) T. Balla, *Physiol Rev.* **2013**, *93*, 1019 - 1137.

[2] (a) K. M. Sureshan, M. S. Shahsidhar, T. Praveen, T. Das, *Chem. Rev*. **2003**, 103, 4477 - 4503; (b) B. Kilbas, M. Balci, *Tetrahedron,* **2011**, *67*, 2355 - 2389.

[3] **From glucose:** (a) A. L. Leavitt, W. R. Sherman, *Carbohydr. Res.***1982**, *103*, 203 - 212; (b) K-I. Sato, S. Sakuma, S. Muramatsu, M. Bokura, *Chem. Lett.* **1991**, 1473 -1474; (c) C. Jaramillo, J-L. Chiara, M-L. Manuel, *J. Org. Chem.* **1994**, *59,* 3135–3141; (d) O. Thum, J. Chen, G. D. Prestwich, *Tetrahedron Lett.* **1996**, *37*, 9017–9020; (e) S. Saito, R. Shimazawa, R. Shirai, *Chemical & Pharmaceutical Bulletin*, **2004**, *52*, 727–732.

From galactose: (a) D. Dubreuil, J. Cleophax, M. V. De Almeida, C. Verre-Sebrie, J. Liaigre, G. Vass, S. D. Gero, *Tetrahedron,* **1997**, *53*, 16747–16766; (b) V. Pistara, P. L. Barili, G. Catelani, A. Corsaro, F. DÁndrea, S. Fisichella, *Tetrahedron Lett.* **2000**, *41*, 3253–3256.

From Pinitol: (a) W. Tegge, C. E. Ballou, *Proc. Natl. Acad. Sci.* **1989**, *86*, 94–98; (b) M. Li, A. Wu, P. Zhou, *Tetrahedron Lett.* **2006**, *47*, 3707–3710; (c) J. B. Hart, L. Kröger, A. Falshaw, R. Falshaw, E. Farkas, J. Thiemb, A. L. Win, *Carbohydr. Res.* **2004**, *339*, 1857–1871; (d) T. R. Zhan, Y-D. Ma, P-H. Fan, M. Ji, H-X. Lou, *Chem. & Biodiversity*, **2006**, *3*, 1126–1137.

From Quebrachitol: (a) A. P. Kozikowski, V. I. Ognyanov, A. H. Fauq, S. R. Nahorsk, R. A. Wilcox, *J. Am. Chem. Soc.* **1993**, *115,* 4429–4434; (b) J. J. Kiddle, *Chem. Rev.* **1995**, *95*, 2189–2202; (c) T. Akiyama, M. Hara, K. Fuchibe, S. Sakamoto, K. Yamaguchi, *Chem. Commun.* **2003**, 1734–1735; (d) S. M. Baars, J. O. Hoberg, *Carbohydr. Res.* **2006**, *341*, 1680–1684.

From Xylose: (a) D. J. Jenkins, B. V. L. Potter, *J. Chem. Soc. Perkin Trans. 1* **1998**, 41– 49; (b) K. Fukase, S. Hase, T. Ikenaka, S. Kusumoto, *Bull. Chem. Soc. Jpn.* **1992**, *65*, 436–445; (c) N. Moitessier, F. Chrétien, Y. Chapleur, C. Humeau, *Tetrahedron Lett*. **1995**, *36*, 8023–8026.

From D-Mannitol: J. L. Chiara, M. Martin-Lomas, *Tetrahedron Lett*. **1994**, *35*, 2960–2972.

From Tartaric acid: (a) F. Colobert, A. Tito, N. Khiar, D. Denni, M. A. Medina, M. Martin-Lomas, J-L. Ruano, G. Solladié, *J. Org. Chem.* **1998**, *63,* 8918–8921; (b) Y. Watanabe, A. Oka, Y. Shimizu, S. Ozaki, *Tetrahedron Lett.* **1990**, *31*, 2613–2616; (c) G. Solladie, *Hetroatom Chem.* **2002**, *13*, 443–452.

From Quinic acid: J. R. Flack, P. Yadagiri, *J. Org. Chem.* **1989**, *54,* 5851–5852.

[4] (a) K. S. Bruzik, M-D. Tsai, *J. Am. Chem. Soc.* **1992**, *114*, 6361– 6374; (b) M. A. Riley, M. F. Mohan, B. V. L. Potter, *Angew Chem. Int. Ed. Engl*. **1997**, *36*, 1472-1474; (c) S. W. Garrett, C. Liu, A. M. Riley, B. V. L. Potter, *J. Chem. Soc., Perkin Trans. 1*. **1998**, 1367-1368. (d) A. M. Riley, H. Y. Godage, M. F. Mahon, B. V. L. Potter, *Tetrahedron Asymmetry*, **2006**, *17*, 171–174; (e) K. M. Sureshan, Y. Watanabe, *Tetrahedron Asymmetry*, **2004**, *15*, 1193–1198; (f) L.T. Padiyar, Y-S. Wen; S-C. Hung, *Chem. Commun.* **2010**, *46*, 5524 –5526; (h) Shane W. Garrett, Ph D Thesis, University of Bath, **1999**.

[5] (a) P. S. Patil, S-C. Hung, *Chem. Eur. J.* **2009**, 15, 1091 – 1094; (b) S-K Chang, Y-T. Chang, E. J. Lee, Y-U. Kwon, *Korean J. of Med. Chem.* **199**8, 8. 18–21; (c) S. Capolicchio, D. T. Thakor, A. Linden, N. Ahmed, H. J. Jessen, *Angew Chem. Int. Ed. Engl*. **2013**, *52*,6912–6916.

[6] (a) B. R. Sculimbrene, A. J. Morgan, S. J. Miller, *J. Am. Chem. Soc.* **2002**, *124*, 11653–11656; (b) Y. K. Wang, W. Chen, D. Blair, M. Pu, Y. Xu, S. J. Miller, A. G. Redfield,| T. C. Chiles, M. F. Roberts, *J. Am. Chem. Soc,* 2008, **130**, 7746–7755

[7] (a) B. Tse, Y. Kishi, *J. Am. Chem. Soc.* **1993**, *115*, 7892–7893; (b) N. Chida, S. Ogawa, *Chem. Commun.* **1997**, 807–813. (c) B. P. Gurale, M. S. Shashidhar, R. G. Gonnade, *J. Org. Chem.* **2012**, *77*, 5801−5807 and references cited therein.

[8] C. Murali, M. S. Shashidhar, R. G. Gonnade, M. M. Bhadbhade, *Chem. Eur. J.* **2009**, *15*, 261 – 269.

[9] A. Mart, M. S. Shashidhar, *Tetrahedron*, **2012**, *68*, 9769-9776.

[10] (a)T. Praveen, U. Samanta, T. Das, M. S. Shashidhar, P. Chakrabarti, *J. Am. Chem. Soc.* **1998**, *120*, 3842-3845; (b) R. G. Gonnade, M. M. Bhadbhade, M. S. Shashidhar, *Chem. Commun*. **2004**, 2530 – 2531; (c) R. G. Gonnade, M. M. Bhadbhade, M. S. Shashidhar, A. K. Sanki, *Chem. Commun.* **2005**, 5870-5872; (d) M. P. Sarmah, R. G. Gonnade, M. S. Shashidhar, M. M. Bhadbhade, *Chem. Eur. J.* **2005**, *11*, 2103-2110; (e) C. Murali, M. S. Shashidhar, R. G. Gonnade, M. M. Bhadbhade, *Chem. Eur. J.* **2009**, *15*, 261-269; (f) S. Krishnaswamy, R. G. Gonnade, M. S. Shashidhar, M. M. Bhadbhade, *CrystEngComm*, **2010**, *12*, 4184–4197; (g) S. Krishnaswamy, M. S. Shashidhar, M. M. Bhadbhade, *CrystEngComm*, **2011**, *13*, 3258-3264; (h) R. S. Sardessai, S. Krishnaswamy, M. S. Shashidhar, *CrystEngComm*, **2012**, *14*, 8010–8016. (i) M. I. Tamboli, M. S. Shashidhar R. G. Gonnade and S. Krishnaswamy, *Chem. Eur. J.* **2015**, *21*, 13676-13682.

[11] R. Parthasarathy, F. Eisenberg, *Biochem. J.* **1986**, *235*, 313–322.

[12] Nomenclature committee – IUB, *Biochem. J.* **1989**, *258*, 1–2.

[13] (a) D. C. Billington, R. Baker, *J. Chem. Soc. Chem. Commun.* **1987**,1011-1013; (b) S. Devaraj, M. S. Shashidhar, S. S. Dixit, *Tetrahedron*, **2005**, *61*, 529-536.

[14] (a) K. Manoj, K. M. Sureshan, R. G. Gonnade, M. M. Bhadbhade, M. S. Shashidhar, *Cryst. Growth Des.* **2005**, *5*, 833-836; (b) K. Manoj, R. G. Gonnade, M. M. Bhadbhade, M. S. Shashidhar, *Cryst. Growth Des.* **2006**, *6*, 1485-1492; (c) K. Manoj, R. G. Gonnade, M. M. Bhadbhade, M. S. Shashidhar, *Acta Cryst*. **2007**, *C63*, o555-558; (d) K. Manoj, R. G. Gonnade, M. S. Shashidhar, M. M. Bhadbhade, *CrystEngComm*, **2012**, *14***,** 1716 – 1722.

[15] F. H. Allen, C. A. Baalham, J. P. M. Lommerse, P. R. Raithby, *Acta Cryst*. **1998**, *B54*, 320-329.

[16] B. P. Gurale, R. S. Sardessai, M. S. Shashidhar, *Carbohydr. Res.* **2014**, *399*, 8-14.

[17] G. Baudin, B. I. Glänzer, K. S. Swaminathan, A, Vasella, *Helv. Chim. Acta* **1988**, 71, 1367-1378.

[18] (a) S. Ozaki, Y. Kondo, H. Nakahira, S. Yamaoka, Y. Watanabe, *Tetrahedron Lett.* **1987**, *28*, 4691-4694; (b) Y. Watanabe, A. Oka, Y. Shimizu, S. Ozaki, *Tetrahedron Lett.* **1990**, *31*, 2613-2616; (c) D-M. Gou, C-S. Chen, *Tetrahedron Lett.* **1992**, *33*, 721-724; (d) K. Laumen, O. Ghisalba, *Biosci. Biotech. Biochem.* **1999**, *63*, 1374-1377; (e) K. M. Sureshan, M. S. Shashidhar, T. Praveen, R. G. Gonnade, M. M. Bhabhade, *Carbohydr. Res.* **2002**, *337*, 2399–2410 (f) M. S. Shashidhar, *Arkivoc*, **2002***, vii*, 63-75.

[19] D. C. Billington, R. Baker, *J. Chem. Soc. Chem. Commun.* **1987**, 1011-1013; (b) H.W. Lee, Y. *J.* Kishi, *Org. Chem*. **1985**, 50, 4402-4404.

[20] G. Bhosekar, C. Murali, R. G. Gonnade, M. S. shashidhar, M. M. Bhadbhade, *Cryst. Growth Des.* **2005***, 5*, 1977-1982.

[21] H. Gerlach, D. Kappes, R. K. Boeckman Jr., G. N. Maw, *Organic Syntheses*, **1998,** *Coll. Vol. 9*, 151; **1993**, *Vol. 71*, 48.

Appendix IV given in Pen Drive, along with Thesis

List of the content in Appendix IV